universität wien

DISSERTATION / DOCTORAL THESIS

Titel der Dissertation /Title of the Doctoral Thesis

Synthesis and Post Polymerization Modification of Polyester and Polyester carbonate Co- and Terpolymers from Carboxylic acid Anhydrides, CO_2 and Propylene Oxide

verfasst von / submitted by

Rudi Eswein, B.Sc., M.Sc.

angestrebter akademischer Grad / in partial fulfilment of the requirements for the degree of

Doktor der Naturwissenschaften (Dr. rer. nat.)

Wien, 2022 / Vienna, 2022

Studienkennzahl lt. Studienblatt / degree programme code as it appears on the student record sheet:	UA 796 605 419
Dissertationsgebiet lt. Studienblatt / field of study as it appears on the student record sheet:	Chemie
Betreut von / Supervisor:	Univ.-Prof. Dr. Kai C. Hultzsch

Kannst du machen nix, musst du lassen so...

„Ein weiser polnischer Maurer”

You cannot do nothing, you must leave it like that…

“A wise Polish bricklayer”

The work presented in this doctoral thesis was conducted between January 2016 and Mai 2020 at the University of Vienna, Austria under the supervision of Univ.-Prof. Dr. Kai Carsten Hultzsch.

Referees:
Prof. Dr. Holger Helten
Prof. Dr. Alexander Bismarck

Herewith I would like to authenticate that I have written this thesis on my own. I have not used other resources, tools or assistance than those reported in this thesis.

Rudi Eswein, October 2022

For my one and only, for my beloved wife.

Acknowledgements

I would like to thank Prof. Dr. Kai C. Hultzsch for giving me the opportunity to conduct the work on my thesis in his research group. In the last couple of years, I learned a lot about my topic, catalysis, chemistry in general, about flying glassware, highly expensive lab equipment, high pressure reactors, gloveboxes, how to light fires, how to extinguish fires, how to present topics that I have no idea about, about myself and that I should never say “explosion” in an Austrian hospital.

I like to thank Prof. Dr. Alexander Bismarck and Prof. Dr. Holger Helten for accepting the assignment as referees.

I would also like to thank my lab inmates who I share many moments of joy, frustration happiness, lab cleaning, inventories, long seminars and smaller and larger celebrations with. Thank you, Natalie, Lisa, Leo, John, Felicity, Fereshteh, Lara and Bruce. I don’t know if it would have worked out without you guys.

Thanks also to our Postdocs Mariusz and Agnieszka who were always there for good-to-knows, as well as hands on and theoretical advice.

Particularly, I like to thank our lab angel Mirjana. If you cannot find something: “It’s in the basement.” 20 minutes later you will always get the perfect glassware, however fancy it might be. Or an, as good, alternative. Thank you, Mirjana that you always keep the group running, Hvala!

Thanks to Dr. Hans Peter Kählig and the ladies from the NMR department and Alexander-Prado-Roller and Natalie Gajic for the crystallographic measurements.

Special thanks also to Prof. Dr. Alexander Bismarck and Claudia Mitterer and Nadine Barna from the Institute of Materials Chemistry who always helped me out with equipment, advice, discussions, long talks and the one or other beer.

Thanks to all my proof-readers. Thanks to Anja and Lars for their incredibly strong friendship despite of the far distance. Additional thanks to Piet, Nöl, Hermann and Willi for all the years as my pseudo siblings.

Acknowledgements

I like to express my deep gratitude to my family and especially to my parents who always encouraged and enabled me to become everything I want, despite all hard times in the past. Although, you certainly don't speak a single word in English I hope you at least like the figures in this thesis. I would gladly give you a translation.

The last one I like to thank is my deeply beloved wife. Although we spent more time apart in the last years than together you always gave me the strength to keep going on. This thesis might not be perfect, but I wrote it for you giving a piece of my heart, the heart that you safely keep. I love you.

Table of Contents

Abstract

In this thesis investigations on the ring opening copolymerization of anhydrides with propylene oxide to polyester and polyester carbonate co- and terpolymers and the characterization thereof is presented. The presented work scope ranges from the synthesis and characterization of a variation of salicyl aldimine ligand derivatives in the following referred as “salen”, to their metal complexes and the modification of the ligand architecture, the polymer synthesis, characterization and post modification. In this context aromatic derivatives, the salphen class, were equally covered. The synthesized base metal catalysts comprise aluminum, cobalt and chromium as coordinated metal ions. The main catalytic investigations were carried out using cobalt coordinated by salen and salphen ligands bearing electronic and steric variations. In that context the copolymerization behavior of maleic anhydride, phthalic anhydride, tetrahydrophthalic anhydride and *cis*-5-norbornene-*endo*-2,3-dicarboxylic acid anhydride, respectively, with propylene oxide was investigated in various monomer combinations. Subsequently, the terpolymerization of different anhydride monomers was investigated to produce random and block terpolymers. As a final investigation, terpolymerization experiments were conducted under CO_2 atmosphere. The reaction systems were kinetically analyzed by *in situ* IR spectroscopy.

All these investigations based on the need of new biobased and biodegradable materials. All monomers were chosen to already have a biobased feedstock or that a biobased feedstock will be accessible in the near future. Additionally, the monomers were chosen to bear a double bond moiety to be used as a “base” polymer for further modifications. First steps towards such modifications were made by catalytic post polymerization modification reactions by means of double bond cross metathesis. Therein, styrene as well as modified nile red and modified fluorescein were chosen as model systems, also to address potential scaffolding in dye sensitization applications.

Kurzzusammenfassung

In der vorliegenden Arbeit werden Untersuchungen der ringöffnenden Copolymerisation von verschiedenen Carbonsäureanhydriden zur Darstellung von Polyester und Polyesterkarbonat Co- und Terpolymeren und deren Charakterisierung präsentiert. Die vorliegende Arbeit beschreibt die Synthese und Charakterisierung von unterschiedlichen Salicylaldiminliganden und deren Derivaten, im Folgenden als „Salen“ bezeichnet, deren Metallkomplexen, zur Polymersynthese, deren Charakterisierung und Modifikation. Die synthetisierten Metallkomplexe beinhalten Aluminium, Kobalt und Chrom als koordinierte Metallionen. Für den Hauptteil der durchgeführten Experimente wurden Cobalt-Salen- und als aromatische Analoga Cobalt-Salphen-Komplexe mit Variationen bezüglich deren sterischen und elektronischen Einflusses verwendet. In diesem Zusammenhang wurde das Verhalten von Maleinsäureanhydrid, Phthalsäureanhydrid, Tetrahydrophthalsäureanhydrid und *cis*-5-Norbornen-*endo*-2,3-dicarbonsäureanhydrid in der Copolymerisation jeweils mit Propylenoxid untersucht. Weiters wurde das Verhalten von verschiedenen Anhydridkombinationen in der Synthese von statistisch verteilten und Blockterpolymeren untersucht. Als letzte Untersuchung in dem Zusammenhang wurden die Terpolymerisationen unter CO_2 Atmosphäre betrachtet. All die genannten Reaktionssysteme wurden mithilfe von *in situ* IR Spektroskopie verfolgt und bezüglich der Reaktionskinetik analysiert.

Die hier präsentierte Forschung greift die Notwendigkeit der Entwicklung neuer biobasierter und bioabbaubarer Kunststoffe auf. Alle Monomere wurden nach bereits heute, oder in naher Zukunft, verfügbaren biobasierten Rohstoffen bzw. Herstellungsprozessen ausgewählt. Gleichzeitig wurden Carbonsäureanhydride in die Untersuchungen einbezogen, die mit vorhandenen Doppelbindungen, die Verwendung der mit ihnen hergestellten Polymere als „Basispolymere“ zur späteren, bedarfsgerechten Modifikation versprechen. Erste Experimente bezüglich der Postmodifikation mittels Doppelbindungsmetathese werden ebenfalls gezeigt. Dabei wurden sowohl Styrol, als auch modifiziertes Nilrot und Fluorescein als Modellsysteme ausgewählt, auch um mögliche Gerüsteffekte der Basispolymere bezüglich lichtinduzierter Farbanregung zu untersuchen.

Abbreviations

$^{13}C\{^{1}H\}$–NMR	Proton Decoupled Carbon 13 NMR
^{19}F–NMR	Fluorine 19 NMR
^{1}H–NMR	Proton NMR
BDI	β-Diketiminato
BnOH	Benzyl alcohol
BPA	Bisphenol A
Calc.	Calculated
Cat.	Catalyst
CHO	Cyclohexane Oxide
Cocat.	Cocatalyst
Conv.	Conversion
COPO	3,4-Epoxytetrahydrofuran
COSY	Correlated Spectroscopy
CPrA	Cyclopropane-1,2-dicarboxylic acid
CTA	Chain Transfer Agent
Cy	Cyclohexyl Group
Đ	Polydispersity
DMAP	4-(Dimethyl) amino pyridine
DMC	Dimethyl Carbonate
DNP	2,4-Dinitrophenolate
DOSY	Diffusion Ordered (NMR) Spectroscopy
DPC	Diphenyl Carbonate
EC	Ethylene Carbonate
ee	Enantiomeric Excess
EO	Ethylene oxide
eq/equiv	Equivalents
ESIMS	Electro Spray Ionization Mass Spectrometry
FA	Furfural
FeTCTPP	Iron tetra-(*p*-chlorophenyl)-porphyrin
Fig.	Figure
g	gram
GPC	Gel Permeation Chromatography
h	Hour
HMBC	Heteronuclear Multiple Bond Correlation
HPPO	Hydrogen peroxide PO process
HSQC	Heteronuclear Single Quantum Coherence
Hz	Hertz (s^{-1})
IR	Infra Red
IV	Intrinsic Viscosity (dL/g)

L	Liter
LA	Levulinic acid
LUMO	Lowest Unoccupied Molecular Orbital
m/z	Mass/Charge
MA	Maleic anhydride
MALDI-TOF MS	Matrix Assisted Laser Desorbtion Ionization Mass Spectrometry
Me	Methyl
MEG	Monoethylene Glycol
MeOH	Methanol
M_n	Number Averaged Molecular Weight
mol	Mol
MPa	Megapascal
MTBE	Methyl–*tert*–butyl ether
M_w	Weight Averaged Molecular Weight
n.d.	Not determined
N/A	Not applicable or not available
NA	cis-5-Norbornene-endo-2,3-dicarboxylic acid anhydride
NMR	Nuclear Magnetic Resonance
Np	Nanoparticles
OAc	Acetate
PA	Phthalic anhydride
PBS	Poly(butylene succinate)
PBAT	Poly(butylene adipate terephthalate)
PC	Polycarbonate
PCE	Power conversion efficiency
PCL	Polycaprolactone
PCT	Poly(cyclohexyl dimethyl terephthalate)
PDI ≡ *Đ*	Polydispersity Index
PET	Polyethylene terephthalate
Ph	Phenyl
PHA	Poly(hydroxy alkanoate)
PLA	Poly(lactic acid)
PO	Propylene oxide
ppm	Parts per million
PPNCl	Bis(triphenylphosphoranyliden)ammonium chloride
PTT	Poly(trimethylene) terephthalate
Quant.	Quantitative
ROCOP	Ring–Opening Copolymerization

ROP	Ring–opening polymerization
SA	Succinic Acid
Salen	Salicyl aldimine
t	Time
TBA	Tetra-*n*-butyl ammonium
*t*Bu	*tert*–Butyl
Temp	Temperature
TFA	Trifluoro acetate
TGA	Thermogravimetric Analysis
THF	Tetrahydrofuran
THPA	Tetrahydrophthalic anhydride
TOF	Turnover Frequency (h^{-1})
Tol./tol.	Toluene
TON	Turnover Number
TPSCl	Triphenylsilyl chloride
UHR TOF	Ultra High Resolution Time Of Flight
UV	Ultra Violet (Light)
VIS	Visible (Light)
Vol%	Volume %
Wt%	Weight %

1 Introduction

To date many different types of polymers are known. The material properties and structure–property relationships are widely well understood. Among the vast variety of industrialized polymers, polyolefins are the by far widest spread polymer type worldwide.[1] Polyolefins have the benefit of making many material properties available depending on the microstructure and the processing of the respective material. Consequently, the majority of gained knowledge in polymer chemistry and processing is based on polyolefin chemistry.

Yet, the material property benefits of polyolefins being tough and resistant and therefore being long lively are at the same time the largest weakness. To date, on a global scale, the recycling of polyolefins is still facing a waste collection problem, as well as, a lack of recycling effectiveness. This leads to an accumulation of plastic waste in the environment. This weakness can be well addressed by modern polyesters and polyester compounds. Particularly in the packaging industry polyesters such as poly(butylene adipate terephthalate) (PBAT), poly(lactic acid) (PLA), poly(hydroxy alkanoates) (PHAs) or PBS poly(butylene succinate) become increasingly important components in polymer blends with increasingly versatile material properties, challenging those of commonly used polyolefins. Although polyolefins are still superior in material properties in many applications and therefore must be recycled thoroughly, biodegradable and preferentially biobased polyesters are one aspect to tackle global waste problem.[2]

1.1 Types of Polymers

Various kinds of polymers are known in the literature. But generally, the main polymer motifs can be divided into five groups: polyolefins, polyesters, polyamides, polyethers and polyurethanes.

Obviously, each group divides in numerous categories with respect to substitution patterns, crosslinking, branching and also architectural categories such as primary, secondary and tertiary structures. Fig. 1 provides an overview about common organic polymer connectivity motifs. In addition to the already mentioned types of organic polymers, inorganic polymers play an important role in modern society. Examples of inorganic polymers are for instance polymeric sulfur or poly(siloxanes). Although inorganic polymers play an important role in modern society, they will not be further covered in this thesis.

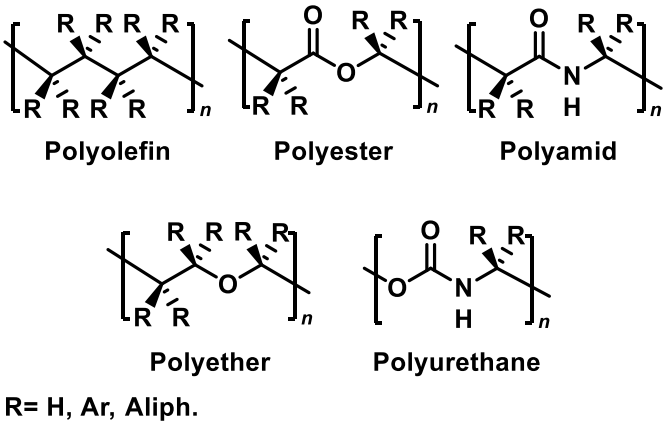

Fig. 1: General polymer connectivity motifs.

Synthetic pathways to produce the mentioned polymers are numerous. Yet, the synthetic principles are similar. The commonly exploited polymerization pathways comprise radical polymerization, anionic and cationic polymerizations, coordination-insertion polymerizations, polycondensations and ring-opening polymerizations.[3] Each of which bears its benefits and drawbacks. In addition to that usually the material property scope of polymers can be broadened by incorporation of two types of monomers leading to copolymers, and thus, to altered material properties compared to the respective homopolymer.[4] A further means to modify the material properties is to modify the microstructure of the polymeric chains to feature alignment effects of the chains. In the following chapter these aspects will be discussed briefly.

1.2 Polymer Synthesis

Modern organic polymers are synthesized essentially in the basic reactions, namely, radical polymerization, ionic polymerization, olefin polymerization, polycondensation and ring–opening polymerization reactions.[3] All of which have various subtypes which are extensively discussed in literature. However, as polyesters and polycarbonates are the focus of this work, the synthesis respectively the industrial production of polyesters and polycarbonates will be covered in the following chapters while the other mentioned polymerization types are discussed elsewhere.[3]

1.3 Industrial Polyester Synthesis

The production of synthetic polyesters is one of the largest processes worldwide. In 2016 76.66 million tons of polyesters were produced of which a large part of 27.5 % was polyethylene terephthalate (PET).[5]

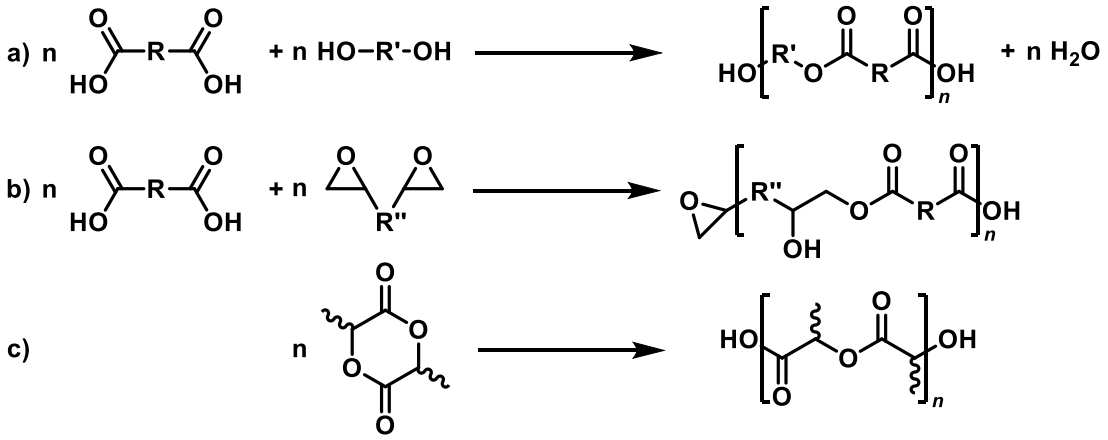

Scheme 1: Examples of polyester syntheses. a) common polycondensation, b) polyaddition reaction, c) ring–opening polymerization.

Obviously, PET is not the only commercially produced polyester. Other patented aromatic polyesters are, for instance, poly(trimethylene terephthalate) (PTT) or poly(cyclohexyl dimethyl terephthalate) (PCT). Besides aromatic polyesters, aliphatic and well degradable polyesters such as polybutyrolactones, polylactides or polycaprolactones are nowadays common materials. Polyesters are widely used as fibers for clothing, coatings, lacquers, as food packaging, as well as components in composite materials such as tires.[5, 6]

Three different strategies can be followed to produce polyesters (Scheme 1). One synthetic pathway is the step growth polymerization which is a condensation reaction in the context of polyester synthesis (Scheme 1a). In this type of polymerization, dicarboxylic acids, or their diester analogues, are reacted with diols at elevated temperatures (200–280 °C, melt). Although, the reaction is auto-catalytic, a Lewis acidic metal catalyst can be employed to decrease reaction times.[6, 7] Generally, the obtained molecular weight distributions are broad and typically in the range of $M_w/M_n >> 2$ because of extensive transesterification reactions at elevated temperatures. The transesterification reaction can, on the other hand, be exploited to produce a polyol oligomer which is then employed in a further polycondensation step. To produce such oligomer, an ester, for instance dimethyl terephthalate, is molten under an inert gas atmosphere. Under these conditions, transesterification reactions proceed in the presence of ethylene glycol upon the release of methanol, which is removed by distillation in the reaction process.[7]

Another strategy is the polyaddition reaction (Scheme 1b). Contrary to polycondensation reactions, no condensates are produced in polyaddition reactions. Thus, polyaddition reactions benefit from the fact that small molecules do not have to be removed and, additionally, polymers with reactive chain ends can be produced.[3] The most prominent example, however, is not the

synthesis of a polyester, but rather the synthesis of polyurethane.[3, 8] Thus, polyaddition reactions remain a specialty in industry in the regime of polyesters to date.

A third synthetic strategy for polyester synthesis is the ring–opening polymerization (Scheme 1c). The benefit of the ring–opening polymerization process is the minimization of side products compared to the polycondensation reaction, as transesterification is minimized. However, ring–opening polymerization processes for polyester syntheses are relatively scarce in industry.[7] ε-Caprolactone can be utilized as monomer to produce polyesters by ring–opening polymerization. Although it is biodegradable, its low melting temperature limits potential applications and makes polycaprolactone, thus, a niche polymer so far.[7] However, a monomer which gained much interest over the last 3 decades is lactide. Lactide can be produced over fermentation of dextrose which leads to lactic acid.[9] The lactic acid can be further oligomerized and subsequently depolymerized to yield lactide. The lactide can further undergo catalytically a ring–opening polymerization to yield poly(lactic acid) (PLA).[9-13] To substitute this two-step process, investigations were performed to catalytically transform the monomeric lactic acid to the dimeric lactide.[14]

Cyclic ethers such as tetrahydrofuran (THF), propylene oxide (PO) or ethylene oxide (EO) are oligomerized in industry to produce macroinitiators which can be employed in the polyurethane synthesis.[15, 16] These polyols are also employed as thickeners or lubricants. Another large field, where the ring–opening polymerization is largely employed, is in the synthesis of epoxy resins, which function as adhesives, coatings or insulations, just to name a few applications.[17] An overview about industrially produced polymers can be found in the *Handbook of Polymers*.[18]

1.4 Industrial Polycarbonate Synthesis

The first industrial process to produce polycarbonates was based on the phosgene-process.[16] This process was industrialized in 1958 by Bayer and 1960 by GE. Subsequently, chemical companies like Idemitsu Petrochemicals, Mitsubishi Chemical and Dow Chemical followed. The process is based on a polycondensation reaction of phosgene, which is highly corrosive and highly toxic, and bisphenol-A (BPA), which is known to be an endocrine disruptor and toxic for reproduction.[19] Still, the process developed to the largest polycarbonate process world-wide. In 2016 over 5000 kilotons were produced mainly by this process.[20] The process is a biphasic process comprising of a dichloromethane layer, which contains the phosgene and an aqueous layer containing a BPA sodium salt. Hence, the process produces a significant amount of

contaminated water and dichloromethane. Scheme 2 represents a schematic polycarbonate synthesis by the mentioned route.

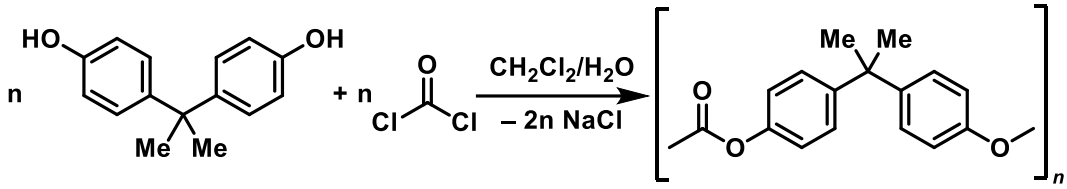

Scheme 2: Polycarbonate synthesis from bisphenol-A and phosgene.

Because of the nature of phosgene, it is produced on site from carbon monoxide by chlorination with chlorine. To avoid storage of toxic gases, carbon monoxide is produced by oxidation of carbon while chlorine is generated by electrolysis of an aqueous NaCl or KCl solution on site. An overview of the process is depicted in Scheme 3.[16]

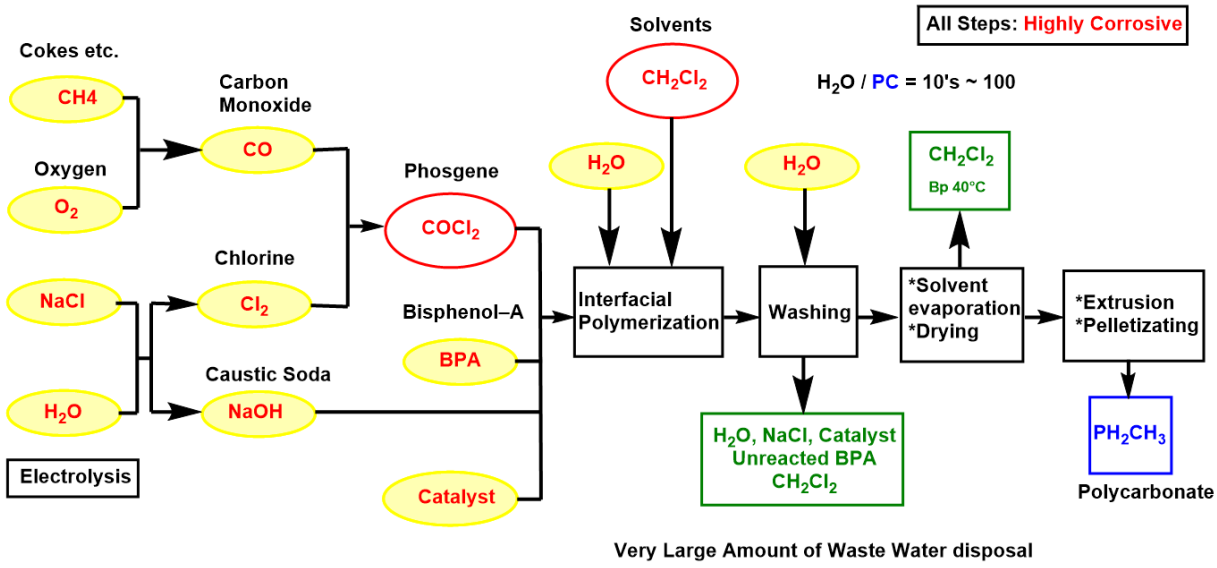

Scheme 3: Overview of the phosgene process.Redrawn from ref.[16]

The drawbacks of this complicated process employing highly toxic and corrosive chemicals lead after years of development to the phosgene-free Asahi Kasei process. The process starts from CO_2 which is reacted with ethylene oxide in the presence of an ion exchange resin bearing quaternary ammonium groups. The resulting cyclic carbonate is further reacted under reactive distillation conditions with methanol to produce dimethyl carbonate (DMC) and monoethylene glycol (MEG). The DMC is further reacted with phenol in another reactive distillation process to yield diphenyl carbonate. The diphenyl carbonate can then be reacted in a polycondensation reaction with bisphenol–A (BPA) to obtain the desired polycarbonate. Scheme 4 summarizes the Asahi Kasei non-phosgene process.

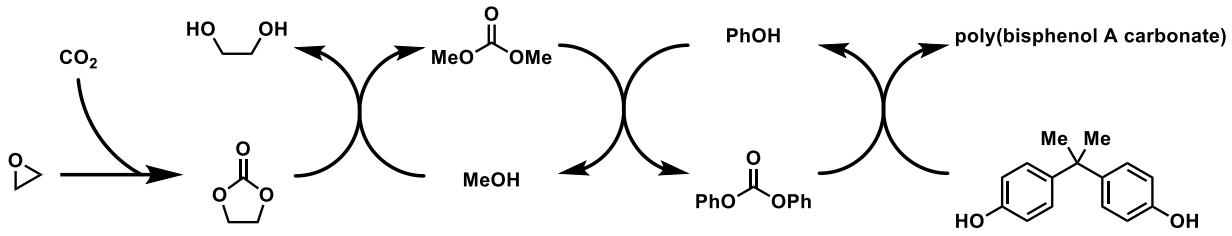

Scheme 4: Asahi Kasei process. Redrawn from refs[16, 21].

Since the process was developed, it was licensed to various companies and about 1/5th of the world production of different polycarbonates is produced by non-phosgene processes.[16] Although, the process comprises several reactive distillations and is therefore highly energy demanding, the popularity of the process benefits from the possibility of complete recyclization of produced intermediates and of the use of CO_2 instead of phosgene. Another benefit of this process is the higher material quality. As no phosgene is employed in the process, no corrosive carryovers are present in the process which leads to materials without corrosion defects.

The Asahi Kasei process already provides a large improvement to industrial polycarbonate production. One drawback of this whole process might be the low flexibility in choosing the substrates or the high energy demand, as well as, the number of steps. However, in academia and in pilot plants (Novomer[22]) polycarbonates can already be produced by ring-opening polymerizations of epoxides and CO_2.

1.5 Monomers from Renewable Feedstocks

As discussed before, one way to improve the sustainability of highly demanded materials is to improve the process itself to give higher selectivities, higher product yields, less by–products and to have lower energy demand. These aspects are not only important from a sustainability but also from the economic point of view. An obvious complementary strategy with respect to a sustainable material feedstock is the exchange of fossil-based feedstock to renewable feedstocks. Not only that it is a crucial step concerning the depletion of fossil feedstock, but it is also important to transform industry from linear to truly circular in that context. Many companies consider recycling of side streams or already consumed products as circular. But as a matter of fact, industry can only become truly circular if the circle between degraded product and the raw material feedstock can be closed. Therefore, material degradation must be considered during the use and after disposal of a product, as well as, during the recycling process of the material. This can lead to serious environmental issues, namely the accumulation of plastic particles in soil and water. Because of this quality degradation, virgin material will still be needed in a circular

economy to maintain material quality. Therefore, the absolute amount of non-degradable plastic increases. This issue can partly be accounted for by changing the feedstock from fossil–based to biobased to improve sustainability and simultaneously to strive for biodegradability or technologies recycling plastic on a molecular level. An extensive overview about synthetic routes to renewable platform chemicals is given elsewhere.[21]

For this work the focus is on the controlled synthesis of advanced polyester materials *via* ring–opening copolymerization of epoxides and anhydrides, potential routes of biobased monomer syntheses will be discussed in the following.

1.6 Industrial and Biobased Production of Propylene Oxide

Many epoxidation reactions with a countless amount of variations can be found in literature. However, they can be divided in four main groups: Jacobsen-Katsuki[23] epoxidation, the Prilezhaev reaction,[24] the Sharpless epoxidation[25, 26] and the Shi epoxidation.[27] Each reaction has its benefits and its drawbacks. Although they are altogether wide in substrate scope, these reactions are not used, as such, in large industry processes, as it would be necessary in plastics industry due to low value stoichiometric byproducts and, particularly, due to expensive starting materials. The reactions are rather employed in small-scale and high-value processes. Only two epoxides are synthesized on large scale in industry: ethylene oxide (EO) and propylene oxide (PO). EO is industrially synthesized directly from oxygen and ethylene. The reaction is catalyzed by a heterogeneous silver based catalyst at temperatures between 220 and 300 °C with selectivities greater than 90 %.[28] The production of propylene oxide is more difficult as overoxidation to acetaldehyde, formaldehyde and carbon monoxide takes place at similar conditions. Hence, four alternative processes are used for the synthesis of propylene oxide in industry. The oldest process is the so-called chlorohydrin process (Scheme 5).[29] In this process chlorine is reacted in the presence of water in the gas phase with propylene to epichlorohydrin and hydrochloric acid. Commonly the process is only viable if the chlorine can be produced on site. In a second step the chlorohydrin and HCl react with $Ca(OH)_2$ to yield propylene oxide, two equivalents of water and one equivalent of $CaCl_2$. Hence, one equivalent of salt waste is produced per equivalent of produced PO. If $Ca(OH)_2$ is replaced by sodium hydroxide, the generated NaCl can be recycled electrolytically to produce Cl_2 and NaOH. In such a setup the chlorine gas and the NaOH can be recycled. However, such an expansion of the process increases the investment costs significantly.[30]

Scheme 5: The chlorohydrin process.

Because of the difficult handling of this reaction using chlorine and the high amount of waste, other processes were developed. The currently mostly used process is the hydroperoxide process. This type of process can be divided in three variants which can be distinguished by the produced coupling product. The produced coproduct is again dependent on the hydroperoxide which is employed in the process. If an organo hydroperoxide is used, for instance, the coupling product is an alcohol which adds value to the process. The first variant produces *tert*–butyl methyl ether (MTBE) as coproduct. Another process produces styrene after an additional reaction step. The third variant produces, besides propylene oxide, *tert*-butyl benzene after two additional steps. Because of the stoichiometrically formed coproduct the economical value of the whole process depends also on the demand of a second component and not only on propylene oxide.[31] A further development of the oxidation of propylene with an additional oxidant leads to the use of hydrogen peroxide as oxidant. This process is currently the most growing process for PO production, mainly replacing the chlorohydrin process.[30] The hydrogen peroxide PO process (HPPO) is the state-of-the-art process in industry and it is catalyzed by the titanium silicate TS-1.[30, 32]

In academia the catalyst development concentrates on direct oxidation of propylene by molecular oxygen. The reaction proceeds either in the liquid or in the gas phase while the majority of the investigated catalyst systems are heterogeneous. In heterogeneous catalysis Cu, Ti, Au, MoO_X, RuO_2, V_2O_5, and TiO_X based catalysts were investigated.[31] Silver based catalysts attracted attention as heterogeneous silver-based catalysts were already successfully employed in ethylene oxide synthesis. More recent investigations on silver nanoparticle catalysts proved even a wider substrate scope, selectively oxidizing bulkier olefin substrates to the respective epoxides, which were not accessible by zeolithe based catalysts.[33]

To summarize, the oxidation of propylene to PO either with an organo hydroperoxide or hydrogen peroxide as oxidant are already industry implemented technologies which will be certainly further developed. Yet, the basis of the newly developed propylene oxidation processes is still propylene, which is mainly produced in the cracking process of crude oil. Hence, the development of processes to produce biobased propylene is an intriguing goal to strive for.

1.7 Renewable Propylene Production

Much effort was undertaken to substitute fuels for the transport sector. The most prominent set up infrastructure in that regard is the production of bioethanol. Bioethanol is widely used either as fuel additive or even as fuel itself. The viability of a changeover of first and second generation bioethanol facilities to produce ethylene and butene in a first step and propylene *via* double bond metathesis in a second step was simulated.[34] Very promising results were already obtained for the ethylene dimerization/isomerization/methathesis step at 80 °C and 30 bar. The ethylene is here produced from dehydration of bioethanol. Another pathway is the oligomerization of ethylene and the subsequent catalytic cracking of the oligomers, also known as SHOP process.[35] These two subsequent steps of first producing biobased ethylene and as second step the oligemerization thereof, can be completed by catalytic cracking to propylene at high temperatures (~500 °C) over zeolite catalysts.[36] An overview is provided in Scheme 6.

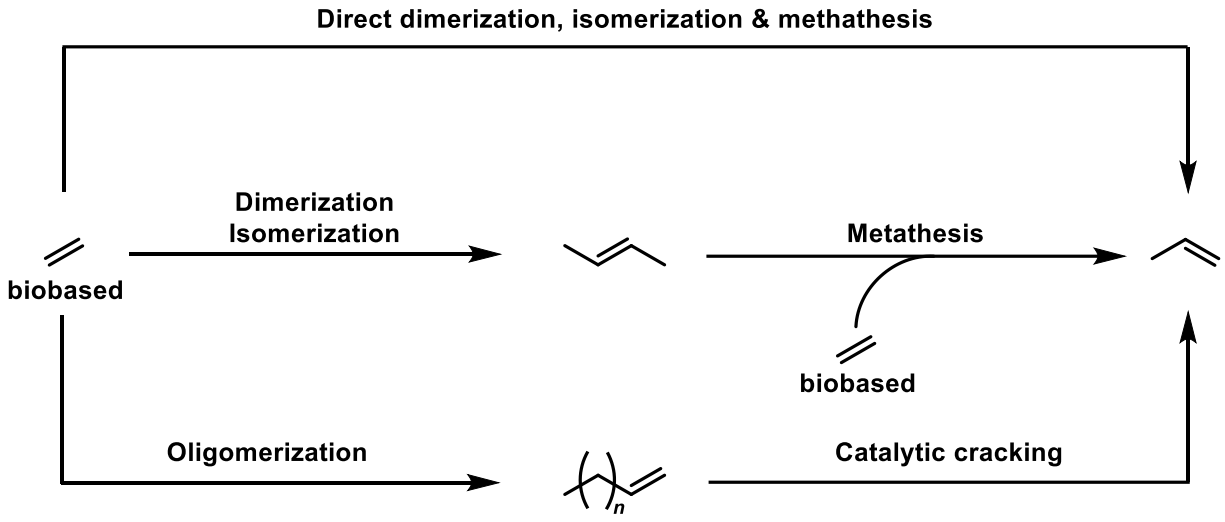

Scheme 6: Reaction pathways to biobased propylene.[21]

Other studies concentrate on furfural as biobased feedstock for the production of butadiene. The reaction sequence would proceed over a decarbonylation of furfural (furan-2-aldehyde) to furan and subsequent hydrogenation to tetrahydrofuran (THF). Furfural can be produced by acidic treatment of hemicellulose. The THF can then be catalytically converted to butadiene with propylene as byproduct. Thus, the process should also be able to be directed towards propylene production.[37] Moreover, the production of light olefins has been shown on laboratory scale and micro pilot scale using fatty acid methyl esters as substrate. The hydrogenation over a Ni_3Al alloy catalyst is followed by a hydrodeoxygenation step over a $NiMoS/Al_2O_3$ catalyst and a subsequent steam cracking step. Here, the product distribution could be even improved to about

62 % towards ethylene, propylene and 1,3-butadiene, compared to 32 % from naphtha processes at similar reaction conditions.[38, 39]

The last process that shall be mentioned here is the catalytic conversion of glycerol to propylene. Glycerol can be produced from transesterification or hydrolysis of fatty acid esters or from fermentation. Glycerol is also a coproduct in biodiesel production.[40, 41] The glycerol can be transformed in a two-step process to propylene. The first step comprises a hydrogenolysis of aqueous glycerol (10 wt%) using different supported noble/rare–earth metal catalysts in loadings as low as 1 wt% for Ir/ZrO_2 (with 0.12 mol% Ir) under 5 MPa hydrogen atmosphere. The produced 1-propanol can be obtained with a selectivity of up to 94 %. The next step in the process is the dehydration of 1-propanol over zeolite catalysts at 250 °C to selectively obtain propylene (Scheme 7).[42] Although, the described processes are still under investigation and are thus so far not industrially viable, important progress was already made to switch the fossil-based production of propylene to a biobased production.

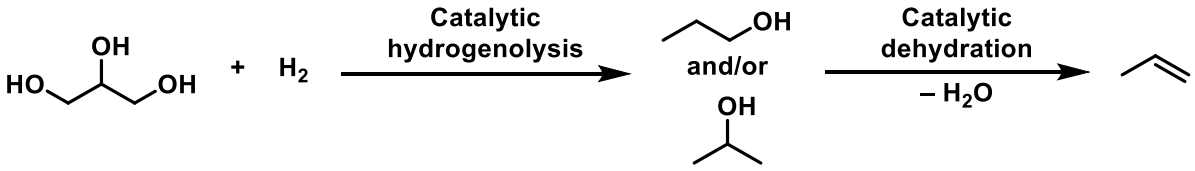

Scheme 7: Synthetic pathway to propylene from glycerol.[21]

1.8 Biobased Anhydrides

In the previous section a potential route to biobased propylene was elucidated as propylene is the basis for the subsequent oxidation reaction to produce propylene oxide. As propylene oxide is only one monomer to produce polyesters *via* ring–opening copolymerization. In this chapter the biobased feedstock of cyclic anhydrides will be discussed. Cyclic anhydrides are a product of the dehydration of organic diacids. Therefore, the renewable production of a variety of organic diacids is of major importance to produce fully biobased polyesters and further to the production polycarbonates and polyester carbonates.

One example is the synthesis of succinic acid. Succinic acid can be produced by oxidation of furfural with H_2O_2 over Amberlyst-15®. Another approach is the oxidation of levulinic acid (LA) with molecular oxygen over ruthenium nanoparticles. Levulinic acid can also be produced from cellulose.[43] The mentioned reactions are depicted in Scheme 8.

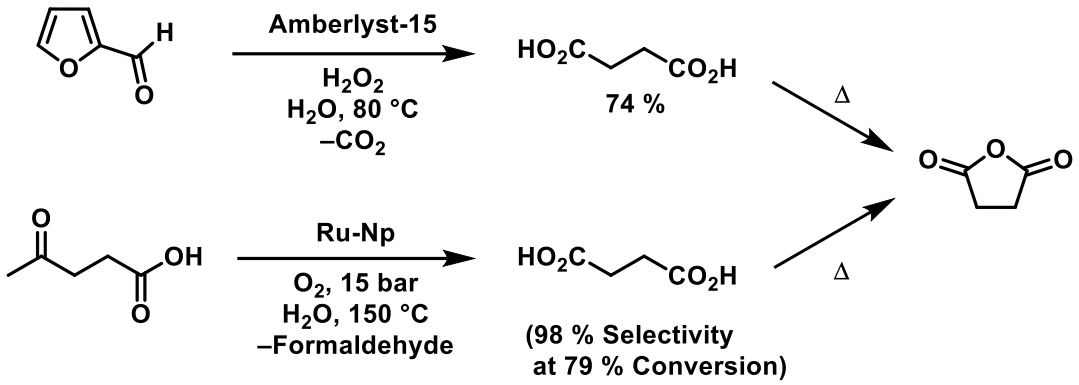

Scheme 8: Synthesis of succinic acid (SA) from furfural (FA), top, and levulinic acid (LA), bottom.

After an additional dehydration step, succinic acid can be transformed to succinic acid anhydride, which can be employed as a monomer in the ROCOP of anhydrides and epoxides with a suitable catalyst. To further gain structural diversity in the anhydride branch of the monomers, additional functionalities are crucial. A very promising functionality in that regard are double bonds. Hence, maleic acid is of major interest as its anhydride gives the possibility for modifications *via Diels-Alder* cyclo addition. Therefore, not only structural diversity can be introduced, but also the reactivity can be significantly altered, as the ring strain of cyclic anhydrides is strongly influenced by the substitution pattern.[44]

A feedstock for maleic anhydride (MA) is provided by furfural, which can be oxidized to maleic acid over heterogeneous $H_3PMo_{12}O_{40}$, $Cu(NO_3)_2/H_3PMo_{12}O_{40}$ or iron tetra-(*p*-chlorophenyl)-porphyrin (FeTCTPP) in solution using molecular oxygen as oxidant or over zeolite TS-1 with H_2O_2 as oxidant (Scheme 9). Here, yields up to 92 % were reached. If formic acid is used as solvent and H_2O_2 as oxidant, furfural can also be converted to maleic acid in a yield of 91 % without a catalyst after 4 h.[21] VO_X/SiO_2 can convert furfural with O_2 in the gas phase at 320 °C directly to maleic anhydride with a selectivity of 73 %. Maleic acid was found here as a byproduct. Unfortunately, some of the reactions still require highly toxic solvents.

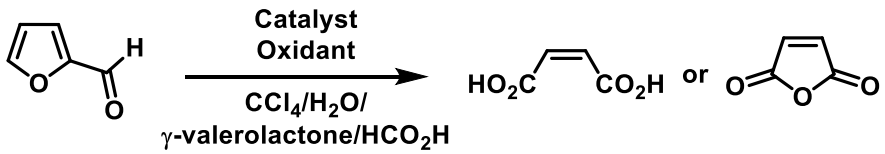

Scheme 9: Maleic acid and maleic anhydride from furfural.

With a renewable feedstock of maleic anhydride available, it can be further reacted *via Diels-Alder* reactions with various furan derivatives to selectively produce oxanorbornene dicarboxylic anhydrides. *Diels-Alder* reactions with maleic anhydride to dehydrated anhydrides were investigated in the last 20 years on many occasions with many substrates. Among the

investigated dienes, furfural derivatives,[45] furan derivatives,[46, 47] conjugated triene fatty acid esters,[48] cyclopentadiene derivatives,[49, 50] and butadiene derivatives[51-53] can be found. Thus, the chemistry of *Diels-Alder* reactions with maleic anhydride is already well investigated. In this context, not only cyclic dienes can be produced from bio-feedstocks but also linear dienes are accessible. Potential substrates would be bioethanol, 1,4-butane diol, itaconic acid, threitol or erythritol. Additionally, many carbonyl compounds are imaginable as substrates for *Hetero-Diels-Alder* reactions, for example acrylates, which can again be bioderived.[21]

1.9 Ring–Opening Polymerization in Academia

In contrast to industrial applications, research in academia focuses on ring–opening polymerization for the synthesis of polyesters. One of the first substrate that was investigated in ring–opening polymerizations with respect to catalysis was L-lactide.[10-13] However, a major drawback of PLA from ROP is the low mechanical stability due to brittleness.[54] Polyesters which were produced by polycondensation reactions, however, exhibit excellent properties accounting brittleness by a broader molecular weight distribution. Nevertheless, polycondensation reactions also intrinsically suffer a lack of reaction control, side product formation and require high reaction temperatures. Thus, one focus in polymer research is to apply the benefits of the ring–opening polymerization to relevant polymers to produce a defined product with the production of materials with high applicability, as known from conventional polyester syntheses.

Cyclic ethers can be easily polymerized, but the resulting polyethers, such as poly(tetramethylene glycol), poly(THF) exhibit a too high flexibility for many application.[18] To improve the properties, comonomers can be introduced. It has been found that strictly alternating monomer incorporation of cyclic anhydrides and epoxides can be achieved by homogeneous catalysis, which leads to polyesters that are structurally similar to industrially produced polyesters synthesized by polycondensation. Additionally, these polyethers can be synthesized under much milder conditions and in a more controlled fashion.[55, 56] Moreover, many potentially valuable monomers can be employed in this type of reaction, which can be produced from renewable feedstocks. This provides the unique opportunity to lower the dependence on petrochemical feedstocks.

1.10 Mechanism of Ring Opening Copolymerizations (ROCOP)

Generally, the ring–opening of epoxides, as well as, of anhydrides is facilitated by metal complexes with various ligand environments.[55, 57] The ring–opening to form the initiating species proceeds via a nucleophilic attack of a complex anion at the epoxide. The formed metal alkoxide

species can then further perform a nucleophilic attack at one carbonyl moiety of a cyclic anhydride molecule which leads to its ring–opening. Since the thus formed carboxylate species is not nucleophilic enough to open another anhydride, a ring–strained epoxide is opened to form an alkoxide species. Obviously, it is possible for an alkoxide group to attack another epoxide, which would result in a polyether. Avoiding such a polyether formation is one of the major challenges in catalyst development in this field. An overview of the described steps is depicted in Scheme 10.

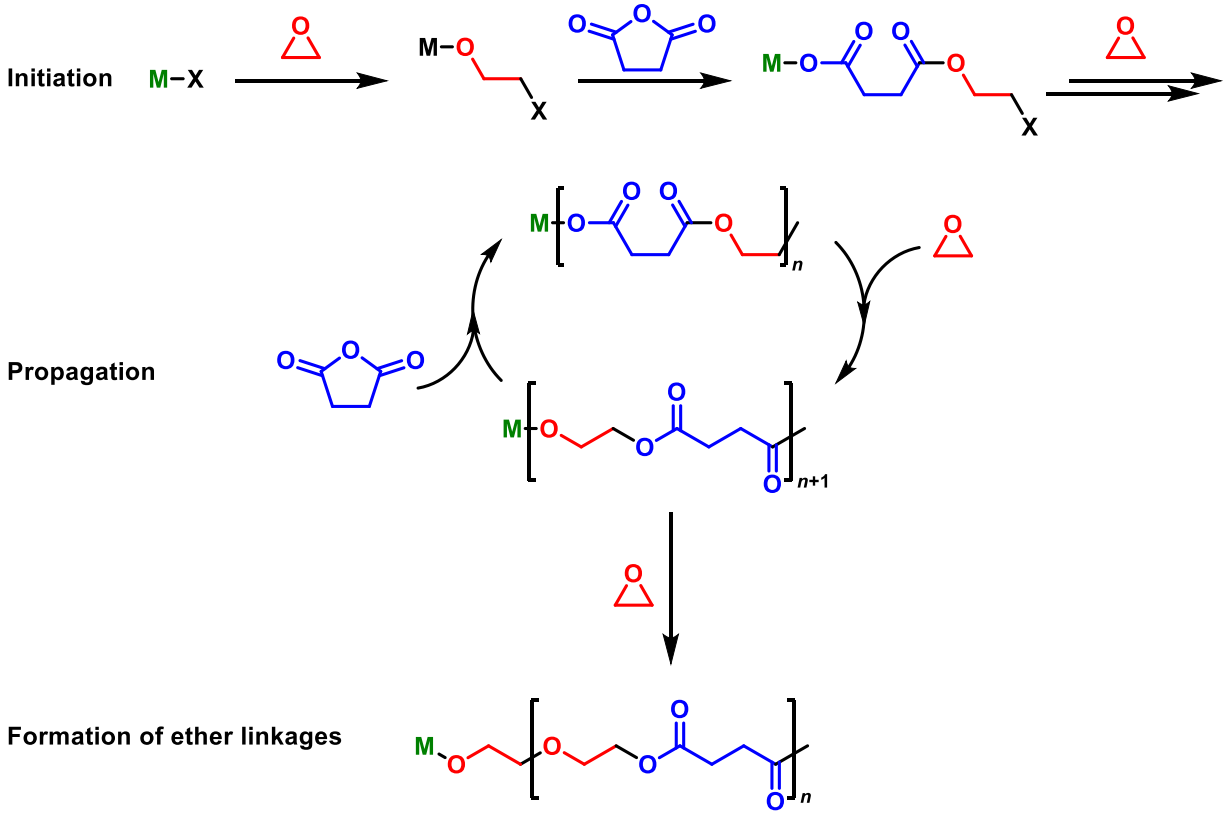

Scheme 10: General mechanism of the ring–opening copolymerization of anhydrides and epoxides. Redrawn from. [56]

In fact, the reaction mechanism depicted in Scheme 10 is oversimplified. Due to the high density of functional groups in the monomer mixture a versatile coordination to the metal centers is possible. Scheme 11 provides an overview on the different possible catalytic cycles involving the anhydride and the epoxide ring–opening with metal salen complexes as catalysts.[55] The first step in cycle 1 is the dissociation of an alkoxide from the dialkoxy complex (**AA**) followed by the coordination of an anhydride to form the alkoxide-carboxylate complex (**AC**). The following nucleophilic attack of the alkoxide at the anhydride leads to the ring opening of the cyclic anhydride. Following cycle 1 the next step can be a displacement of the formed carboxylate by a new epoxide which is then opened by a nucleophilic attack of the carboxylate anion. Another possible pathway is represented by cycle 2. Starting from the alkoxide-carboxylate complex

(**AC**), the coordinated alkoxide can dissociate and is replaced by an anhydride which then coordinates to the metal center *via* the carbonyl moiety. The previously dissociated alkoxide can then attack the activated carbonyl group leading to the ring–opening of the anhydride, resulting in the formation of the dicarboxylate complex (**CC**). The species **AC** is formed again after dissociation of one carboxylate and insertion of an epoxide. The third possible cycle starts similarly from the alkoxide-carboxylate complex **AC**. There the carboxylate is substituted by an anhydride. The carbonyl of the anhydride is then attacked by the neighboring alkoxide leading to an insertion of the anhydride. Complex **CC** is formed after coordination of the previously dissociated carboxylate. At this point cycle 3 follows the reaction pathway of cycle 2. In comparison to the other two cycles, cycle 3 requires a geometry change in the coordination sphere of the complex. Depending on the respective ligand this might not be necessarily possible, as the alkoxide and the anhydride would have to be in *cis* position with respect to each other. The other two reaction pathways would proceed with the alkoxide/carboxylate in axial positions.

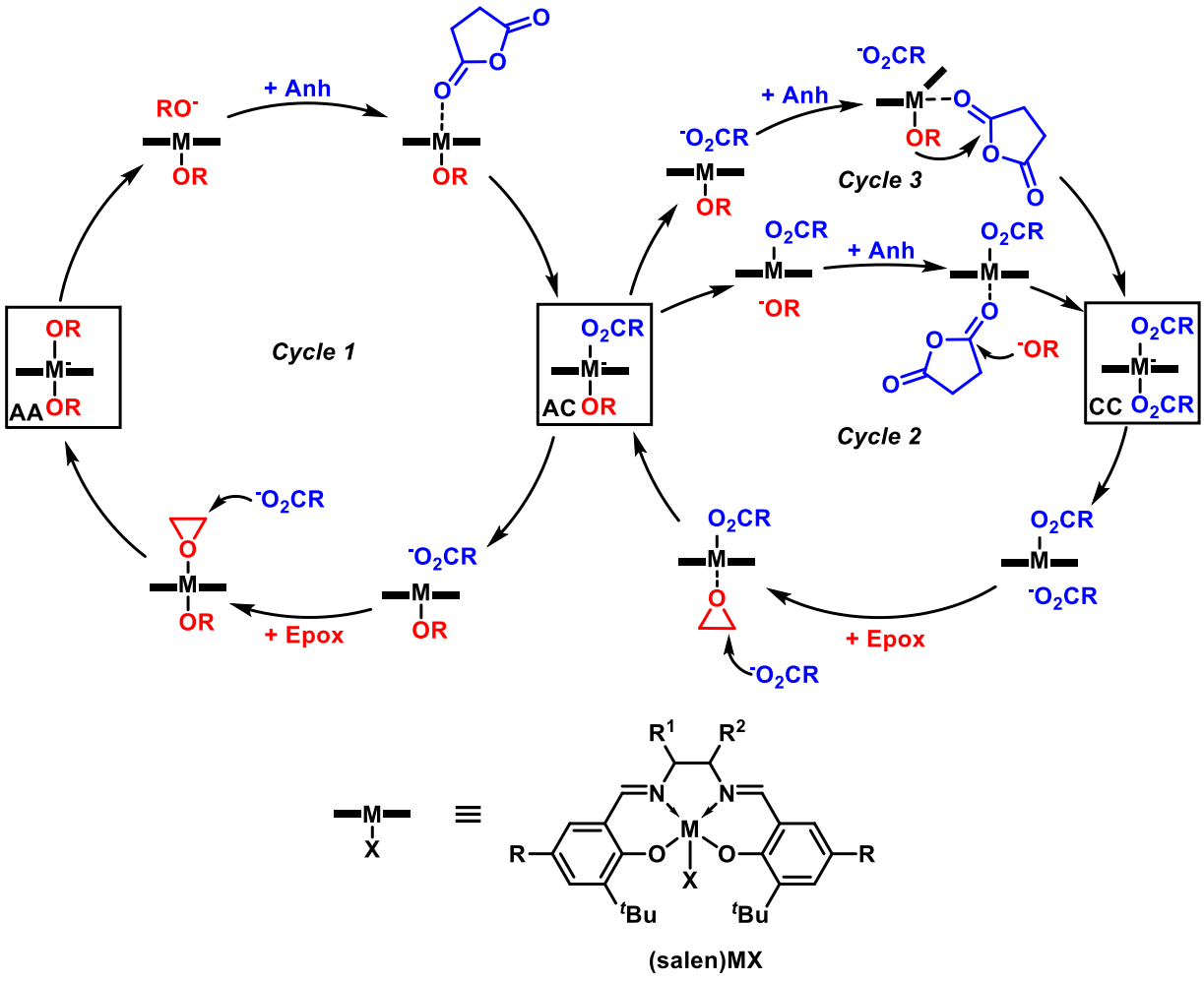

Scheme 11: Possible catalytic cycles of epoxide/anhydride copolymerization catalyzed by (salen)MX complexes M=Cr.[55]

Besides polyether formation another side reaction can occur. Both, the alkoxide and the carboxylate can easily be protonated and, hence, be transformed into a dormant species. As a result, the active chain is transferred to another "nucleus", namely H^+, and then further to a new catalyst molecule. Basically, every protic compound can be employed as chain transfer agents (CTA). However, if CTAs are employed, water or alcohols are usually used. Scheme 12 depicts the chain shuttling process.

Chain Transfer (generated by addition of ROH)

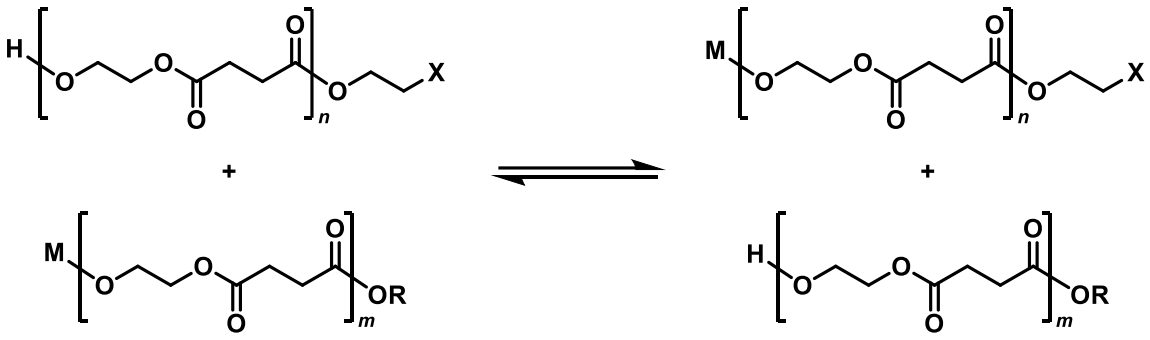

Scheme 12: Chain shuttling in ring–opening polymerizations of cyclic anhydrides and epoxides. Redrawn from.[56]

The concentration of CTAs in the reaction solution has a direct impact on the resulting molecular weight of the synthesized polymer. As shown in Scheme 12, the overall amount of monomer is divided by an increasing number of polymer chains. Thus, the overall molecular weight is decreasing. Another effect of the presence of CTAs is that the resulting molecular weight distribution is significantly narrowed, as the absolute number of polymer chains increases and the number average molecular weight (M_n) increases relatively to the weight average molecular weight (M_w). Hence, CTAs can lead to a better defined and more uniform polymer. At the same time, the polydispersity (*Đ)* of a sample can provide a measure to estimate the purity of the employed reaction conditions. Water as a CTA can influence the reaction rate of polymerization reactions, which will be presented later in this thesis (see chapter 3.2.1).

A third side reaction during the polymerization process is the transesterification reaction. However, the catalytic epoxide/anhydride copolymerization proceeds at much milder conditions than transesterifications and epimerization reactions, which usually appear at elongated reaction times and high conversions.[58] Extensive transesterification leads to a significant increase of the polydispersity of the resulting polymer and, thus, to an additional means to adjust material properties.

1.11 Epoxide/CO_2 Copolymerization

The copolymerization of epoxides and CO_2 underlies the very same principles as the ROCOP of anhydrides and epoxides catalyzed by salen complexes. The key to a functioning catalytic cycle is the carbonyl moiety of CO_2, similar to the anhydride in the former case (Scheme 13).[55, 57, 59] However, due to the nature of the reaction system, a smaller number of coordination modes is possible. Either the epoxide is coordinated to the metal center, which is then opened and inserted into the growing chain, or the CO_2 is coordinated and inserted. The initiation of the polymerization proceeds *via* a displacement of the coordinated anion X at the metal center by an epoxide. The displaced anion subsequently attacks the preferred carbon of the respective epoxide. The preferential carbon of the epoxide is strongly determined by the substitution pattern of the epoxide and the ligand sphere of the catalyst.

After the epoxide is opened, the first CO_2 molecule can insert into the alkoxide-metal bond. The chain growth is continued by a displacement of the carboxylate by a new epoxide. The epoxide is then attacked by the carboxylate and the chain grows by forming the carbonate segment. A typical side reaction is an attack of the carboxylate chain end at the γ-carbon, which leads to the formation of a cyclic carbonate and which shortens the already formed polymer chain. Compared to the intended polymerization, the formation of cyclic carbonate by ROCOP of epoxides is less exothermic, thus, the cyclic carbonate represents an entropic–favoured product. Another side reaction is the so called, backbiting of the terminal alkoxide in the absence of CO_2. The alkoxide backbiting reaction has a lower activation energy barrier than the carboxylate backbiting. Therefore, the alkoxide backbiting is more dominant compared to the carboxylate backbiting reaction if the metal–alkoxide bond is weak.[59] However, using the current state of the art polymerization catalysts backbiting, and thus, cyclic by–product formation, is minimized as the energy barriers of the side reactions are significantly higher compared to the alternating incorporation of epoxides and CO_2 into the growing chain.

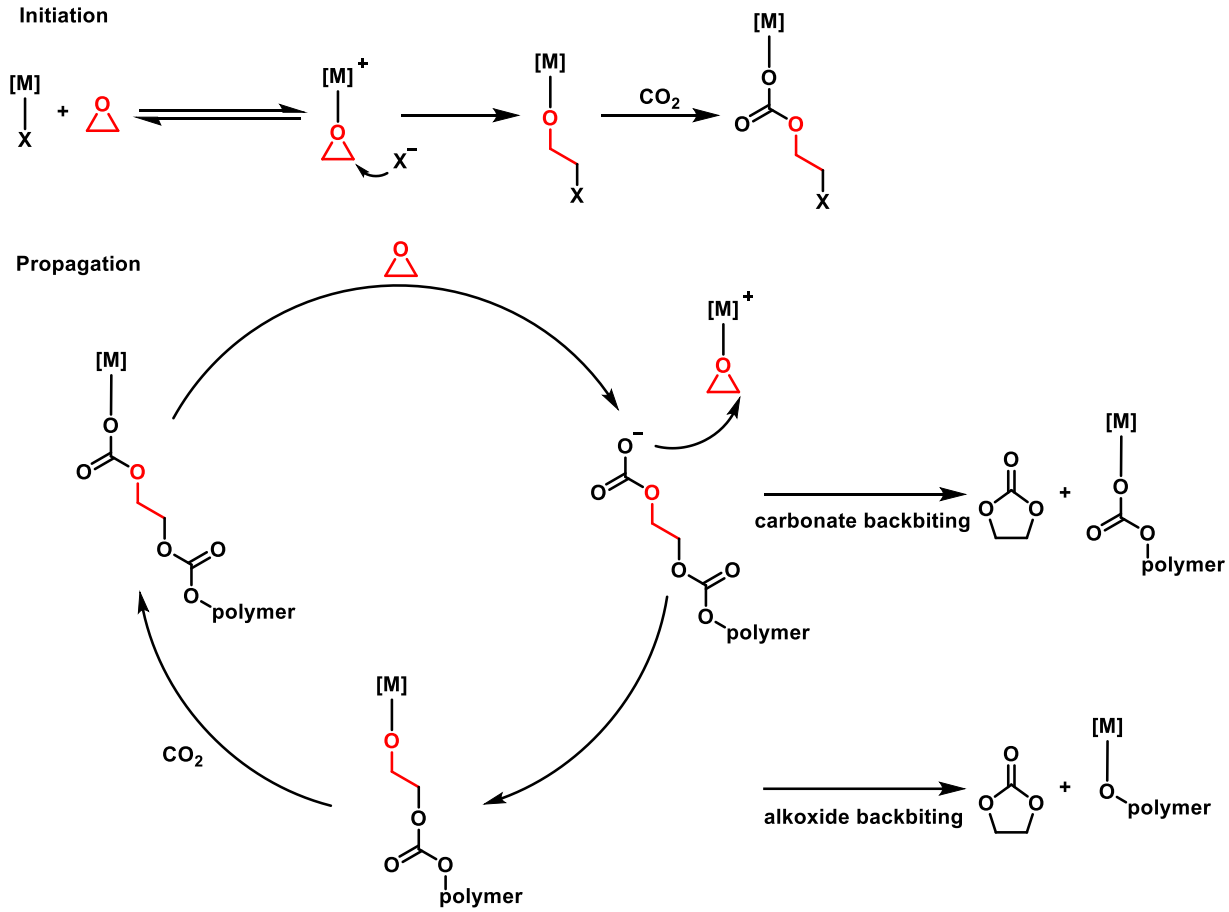

Scheme 13: Schematic mechanism of CO_2/epoxide copolymerization including side reactions according to ref.[59]

1.12 Microstructure Control Mechanisms

The polymerization reactions to polyesters and polycarbonates discussed above are homogeneously catalyzed. Homogeneous catalysis gives the unique opportunity to tune the ligand geometry and hence influence the binding of the respective substrate and the energy of the reaction transition states. Just as in many other catalytic processes the ligand has a major role in the reaction process and the outcome, as well. Chiral ligands can induce stereoregularity in the polymer. With the introduction of stereoregulartiy, the macroscopic material properties can be strongly influenced by a controlled microstructure. However, not only the ligand sphere has an impact on the enantioenrichment, hence on the microstructure of the polymer but also the interaction of the last incorporated monomer unit(s) with the catalyst. Note that both effects usually occur in combination.

Therefore, applying the concept of classical olefin polymerization, one can divide the control mechanisms in chain-end-control, where the last chain segment determines the subsequent

mode of addition of the next monomer, and in enantiomorphic site control, where the ligand sphere is the microstructure–determining factor.[60, 61]

Considering the chain-end-control mechanism, it becomes clear that the steric demand of the respective monomer unit is crucial because of the fact that the insertion reaction occurs in close proximity to the substituents of the previously incorporated monomer unit. Thus, the steric demand of the growing chain segments has to be sufficiently large to obtain a dominating chain-end-control. At the same time, the ligand sphere of the catalyst must be sufficiently small to not have an influence.

Considering the enantiomorphic-site-control, the ligand design dominates the configuration of the growing polymer chain. The steric bulk of the ligand blocks a certain trajectory to incoming monomers and favors one enantiomer in a racemic monomer mixture for polymerization. These two mentioned mechanisms are not only valid for olefin polymerization, but can also be applied for ring–opening copolymerization. Scheme 14 provides a hypothetic example of the two control mechanisms for the ring–opening copolymerization of 4,7-dimethylhexahydro-4,7-methanoisobenzofuran-1,3-dione with a PO racemate.

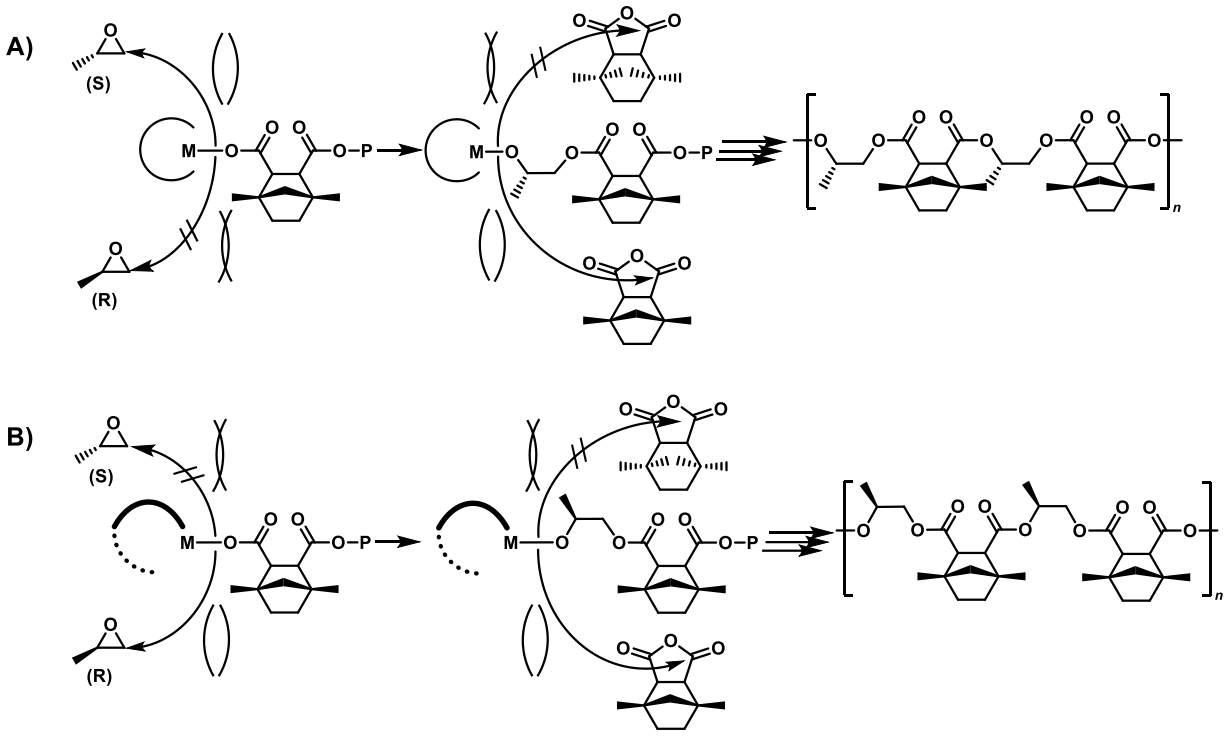

*Scheme 14: Example of chain-end and enantiomorphic-site control. **A**: Small ligand, chain-end control. **B**: Large ligand with stereo-information. Concept adapted from polyolefin synthesis from ref. [62]*

The reaction depicted in Scheme 14A) gives an example for a polymerization with of a small influence of the ligand sphere on the catalysis. The steric bulk of the already incorporated anhydride is comparatively large. Additionally, the copolymerization is carried out with a racemic

mixture of PO. If the influence of the ligand is small, the last incorporated anhydride determines which PO enantiomer is added next with a minimum energy barrier. Thus, the probability of the incorporation of (*S*)-PO is higher compared to (*R*)-PO. The ring–opening of the anhydride can theoretically occur at either of the two carbonyls. Yet, due to the steric hindrance by methyl substituents of the former anhydride, one orientation is preferred. This would lead to an overall alternation of the steric demand in the polymer backbone. The exact fashion of this process is determined by the very first monomer incorporated in the active chain. Thus, the incorporation of new monomers underlies a chain-end-control.

The example Scheme 14B implies a catalyst with a chiral ligand with an unsymmetric steric distribution. In contrast to the previous example, the steric bulk of the ligand dominates the steric interactions and leads to a resolution of the PO enantiomers. Instead of (*S*)-PO, (*R*)-PO is preferentially incorporated. Thus, the ligand design of the catalyst facilitates the “choice” of the higher energy state by increasing the energy barrier for the pathway of (*S*)-PO incorporation. Overall, the two hypothetic materials can be expected to show different material properties. Among many other examples, *Coates et al.* provided an example of the synthesis of semicrystalline polyols of polypropylene oxide which were produced by a chiral bimetallic catalyst.[63]

1.13 Catalyst Systems in Epoxide/Anhydride ROCOP and Epoxide CO_2 Copolymerization

In the following chapters examples of catalytically active metal complexes of the fields of copolymerization of epoxides, anhydrides and CO_2 will be briefly discussed. Because of the large field of different complexes not every complex can be discussed in detail. Thus, the discussion will be focused on the most important ligand classes and “milestones” of catalyst development. First, an overview of the ligand classes leading to monometallic catalysts will be given. Second, the most relevant examples for bimetallic catalysts will be discussed. Salicyl aldimine and related complexes will be mentioned separately in the third part of this section, focusing on their catalytic reactions regarding the polyester synthesis, the polycarbonate synthesis and the combined syntheses to polyester carbonates. The mentioned examples are chosen to be the most relevant to this work. The field was reviewed over the last years several times in excellent reviews.[55, 56, 64-68]

1.14 Monometallic Catalyst Systems

Various well-defined catalyst systems are known in the literature to promote the ROCOP of anhydrides with epoxides.[55] Most catalyst systems have in common that not only a metal complex is required but also a cocatalyst is necessary to act as an initiator. Depending on the respective transition metal complex, ammonium or phosphonium salts, Lewis bases or inorganic salts might be used. Among all examples 4-(dimethylamino)pyridine (DMAP) and bis(triphenylphosphine)iminium halides (PPNX, X = Cl, Br, NO_3,…) were predominantly used. Recently, a number of investigations on metal-free catalyst systems in the ROCOP of anhydrides and epoxides with promising results were published where *Lewis* acid-base interactions, conceptionally similar to metal–based catalysis, facilitate the ring–opening. However, these investigations exceed the scope of this thesis and will not be discussed further.[69-78]

Among the main group and transition metal complexes, predominantly four ligand classes were investigated, namely porphyrin, *β*-diiminate, salen and Robson-type ligands of which some were employed to synthesize hetero- or homo-bimetallic complexes.

Some of the first catalysts utilized prophyrin ligands in combination with Al(III), Cr(III), Co(III), Mn(III), and Fe(III) centers.[56, 79-86] Although many metal and ligand variations and modifications were investigated, Cr(III) tetraphenyl porphyrinato complexes showed the best performance (Fig. 2).[55]

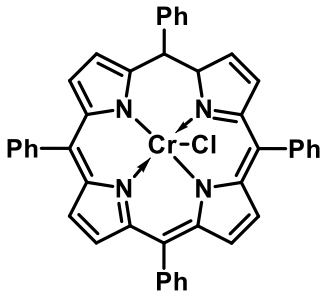

I

Fig. 2: Chromium tetraphenyl porphyrinato chloride catalyst for the anhydride/epoxide ROCOP.

The successfully employed porphyrin complexes were later outperformed as *Coates and coworkers* introduced *β*-diketiminato (BDI) complexes to this copolymerization in 2007.[55] This type of complex was previously used for the copolymerization of CO_2 and epoxides.[57, 87] As *Coates* and coworkers applied the Zn(BDI) acetate complex in the ROCOP of diglycolic anhydride with various epoxides, such as vinyl cyclohexyl oxide, propylene oxide or *cis*-butene oxide, they could prove the complex to be highly active, affording polymers with high molecular

weights with up to 55 kg/mol.[88] Electronic variations in the ligand backbone strongly affect the complex stability and the catalytic performance.[56, 88, 89] Electron deficient CN substituted backbones were observed to be the most efficient.

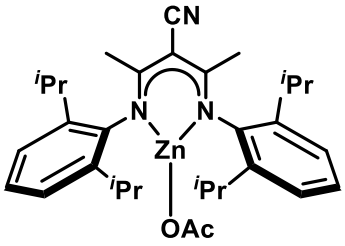

II

Fig. 3: Zn(BDI)OAc catalyst introduced by Coates et al. in the ROCOP of epoxides and anhydrides.

The third and one of the most prominent ligand classes are salicyl aldimine based ligands. The ligand class can be further divided into two subgroups. The first subgroup is characterized by an aromatic ligand backbone (salphen ligands) and the second subgroup is characterized by an aliphatic backbone (salen ligands) bridging two side arms. This ligand class gained much attention as it is compatible with a variety of metal ions on the basis of Cr, Al, Co, Mn, Zn and Fe.[68] Hereby, the respective metal can be coordinated to the ligand in the oxidation states II-IV, depending on the metal. Additionally, the complexes are usually not very air or moisture sensitive and comparatively easy to synthesize. Salen catalysts proved to be active in kinetic resolution of epoxides,[90] in the copolymerization of CO_2 with a variety of epoxides and as well in the ROCOP of epoxides and anhydrides.[55, 56] In 2011 the groups of *Coates, Duchateau* and *Thomas* reported the first polymerization reactions with chromium salen complexes.[82, 83, 91] As mentioned above, an additional initiator had to be employed in all studies. For instance, **IIIa**/DMAP (Fig. 4) successfully copolymerized cyclohexene oxide with succinic anhydride (SA, cyclopropane-1,2-dicarboxylic anhydride (CPrA) or phthalic anhydride (PA, which yielded polymers with up to 1800 g/mol).[55, 82, 92, 93] However, the obtained polymers exhibited a significant amount of ether linkages. Aluminum analogues of that complexes (**IIIb**) were reported, as well.[55]

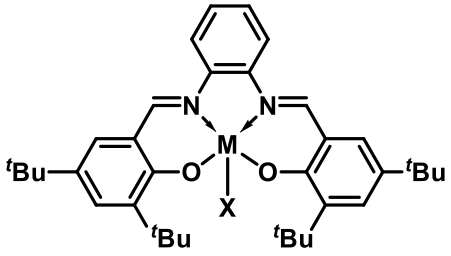

IIIa: M = Cr, X = Cl
IIIb: M = Al, X = Cl

*Fig. 4: Chromium and aluminum salphen complexes **IIIa** and **IIIb**.*

At this point the investigated chromium salphen complex (**IIIa**) was less efficient compared to the chromium tetraphenylporphyrinato chloride complex (**I**) (Fig. 2). In the same year *Coates* and his group showed chromium (**IV**) and cobalt salen (**V**) complexes to be active in the copolymerization of maleic anhydride and propylene oxide.[83] As no cocatalyst was employed in these studies, the reactions proceeded relatively slow with a TOF of 6 h^{-1} and 13 h^{-1} for **IV** and **V**, respectively. *Thomas* and his group showed additionally an aluminium salen complex (**VI**) to be active in this type of copolymerization, as well.[82] He successfully polymerized camphoric anhydride with limonene oxide in the presence of PPNCl as cocatalyst to obtain a polymer with 27 kg/mol after a reaction time of 45 h.[82, 83, 94]

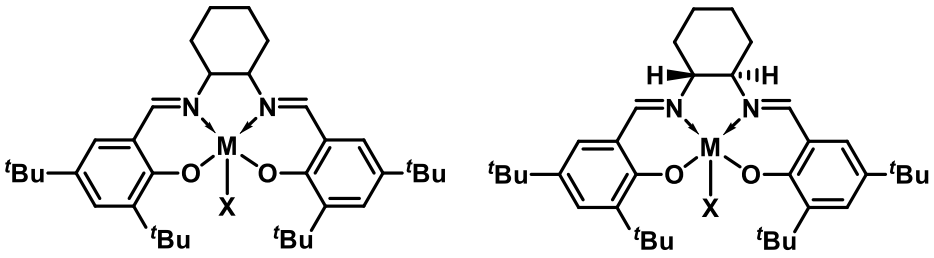

IV: M = Cr, X = Cl
V: M = Co, X = O_2CPh^{F5}
rac

VI: M = Al, X = Cl

Fig. 5: Cr, Co and Al salen complexes employed in the copolymerization of epoxides and anhydrides.

Since salen complexes belong to the “privileged” class of complexes and are therefore predominantly used in this field, not only the coordinated metals, anions or cocatalysts were varied.[95] A sophisticated ligand design strategy in the field led to ligand designs with, for instance, the necessary cocatalyst attached directly to the ligand or polar moieties for catalyst recycling strategies.[96] The degree of structural changes strongly varies thereby. *Coates* introduced a minor structural change by replacing a *tert*–butyl group by fluorine (**VII, IX,**) or

chlorine (**VIII**) in *para* position of the ligating alkoxide (Fig. 6). The electron–withdrawing fluorine led to a decreased reaction rate compared to **VI** but in turn strongly suppressed the epimerization side reactions at elongated reaction times in the copolymerization of epoxides and anhydrides. The less electron withdrawing chlorine did not show such a strong effect.[58, 97-99]

Additionally, *para* fluoro substituted analogues of **X** showed an increase of reaction rate in the maleic anhydride/propylene oxide copolymerization compared to the *tert*–butyl substitution pattern. However, **X** was shown to copolymerize phthalic anhydride and propylene oxide more efficiently compared to its *para* chloro substituted analogues.[97, 100]

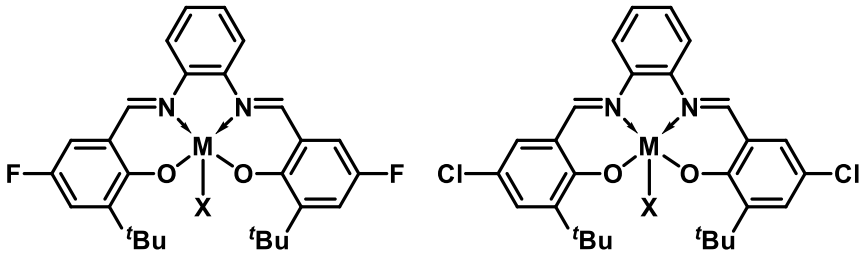

VII: M = Al, X = Cl **VIII: M = Al, X = Cl**

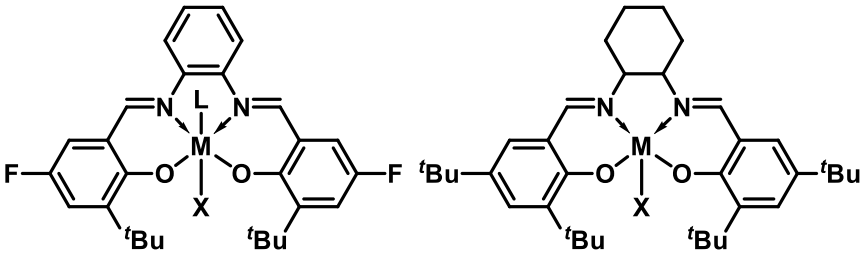

IX: M = Al, X = OTf, L = THF

Xa: M = Co, X = NO_3
Xb: M = Co, X =TFA
rac

Fig. 6: Ligand variations for Al und Co catalysts for epoxide/anhydride copolymerizations.

Other cobalt complexes with other modifications were presented by *Liu* and *Lee* and their respective coworkers (Fig. 7). In their works an additional functionality was tethered as intramolecular initiating cocatalyst to the ligand backbone (**XI**, **XII**, **XIV**).[101, 102] This ligand modification leads to a perfect 1/1 ratio of catalyst and cocatalyst, while, at the same time, increasing the reaction rate for certain polymerization systems. Another efficient design was published by *Lee* and coworkers who linked up to four alkylammonium groups to the ligand to recycle these types of complexes by simple silica gel filtration.[96] All mentioned complexes were very active in CO_2/epoxide and epoxide/anhydride polymerizations.[96, 102]

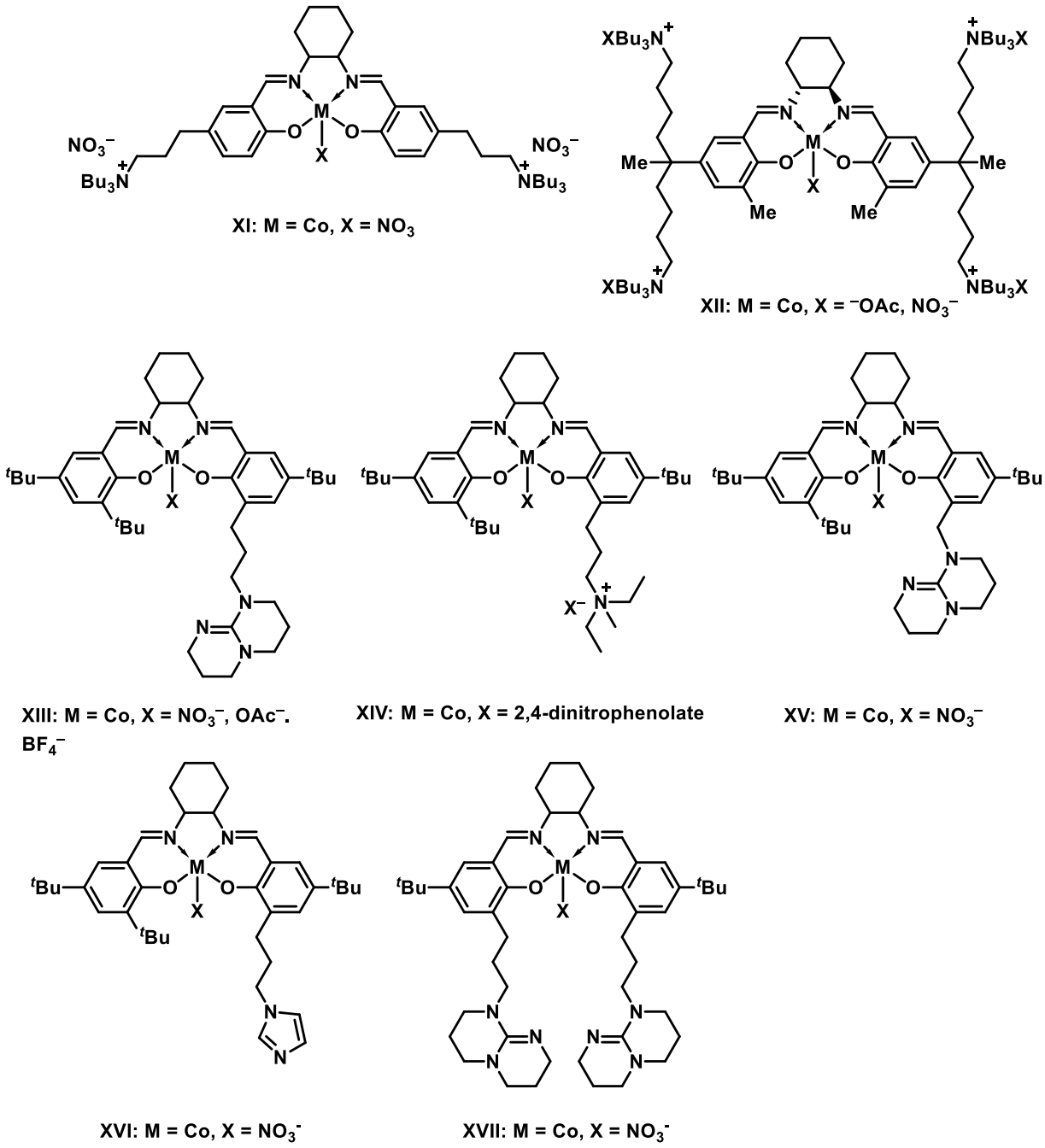

Fig. 7: Salen ligand modifications with cocatalysts tethered to the side arms.

Later a very active system was presented by *Coates*, which comprised an aminocyclopropenium group.[103] This modification leads to a significantly higher stability, productivity and debased the mentioned epimerization or transesterification side reaction (Fig. 8).

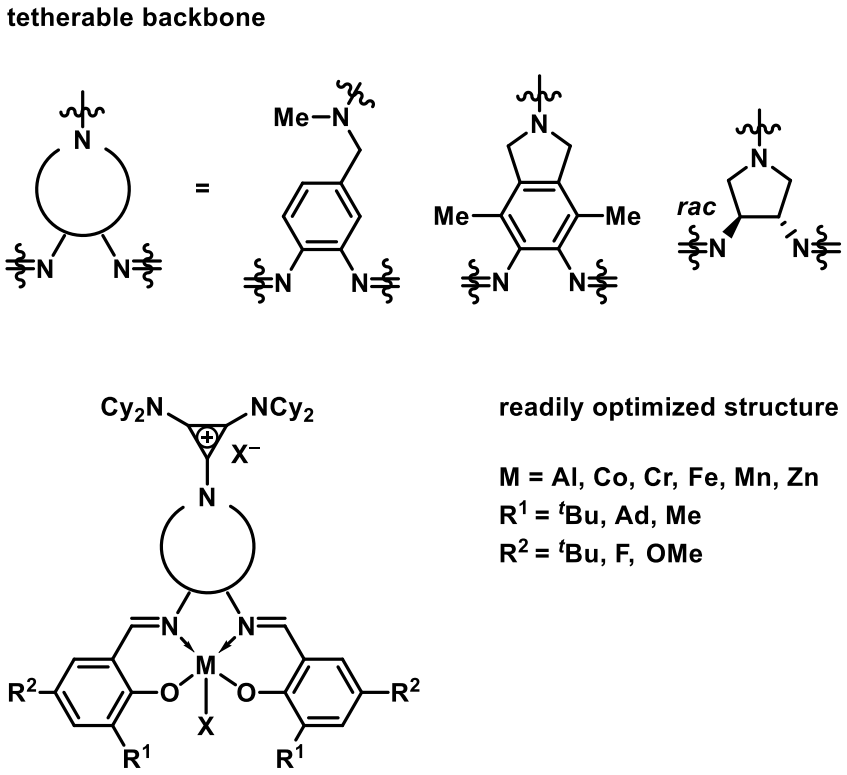

Fig. 8: Structurally modified Co-salen complexes with cocatalysts tethered to the ligand backbone. Figure adapted from ref.[103]

However, besides positively charged alkylammonium groups, also Lewis bases were employed in ligand modification and proved to be among the most active catalysts in polycarbonate synthesis (**XIII**, **XV**-**XVII**).[104] At this point it is noteworthy that the distance of the linked group to the metal center plays a crucial role for the activity of the complexes. Complex **XVI** was observed to have only a poor TOF of 25 h^{-1} compared to almost 11,000 h^{-1} for complex **XIII**-OAc in CO_2/PO copolymerization. The mentioned complexes are summarized in Fig. 7. As it is obvious from the fact that most catalytic systems, presented so far, need a suitable cocatalyst to operate at a reasonable rate, the second functionality was, therefore, implemented directly into the ligand backbone to provide the perfect stoichiometric ratio and a well-chosen distance of catalyst and cocatalyst. Thus, the scope of a doubled functionality was broadened by the introduction of a second metal center.

Although the bifunctional complex systems show promising and great performances, they do have an issue to account for. In particular, the synthesis of the asymmetric analogues can be very challenging with respect to purity and yields.

1.15 Bimetallic Catalyst Systems

In the literature mainly two different ligand classes were employed to synthesize bimetallic catalysts. The previously mentioned salen and salphen ligand systems were expanded to design ligands which can bear two metal centers.[105, 106] The other widely known system comprises the *Robson*– and reduced *Robson*–type ligands.[107] A third, but by far less investigated class of complexes in this field, are corrole complexes, which are oxo-bridged dimers and which are very different in ligand conception.[81] The *Robson*–type ligand was first published in 1970.[107] The original ligand was, just as salen ligands, coupled *via* a *Schiff* base to a macrocycle. However, often the reduced analogue is employed in the literature. Among others the group of *Williams* investigated extensively its activity in catalytic CO_2/epoxide copolymerization and epoxide/anhydride copolymerization. In their investigations the group showed not only that the bimetallic design of this ligand system is crucial for the activity, but they also found that heterobimetallic active sites lead to a significantly higher activity compared to homobimetallic analogues. Moreover, it was shown successfully that in addition to epoxides, CO_2 and anhydrides, also CO_2 and lactones could be copolymerized.[105, 106, 108-117] Fig. 9 gives an overview of the most prominent reduced *Robson*–type complexes that were employed by *Williams et al.* The homobimetallic complex **XX** showed a TOF of 17 h^{-1} while the heterobimetallic complex **XXI** a TOF of 188 h^{-1} in the copolymerization of cyclohexene oxide (CHO) and phthalic anhydride (PA).

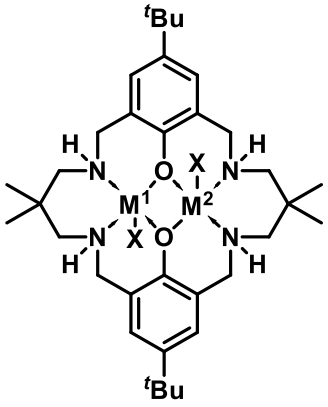

XVIII: M^1 = Mg, M^2 = Mg, X = μ-OAc, TOF = 97 h^{-1}
XIX: M^1 = Zn, M^2 = Zn, X = μ-OAc, TOF = 27 h^{-1}
XX: M^1 = Mg, M^2 = Mg, X = Br, TOF = 9 h^{-1}
XXI: M^1 = Zn, M^2 = Zn, X = Br, TOF = 17 h^{-1}
XXII: M^1 = Mg, M^2 = Zn, X = Br, TOF = 188 h^{-1}
XXIII: M^1 = Zn, M^2 = Zn, X = Ph, TOF = 25 h^{-1}

Fig. 9: Reduced Robson type complexes investigated by Williams and coworkers. Figure adapted from.[55]

As already mentioned, the *Robson* type complexes are conceptionally similar to salen ligands. Therefore, it is not unexpected that similar metal coordination modes were adapted to salen ligands to catalyze the very same reactions. The investigated salen–type complexes were found to be similarly active as the reduced *Robson*–complexes, for instance as **XXIV** and **XXV**,

respectively. The complexes are depicted in Fig. 10. Other similar complexes were applied for CO_2/epoxide copolymerization by Ko.[106, 118-122] Even trimetallic complexes were investigated in ring–opening polymerizations, which will not be further covered, here.[123-125]

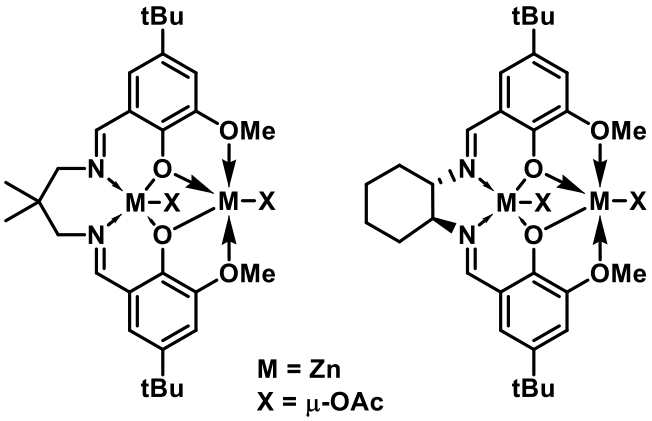

Fig. 10: "Robson like" homobimetallic salen complexes for the copolymerization of CHO and PA.[106]

Another catalyst concept in the context of ring–opening polymerizations is to generate a second coordination site next to the salen pocket. Unlike the complexes shown in Fig. 10 *Mazzeo* and coworkers presented aluminum complexes where the *Schiff* bases were linked with an aliphatic chain.[126] The length of the spacer fragment was varied between *n* = 1 and *n* = 3 to generate different metal distances (Fig. 11).

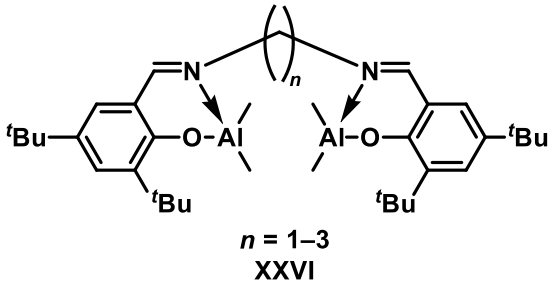

Fig. 11: Bimetallic aluminum complex with varied linker lenghts n.[126]

The complexes are active in the ring–opening polymerization of lactide and lactones, as well as in the ROCOP of epoxides with cyclic anhydrides and lactones. However, the formation of polyether segments could not be fully avoided in the copolymerization of cyclic anhydrides and epoxides, yet.[126-128]

A third strategy to generate bimetallic catalysts utilizes a ligand bridge between the two ligand fragments. This concept was applied to a number homobimetallic salen and salphen complexes (Fig. 12). The cobalt complex **XXVII** uses a dimethylpiperazinyl linker and was successfully

employed in the CO_2/PO copolymerization with TOFs up to 257 h^{-1} with 99 % carbonate selectivity.[129] While **XXVII** does not induce stereo regularity, a stereoinduction could be observed for the chromium complex **XXVIII**[130] in the copolymerization of PA with stilbene oxide by exploiting the axial chirality along the biphenyl bridge. Here, the two salen ligands are linked by a rather flexible biphenyl linker. With this complex, polymers with a M_n up to 14.5 kg/mol at TOFs of 175 h^{-1} were produced. Similar turnover frequencies were found for the aluminium complex **XXIX** with CHO/PA and 3,4-epoxytetrahydrofuran (COPO)/PA systems leading to highly enantioenriched polymers with a M_n around 8 kg/mol exploiting the same principle as **XXVIII**.[131] In the same publication *Lu* presents complex **XXX** linked by a 4,5-dicarboxy-9,9-dimethylxanthen backbone and complex **XXXI** connected also by a biphenyl linker, which also provide, a strong enantioenrichment in the polymer backbone in case of **XXXI**; however, they are significantly less active.[131] A somewhat different approach was taken by *Nozaki* and coworkers. Instead of coupling the two cobalt moieties *via* a biphenyl, a rigid naphthyl moiety was employed as bridging unit (**XXXII**). Obviously, the axial chirality is not present in this example, anymore. However, this connectivity of the rest of the ligand to the naphtyl bridge was altered but did not show acceleration of the polymerization compared to the monometallic analogues. The complex showed a TOF of 254 h^{-1} in the CHO/PA copolymerization.[132] Very recently *Lu* and his coworkers proved complex **XXXIII** to be active in the copolymerization of epoxides and CO_2. As commonly reported in the literature, an ammonium salt (bis(triphenylphosphino)-iminium-2,4-di(nitro) phenolate, PPN(DNP)) was used as a cocatalyst, enabling the catalyst to produce selectively poly(cyclohexane carbonate) and poly(propylene carbonate). Moreover, *Lu* showed the formation of block polycarbonates using 3-buten-1-ol as chain shuttling agent and PO and CHO as epoxides. The block architecture was conveniently generated by a step addition process.[133] The selected examples of the different types of bimetallic salen complexes are depicted in Fig. 12. Furthermore, various other di- and trimetallic complexes were investigated by *Chen* and coworkers.[134-143]

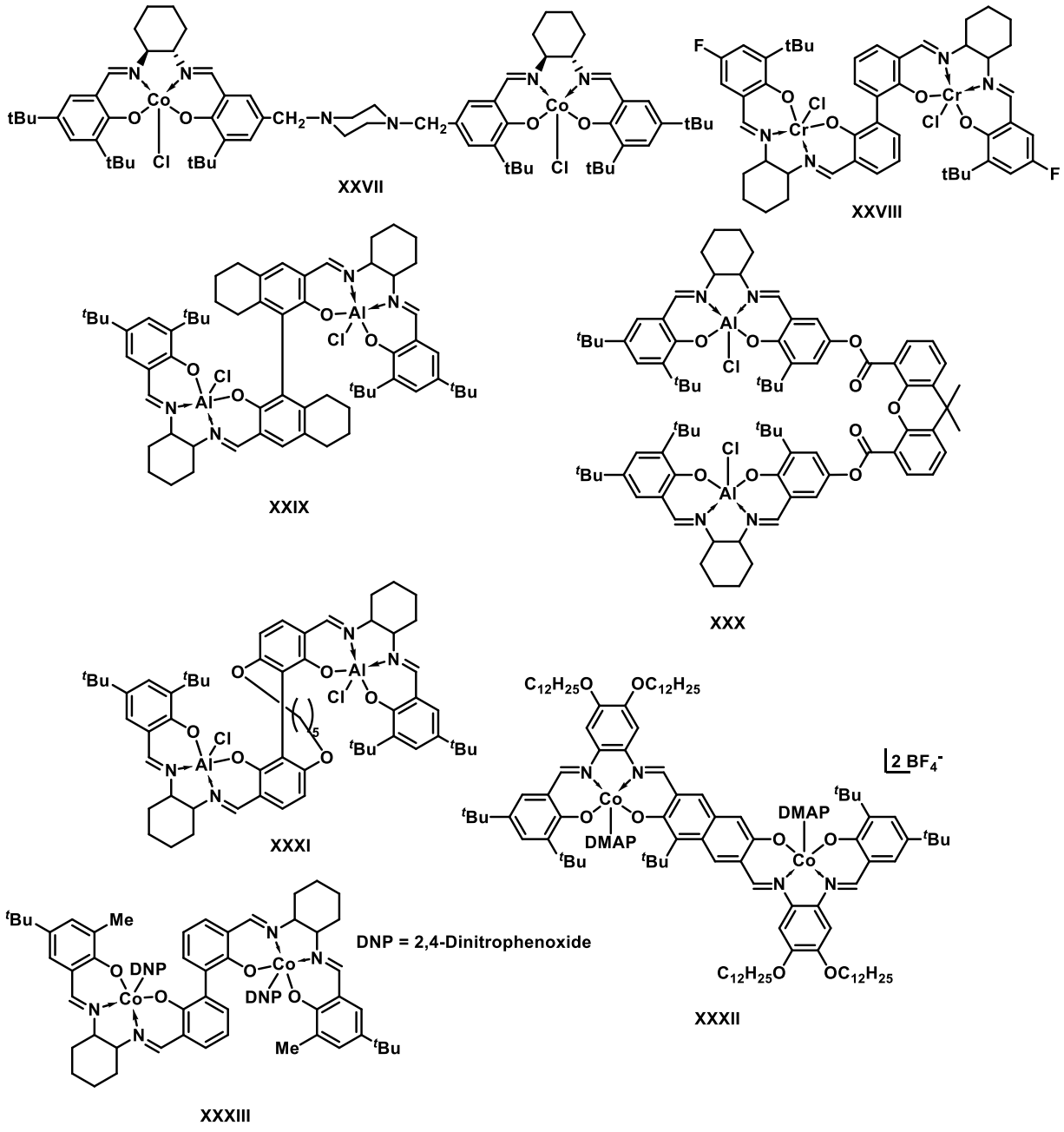

Fig. 12: Sidearm connected bimetallic salen and salphen complexes.[129-133]

1.16 Comparison of Literature Catalysts

An exact comparison of reported catalytic activities is very difficult, because in many cases the turnover frequency is not provided. The turnover frequency (TOF) determines how much substrate is converted on average per hour and mols of catalyst. An additional difficulty of a comparison are the slightly different conditions, catalyst loadings and substrate variations. To give an idea about catalyst performances in the anhydride/epoxide copolymerization, some complexes from chapter 1.13 were chosen and the catalytic data of some benchmark substrates

is compared (Table 1). Thus, substrates were chosen which are closely related to this work (Fig. 13). Additionally, it is noteworthy that the reaction conditions in the presented examples are not identical. This can lead to a major difference in reaction outcome. However, the reaction conditions are usually similar enough to enable a qualitative comparison.

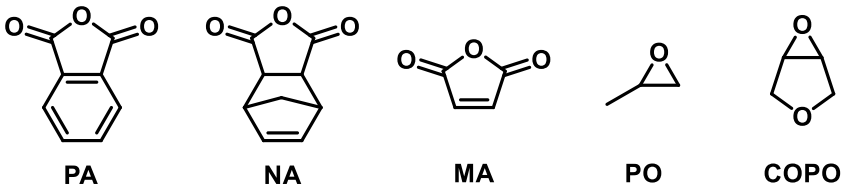

Fig. 13: Considered monomers in this thesis for catalyst comparison.

Table 1: Comparison of complex activity in anhydride/epoxide ring opening copolymerization.

Complex	Cocatalyst	Monomers	Conv. (%)	TOF (h^{-1})	M_n (kg/mol)	*Đ*	Ref.
IIIa	DMAP	PA/CHO	40	400	5.5	1.17	[144]
IV	PPNCl	PA/CHO	90	75[a]	16.1	1.2	[145]
VI	PPNCl	PA/PO	95	2[a]	18.1	1.77	[115]
VII	PPNCl	NA/PO	99	198[a]	9.8	1.16	[58]
IIIb	PPNCl	NA/PO	99	330	8.1	1.39	[58]
Xa	PPN(NO_3)	PA/PO	n.d.	107	5.4	1.25	[100]
XII	/	PA/PO	100	1900	59	1.61	[102]
XXII[b]	/	PA/CHO	94	188	10.9/5	1.04/1.09	[110]
XXIX	PPNCl	PA/COPO	93	155	8.3	1.11	[131]

[a]Calculated from original publication or respective supporting information. [b]Two values for number average molecular weight M_n and polydispersity Đ are given by the original author because of the bimodal distribution in the GPC trace.

The chromium salphen complex **IIIa** (Fig. 4) is one of the complexes with the simpler ligand designs. Still **IIIa** is among the most active catalysts for this type of polymerizations. In the chosen example dimethylaminopyridine (DMAP) was employed as cocatalyst in the copolymerization of PA and CHO. The reaction reached a TOF of 400 h^{-1} with 40 % conversion of PA. As described above a common side reaction in the ROCOP of anhydrides and epoxides is the formation of polyethers. **IIIa** produced only a minor fraction (5 %) of ether segments with a narrow molecular weight distribution (*Đ)* of 1.17 of the polymer. The analogue with an aliphatic linker, complex **IV**, activated with PPNCl (Fig. 5) as cocatalyst achieved a TOF of 75 h^{-1}. No

significant difference in catalytic performance when DMAP was used under identical conditions was observed, except for a slightly higher M_n.[145] The reactivity dropped to approximately a third when the coordinated metal was changed from Cr to Al (**VI**). 95 % conversion with 95 % ester selectivity was reached after a reaction time of two days. Moreover, the prolonged reaction time led to a strong increase of *Đ* with still comparatively high molecular weight. Complex **VII** comprises an Al central atom, as well as, an aromatic backbone. The ligand was modified by *Coates'* group by introducing a fluoro substituent in the *para* position to the phenolate moiety. This led to a superior reduction of side reactions, arising from epimerization, compared to the *tert*–butyl analogue. However, the catalyst converted NA to 99 % within 2.5 h leading to a TOF of 198 h^{-1}. M_n of almost 10 kg/mol with a *Đ* of 1.16 was reached. The *tert*–butyl substituted analogue was faster in conversion and reached a TOF of 330 h^{-1} under identical reaction conditions, but the polydispersity increased drastically after the norbornene anhydride was fully converted (**IIIb**).[58] Another example with a particular difficult to polymerize substrate is the copolymerization of maleic anhydride and epoxides.[97] In addition *Hiranoi* and *Nakano* showed a good activity for the cobalt salen complexes **Xa** (Fig. 6) in the copolymerization of PA and PO.[100] This particular system did not reach the TOF of the previously discussed complexes.

The bimetallic aluminum complex **XXIX** is structurally very interesting (Fig. 12).[131] Although, this complex does not show high activity, it does provide superior stereocontrol. Because of its axially chiral linking unit, the complex selectively incorporates one enantiomer of the epoxide. An enantiomeric excess (*ee)* of 99 % was observed after hydrolysis and derivatization of the resulting diol. Besides stereocontrol, multifunctional catalyst systems provide the unique potential of cocatalyst incorporation. However, the ligand synthesis is very challenging due to these ligand design features. On the other hand, no additional cocatalyst needs to be added to the polymerization reaction. One example of this type is provided by complex **XII** (Fig. 7). It comprises four attached quaternary ammonium moieties. These groups act as very effective initiators which leads to an outstanding TOF of 1900 h^{-1}. Unfortunately, a loss of control over the molecular weight distribution can be attributed to some extend to the high catalytic activity. A comparatively broad *Đ* of 1.61 was achieved in this example. Complex **XXII** (Fig. 9) was chosen as a last comparison to span a bridge to another very successful complex type in the field. **XXII** comprises a heterobimetallic core, ligated by a reduced *Robson*–type ligand. This type of complex also does not necessitate the use of a cocatalyst. With respect to salen and salphen complexes, the catalyst provides a comparable TOF of 188 h^{-1}. Here, the molecular weight distribution is narrow by nature, as the author provided a separate analysis of each mode in the bimodal distribution of the analyzed PA/CHO polyester. Still the overall distribution can probably be considered relatively narrow.

To summarize, a wide range of ligand systems can be found in the field of ring–opening copolymerizations of anhydrides and epoxides. Among the vast amount of ligand variations, generally Cr salen/salphen complexes are among the most active, not taking into account larger ligand systems with tethered cocatalyst substituents.

2 Aim of Work

In this work the synthesis of polyesters *via* ring–opening copolymerization of diacid anhydrides and propylene oxide, catalyzed by base metal salen- and salphen catalysts, should be investigated. Hereby, the effect of variations of ligand substitution patterns, of the complex anions and central metals on the catalyst's activity shall be considered. In addition, monomer mixtures of different anhydrides and propylene oxide should be investigated with respect to preferential incorporation into the polymer backbone. To combine two polymerization systems namely, polyesters and polycarbonates, reactions should be carried out not only under inert atmosphere, but also under CO_2 atmosphere. As last aspect double bond moieties, introduced into the polymer backbone by choosing appropriate anhydride monomers, should be investigated regarding their potential to be substituted in the isolated polymer. These latter studies should be understood as preliminary studies to utilize polymer backbones in molecular scaffolding applications.

3 Results and Discussion

The presented work herein is divided in two parts. The first part presents the catalyst syntheses and the investigated polymerizations. The first part also comprises of investigations on solvent-, ligand-, and substrate effects in the catalysis. The second part presents investigations on post polymerization modification of previously synthesized polymers. The laboratory work for the second part was performed in close collaboration with Christian Markl and is additionally represented in his Master thesis.[175]

3.1 Ligand and Catalyst Syntheses

3.1.1 Ligand Syntheses

Some of the ligands which will be mentioned below were employed to synthesize complexes with different metals. Generally, all synthetic procedures are described in detail in the experimental section of this work. At this point it is important to mention that ligands and complexes discussed below are not drawn separately. The ligands and the complexes are numbered according to the order of their appearance in this work. The respective ligands are named accordingly with the prefix "L". That is, "**L1**"represents the ligand for complex **1**. This coding system shall save time for the reader to distinguish between similar complexes.

One reason for choosing salen type ligands as basis for the complex syntheses is the comparatively uncomplicated ligand synthesis. If the ligand of **1** is considered (Fig. 14) the synthesis starts from 2,4–di(*tert*–butyl) phenol which is formylated *via* paraformaldehyde and $MgCl_2$ to 2,4–di(*tert*–butyl) salicyl aldehyde.[146] If the racemic analogue of **1** is the target compound, the synthesized salicyl aldehyde can be directly reacted with a racemic mixture of 1,2-diamino cyclohexane. Otherwise, the racemic 1,2-diamino cyclohexane is resolved *via* diasteromer resolution as tartrate salt.[147] The resolved 1,2-diamino cyclohexane can be subjected to the imine formation with the previously synthesized salicyl aldehyde to give the enantiomerically pure ligand of **1**. With an even more practical procedure the backbone can be altered to be fully aromatic. In that case 1,2-phenylene diamine can be directly reacted with 2,4–di(*tert*–butyl) salicyl aldehyde to give the respective ligand of **2**.[148] Analogue imine formations can be found in Scheme 16 (page 38) and Scheme 17 (page 39). For the ligand synthesis of **3** the synthetic procedure of the salicyl aldehyde is altered by an acid catalyzed alkylation reaction

of *p*–fluorophenol with *t*BuOH. The synthesized 2–*tert*–butyl–4–fluoro phenol is then further formylated with paraformaldehyde. The formation of the ligand of **3** proceeds in the same fashion as for the other two already mentioned procedures. Thus, the synthesis of simple salen and salphen ligands is a straightforward reaction sequence which is moreover not very sensitive to scaling effects throughout all steps.

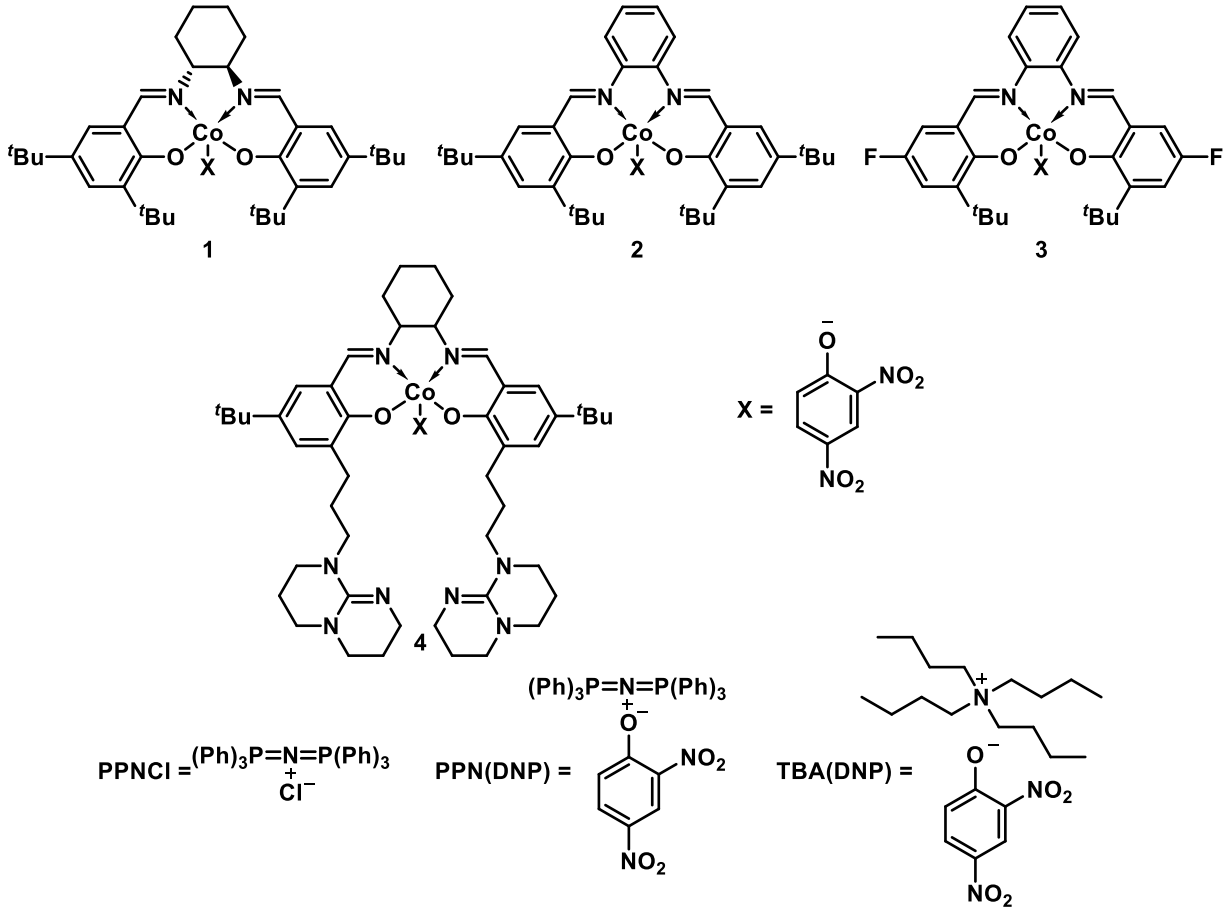

Fig. 14: Catalysts and cocatalysts covered in this work.

As already mentioned in the introductory section, the complexes in this ligand class usually need the addition of an activating cocatalyst. Hence, ligand modifications with a tethered cocatalyst might be highly interesting in the ROCOP of anhydrides and epoxides as such ligand architecture proved itself already effective in catalyzing the copolymerization of CO_2 and epoxides and in the ROCOP of epoxides and anhydrides (Table 1). Therefore, two ligands with tethered cocatalysts were synthesized. Initially the synthetic procedure of *Lu* was followed.[104] However, because of issues with reproducibility a larger part of the synthetic pathway (**S1** to **S3**) was newly developed in a more modern fashion compared to the literature procedure (Scheme 17, page 39). The first reaction step is the methoxy protection of 4–*tert*–butyl phenol. Subsequently, the *ortho* position could be conveniently and selectively mono iodinated to

prepare the precursor for a subsequent *Sonogashira coupling* using $Pd(PPh_3)_2Cl_2$ as catalyst and 1–propynol as coupling partner. The thus synthesized compound **S3** could be obtained in good yield of 83 %. A subsequent hydrogenation step yielded the corresponding alcohol. At this point of the reaction sequence the solvent mixture is crucial. As hydrogenations over Pd/C are commonly performed in ethanol, using ethanol as the sole solvent leads in this case to a large amount of dehydrated byproduct. The hydrogenation of alkynes proceeds over an intermediate alkene. In this case the alkene is an allylic alcohol and is, hence, prone to dehydration reactions (Scheme 15).

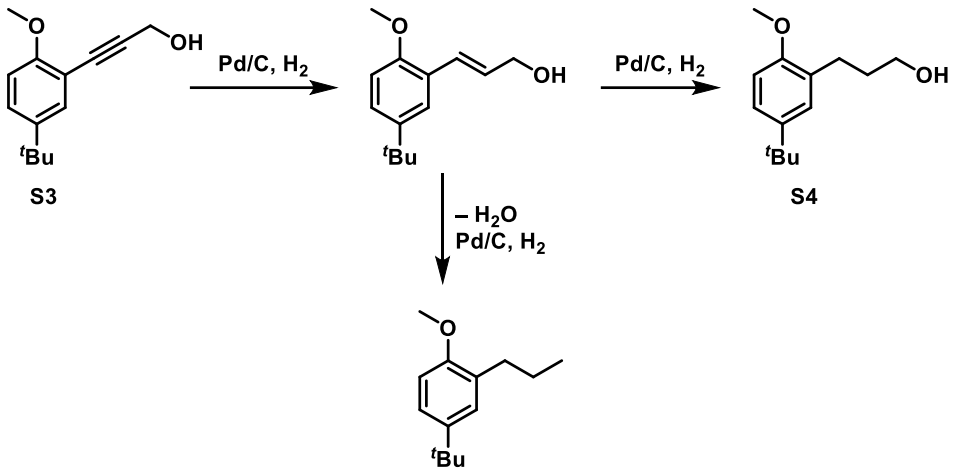

*Scheme 15: Hydrogenation step to **S4**.*

It was found that the side product formation can be limited by strong dilution of ethanol with heptanes, improving the yield up to 96 %. From this point the remaining synthetic route was carried out according to *Lu*.[104] The substitution of the hydroxy group by bromine, the subsequent substitution of the bromine by 1,5,7-triazabicyclo[4.4.0]dec-5-ene (TBD) and the following methoxy deprotection were carried out with good yields. Unfortunately, the formylation reaction to **S8** proved itself very difficult in terms of product purity, yield and purification. Several chromatographic purification steps were commonly necessary to purify the crude product. This and the already poor crude product yield affected the yield for this step to be at best 52 %. The last step of the reaction sequence was found to be even more difficult. The selective imination to the 1,5,7-triazabicyclo(4.4.0)dec-5-en (TBD) anchored ligand was, unlike described in literature[104], very difficult. The originally targeted compound after the whole synthetic route was complex **5**. According to literature procedures the ligand formation step could simply be carried out by the combination of a 1:1 ratio of the respective 2,4–di(*tert*–butyl) salicyl aldehyde and aldehyde **S8** together with the respective diamine. This could not be reproduced successfully. Consequently, the reaction was divided into two parts (Scheme 16). First, the 1,2–diamino cyclohexane was transformed to the dihydrochloride. The dihydrochloride was subjected to a

monoimination reaction with 2,4–di(*tert*–butyl) salicyl aldehyde. The isolated iminoamine is reacted in the following step with aldehyde **S8** to, eventually, yield the mono-anchored ligand **L5**. Detailed reaction conditions can be found in the experimental section of this work. A brief overview about the reaction sequence is provided in Scheme 16.

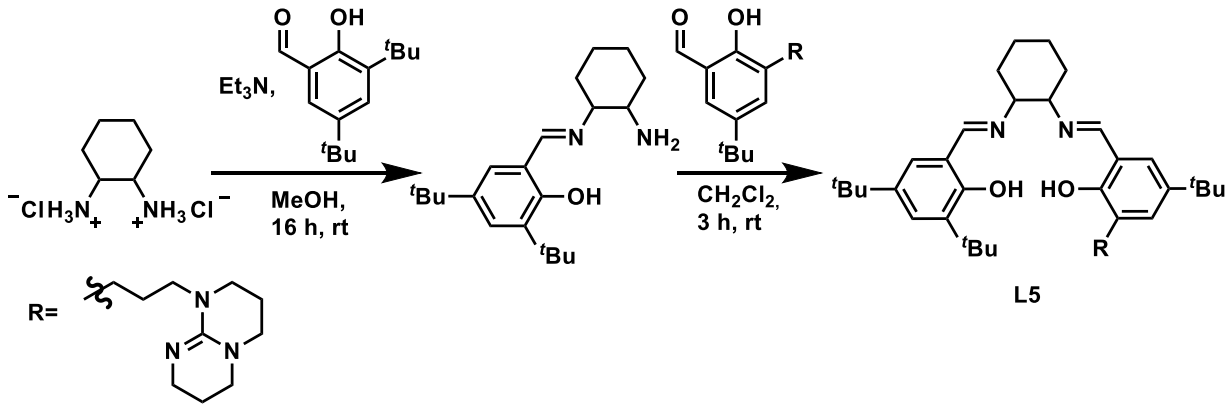

*Scheme 16: Ligand formation step to **L5**.*

The crude ^{1}H–NMR product spectrum showed the desired product, as well as, signals of the symmetric ligand analogue of complex **1** (**L1**). After the attempted purification by column chromatography the product almost decomposed completely. Instead, a broad product spectrum could be found. The two major compounds that could be identified were the **L1** and the ligand of complex **4** (**L4**). Further literature research on this topic showed a possible transimination side reaction in the presence of free amines. Hence, not fully consumed starting material could facilitate the transimination.[149] However, since the ligand synthesis is only one part of this work, the nature of the side reactions was not investigated further.

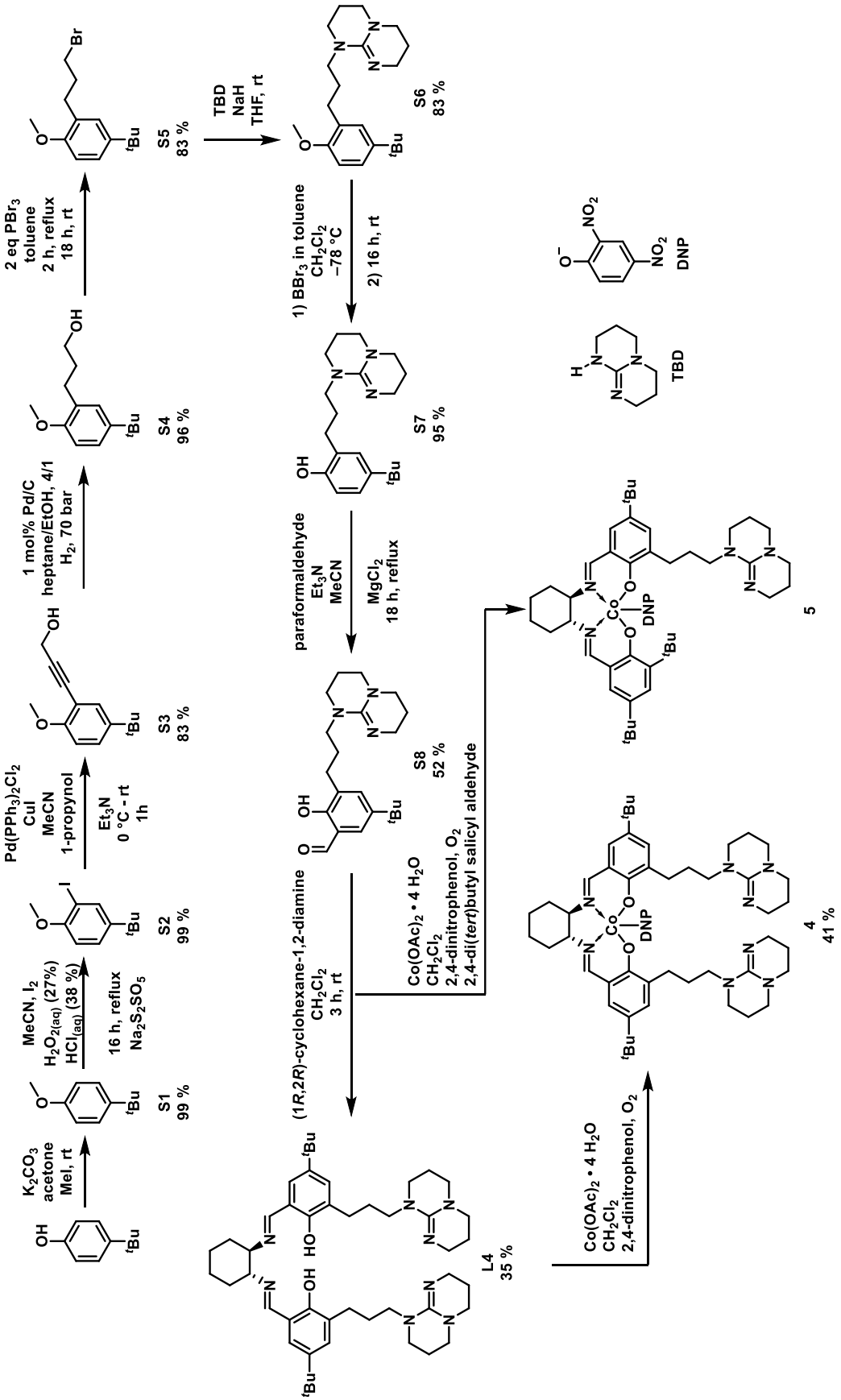

*Scheme 17: Synthetic pathway of **L4** and complex **4**.*

In addition, to the already mentioned ligands and ligand modifications, the *ortho* substituent of the salicyl aldehyde was varied to investigate a potential effect on epoxide/anhydride ROCOP. Thus, two additional ligands were synthesized: one ligand comprising *tert*–butyl–dimethylsilyl substituents and one ligand with a triphenylsilyl substituent. The chosen synthetic route proved itself as very reliable for both silyl substituents and is summarized in Scheme 18.[150, 151] Starting from *p–tert*–butyl phenol a bromination leads to the *ortho* dibrominated phenol. The subsequent silyl ether formation is mediated by imidazole activating the silyl chloride.The last reaction in the synthetic route for *ortho* silylated salen ligand precursors is the *retro Brook rearrangement.*[152] This one-pot-two-step reaction does not only transfer the silyl group but gives, moreover, the possibility to directly introduce aldehyde functionalities.

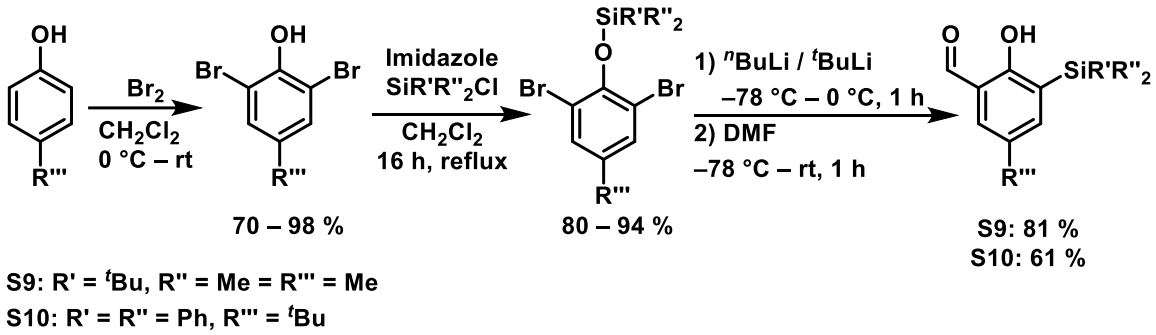

*Scheme 18: Synthetic route for silyl substituted ligand precursors **S9** and **S10**.*[150]

The two, such synthesized, ligand precursors were subsequently reacted to the respective salen and salphen ligands. In this context **S9** was converted to the ligand of **6** (**L6**) and **S10** to the ligand of **7** (**L7**). The corresponding complexes are shown in Fig. 15.

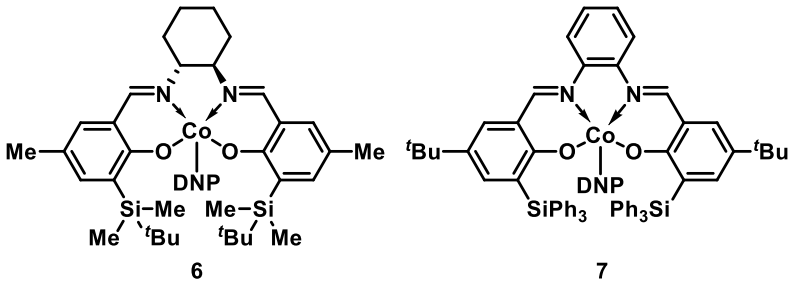

Fig. 15: Ortho silyl substituted salen/salphen complexes.

3.1.2 Complex and Cocatalyst Syntheses

In this work, mainly Al and Co were employed. The metal precursor for Co complex syntheses, regardless of the ligand, was $Co(OAc)_2 \cdot 4\ H_2O$. The cobalt acetate was dehydrated prior to use. Metal precursors for aluminum complexes were either $AlEt_2Cl$ or $AlMe_3$. In the synthetic procedure for aluminum complexes no additional reaction step is necessary, as aluminum is already in the +3 oxidation state. In the cobalt precursor the Co naturally is in its +2 oxidation state directly after the complexation reaction. All employed Co catalysts, however, were oxidized to Co(III) using molecular oxygen as oxidant and the respective counter anion was introduced. Addition of dinitrophenol was sufficient in the syntheses for dinitrophenolate (DNP) complexes in the oxidation step. For other counter anions, such as trifluoroacetate, the chloro complex was synthesized first. The chloride was then exchanged by salt metathesis reactions using Ag(TFA).

The oxidation of Co(II) to Co(III) in the cobalt salen type complexes is critical to the catalytic activity in ROCOP reactions as only Co(III) appears to be catalytically effective in polymerizations. But the +3 oxidation state of cobalt is not only critical to its catalytic activity, but also to the solubility properties. Co(III) salen type complexes are readily soluble in methanol, whereas Co(II) salen type complexes precipitate from methanol. Additionally, a color change from usually brick red to brownish-green indicates oxidation. The exact color tone depends on the employed anion. This convenient situation allows already in the course of the synthetic work to distinguish between the two oxidation states and potentially undesired oxidation. Moreover, ^{1}H–NMR spectroscopy is indicative for the oxidation state of the synthesized complex. As Co(II) is paramagnetic, a strong signal broadening can be observed. The diamagnetic nature of Co(III) does not show this broadening, as long as, the complexes do not show fluctual ligand behavior. Fig. 16 shows a ^{1}H–NMR spectrum of a paramagnetic Co(II) complex. In contrast to that Fig. 17 represents a ^{1}H–NMR spectrum of a diamagnetic Co(III) complex.

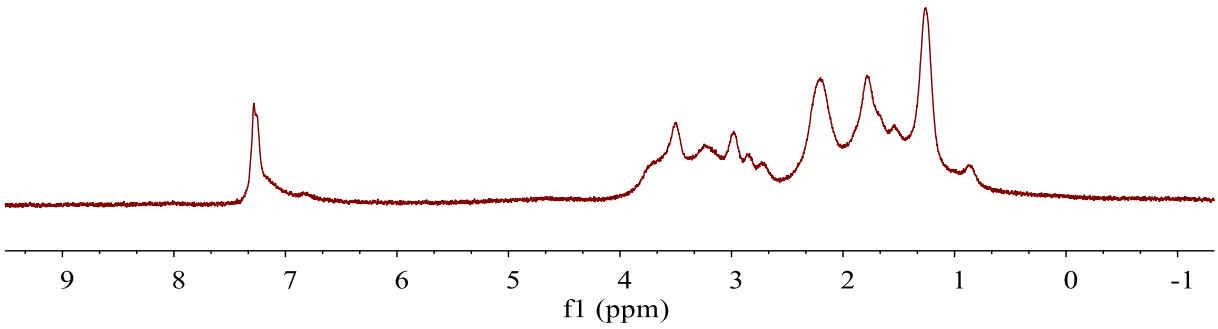

*Fig. 16: ^{1}H–NMR spectrum of a Co(II) complex of ligand **L1** (Co^{2+}–L1), in DMSO-d_6 at 25 °C.*

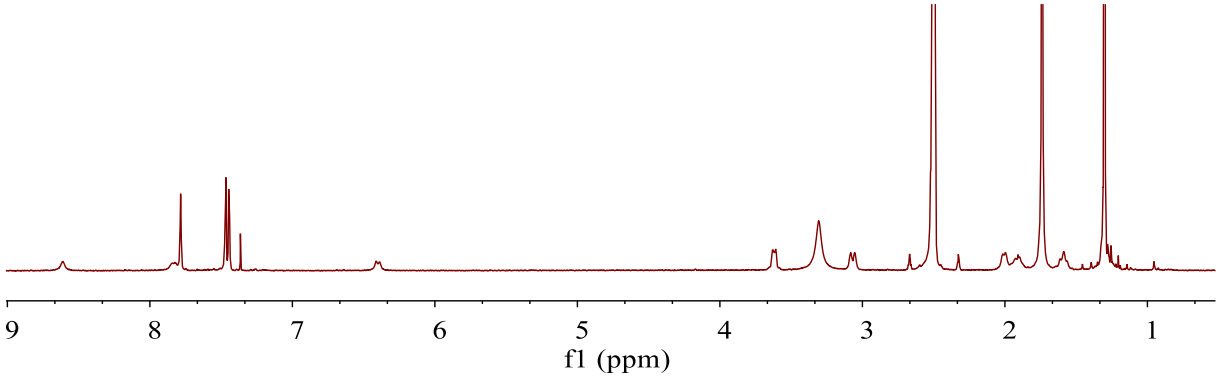

*Fig. 17: ^{1}H–NMR spectrum of **1** (see Fig. 14) in DMSO-d_6 at 25 °C.*

The synthesis of the cocatalysts presented in Fig. 14 could be conveniently carried out in a two-step procedure. First sodium dinitrophenolate was synthesized by a deprotonation of 2,4-dinitrophenol with NaH. The isolated sodium-2,4-dinitrophenolate (NaDNP) can then be reacted with PPNCl or tetrabutylammonium bromide (TBABr) in a salt metathesis to PPN(DNP) or TBA(DNP) while the precipitation of NaCl or NaBr shifts the equilibrium to the product side. PPNCl is commercially available.

3.2 Polymerization Catalysis

In this work three different anhydrides will be discussed in their co- and terpolymerization properties. The following two sections mainly focus on the copolymerization of maleic anhydride and tetrahydrophthalic anhydride with propylene oxide, respectively. These two sections comprise additionally phthalic anhydride chemistry which is closely related to the mainly investigated anhydride in the respective section. Phthalic anhydride itself will be considered in a larger context including kinetic considerations with respect to norbornene anhydride and CO_2 (NA, see Fig. 13).

3.2.1 Maleic Anhydride (MA)

Maleic anhydride is an important and comparatively easy to access potential monomer in the ring opening copolymerization of epoxides and anhydrides. As discussed in the introduction, maleic anhydride can be accessed *via* furfural, which itself, can be derived from sugar. Maleic anhydride does not only have the advantage of bioderivability, but moreover, it has the potential of post–polymerization modification. That is, a basic polymer can be modified by exploiting the reactivity of the double bond incorporated into the polymer backbone. Several studies with different catalysts were already published in this

field. In early investigations double metal cyanide catalysts based on Zn and Co were employed in the PO/MA copolymerization, which yielded only low molecular weight polymers.[153] Other mixed metal cyanide or Zn glutarate complexes were employed in the investigations on PO/MA/CO_2 terpolymerization.[154, 155] Investigations on the activity of salen type complexes on the PO/MA polymerization are scarce.[83, 92, 97] Other epoxides, on the other hand, are better investigated.[55]

To start the investigation, common salen complexes were studied first. Although it was known that cobalt complexes usually show better performance in the epoxide/anhydride related polymerization systems, aluminum complexes were tested, as well. For that three different Al-salen complexes were synthesized Scheme 19. This first experiments should provide a first idea about the general activity of these complexes.

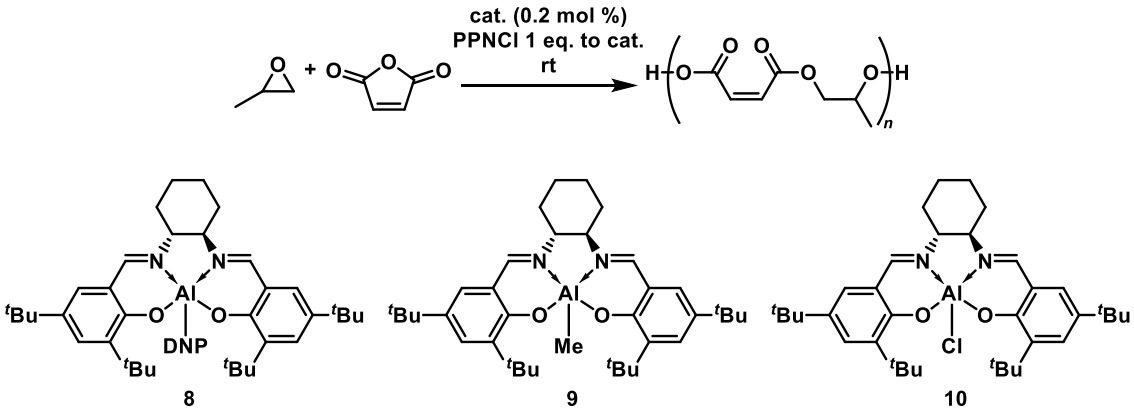

Scheme 19: Al-salen complexes tested in the copolymerization of PO & MA.

All complexes showed very low reactivity at room temperature. Still, some conversion of maleic anhydride could be observed by ^{1}H–NMR spectroscopy. Complex **8** converted 13% of the anhydride after 24 h of reaction time. Less anhydride was converted after 18 h (10 %) by **9**. Considering the somewhat shorter reaction time **8** and **9** can be considered as similarly active. Even after 2 days complex **10** converted only 29 % of the maleic anhydride. Unfortunately, in none of the cases the presumably formed polymer could be isolated by precipitation into MeOH.

As a generally poor reactivity was observed, it was hypothesized that the activation of the maleic anhydride was very poor. It is reported in literature that aluminum salen complexes can also catalyze the copolymerization of CO_2 and epoxides.[156] It was further hypothesized that during the proceeding copolymerization of CO_2 and propylene oxide the catalytically active species might activate the maleic anhydride to some extent. Unfortunately, in a reaction system with maleic anhydride, propylene oxide and CO_2 being present, not even the copolymerization of CO_2 and propylene oxide could be observed.

Additional heating of the reaction to 60 °C under CO_2 atmosphere did not lead to an improved outcome.

As this part of the work was aimed to find catalysts which were operational at mild conditions these complexes were not further investigated. Instead, the chromium salen complex **13** (Fig. 18) was synthesized and tested in the copolymerization together with PPNCl as cocatalyst. Also, in this case, some reactivity could be observed. After 24 h at room temperature about 29 % of the anhydride was converted, while complete conversion after 2 additional days of reaction time was observed. In contrast to the former cases some polymer could be isolated and characterized by NMR spectroscopy and GPC. The product was found to be a mixture of the desired polypropylene maleate, the fumarate isomer and polypropylene glycol. Thus, the chromium complex facilitates not only the polyester formation but also the polyether formation at prolonged reaction times. According to GPC measurements the M_n of the isolated polymer is about 27 kg/mol with a $Đ$ of 2.4. Hence, the complex does not show extraordinary catalytic performance in this reaction and, moreover, facilitates polyether formation leading ill-defined polymer mixtures. At this point the focus was rather shifted to cobalt complexes.

For that, eight different complexes were tested in overall three different reaction setups. That is:

- MA was employed as the sole anhydride in the copolymerization with PO
- PA and MA were employed in a directly mixed fashion
- PA and MA were employed in combination in a sequential order of addition

However, not every complex was tested in every combination. All employed Co complexes in the investigations of PO/MA copolymerization are summarized in Fig. 18. In addition to that, the scope of the employed cocatalysts was expanded from PPNCl to PPN(DNP) and TBA(DNP).

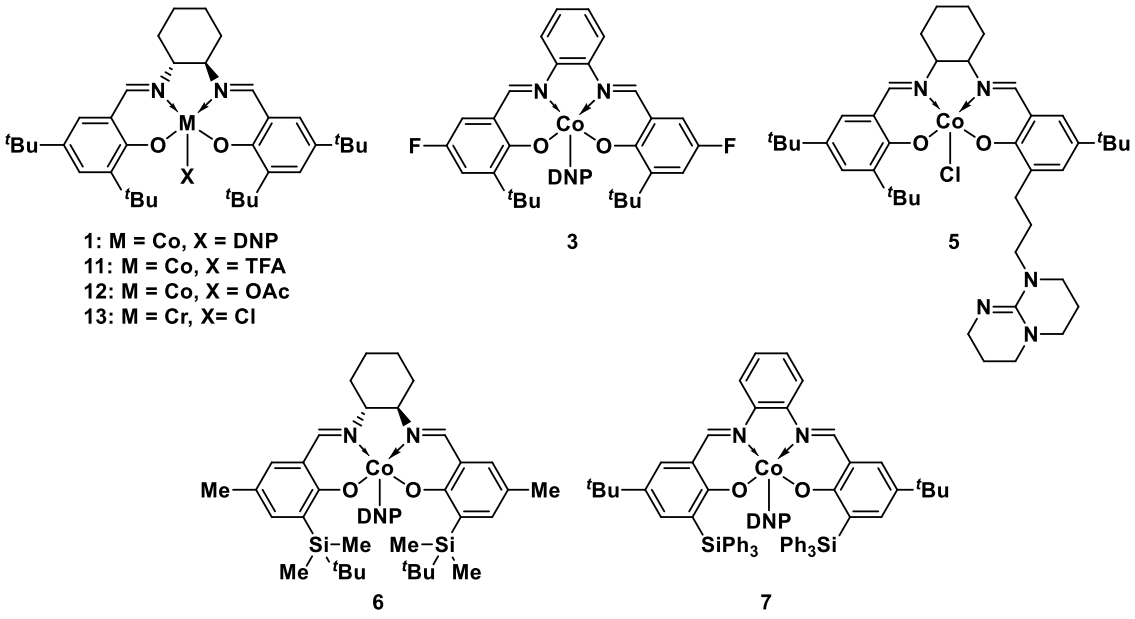

Fig. 18: Cr- & Co-complexes, tested in the copolymerization of PO & MA.

Similar to complex **13**, complex **1** was employed under the same conditions. While the Cr-Cl complex **13** converted 29 % of the maleic anhydride after 24 h, complex **1** converted 55 % of the anhydride after 18 h of reaction time. An ^{1}H–NMR spectroscopy analysis of the crude reaction mixture showed poly(propylene maleate) exclusively. However, after workup by precipitation into a 1 M solution of HCl in MeOH, the isolated polymer had isomerized partly to poly(propylene fumarate) to a degree of 25 %. In this type of polymer isomerization is easily detectible as additional double bond proton signals appear at about 6.88 ppm representing the fumarate. The original maleate protons appear further upfield shifted to 6.26 ppm.[83] Contrary to the polymer obtained from the catalyst system based on complex **13**/PPNCl, the catalyst system **1**/PPNCl yielded a very low molecular weight polymer. In fact, the molecular weight could not be determined by GPC analysis, which is consistent with the difficult isolation.

In 2016 *Coates et al.* showed the importance of electronic variation in the ligand backbone. In this study the *t*Bu group in *para* position was exchanged by fluoride in **L1** which led to a dramatic increase in activity.[97] Thus, the system was utilized in **L3** with an aromatic backbone (**3**). As a first experiment in the study, to elucidate the general reactivity of the catalyst system based on **3**/PPNCl, the reaction temperature of the copolymerization of maleic anhydride and propylene oxide was changed from room temperature to 50 °C. The catalyst loading was maintained the same. After a reaction time of 24 h, no significant conversion could be observed. Complex **5** was tested without the addition of a cocatalyst, because the tethered TBD moiety is believed to act as a cocatalyst. No reaction could be observed. An overview of the described reactions is provided in Table 2.

Table 2: Activity tests of complexes in the copolymerization of PO & MA.

Entry	Cat.	Cocat.	Conv. (%)[a]	t (h)	Temp.	M_n (kg · mol^{-1})[b]	$Đ$[b]
1[c]	**8**	PPNCl	13	24	rt	N/A	N/A
2[c]	**9**	PPNCl	10	18	rt	N/A	N/A
3[c]	**10**	PPNCl	29	48	rt	N/A	N/A
4	**13**	PPNCl	29	72	rt	27	2.4
5[c]	**1**	PPNCl	55	18	rt	N/A	N/A
6[c]	**3**	PPNCl	5	24	50	N/A	N/A
7[c]	**5**	/	/	18	50	N/A	N/A

[cat]/[cocat]/[PO]/[MA] = 1/1/5000/500. Reactions were carried out in neat PO in an Ar filled glovebox. [a]Reaction progress was followed by ^{1}H–NMR spectroscopy. [b]Determined by GPC calibrated with polystyrene standards and triple detection. [c]No polymer could be isolated.

A brown precipitate could be observed during the catalytic reactions in every setup. Although the amount of formed precipitate differed from complex to complex, it was hypothesized that the catalyst is deactivated during the reaction. NMR spectroscopic analysis of the precipitate did neither allow the identification of a distinct product nor to provide further information on the identity of the unknown number of substances. All crystallization attempts of the precipitate failed. It was shown in literature that the α-proton of the maleic anhydride could be acidic enough to protonate DMAP.[73, 157] Obviously, this is not plausible in the discussed cases. Nevertheless, the precipitate formation could only be observed when maleic anhydride is applied. Hence, it was hypothesized that the ring–opening of the anhydride does not proceed under these conditions as the alkoxide formation readily occurs.[158] To test the ring–opening of the anhydride, water was introduced into the reaction system in a controlled fashion. For this **1**/PPNCl was employed as catalyst system and water was added to the common reaction mixture containing PO and anhydride in 1, 5, and 10 equivalents with respect to the amount of employed catalyst. The progress of the anhydride consumption was monitored by taking small aliquots for ^{1}H–NMR spectroscopic analysis. This set of reactions was carried out with and without toluene as cosolvent for comparison. The effect of cosolvents in the investigated polymerization systems is separately discussed in section 3.2.3.1. Considering the system with added toluene a clear trend could be found. The more water was added to the system the more the reaction accelerated. Considering the fact that without the addition of water the catalyst

system **1**/PPNCl was inactive, already one equivalent of water appears to be sufficient to prevent catalyst deactivation. Still, the conversion after 20 h of reaction time did not exceed 10 %. Five equivalents of added water increased the conversion to 30 % after 20 h. When 10 equivalents of water with respect to the amount of catalyst were added to the system, 57 % of the initially employed maleic anhydride were converted (see Table 3, entry 1–3). The Fig. 19a shows the reaction progress. Fig. 19b represents the molecular weight distribution plot.

As expected, the molecular weight distribution shifts to lower molecular weights. Two domains can be found in this plot. The first domain (black box) shows a gaussian distribution as polymerization statistics would predict. The second domain probably can be attributed to high molecular weight aggregates which could also be observed in the light scattering detectors. The determined molecular weights provide additional insight into the polymerization. Although the earlier mentioned precipitate could not be characterized, the obtained M_n of about 103 kg/mol for the setup with 1 equivalent of water points towards a strong but incomplete deactivation of the catalyst. This deactivation shifts the potential molecular weight to higher values. Even if the molecular weight is highly overestimated (which might be the case) this presents the deactivation of the catalyst by the substrate more plausible than just a low reactivity. In fact, in this polymerization system a comparatively low reactivity of MA towards polymerization and a catalyst deactivation might be both present. When 5 equivalents of water are present in the system the catalyst does not seem to be deactivated as easily but shows a low reactivity at the same time. Here, the molecular weight drops to M_n 6.6 kg/mol with 30 % conversion. With 10 equivalents the M_n, determined by the GPC software, reaches 24.8 kg/mol. Comparing the average numbers calculated by the GPC software with the actual distribution plot inconsistencies become obvious. At this point it is important to note that the *Đ* are very high in all cases: 9.43 for the setup with 1 equivalent of water, 63.9 for 5 equivalents and 6.8 for 10 equivalents of water, respectively. Because of this seemingly unrealistic averaged data, stated above, the distribution plot and not the averaged data is provided in this case, which show consistent decrease of molecular weight with increased amounts of water present. Even if the numbers were not correct, the derived data still points towards a combined effect of catalyst deactivation, low reactivity and, since water is employed, chain shuttling, to some extent.

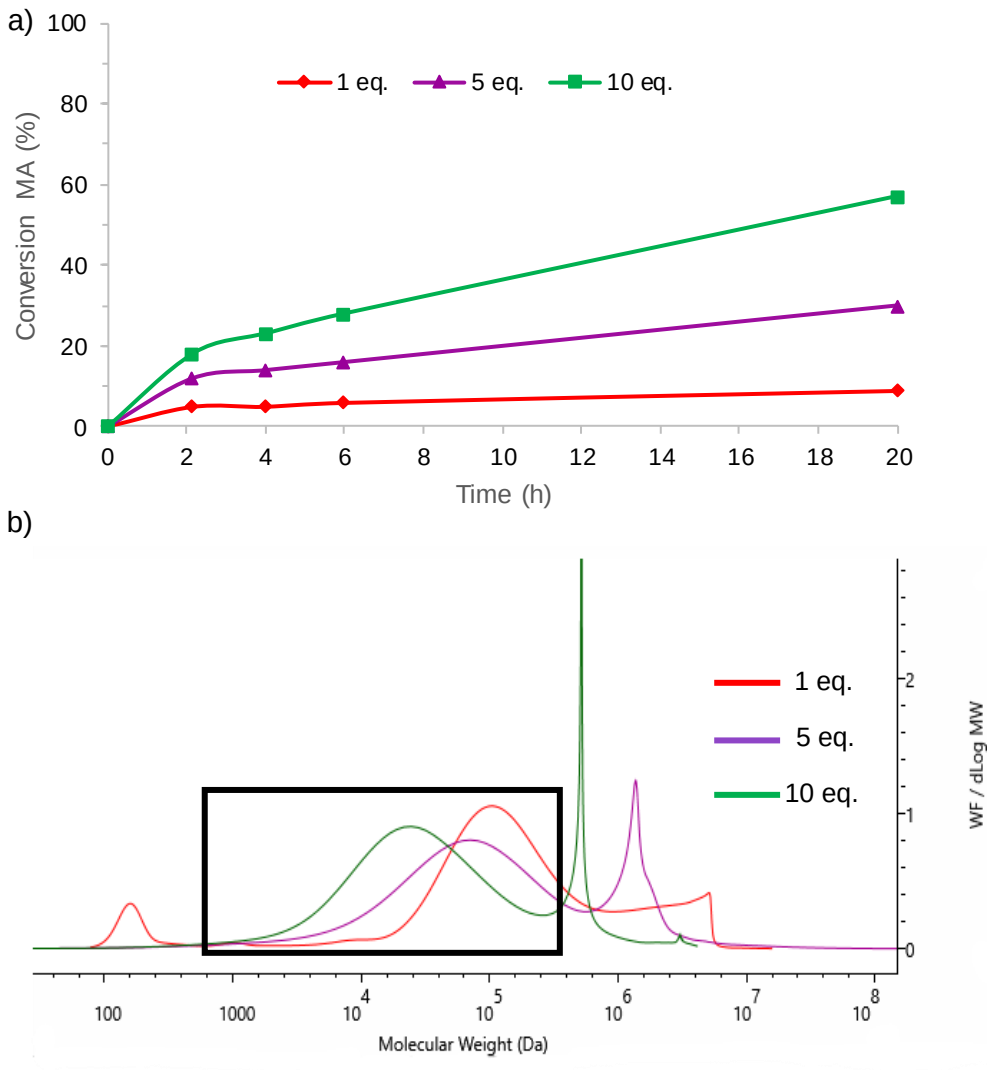

Fig. 19: a) Reaction progress of PO/MA polymerization catalyzed by 1/PPNCl in the presence of 1, 5 and 10 equivalents of H_2O. The connecting line between the data point is a guide to the eye. b) Molecular weight distribution plot of the isolated polymers. [cat]/[cocat]/[PO]/[MA]/H_2O = 1/1/5000/500/X, 50 °C with 50 vol% of toluene. Black box: Gaussian distribution domain of molecular weight.

If the same reaction is carried out in the absence of toluene as a co-solvent the increase in conversion over different water contents was non-linear (Fig. 20). While the conversion was comparatively similar with 1 equivalent and 5 equivalents of water, the conversion of MA increased significantly in the presence of 10 equivalents. After 4 h of reaction time, for instance, 1 equivalent of water gave 6 % conversion and 5 equivalents 9 % conversion. With 10 equivalents of water present, 23 % conversion was reached after 4 h. After 20 h 10 %, 17 % and 49 % of MA was converted with 1, 5 and 10 equivalents water present, respectively (Table 3, entries 4–6). The increase in conversion between the setups was not only non-linear in the absence of toluene, but the determined M_n values are noteworthy higher, as well. While no polymer could be isolated with 1 equivalent of water, 5

equivalents led to an M_n of 123 kg/mol and 10 equivalents to 17 kg/mol with *Đ* of 3.0 and 4.3 (Table 3, entries 4–6). Also in this case, at least the setup with 5 equivalents of water, the molecular weight measurement might have overestimated the average molecular weight considering the low conversion (Fig. 20b). However, the 10 equivalent setup leads to an averaged molecular weight which appears to be more plausible with a conversion of 49 % and a broader distribution. Fig. 21 represents an equivalent polymerization setup as described before, but with **11**/PPNCl instead of **1**/PPCl as catalyst. If Fig. 19, Fig. 20 and Fig. 21 are compared, a discrepancy regarding the 5 equivalent setup becomes evident. As the increase in the conversions and water content are similar in the experiments shown in Fig. 19 and Fig. 21, the data points for 5 equivalents in Fig. 20 do not seem to follow the same pattern. Considering the small quantities of employed water, a measurement error cannot be fully excluded here.

Overall, toluene has a positive effect on the polymerization outcome. Not only the obtained molecular weights are higher, but also the conversion of the maleic anhydride proceeds slightly quicker than without toluene present as a co–solvent.

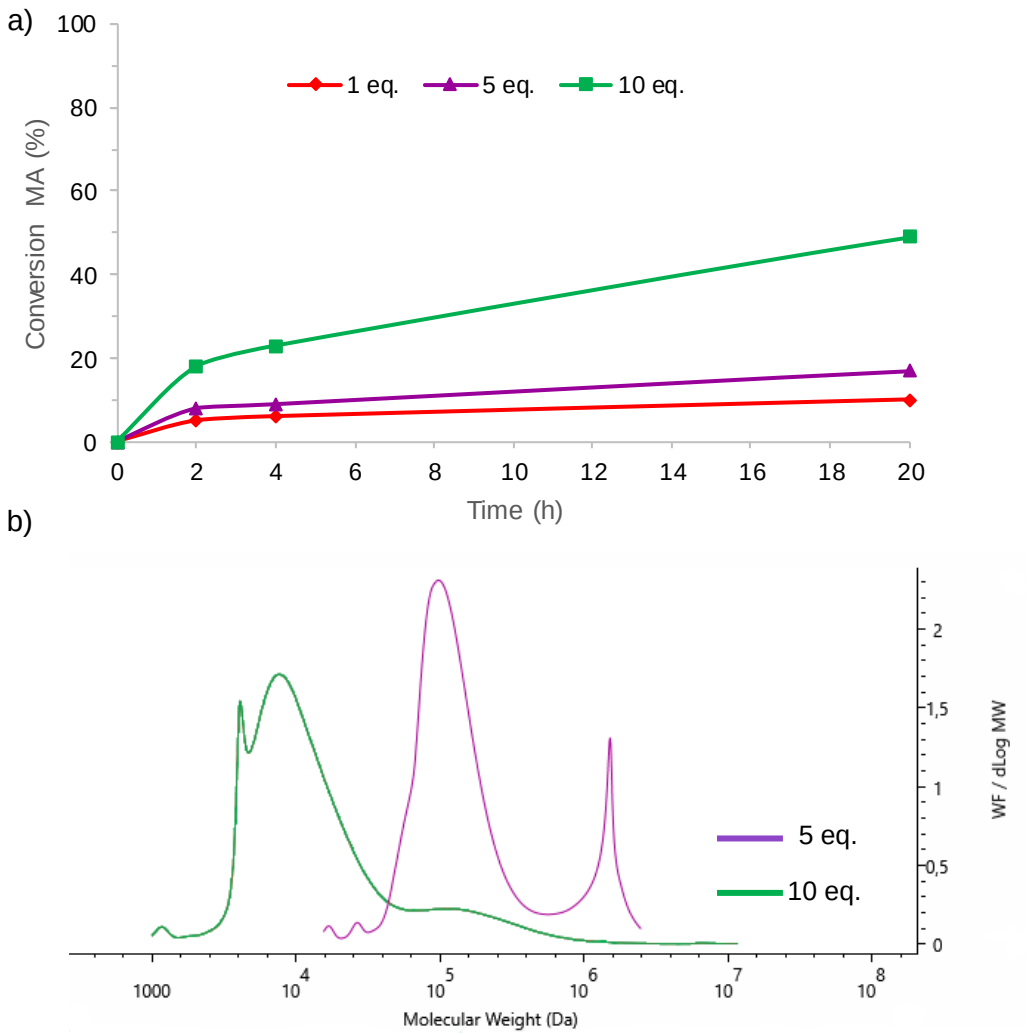

*Fig. 20: a) Reaction progress of PO/MA polymerization catalyzed by **1**/PPNCl in the presence of 1, 5 and 10 equivalents of H_2O. The connecting line between the data point is a guide to the eye. b) Molecular weight distribution plot of the isolated polymers. [cat]/[cocat]/[PO]/[MA]/H_2O = 1/1/5000/500/X, 50 °C.*

The nature of the anion coordinated to the core metal is of major importance to the catalytic activity. Therefore, not only **1** was tested in the above discussed manner, but also the trifluoroacetate analogue **11** of complex **1**. The same trend as with complex **1** is found. With increasing amount of introduced water, the rate of the anhydride consumption increases. In contrast to the former catalysis set, using catalyst **11**, no polymer of the reaction with one equivalent of water present could be isolated. Following the similarity between the two sets of catalytic experiments with **1** and **11** as catalyst, the molecular weight distribution shifts consistently to lower molecular weights with an increased amount of water (5 equiv: M_n = 80.9 kg/mol, 10 equiv M_n = 22.4 kg/mol). Still, the calculated average values of M_n seem to be highly overestimated in both cases, as also here large aggregates in low concentrations cause a strong light scattering response. This in turn leads to an overestimation of the actual M_w leading to *Đ* of 3.62 and 9.73 for 5 equivalents and for 10

equivalents of employed water, respectively. The discussed reactions are summarized in Table 3.

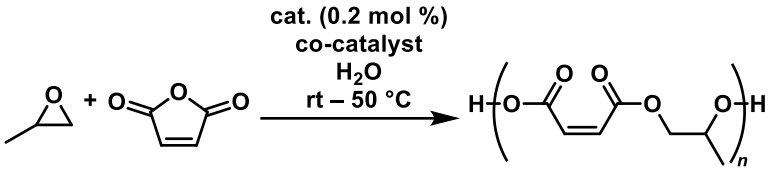

Scheme 20: Copolymerization of maleic anhydride (MA) and propylene oxide (PO) with the addition of H_2O.

Table 3: Summary of polymerization experiments with H_2O addition.

Entry	Cat.	Cocat.	H_2O	Solv.	Conv. (%)[a]	t (h)	M_n (kg · mol^{-1})[b]	$Đ$[b]
1	**1**	PPNCl	1	Tol.	10	20	103	9.43
2	**1**	PPNCl	5	Tol.	30	20	6.6	63.9
3	**1**	PPNCl	10	Tol.	57	20	24.8	6.8
4	**1**	PPNCl	1	/	10	20	N/A	N/A
5	**1**	PPNCl	5	/	17	20	123	3
6	**1**	PPNCl	10	/	49	20	17.0	4.3
7	**11**	PPNCl	1	Tol.	13	20	N/A	N/A
8	**11**	PPNCl	5	Tol.	23	20	80.9	3.62
9	**11**	PPNCl	10	Tol.	36	20	22.4	9.73

[cat]/[PPNCl]/[PO]/[MA]/H_2O = 1/1/5000/500/X, 50 °C. [a]Determined via ^{1}H–NMR analysis. [b]Determined by GPC calibrated with polystyrene standards and triple detection.

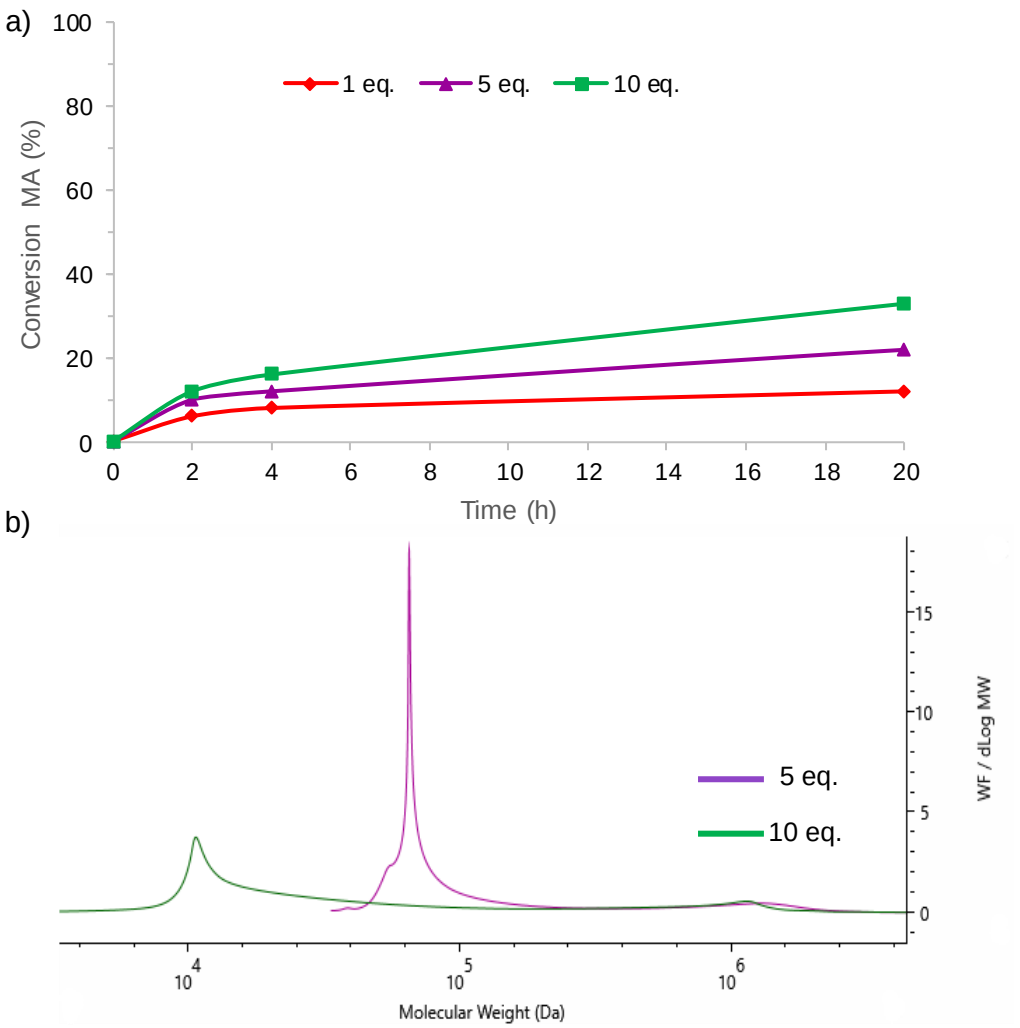

*Fig. 21: a) Reaction progress of PO/MA polymerization catalyzed by **11**/PPNCl in the presence of 1, 5 and 10 equivalents of H_2O. The connecting line between the data point is a guide to the eye. b) Molecular weight distribution plot of the isolated polymers. [cat]/[cocat]/[PO]/[MA]/H_2O = 1/1/5000/500/X, 50 °C with 50 vol% of toluene.*

In summary, the discussed experiments prove a certain deactivation of the catalyst by maleic anhydride or potentially by a strong coordination of the respective carboxylate. To further elucidate whether the carboxylate is too strongly coordinated to the metal center leading to catalyst deactivation or if other deactivation mechanisms are present, highly concentrated reaction setups could be analyzed by *in situ* IR spectroscopy. If the anhydride is opened and coordinated as carboxylate a strong band shift of the carbonyl band should be observable. While the necessary *in situ* IR spectrometer was not accessible at that time, this question was addressed in another fashion. Additional steric demand in the *ortho* position of the ligand was introduced to investigate the effect of the steric demand of the ligand on catalyst deactivation. The size of the introduced substituents was increased in two steps. First dimethyl–(*tert*–butyl)silyl groups were introduced instead of the *t*Bu groups (complex **6**). In a second ligand the *t*Bu groups were

substituted by triphenyl silyl groups (complex **7**). It is noteworthy that in the context of other catalytic experiments it was found that an aromatic backbone might increase the reaction rate. That is, **7** was synthesized bearing a fully aromatic backbone. Unfortunately, neither complexe **6** nor **7** showed significant reactivity towards the copolymerization of PO and MA. On the other hand, no precipitate formation could be observed, even after 48 h of reaction time. Thus, no catalyst deactivation according to the earlier experiments could be observed. To cross check the reactivity towards other anhydrides, **6** was employed as catalyst in the copolymerization of PO and PA. The reaction did neither yield a previously observed precipitate, nor catalytic activity. Therefore, the dimethyl–(*tert*–butyl)silyl substituents are considered too large to allow catalytic activity. Although, phthalic anhydride is much more sterically demanding than maleic anhydride, all these findings still suggest that the catalyst is deactivated by MA as substrate and does not only show a low reactivity towards polymerization under these conditions. As a next step to understand the deactivation, complex system **1**/PPNCl was employed to investigate the reversibility of the deactivation. For it is known that **1**/PPNCl provide a good activity towards the PO/PA ROCOP, a 1/1 mixture of maleic anhydride and phthalic anhydride with 500 equivalents with respect to the catalyst was subjected to the polymerization. No conversion of the anhydrides was observed (Scheme 21).

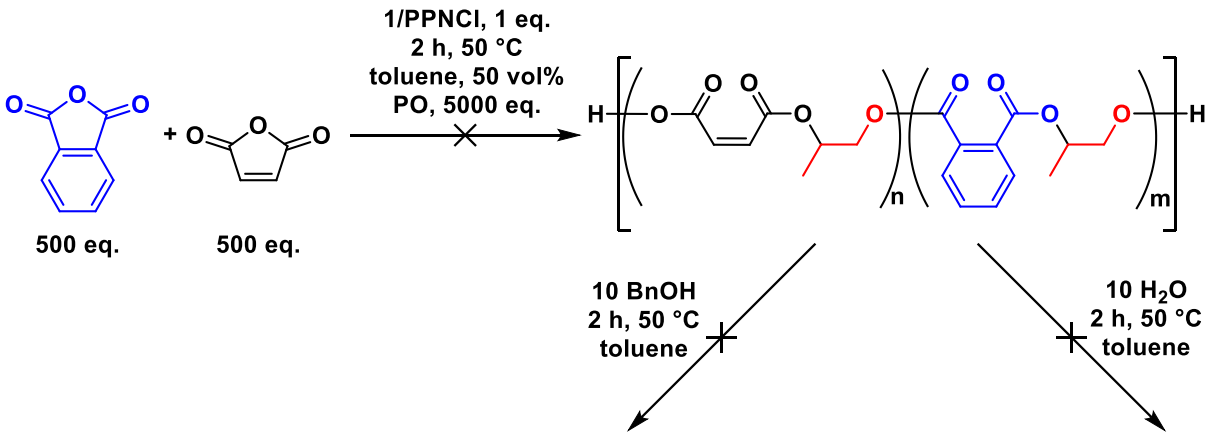

Scheme 21: Attempted PO/PA/MA terpolymerization and catalyst reactivation with BnOH and H_2O.

Furthermore, it was tested whether the complex could be reactivated. For that the same setup was repeated with the difference that after 2 h of reaction time at 50 °C the reaction mixture was divided into two separate, equal volume parts. In one part, 10 equivalents with respect to the catalyst of H_2O and in the second part 10 equivalents of benzyl alcohol were added. The reaction mixtures were stirred for additional 2 h at 50 °C under argon atmosphere. ^{1}H–NMR spectroscopic analysis of the crude reaction mixtures did not show

any polymer formation. Thus, the deactivation process of the catalyst by MA appears to be irreversible.

Another possibility to prevent catalyst deactivation is to provide water or benzyl alcohol directly at the start of the reaction (Scheme 22). The reactivation experiments were repeated in two separate setups using the same amounts of water and benzyl alcohol. Still, no conversion of the anhydrides was observed in the setup with benzyl alcohol. The setup with 10 equivalents of water did show anhydride conversion, on the other hand. After 19 h of reaction time 27 % of the maleic anhydride were converted according to ^{1}H–NMR spectroscopic data. Phthalic anhydride was converted to roughly 10 % indicating a stronger affinity of maleic anhydride to coordinate to the catalyst compared to phthalic anhydride, as the latter can be copolymerized with PO conveniently under the same conditions, separately. Although, the crude ^{1}H–NMR spectrum showed poly(propyl maleate) signals, the polymer could hardly be isolated from the reaction mixture for further analysis because of very similar solubility properties of the PO-MA oligomers and the other solution components.

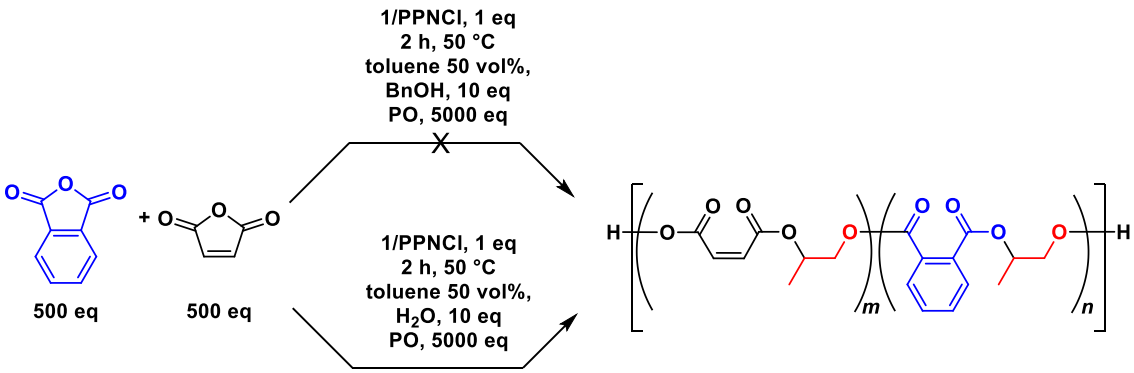

Scheme 22: Attempted terpolymerization of phthalic anhydride, maleic anhydride and propylene oxide in the presence of water and benzyl alcohol.

As a next step a sequential addition of phthalic anhydride and maleic anhydride was considered, aiming towards block terpolymers. For the following polymerization reactions complex **1** was used in combination with PPNCl, PPN(DNP) and TBA(DNP) as cocatalysts. Therefore, PA was first copolymerized with PO in the presence of **1** and the respective cocatalyst. Subsequently, maleic anhydride was added to the reaction mixtures and the reaction progress was followed *via* ^{1}H–NMR spectroscopy. In each setup maleic anhydride was added after 4.5 h of reaction time with only phthalic anhydride present with PPNCl as cocatalyst. Maleic anhydride was added to the system at 80 % PA conversion. While the conversion of PA immediately stopped, maleic anhydride was converted to 89 % after 48 h of reaction time. The ^{1}H–NMR spectrum of the isolated polymer showed 35 %

total propyl maleate moieties (Scheme 23, a1). For comparison a similar polymerization setup was performed with a shorter reaction time. After 20 h of reaction time the second setup reached a MA conversion of 56 % which is comparable to a conversion of 59 % after 24 h in the former reaction setup. Yet, the reaction was stopped and the formed polymer was isolated. Contrary to the former polymerization setup, the latter setup yielded a polymer which mainly consisted of poly(propylene phthalate). Only 5 % of the total amount of ester moieties could be assigned to propyl maleate segments. The formed poly(propyl maleate) was not isolated during workup (Scheme 23, b). Thus, the prolonged reaction time leads to an increasing amount of terpolymer. This observation points strongly towards transesterification facilitating the incorporation of the two polymers into each other. The transesterification will be addressed separately at the end of this chapter.

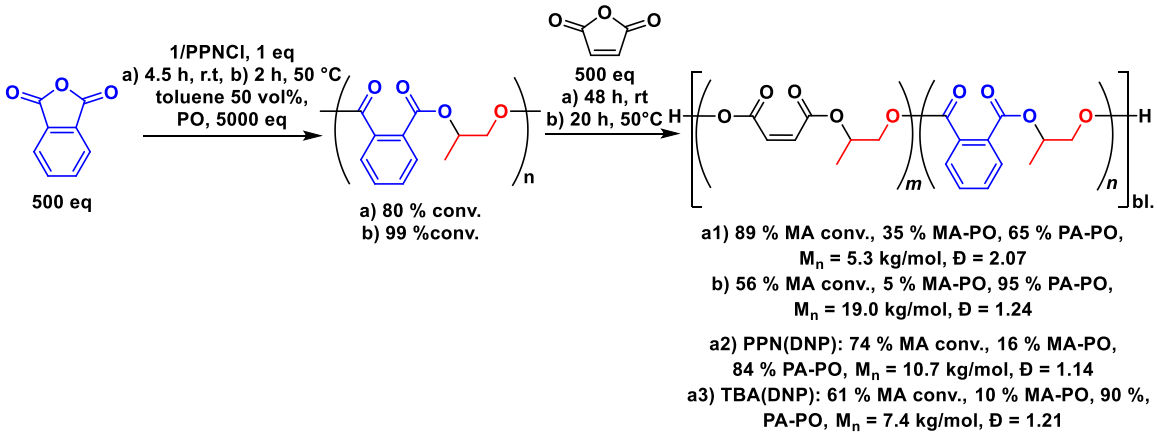

Scheme 23: Sequential anhydride addition in PO/PA/MA terpolymerization. MA-PO: propyl maleate segment, PA-PO: propyl phthalate segments. conv.: conversion.

A variation of the cocatalyst to PPN(DNP) Scheme 23, a2) or TBA(DNP) (Scheme 23, a3) led to a fair conversion of MA, as well. However, the incorporation of propyl maleate units was significantly less effective. If PPN(DNP) is employed as a cocatalyst only 16 % of all ester moieties in the isolated polymer can be assigned to propyl maleate segments. With TBA(DNP) the ratio is even lower where only 10 % propyl maleate is present in the isolated polymer. In all reactions the determined molecular weight is significantly lower than the predicted theoretical molecular weight. For instance, the M_n of the produced poly(propyl phthalate) under conditions b) should theoretically yield a polymer with 56 kg/mol. Instead of an increasing molecular weight with a further addition of maleate segments, the molecular weight of the isolated polymers was found to be significantly lower than the theoretical value. This effect appears to be even stronger with prolonged reaction times. In fact, the isolated terpolymer under conditions a) showed a *Đ* of 2.07 which clearly indicates transesterifications. However, all other isolated polymers in this

study exhibited a narrow *Đ* between 1.14 and 1.24 which are very common values for PO/PA copolymerizations with these catalyst systems. As mentioned above, the fact that PO/PA copolymerization stopped after addition of maleic anhydride might be an important aspect to explain the noticeable conversion of the employed maleic anhydride, and, at the same time, the poor incorporation thereof. As maleic anhydride (or the respective carboxylate) exhibits a higher binding affinity towards the catalyst, it blocks on the one hand the catalyst for binding of phthalic anhydride, but does not react to higher molecular weight polymers, on the other hand. As probably the determined molecular weights in Table 3 are overestimated, the conversion of maleic anhydride (Scheme 23) might only be explained by the formation of cyclic ester oligomers, which are well soluble in organic solvents. This behavior would be similar to widely observed backbiting side reactions in polycarbonate synthesis. The formation of cyclic polyesters is not very well explored with this catalyst systems. Still, the transesterification of the cyclic poly(propyl maleate) and poly(propyl phthalate) explains the high content of PO-MA segments from Scheme 23, a1. Very recently *Milione* and his group reported a similar catalyst system using an Fe-[OSSO] complex which is able to produce cyclic poly lactide.[159] His findings could support the hypothesis of the formation of cyclic poly(propyl maleates). As this topic was not further followed, the nature of the PO/MA copolymerization product was not further investigated.

A side reaction which was further investigated is the mentioned transesterification reaction. It was hypothesized that at given reaction conditions the catalyst system exhibits potential activity to catalyze the transesterification at prolonged reaction times. Thus, the observations which were made for the PO/MA/PA terpolymerization should be reproducible using other polyesters under the same reaction conditions. To prove this, ε-caprolactone was homopolymerized to a waxy, low molecular weight polycaprolactone (PCL, Scheme 24).

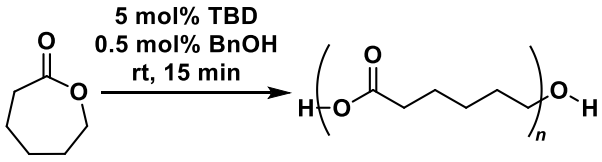

Scheme 24: TBD catalyzed homopolymerization of ε-caprolactone.

The molecular weight of the PCL was found to be below the detection limits for the used OmniSec GPC instrument even at high concentrations as of 9.45 mg/mL because of the low diffraction index increment (dn/dc) values and the low molecular weight. Initially, the theoretical molecular weight was determined to be 2.3 kg/mol based on the

monomer/catalyst ratio. This low molecular weight polyester was added (236 mg) to a freshly prepared poly(propyl phthalate) which was still unisolated in the reaction mixture. Before addition of the PCL, an aliquot of the poly(propyl phthalate) was taken and isolated. A characterization by GPC proved a high molecular weight of 44.5 kg/mol and a *Đ* of 1.15. The mixture of the two polymers was stirred for 40 h at typical polymerization conditions (50 °C, Ar atmosphere, glovebox). The resulting polymer exhibited only a molecular weight of 5.2 kg/mol with a *Đ* of 1.91. To further verify the results ^{1}H–NMR spectroscopic analysis was performed. Fig. 22 shows the stack plot of the three mentioned polymers. The ^{1}H–NMR spectrum of the terpolymer clearly comprises both signal sets of poly(propyl phthalate) and polycaprolactone, respectively.

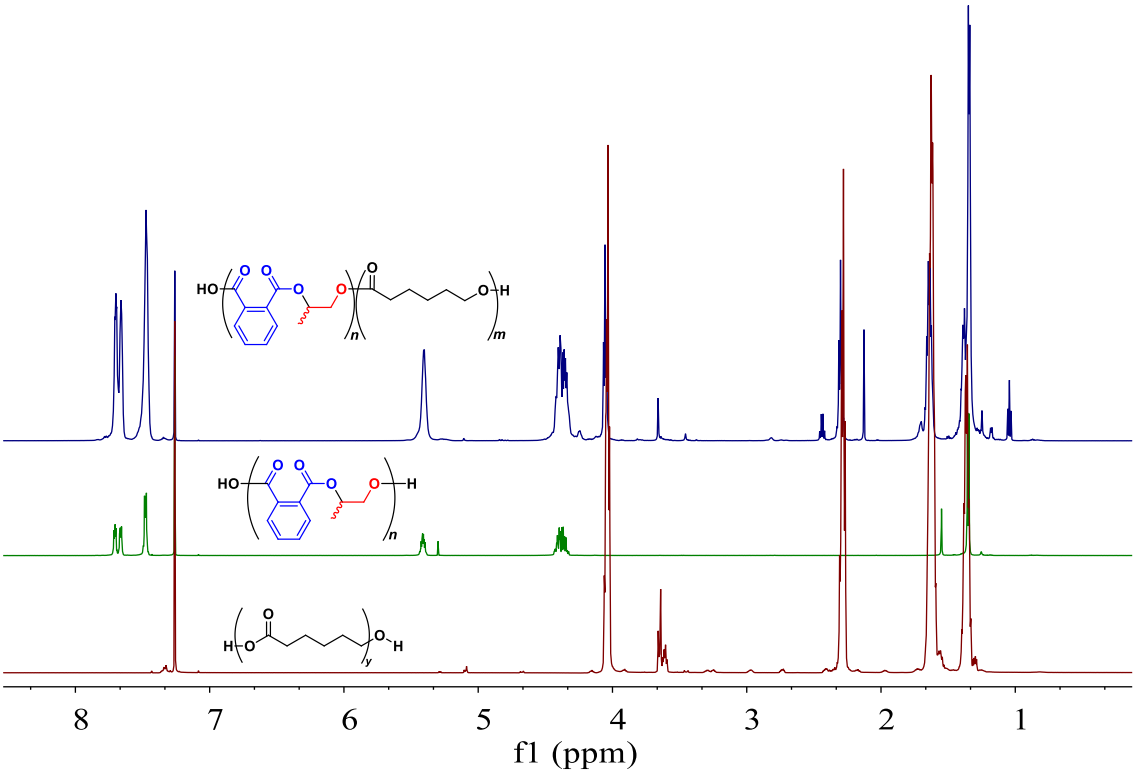

Fig. 22: Stack plot of ^{1}H–NMR spectra of PCL, poly(propyl phthalate) and PCL-poly(propyl phthalate) terpolymer, measured in $CDCl_3$ at 25 °C.

Because, the measured polymer could consist of a blend of the two polymers additional analytical evidence must be collected. To clearly distinguish between a blend and one polymer species comprising both ester segments, DOSY NMR spectra were recorded. Fig. 23 shows an overlay of two ^{1}H–DOSY spectra. The upper trace represents the mentioned terpolymer. The lower trace represents the parent PA-PO polyester before transesterification. As the parent polymer was shown to have a much higher molecular weight compared to the transesterification product, the diffusion is significantly slower compared to the terpolymer. The parent PA-PO polymer shows a diffusion coefficient of $8.4 \cdot 10^{-7}$ cm^2/s while for the terpolymer a diffusion coefficient of $1.2 \cdot 10^{-6}$ cm^2/s was found.

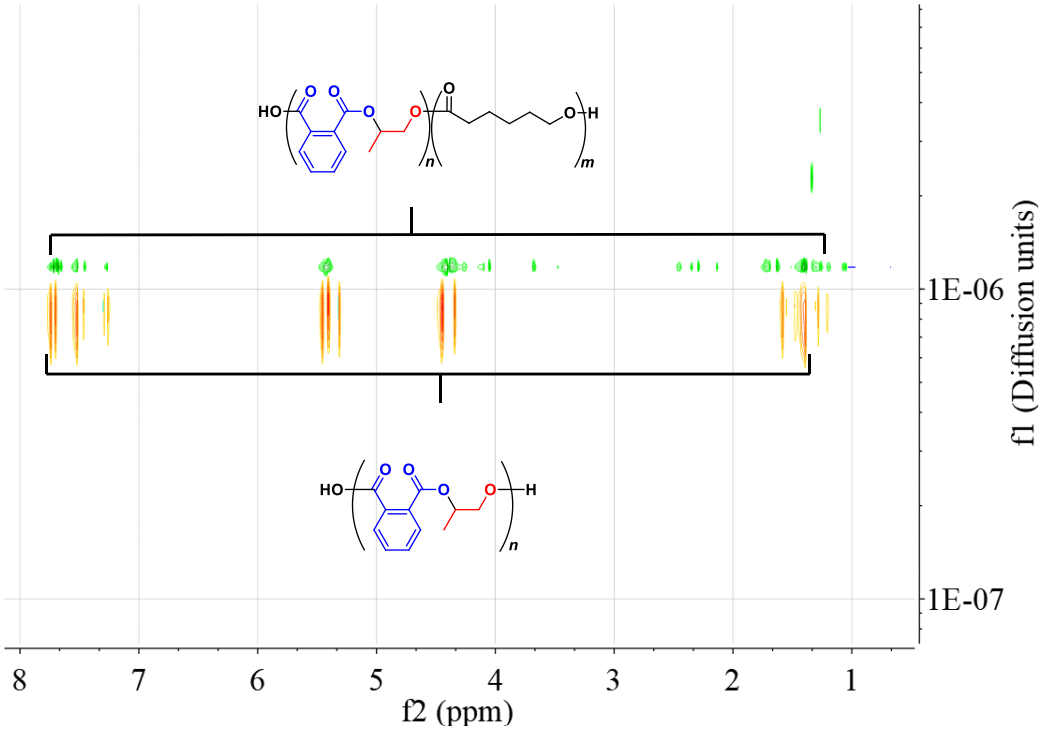

Fig. 23: Overlay of ^{1}H–DOSY NMR spectra of poly(propyl phthalate) and PCL-poly(propyl phthalate) terpolymer. Diffusion units: cm^2 · s^{-1}.

In addition to the presented **1**/PPNX catalyst system, three other catalysts were tested in the copolymerization of MA and PO. Table 4 summarizes the additional catalytic reactions. Similar to **1**/PPNCl under conditions b) (Scheme 23) complexes **11**, **12** and **5** performed well in the copolymerization of PA and PO, but they did poorer in the copolymerization of MA and PO. The conversion of maleic anhydride and the poor incorporation in the isolated polymer are comparable to the earlier example. Interestingly, using complex **5** without PPNCl the determined molecular weight of the isolated polymer remained high. Hence, the cocatalyst appears to have a crucial role in the

transesterification process as the tethered cocatalyst in **5** functions as Lewis base, contrary to the ammonium in PPNX cocatalysts.

Table 4: Additional catalysts tested in the PO/PA/MA block terpolymerization. Inc.: incorporation, ratio of MA-PO segments to all ester segments (see Scheme 23, conditions b)).

Entry	Cat.	Conv. PA (%)[a]	Conv. MA (%)[a]	Inc. MA (%)[a]	M_n (kg/mol)[b]	$Đ$[b]
1	**11**	99	62	6	19.6	1.12
2	**12**	99	57	5	18.9	1.12
3[c]	**5**	99	44	2	43.7	1.35

[cat]/[PPNCl]/[PO]/[PA]/[MA] = 1/1/5000/500/500, 50 °C, 2 h (reaction conditions b Scheme 23). [a]Determined via ^{1}H–NMR spectroscopic analysis. [b]Determined by GPC calibrated with polystyrene standards and triple detection. [c]Catalysis run without PPNCl.

In summary, it could be shown that the copolymerization of maleic anhydride and propylene oxide with Co-salen type complexes is strongly hampered by catalyst deactivation. This catalyst deactivation can be slowed down by the addition of trace amounts of water to the reaction system. The water is assumed to coordinate to the catalyst and, therefore, decelerate the catalyst deactivation, which could be shown by variation of the amounts of water added. At this point hydrolysis of the maleic anhydride can be widely excluded, as the reactions were performed in predried, sealed vessels and the water was added under a dry argon shower. Thus, the conversions were found to be too high to be exclusively caused by hydrolysis by the trace amounts of water. Additionally, the block terpolymerization of MA, PA and PO was investigated. Here, the carboxylate end groups of the previously polymerized phthalic anhydride showed an effect on the catalyst activity towards the copolymerization of MA and PO. As MA was added in the two step experiments, the conversion of the remaining phthalic anhydride stopped while the maleic anhydride was slowly converted. Using PPNCl as cocatalyst, PO/MA ester segments were well incorporated into the polymer backbone at prolonged reaction times. Due to the long reaction time, transesterification was attributed to cause the good incorporation as the incorporation was generally poor with shorter reaction times. This was even the case for reactions with significant conversion of maleic anhydride. The transesterification was successfully proven by combination of poly(propyl phthalate) with a previously synthesized PCL under standard reaction conditions. In this context PPNX species as cocatalyst were found to facilitate not only the copolymerization of anhydrides and epoxides together with analogues of **1**, but, moreover, facilitating transesterification. The poor incorporation at shorter reaction times is presumably due to cyclic poly- or oligoester formation of maleic

anyhdride and propylene oxide. This would explain the poor content of propyl maleate segments in the polymer backbone. The incorporated maleate is considered as end groups, as the respective propyl ^{1}H–NMR spectroscopic signals of the maleate segments are well separated from the residual phthalate signals.

3.2.2 Tetrahydrophthalic Anhydride (THPA)

Tetrahydrophthalic anhydride (THPA) represents and alternative monomer in the ROCOP with propylene oxide. The anhydride moiety in THPA is expected to have a higher ring strain than MA, while at the same time the double bond is retained giving the possibility of post polymerization modification (Scheme 25).

In this context first **1**/PPNCl was tested and the results were subsequently compared to experiments with **2**/PPNCl as catalyst system. The anhydride was not only investigated in the copolymerization with propylene oxide, but also in the potential of forming terpolymers with phthalic anhydride. Thus, the order of addition was again altered between direct and sequential addition of the anhydride monomers.

It is important to note that the copolymerization of THPA and PO proved to be similarly difficult as maleic anhydride with the investigated systems to begin with. However, compared to maleic anhydride THPA did not noticeably deactivate the catalysts. Still, THPA was converted at a comparable slow rate as MA. **1**/PPNCl, for instance, as catalyst system converted 73 % of the THPA after 48 h. A low molecular weight polymer could be isolated with 2.0 kg/mol and a *Đ* of 1.55. **2**/PPNCl as catalyst system produced under the same conditions after 3 h with full THPA conversion a significantly higher molecular weight polymer with 12.6 kg/mol but a *Đ* of 9.5.

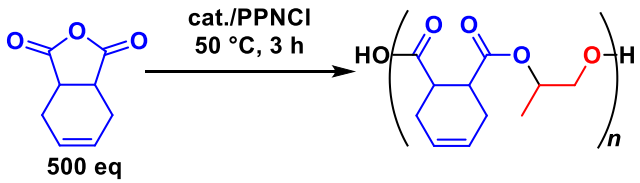

Scheme 25: Copolymerization of THPA and PO.

Importantly, it must be noted that these results have to be taken with care in terms of the absolute numbers. The former polymer gave only a poor light scattering response so that the measurement error might be significant. The latter polymer gave better light scattering responses in the GPC measurement but showed additionally a certain amount of larger aggregates in solution and sample fractions, which could not be dissolved completely.

Thus, after initial experiments with **1**/PPNCl and **2**/PPNCl as catalysts the copolymerizations were left aside and phthalic anhydride was introduced as additional monomer.

In first terpolymerization experiments THPA and PA were directly combined at the beginning of the reaction and reacted with PO in the presence of **1**/PPNCl. In the previous section the influence of water on the copolymerization of MA and PO was discussed. Based on these observations one equivalent of water with respect to the catalyst was added to the reaction system, also in this case.

To follow the consumption of the respective anhydride the reaction was carried out using an *in situ* IR spectrometer, measuring time resolved IR spectra. The reaction was stirred for 48 h at 50 °C. The respective IR bands were identified, and the time resolved trends of the respective IR band were followed. The reaction progress was modelled to obtain the consumption curves of the anhydrides in absolute concentration instead of in signal intensity differences. As it becomes clear in Fig. 24, the two anhydrides are consumed almost simultaneously. Interestingly, phthalic anhydride is converted significantly slower than it would be the case in the separate copolymerization of PO and PA under the same conditions (compare Table 5, entry 1, page 77). In this experiment 65 % of PA and 73 % of THPA were consumed. Although, 250 equivalents of the respective anhydride were weighed in, which should lead to a theoretical molecular weight around 34 kg/mol for double initiation at the catalyst in the presence of one equivalent of water, only a molecular weight M_n of 2.2 kg/mol was observed. A calculation error in the GPC software due to low concentration can be excluded at this point, since the signal intensity of the refractive index signal is in the range of the measured standards. The $Đ$ of 1.3 can be considered as narrow. Because of this narrow polydispersity transesterification appears to be less likely causing the low M_n. Hence, cyclization could be a potential cause for the low molecular weight. In the previous section a similar experiment was presented with a low PA conversion of 10 % and 27 % MA conversion (see Scheme 22), where the formed product could not be properly isolated. Contrary to that, the PO/PA/THPA terpolymer from this experiment could be isolated and characterized. NMR spectroscopic analysis of the isolated polymer proved the presence of both, PO-PA and PO-THPA, segments in the polymer in a 1/1 ratio. As the anhydrides were consumed simultaneously no polymer block formation can be expected. That is, particularly the ^{1}H–NMR spectroscopic signals of the methylene protons of the ester segments are expected to strongly overlap, which is indeed found. The overlap of the signals is caused by the similarity of the environments in the transition between a PO-PA and PO-THPA segment. Block terpolymers give well separated signal sets while strictly alternating structures would theoretically give only one signal set in that region without strong overlap because of the well-defined methylene

environment. A more detailed discussion and examples on that topic will be given in chapters 3.2.3.6 and 3.2.3.7. The discussed ^{1}H–NMR spectrum is provided in Fig. 25. Hence, in this example the simultaneous consumption of the anhydrides points towards a random incorporation of the two anhydrides into the polymer backbone. Additionally, if the consumption in this experiment is compared to the copolymerization of PO and THPA with **1**/PPNCl, both reactions show the same conversion in THPA of 73 % after 48 h. This can lead to the conclusion that the ring–opening of THPA is also rate determining in the terpolymerization of PO, THPA and PA, as the copolymerization of PO and THPA yielded 73 % of THPA conversion after 48 h, as well. However, considering the proposed reaction mechanics of epoxide/anhydride copolymerization (Scheme 11, complex CC), this observation supports the hypothesis of a preferentially mixed coordination of the two respective anhydrides at the catalyst in an octahedral coordination. This might slow down also the PA/PO copolymerization to the rate of the THPA/PO copolymerization.

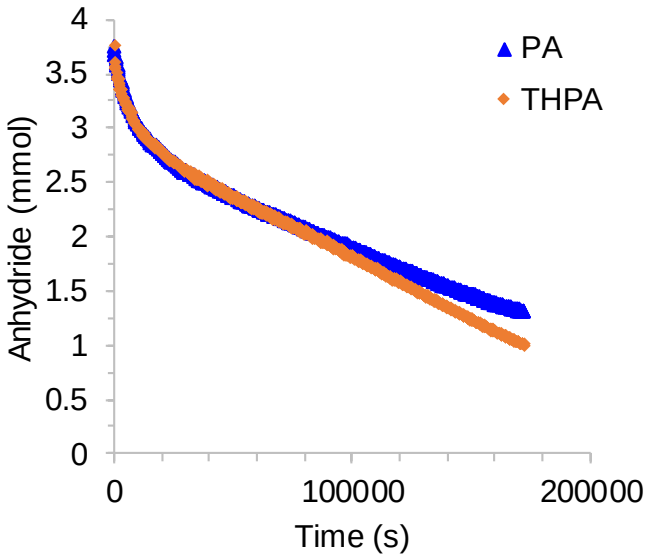

Fig. 24: Time dependence consumption of PA and THPA as detected with in situ IR spectroscopy with at direct addition of both anhydrides. [1]/[PPNCl]/[PO]/[PA]/[THPA]/[H_2O] = 1/1/5000/250/250/1, 50 vol% toluene, 50 °C, 48 h.

Another question that has to be answered in this context is the connectivity of the respective ester segments. As THPA plays a rate determining role in this polymerization it does not necessarily lead to 1:1 incorporation of both possible ester segments into the polymer chain. Another possibility is that a polymer blend is formed and that the THPA debases the reaction rate by coordination to the catalyst, assuming a similar behavior as observed for maleic anhydride. To clarify whether the formed polymer product is a blend of poly(propyl phthalate) and poly(propyl tetrahydrophthalate) one has to consider several facts. One aspect is a DOSY NMR spectroscopic analysis. In the case of a blend two

different diffusion coefficients should be observable if the hydrodynamic radii of the polymer particles in solution are sufficiently different in size. Because in this experiment the two anhydrides were employed in equimolar amounts, this is not necessarily the case. However, the uniformity of the diffusion trace is remarkable with respect to the different conversions of the anhydrides (Fig. 26).

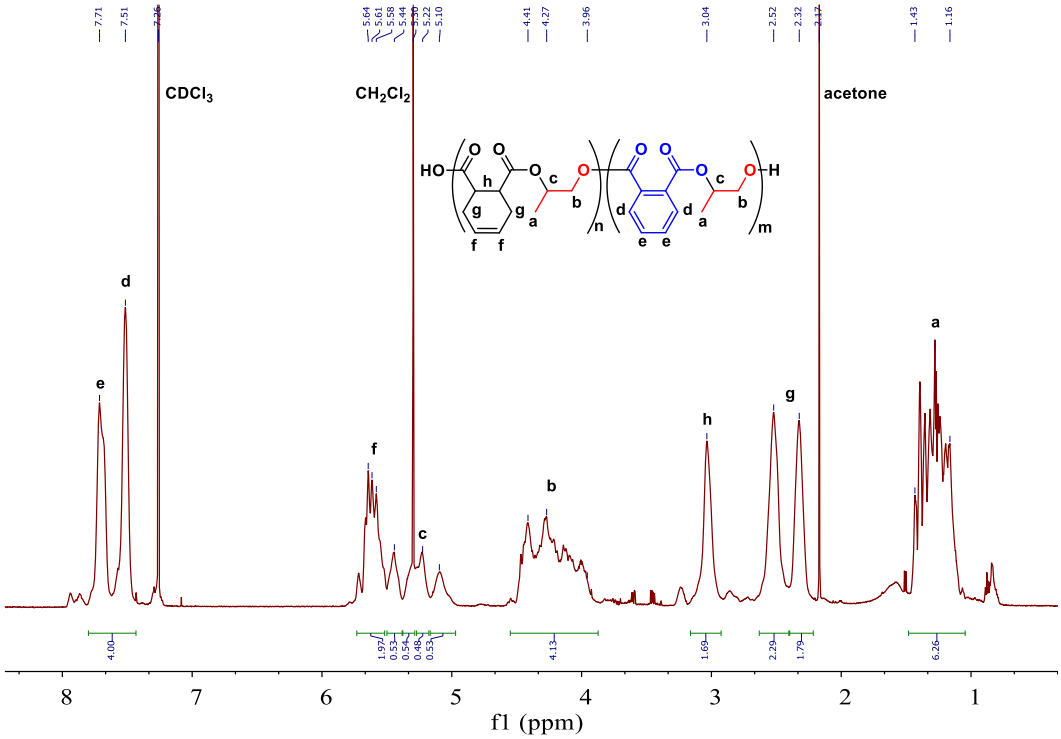

Fig. 25: ^{1}H–NMR spectrum of a PO/THPA/PA terpolymer from direct addition in $CDCl_3$ at 25 °C. [1]/[PPNCl]/[PO]/[PA]/[THPA]/[H_2O] = 1/1/5000/250/250/1, 50 vol% toluene, 50 °C, 48 h.

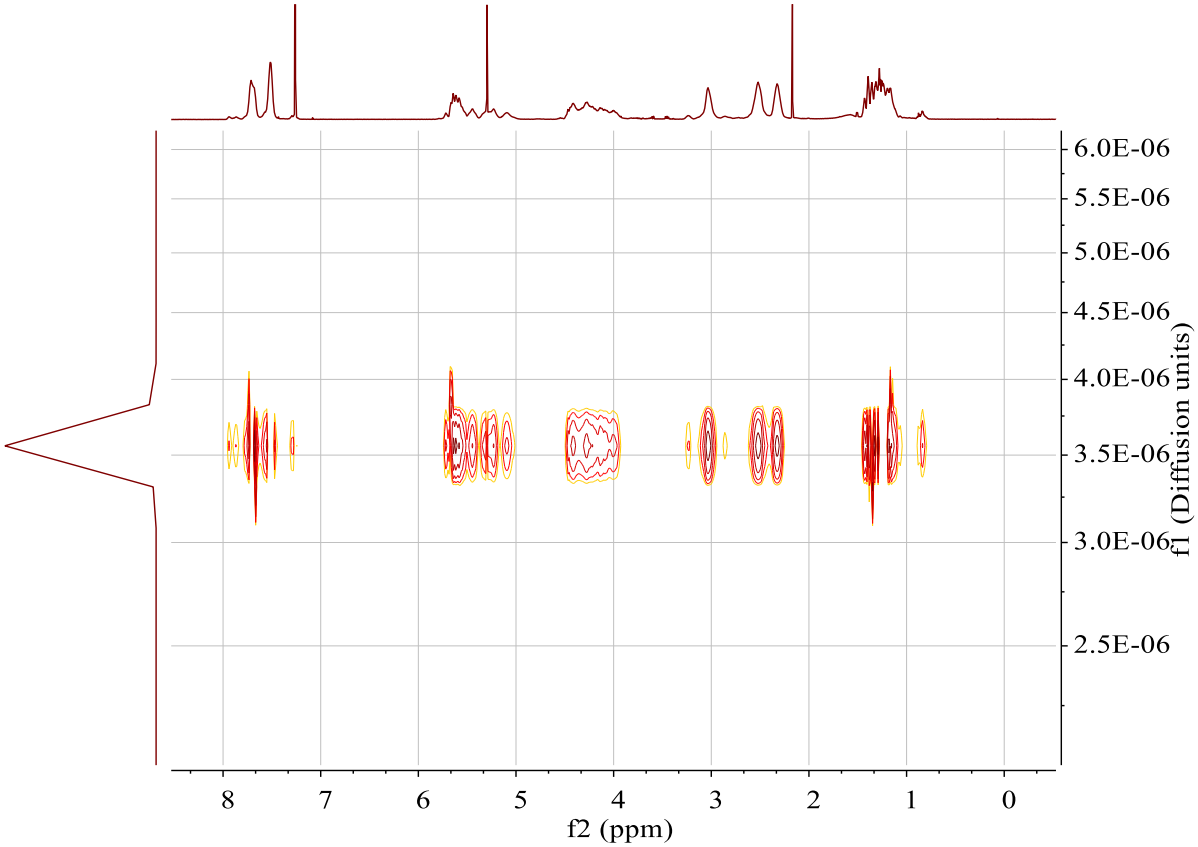

Fig. 26: ^{1}H–DOSY NMR spectrum of PO/THPA/PA terpolymer with 2.2 kg/mol in $CDCl_3$ at 25 °C. Diffusion units: $cm^2 \cdot s^{-1}$.

Another aspect is the obtained molecular weight. It is known from previous experiments for the polymerization system of PO/PA with **1**/PPNCl that the polymerization leads to significantly higher molecular weights for poly(propyl phthalate) under these conditions than it was determined for PO/PA/THPA terpolymer. Therefore, even with long reaction times and the occurrence of transesterification, the obtained number averaged molecular weight of 2.2 kg/mol does not seem to be reasonably high for separate PO/PA and PO/THPA polymerizations. Moreover, GPC analysis should indicate at least a bimodal molecular weight distribution for a polymer blend or a broad *Đ*, which is not the case in this experiment. However, a closer look at the molecular weight distribution plot shows three distinct spikes in mass fractions (Fig. 27). Considering the hypothesis for the formation of cyclic oligomers as discussed for the PO/MA copolymerization and assuming the 1/1 incorporation of THPA and PA in the sample, the peaks in the distribution could represent 6, 8 and 10 membered macrocycles of the present ester segments. Because of the similarity of molecular weight of the two anhydrides it cannot be concluded on the anhydride incorporation pattern from this plot.

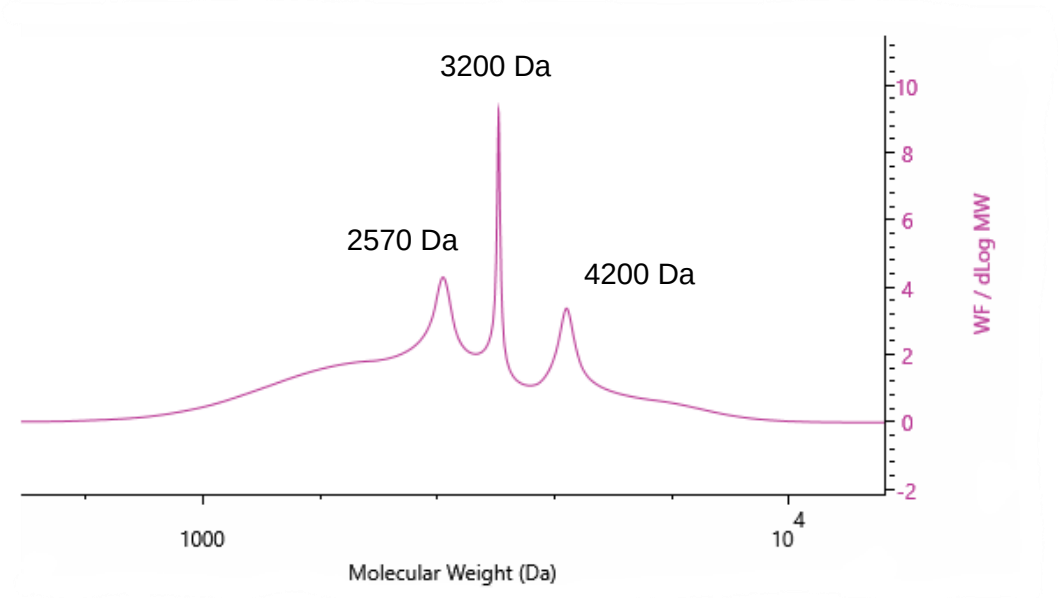

Fig. 27: Molecular weight distribution plot of a PO/THPA/PA terpolymer from direct anhydride addition.

A thorough MALDI-TOF MS investigation should proof the presence of cyclic oligomers based in the absence of end groups.

2/PPNCl was investigated next in the direct terpolymerization of PO/THPA and PA. This experiment was performed by ^{1}H–NMR spectroscopy in the glovebox without water present. Initially, the absence of water in the reaction system was considered to be problematic in terms of comparability between the two catalysts. Nonetheless, the small amount of inserted water in the other experiments and the significantly faster transesterification might diminish the importance of one equivalent of water in retrospect. The direct terpolymerization of PO, THPA and PA, **2**/PPNCl lead to a full conversion of both anhydrides after 3 h in agreement to the observation in the copolymerization of THPA and PO. In order to be certain of the incorporation of THPA into the polymer backbone, the amount of THPA was lowered to a 1:3 ratio of THPA to PA. This should additionally maintain a distinguishability of polymeric or oligomeric species by diffusion coefficient in the DOSY NMR spectroscopic analysis. In fact, NMR spectroscopic analysis proved an almost full incorporation of THPA in the isolated polymer. 23 % of the ester moieties found by ^{1}H–NMR spectroscopic analysis were assigned to PO-THPA segments with a determined M_n of 15.3 kg/mol and a $Đ$ of 1.43. The diffusion coefficient could be calculated to 2.65 · 10^{-6} cm^2/s. Moreover, the DOSY spectroscopic analysis showed only one polymeric species in the pseudo 2D DOSY plot (see Fig. S9, page 163). Contrary to the direct terpolymerization with **1**/PPNCl, the product of this experiment could be easily

isolated and could hence be further analyzed by DSC. The glass transition was found at 43 °C after two and three cycles which is about 8 °C lower compared to a racemic poly(propyl phthalate) polymer (51 °C). Moreover, the polymer was found to be semicrystalline. A zoom to the respective region is provided in Fig. 28. Interestingly, a melting point shift was observed between the second and third heating cycle for poly(propyl phthalate). In the second cycle a melting point of 296 °C with a melting enthalpy of 0.078 J/g was determined, while in the third lower a lower melting point of 284 °C and a lower melting enthalpy of 0.058 J/g were observed. Taking a closer look at the region around the melting peak of the second cycle, partial decomposition of the sample can be observed. That is, the crystallinity of the polymer decreased between the two cycles. This leads to the formation of less and smaller crystallites upon cooling. This results in a shifted melting point and smaller melting enthalpy that was observed in the third measurement cycle.

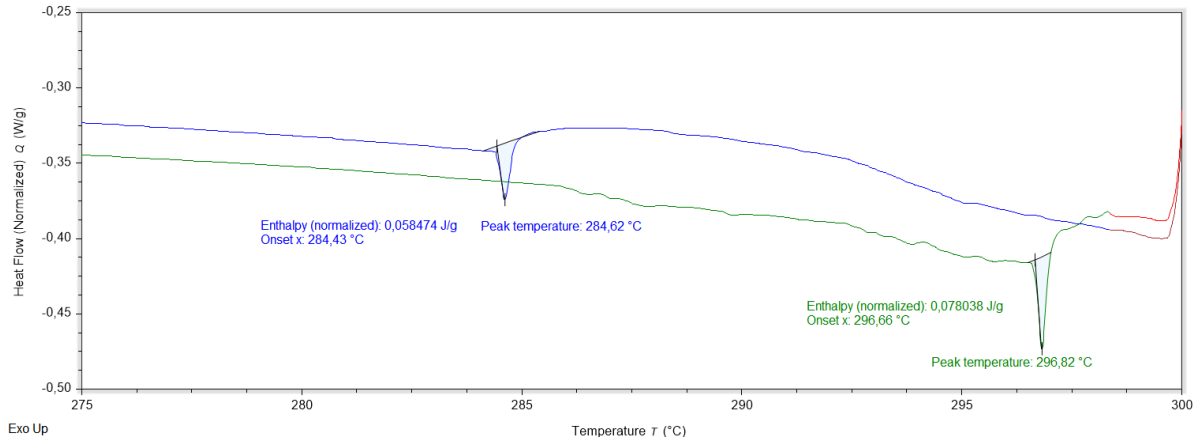

Fig. 28: Zoom to the melting region of a DSC plot of a PO/THPA/PA terpolymer with 23 % PO-THPA segments and M_n = 15.3 kg/mol and Đ = 1.43. Green curve: second cycle, blue curve: third cycle.

As **2**/PPNCl was found to be efficient in the polymerization, as well as, in the incorporation of PO-THPA segments into the polymer backbone, the catalyst system was also tested and compared to **1**/PPNCl in the sequential terpolymerization of PO, THPA and PA.

Next, the sequential addition of PA and THPA in the polymerization process, was studied using catalyst systems **1**/PPNCl and **2**/PPNCl. In the first step of the reaction sequence, phthalic anhydride was copolymerized with propylene oxide under standard reaction conditions at 50 °C under argon atmosphere and 0.4 mol% catalyst loading (250 equivalents of PA with respect to catalyst). After 5 h of reaction time both catalyst systems

reached 96 % conversion. Then 250 equivalents of THPA were added to the reaction and stirring was continued. After additional 6 h of reaction time, 50 % of the reaction volume was removed for analysis (Scheme 26).

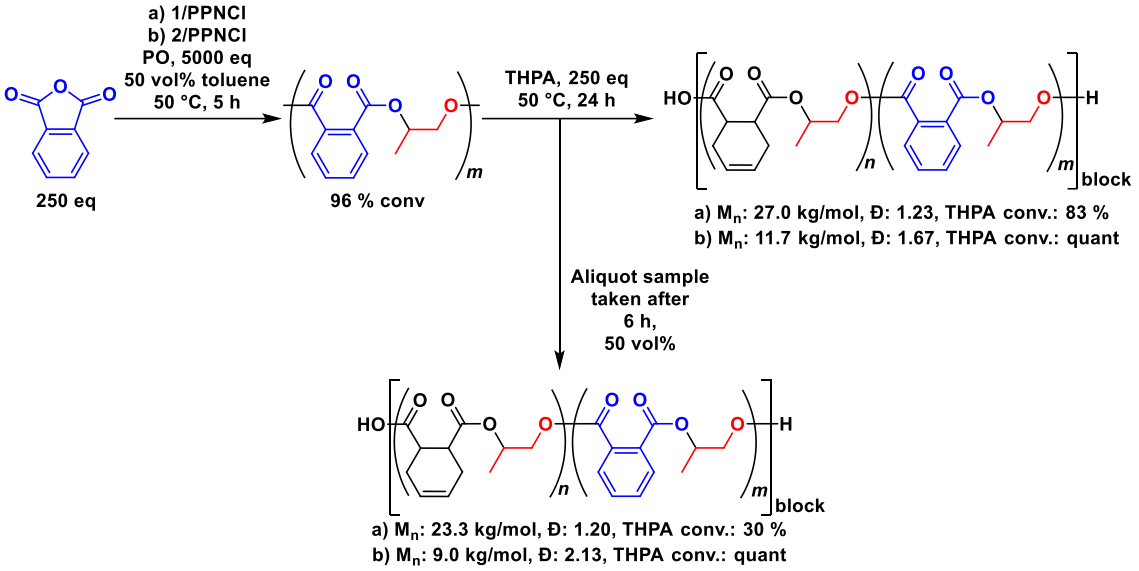

Scheme 26: Synthesis of PO/PA/THPA terpolymer by sequential anhydride addition. The reaction was carried out in the glovebox with no water present. conv.: conversion, quant.: quantitative.

For the analyzed aliquot from catalyst **1**/PPNCl Scheme 26 a) a M_n of 23.3 kg/mol and a narrow polydispersity were found. This value is close to the expected theoretic molecular weight of 25 kg/mol for poly(propyl phthalate). Although 30 % of the initially employed tetrahydrophthalic anhydride was consumed, only 5 % of all ester moieties could be attributed to propyl tetrahydrophthalate segments. The acidified methanolic solution containing hydrolyzed THPA, catalyst and byproducts was not further analyzed in depth, as the work was more focused on the copolymerization and incorporation behavior of the anhydride and not on the side product formation. With **2**/PPNCl as catalyst system significantly lower molecular weights were obtained. Moreover, the broad distribution represents extensive transesterification behavior. As noted earlier, the used types of catalyst systems seem to facilitate transesterifcation reactions as the catalyst is “unoccupied” at high conversions. This also explains the high content of PO-THPA segments in the polymer chain after 24 h of reaction time. ^{1}H–NMR spectroscopic analysis revealed 30% of PO-THPA segments. Thus, 1/3rd of all ester segments are derived from THPA. A DOSY NMR spectrum was recorded to verify that the two polyester blocks are interconnected (Fig. 29). Interestingly, three different species can be distinguished by diffusion coefficient. All three species contain both types of ester segments. One of which diffuses relatively fast with $4.85 \cdot 10^{-5}$ cm^2/s, while the other two species exhibit a rather

similar diffusion coefficient of $3.58 \cdot 10^{-6}$ cm^2/s and $2.3 \cdot 10^{-6}$ cm^2/s, respectively (compare Fig. 26). Within the three DOSY traces the trace for the smallest diffusion coefficient is significantly more prominent compared to the other two traces, as indicated by the different intensity in the diffusion dimension of the DOSY NMR spectrum in Fig. 29. The determination of the content of the respective ester groups by ^1H–NMR spectroscopic analysis is impossible, because all signals of the species are perfectly superimposed. However, with a fitting transformation algorithm of the respective single spectra to the pseudo 2-D DOSY NMR plot one can gain a little bit of insight into the distributions. It is important to note that measurement artifacts caused by shimming, signal drifts or inhomogeneity of the magnetic field gradient can affect the plot. In this case a Bayesian transformation algorithm built-in the used MestreNova NMR analysis software was employed. Bayesian transformation is a statistical method where the probability of the occurrence of a signal at a specific chemical shift is statistically calculated and correlated with the measured diffusion coefficient caused by a detected response in the NMR spectrum. Overall, a simulation based in the input data from the signal decay along the field gradient was performed.

After setting two-dimensional integration borders a ratio of the two possible ester segments in the fastest diffusing species close to 1/1 was integrated. The species at $3.58 \cdot 10^{-6}$ cm^2/s only provides a PO-THPA segment content of 20 % while the major species shows a poor 13 % incorporation PO-THPA segments (Fig. 29, integrations in red box).

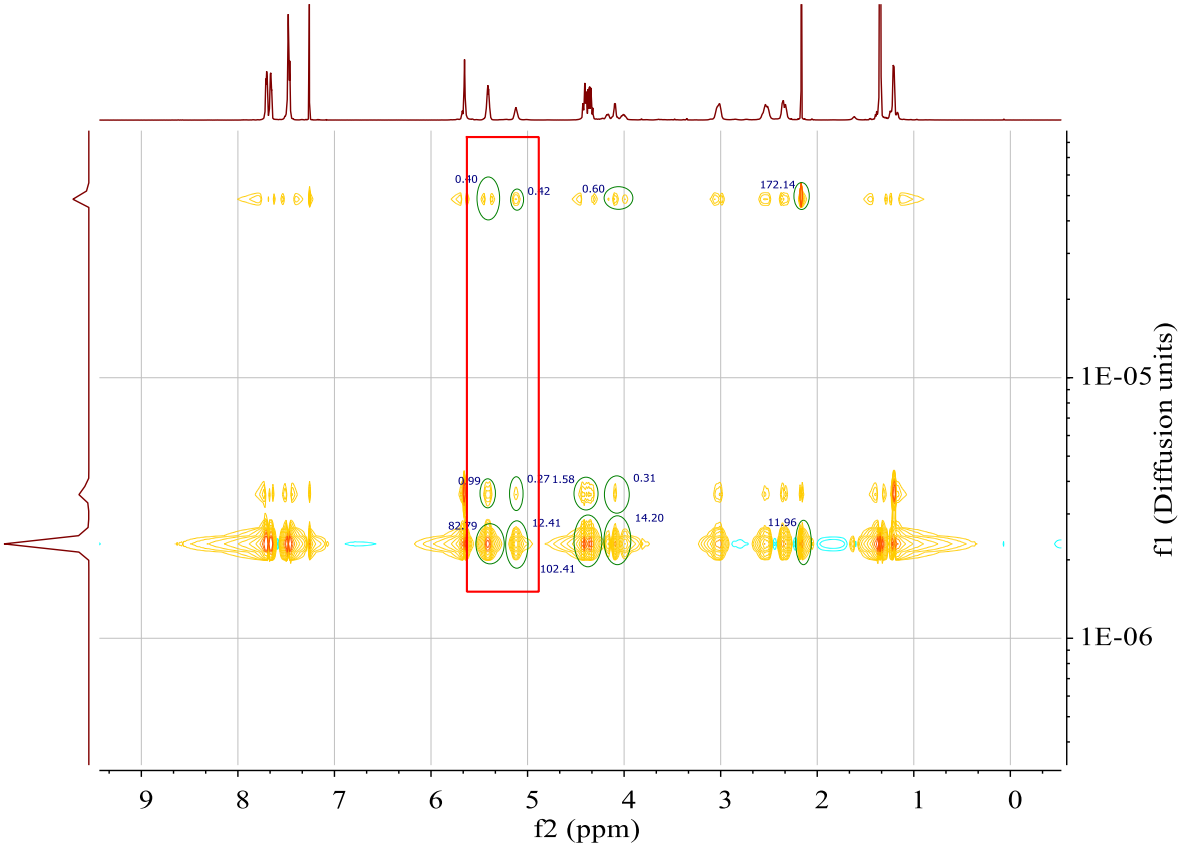

*Fig. 29: ^{1}H–DOSY NMR spectrum of a block PO/PA/THPA terpolymer, produced by **2**/PPNCl after 6 h (see Scheme 26 b). Diffusion units: cm^2 · s^{-1}.*

2/PPNCl as catalyst system, therefore, leads to an extensive transesterification with THPA-PO ester segments present in the reaction system. On the other hand, transesterification can also lead to an increase of PO-THPA segments in the polymer backbone. As a matter of fact, this could be utilized for the synthesis of modifiable polyester resins. Nonetheless, the process is not very well controlled at this point.

Considering the second part of the reaction pathway, no significant changes could be found. The reaction with **1**/PPNCl yielded a polymer with slightly increased molecular weight. Unfortunately, the increase is insignificant in the isolated product. The catalyst system **2**/PPNCl with the aromatic backbone yielded a slightly higher molecular weight as well. Interestingly, the *Đ* decreased to only 1.67. This fact is somehow counterintuitive as it was found earlier that the transesterification proceeds further with reaction time. This observation could not be rationalized with certainty. One possibility is that the transesterification indeed proceeded, yielding to a somehow entropy driven "depolymerization" of higher molecular weight chains to the benefit of the polymer chains with shorter chain lengths. Thus, with an increased number of chains the M_n gains a higher impact.

The sequential addition procedure was repeated to further elucidate the two reaction systems, and the reaction progress was monitored by *in situ* IR spectroscopy (Fig. 30). The reaction conditions were chosen to be comparable to the IR experiment with direct, simultaneous addition of the anhydrides (see Fig. 24). Therefore, one equivalent of water was added together with the THPA to the reaction. The reaction progress in the PA consumption is comparatively similar for both catalyst systems. The consumption of THPA, on the other hand, is significantly different between the two catalyst systems. While PA is fully consumed after 4 h with **1**/PPNCl and after 2 h with **2**/PPNCl the employed THPA is consumed after 18 h with **1**/PPNCl and after only 3 h with **2**/PPNCl after addition.

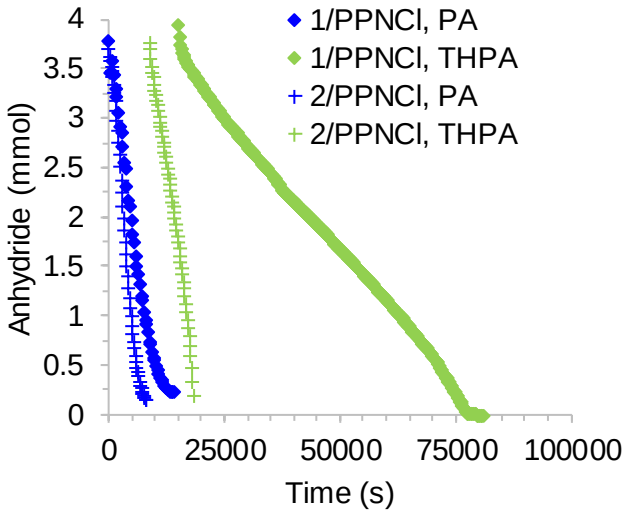

Fig. 30: PA and THPA consumption in a sequential anhydride addition polymerization sequence, followed by in situ IR spectroscopy. [1]/[PPNCl]/[PO]/[PA]/[THPA]/[H_2O] = 1/1/5000/250/250/1, 50 vol% toluene, 50 °C. 1 equivalent of water was introduced together with THPA to the reaction.

Although the reaction conditions with the IR measurement and the reaction conditions in the glovebox are not identical and can lead to slightly different outcomes, these findings reflect the previously made observations of a strong difference in activity of **1** and **2** with respect to PO/THPA copolymerization. A study of the effect of the two different setups on the polymerization outcome will be addressed later. Contrary to the previously discussed sequential addition experiment, here, both complexes lead to similar M_n with 28.1 kg/mol and *Đ* of 1.31 for **1**/PPNCl and 26.5 kg/mol and *Đ* of 1.5 with **2**/PPNCl. Therefore, also here the observations of transesterification reactions are consistent. A further comparison of the recorded GPC data discloses great differences between the two polymers. First of all, the refractive index increment (dn/dc) is very different with 0.11 for **1**/PPNCl and 0.04 for **2**/PPNCl which is one indicator for a difference in the nature of the polymer. The GPC data show furthermore a large difference in the hydrodynamic radii for the polymer

particles in solution despite of a similar molecular weight. The polymer from **1**/PPNCl exhibits a number averaged hydrodynamic radius Rh_n of 4.18 nm while the polymer from **2**/PPNCl yields an almost 40 % smaller particle with 2.66 nm in Rh_n. Another difference is the shape of the particles. As the former sample is random coil shaped with a *Mark Houwink α* parameter of 0.56, the latter polymer has an *α* of 0.77 and is therefore rather rod shaped.[160] These findings correspond with the NMR analyses. As far as the diffusion behavior is concerned, the polymer from **1**/PPNCl diffuses with $3.46 \cdot 10^{-6}$ cm^2/s significantly faster than the polymer from **2**/PPNCl $1.31 \cdot 10^{-6}$ cm^2/s. At the first glance this seems to be counter intuitive as the hydrodynamic radii are in reverse order. However, it is known that shape has a certain influence on the diffusion coefficient. While in the domain of small particles (benzene sized) spherical particles tend to diffuse a little bit slower than planar or linear shaped ones, this order can be reversed with larger particle. This explains the slower diffusion of the smaller particle in this context.[161] Note that both isolated polymers consisted only of one species according to DOSY analysis, respectively. Considering the ratio of ester segments, **1** again gives a poor incorporation of 13 % of PO-THPA segments. **2**/PPNCl incorporates double the amount and a PO-THPA content of 27 % was observed.

It is important to realize that although these results are already improved compared to results presented earlier, still in the best case 73 % of the employed tetrahydrophthalic anhydride was not incorporated.

The investigation discussed above indicate the importance of monomer-monomer and chain end-monomer cooperative effects and, in this context, the importance of the order of monomer addition, even if the copolymerizations of the respective anhydride with propylene oxide might be strongly different in reaction rate. As a second possibility of a sequential fashion of anhydride addition, THPA can be copolymerized first with PO, while PA can be added to the reaction system, subsequently. The reaction sequence is summarized in Scheme 27.

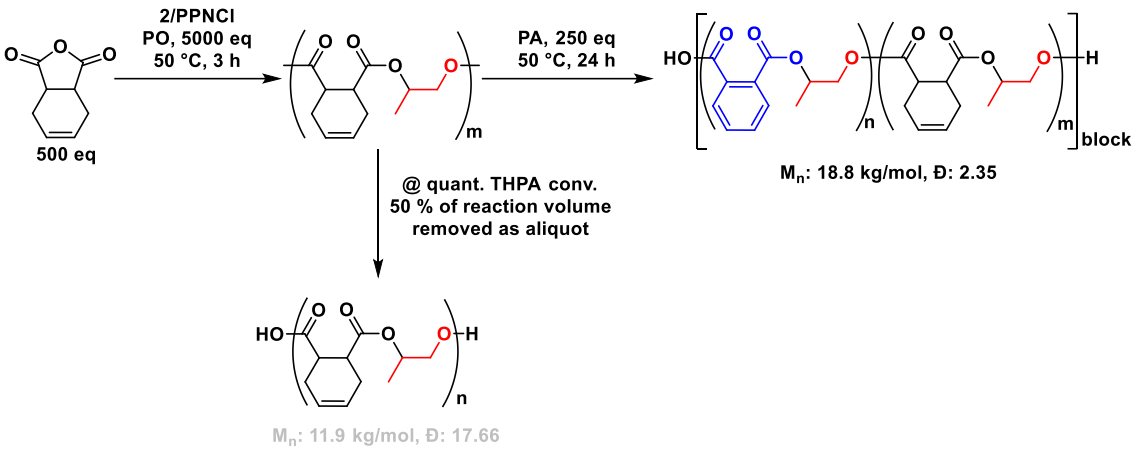

Scheme 27: Reaction sequence to poly(propyl tetrahydrophthalate)-b-poly(propyl phthalate) terpolymer by sequential anhydride addition. conv.: conversion, quant.: quantitative. The grayed-out results are not fully reliable.

Therefore, first THPA was copolymerized with PO at 50 °C under argon atmosphere with **2**/PPNCl. After 3 h of reaction time and full THPA conversion, 50 % of the reaction volume was removed and the polymer was isolated for analysis. The isolated product was already discussed at the beginning of this chapter. Subsequently, 250 equivalents of PA with respect to the catalyst were added to the reaction so that the ratio of the catalyst to PA remained the same as the ratio of catalyst to THPA at the beginning of the reaction. The reaction was carried out in the glovebox and, therefore, no water was present. The reaction mixture was stirred for additional 24 h and the reaction progress was controlled by ^{1}H–NMR spectroscopic analysis. After 24 h of reaction time 53 % of the introduced PA were converted. For the isolated polymer a M_n of 18.8 kg/mol with a *Đ* of 2.35 was observed. Considering the broad molecular weight distribution, one should not expect a block architecture as in Scheme 26 b). Nonetheless, the methylene signals of the propyl moieties of the respective ester segments are well separated in the ^{1}H–NMR spectrum. Additionally, the DOSY spectrum shows a single polymeric species comprising both types of ester segments (Fig. 31).

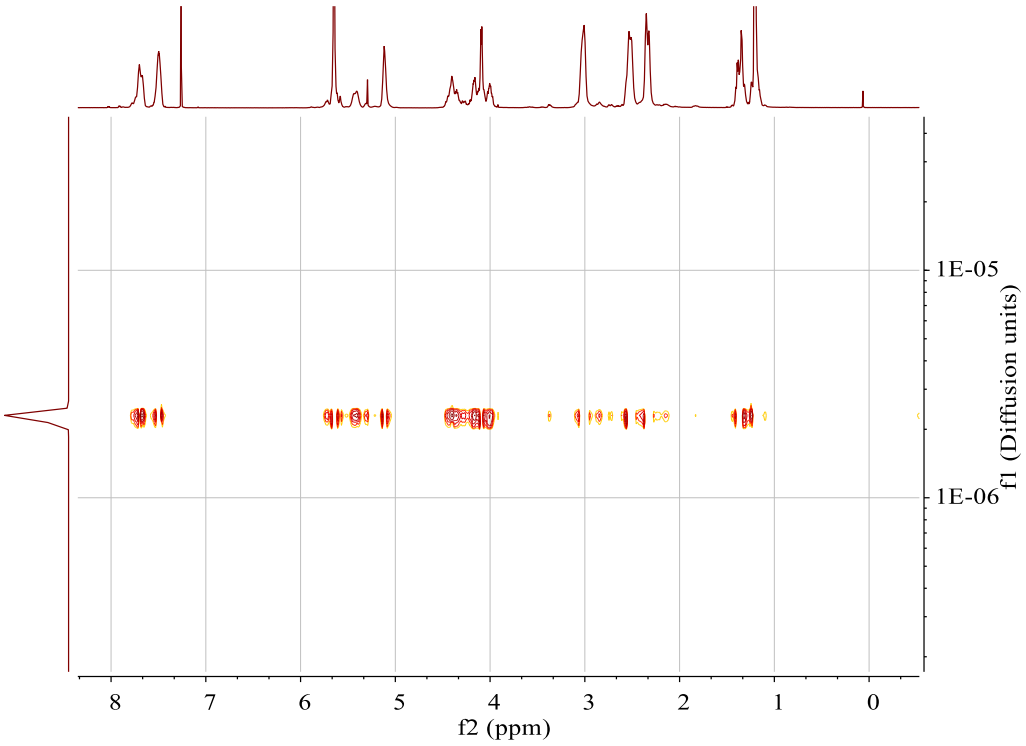

*Fig. 31: ^{1}H–DOSY NMR spectrum of poly(propyl tetrahydrophthalate)-b-poly(propyl phthalate) from sequential anhydride addition and **2**/PPNCl. Diffusion units: cm^2 · s^{-1}.*

Together with the ^{1}H–NMR spectrum a PO-PA content of 33 % was detected. The successful incorporation of PO-PA segments in a block polymer is also indicated by the trend of the intrinsic viscosity of the polymer with increasing molecular weight. The connection of the intrinsic viscosity to the polymer density can be used as a measure for changes in the structure of the polymer, which are introduced by the presence of poly(propyl phthalate) blocks, in this instance. The intrinsic viscosity (IV) is increasing with increasing molecular weight. If an increase in the molecular weight is accompanied by structural changes the IV plot shows “bends” in the trend at characteristic molecular weights. The distribution plot of the polymer provides a good overview on these changes (Fig. 32, IV plot in black boxed regions).

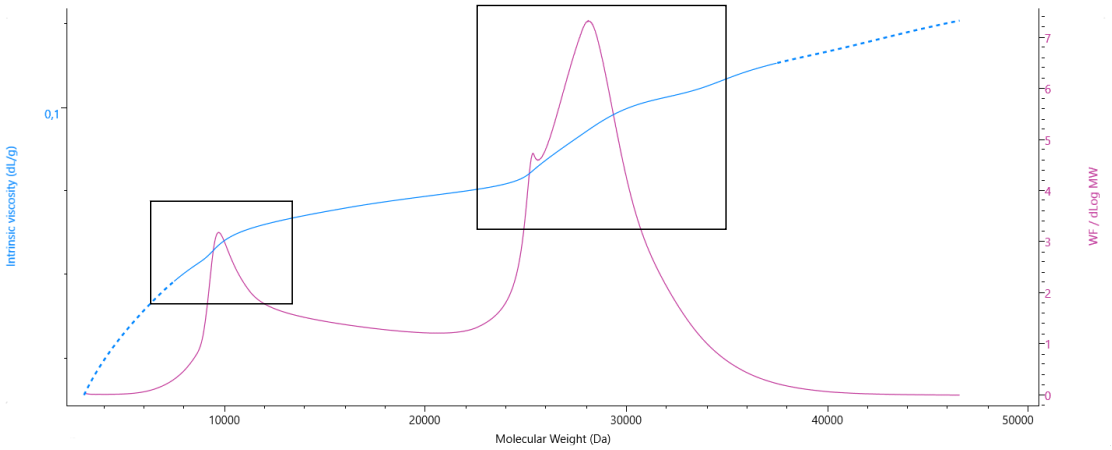

*Fig. 32: Overlay of Molecular weight distribution plot (red scale on right side) and intrinsic viscosity (IV) plot (blue scale on left side) of poly(propyl tetrahydrophthalate)-b-poly(propyl phthalate) from sequential anhydride addition and **2**/PPNCl. Black boxes can be seen as guide to the eye for slope changes in the IV plot.*

The obtained distribution plot indicates two major fractions with comparatively similar molecular weights in the same order of magnitude. At the major fraction the intrinsic viscosity increases rapidly which indicates a strong increase in density. This structural change can be attributed to the introduction of propyl phthalate blocks to the polymer.

To summarize this section, tetrahydrophthalic anhydride proved itself to be not straightforwardly copolymerizable. Particularly, the copolymer synthesis with the employed catalyst systems **1** and **2** is challenging, as the copolymerization proceeds with formation of byproducts and a lack of control. This reaction behavior remains a challenge, particularly with respect to the polymer characterization. This reaction behavior could be addressed to some extend by the introduction of phthalic anhydride. Here, unexpected cooperative effects between the anhydride monomers and the monomeric unit at the active chain ends could be observed. Ultimately, block copolymers of poly(propyl tetrahydrophthalate) and poly(propyl phthalate) could be synthesized successfully. Unexpectedly, a simultaneous copolymerization of both anhydrides was unsuccessful, despite of the difference in reactivity of phthalic anhydride and tetrahydrophthalic anhydride. Still, clear criteria to distinguish the identity of block terpolymers from random terpolymers could be elucidated.

3.2.3 Phthalic Anhydride and Norbornene Anhydride (PA & NA)

3.2.3.1 Solvent effects on PO/PA ROCOP

First, the general impact of the solution mixture on the polymerization mixture was elucidated in the ROCOP of propylene oxide (PO) and phthalic anhydride (PA) for four different complexes (Fig. 14, page 36). With respect to the reaction temperature of 50 °C and to the excess of the low boiling propylene oxide, higher boiling solvents, commonly used in literature, were tested. Therefore, a series of polymerization reactions was performed in toluene, THF and under neat conditions. As anticipated the solvent proved to have a crucial effect on the reaction rate (Table 5, entry 1, 5–9). While the reaction with 50 vol% of toluene (Table 5, entry 1) was almost finished after 3 h of reaction time, the reaction with THF as cosolvent (Table 5, entry 5) led to a conversion of phthalic anhydride to 65 % after 6 h. The neat reaction was slightly faster leading to 86 % conversion of PA after 6 h (Table 5, entry 6). The polydispersities (*Đ*) of the produced polymers in entries 1 and 5 are expectedly narrow. The obtained polymer from the reaction without a solvent additive (Table 5 ,entry 6) shows a somewhat larger *Đ* and exceeds the theoretical molecular weight by ~ 30 %, which implies a potential competitive coordination between an unopened epoxide and the active chain end to the cobalt center. This would lead decrease the reactivity at, at least, one coordination site of the catalyst molecule (less double initiation character) and, therefore, to an increased molecular weight and a broader *Đ* in accordance to the reaction mechanism proposed by *Coates*.[55] Considering the nature of THF as coordinating solvent the decrease of reaction rate can be explained in a similar manner. On the contrary, the reaction in entry 1 shows a significantly lower molecular weight compared to the theoretical value. This observation was generally made for all reactions whose progress was monitored by *in situ* IR measurements. A reaction carried out in the glovebox (Table 5, entry 2) gave similar results to Table 5, entry 6, indicating an insignificant influence of another 5000 equivalents of PO with respect to the catalyst. Therefore, the lower molecular weight obtained from the IR setup can be attributed to contaminations introduced together with the IR probe, despite of thorough cleaning and drying of the probe. Additionally, extended reaction times of 24 h were tested in that context, which led to a strong increase of the *Đ* in all cases due to transesterification (Table 5, entry 7–9). While toluene as solvent is beneficial to the rate of copolymerization, it apparently also increases the rate of transesterification. Still, the *Đ* remains narrow if the reaction is stopped at full conversion. An additional benefit of employing toluene as a

solvent compared to the neat reaction is the overall lower vapor pressure in the reaction vessel at the applied reaction conditions, lowering the risk of PO exposure.

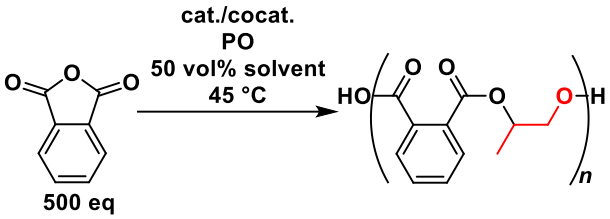

*Scheme 28: ROCOP of PA and PO with catalyst, cocatalyst and cosolvent variation. Cat: complexes **1** or **2**; cocat: PPNCl or PPN(DNP) or TBA(DNP); solvent: toluene or THF or none. The specific reaction setups and results are summarized in Table 5.*

Table 5: Variation of cocatalyst, solvent additive and reaction time in PA/PO ROCOP.

Entry	Cat.	Cocat	Solv.[b]	Conv. (%)	t (h)	TOF (h^{-1})	M_{calc} (kg · mol^{-1})[e]	M_n (kg · mol^{-1})[f]	$Đ$[f]
1[c]	**1**	PPNCl	Tol.	96	3.2	152	49.5	35.5	1.33
2[d]	**1**	PPNCl	Tol.	93	5	93	47.9	59.5	1.41
3[c]	**1**	PPN (DNP)	Tol.	96	2.0	235	49.5	32.6	1.30
4[c]	**1**	TBA (DNP)	Tol.	89	7.5	59	45.9	25.0	1.20
5[d]	**1**	PPNCl	THF	65	6	83	33.5	35.4	1.30
6[d]	**1**	PPNCl	Neat	86	6	83	42.3	54.6	1.47
7[d]	**1**	PPNCl	Tol.	100	24	20	51.5	45.2	1.72
8[d]	**1**	PPNCl	THF	100	24	20	51.5	63.4	1.45
9[d]	**1**	PPNCl	Neat	100	24	20	51.5	55.5	1.55
10[c]	**2**	PPNCl	Tol.	97	3	161	50.0	17.4	1.35
11[d]	**2**	PPNCl	Tol.	96	5	96	49.5	40.0	1.19
12[c, g]	**3**	PPNCl	Tol.	96	5	96	51.5	26.7	1.33
13[c]	**4**	PPNCl	Tol.	99	2.9	171	51.5	31.2	1.49
14	**4**	–	Tol.	85	2.9	147	43.8	14.6	1.34

[a][cat]/[cocat]/[PO]/[PA] = 1/1/5000/500, 45 °C. [b]50 vol%. [c]Reaction was performed in react IR setup, reaction progress was followed with in situ react IR spectroscopic measurement under Ar atmosphere. [d]Reaction was performed in a glovebox under Ar atmosphere, reaction progress was followed by ^{1}H–NMR spectroscopy. [e]Theoretical molecular weight was calculated by $[(conv \cdot M_{Anh+PO} \cdot n_{Anh})/(2n_{cat})]$, assuming a double initiation. [f]Determined by GPC calibrated with polystyrene standards and triple detection. [g]Reaction was performed at 48 °C.

3.2.3.2 Ligand Environment

The ligand backbone and the electronic structure of the ligand was altered in order to investigate the influence of the ligand sphere on the Co center and thus on the polymer formation. Therefore, three complexes were prepared with incremental changes from an aliphatic *R*,*R*-backbone in **1** (Fig. 33) to an aromatic backbone in **2** to an aromatic backbone with *para* fluoro substituents in **3**. The respective anion of the complexes was kept the same.

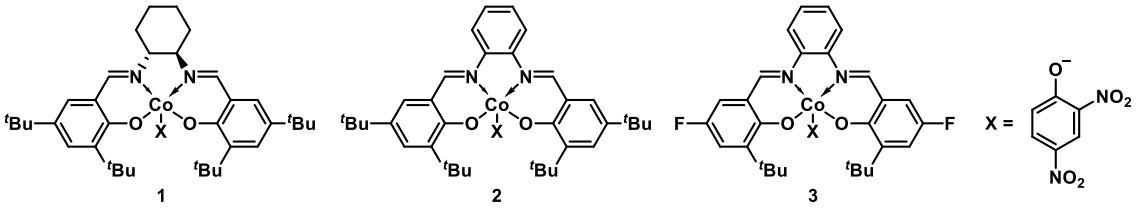

Fig. 33: Incremental changes in Ligand environment in complexes 1 to 3.

Interestingly, the difference in TOF is not as significant as anticipated when the aliphatic *R,R*-backbone is exchanged for an aromatic backbone. The exchange does neither affect the reaction rate in PO/PA (Table 5, entry 1–2 & 10–11), nor in the PO/NA ROCOP (Table 6, entries 1 & 4, page 82), significantly. Although, the overall TOF of the reactions is not affected, the sensitivity of the reaction, and the structure of the resulting polymer, however, is (Table 5, entry 1 vs. 10). Since a racemic mixture of PO was employed, a match/mismatch situation of the PO enantiomers with the complex **1** is occurring. Thus, one enantiomer is preferentially incorporated into the polymer backbone resulting in a resolution of the PO enantiomers.

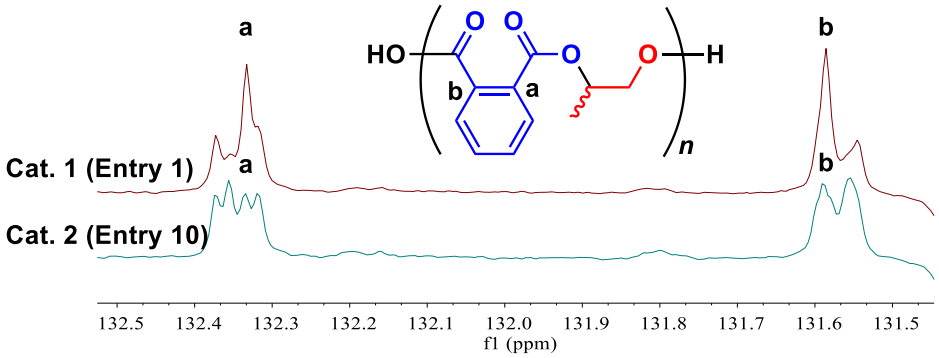

Fig. 34: ^{13}C-NMR spectrum of the aromatic quaternary carbons of the polymers listed in Table 5, entry 1 & 10. The full NMR ^{1}H– and ^{13}C–NMR spectra can be found in Fig. S1 & Fig. S2.

As shown in Fig. 34, complex **1**, in fact, predominantly incorporates one enantiomer. While complex **2** does not differentiate between *R*- and *S*-PO. This could be additionally verified *via* a basic hydrolysis of a representative enantioenriched polyester sample. The hydrolysis of the polyester proceeds with retention of the stereochemistry. Thus, incorporation of *S*-PO in the polymer formation leads to an *S*-stereocenter at the methine carbon of the propylene glycol. To qualitatively support the hypothesis, the resulting propylene glycol was isolated and derivatized using (*R*)-Mosher's acid chloride which was further analyzed by ^{19}F–NMR spectroscopy. A comparison was made by hydrolysis of *R*-PO resulting in predominantly *S*-propylene glycol.[162] Fig. 35 shows the ^{19}F–NMR spectra

from the Mosher esters of the respective propylene glycols. Only two dominant signals were found, one signal which corresponds to the excess of the employed Mosher acid chloride and the other for the propylene glycol derivatives, showing identical chemical shifts. At this point it needs to be mentioned that for an additional verification the procedure should be repeated with racemic or *S*-PO for a comparison, which could not be done in this work because of time restrictions.

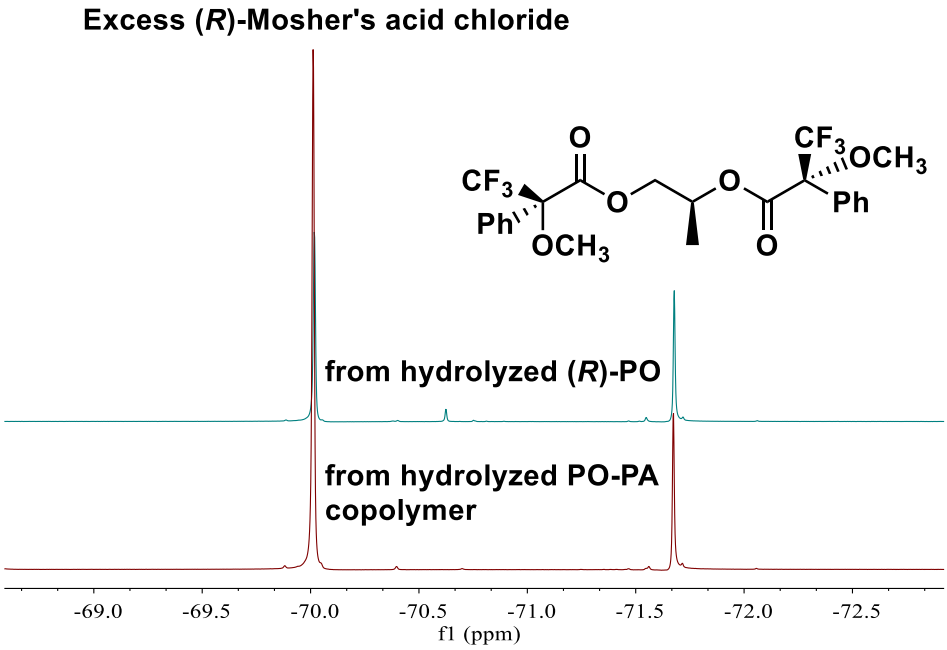

Fig. 35: ^{19}F–NMR spectra of derivatized propylene glycol, obtained from R-PO and from hydrolyzed, enantioenriched PO/PA copolymer.

If the PO/NA copolymerization is considered, the same effect can be observed (Table 6, entry 1 & 4, see page 82). The respective ^{13}C double bond signals are depicted in Fig. 37. If a complex without the preference of one PO enantiomer is employed, an approximate ratio of integrals of 1:2:1 should be found for the *S*,*S*–, the *S*,*R* / *R*,*S*– and the *S*,*S*–dyads of the polymer (see Fig. 37, page 81), which is found in fact for complex **2** (Table 6, entry 4).

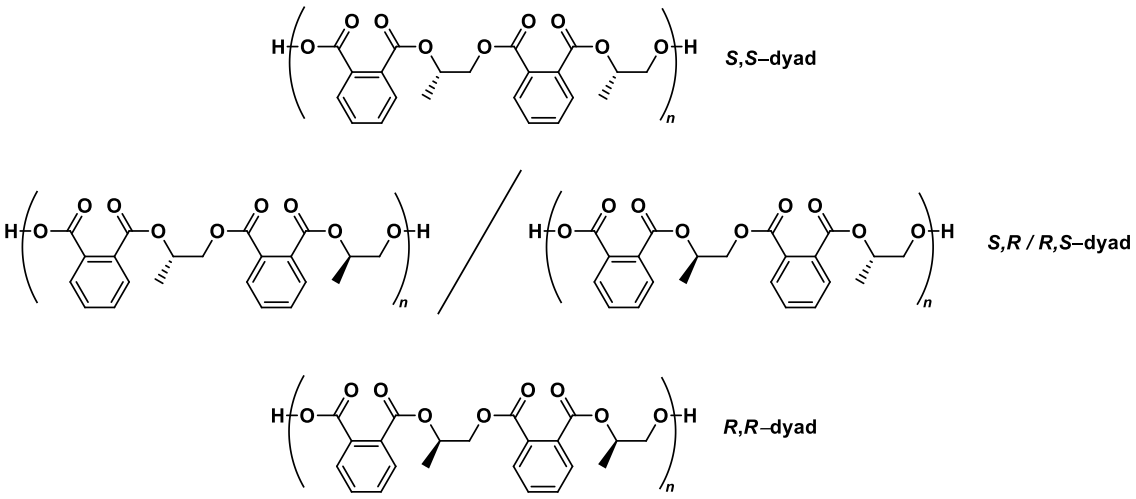

Fig. 36:Possible dyad combination of PO-PA compolymers.

When complex **1** is employed in the polymerization the *S*,*R* / *R*,*S* – *dyads* should be found deminished, resulting in a change of the signal pattern (a) from entry 4 to entry 1 in Fig. 37. Additionally, in the carbonyl region (b) a slight upfield shift of the signals for the enantioenriched polymer alongside with a change in signal pattern can be found. Hence, although the polymer is presumably not fully enantiopure, an enantioenrichment of the polymer becomes evident in this case, as well.

However, the enantioenrichment strongly influences the thermal properties of the material. The enantioenriched PO/PA copolymer shows, interestingly, a decrease of the glass transition temperature (T_g) from 52 °C for the racemic polymer to 47 °C for the enantioenriched polymer (Table 5, entry 1 vs. 4). This observation is counterintuitive to some extent, because an enantioenrichment should lead to a higher degree of crystallinity, which should shift the T_g to higher temperatures as the glass transition temperature correlates often with the melting temperature of polymers.[3] However, as complex **2** is achiral, no PO enantiomer should be preferred. This is additionally represented by Fig. 34, entry 10 **a**, with equal intensities for *ii, ss, is* and *si* connectivity. Considering that both, the enantioenriched and the racemic polymer are fully amorphous, the random incorporation of the PO into the polymer backbone could facilitate a higher degree of entanglement than in the enantioenriched analogue, because of a lower mobility of chain segments. This would lead to an increase of the measured T_g, as well.

In the copolymerization of NA with PO complex **1** produces a polymer without a observable T_g or melting point. Complex **2** on the other hand, provides a polymer with a T_g observed at 126 °C. Because of the bicyclic nature of the norbornene anhydride the chain stiffness would be reduced in this case (see Scheme 14, see page 18).

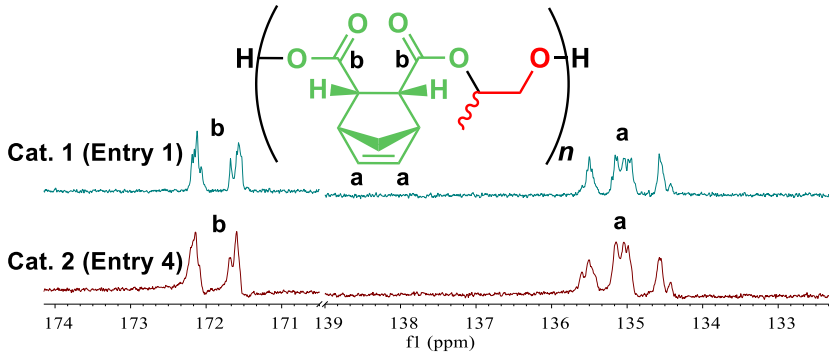

Fig. 37: ^{13}C–NMR spectrum of the double bond (a)- and the carbonyl carbons (b) of polymers listed in Table 6 (page 82), entry 1 & 4. The full NMR ^{1}H– and ^{13}C–NMR spectra can be found in Fig. S3 & Fig. S4.

As already shown by *Coates*[58], ligands decorated with electron withdrawing substituents in *para* position lead to a slower reaction rate, but also avoid epimerization reactions in PO/NA ROCOP in aluminum complexes. An increase in Lewis acidity leads not only in *Coates'* system to a decreased reaction rate, but also when Co is employed as coordinated metal. The *para*–fluorinated Al system showed a debase of 45 % in TOF while the Co–based systems where slightly less affected and performed only 40 % slower in, both, PO/PA and PO/NA ROCOP, because of the generally lower Lewis acidity of Co vs. Al (Table 5, entry 10 vs. 12, page 77; Table 6, entry 4 vs. 5, page 82). At longer reaction times the aluminum complexes showed epimerization of the polymer which could be clearly identified by the carbonyl signals in ^{13}C–NMR spectra according to *Coates'* studies. As mentioned earlier the polymerization reactions that were monitored by *in situ* IR measurements led to a lower molecular weight polymer compared to reactions performed in the glovebox. Cat. **3** ≡ complex **3** with the *para*–fluoro–substituted ligand resulted in an increase of molecular weight in the PO/PA ROCOP (Table 5, entry 12, page 77) by 53 % compared to cat. **2** ≡ complex **2**, indicating diminished amount of side reactions. For the PO/NA ROCOP no epimerization could be observed in our experiments.

Table 6: Catalyst and cocatalyst variation in PO/NA ROCOP.

Entry[a]	Cat.	Cocat.	t (h)	TOF (h^{-1})	M_{calc} (kg · mol^{-1})[b]	M_n (kg · mol^{-1})[c]	$Đ$[c]
1	**1**	PPNCl	3.5	114	55.5	36.7	1.22
2	**1**	PPN (DNP)	3.6	140	55.5	38.0	1.20
3	**1**	TBA (DNP)	23	21	55.5	23.2	1.50
4	**2**	PPNCl	3.9	122	53.3	36.4	1.21
5	**3**	PPNCl	6	72	55.5	32.5	1.27
6	**4**	PPNCl	2.5	185	52.5	26.8	1.32
7[d]	**4**	–	6.8	73	55.5	20.9	1.29

[a][cat]/[cocat]/[PO]/[NA] = 1/1/5000/500, 47 °C, 50 vol% toluene, reaction progress was followed by in situ react IR spectroscopic measurement under Ar atmosphere. [b]Theoretical molecular weight was calculated by [($conv_{Anh}$ · M_{Anh+PO} · n_{Anh})/$2n_{cat}$]. [c]Determined by GPC calibrated with polystyrene standards employing triple detection. [d]Reaction was performed at 40 °C. All substrates were fully converted. Slight variations in M_{calc} are due to weighing inaccuracies.

In addition, to complexes **1**–**3**, the racemic complex **4** was tested for both copolymerization reactions. The ligand system was described by *Lu* in the context of the copolymerization of CO_2 with epoxides and it was shown that no cocatalyst was required if the ligand already comprises a cocatalyst moiety.[104] For initial catalytic experiments with **4**, copolymerization reactions with and without PPNCl were performed (Table 5, entry 13 & 14, page 77 Table 6, entry 6 & 7, page 82). PPNCl accelerated the reaction in both polymerization reactions in comparison to complex **1**/PPNCl. The copolymerization of PO with PA (Table 5, entry 13 & 14) led to a TOF of 147 h^{-1} without additional cocatalyst. In the presence of one equivalent of PPNCl the reaction accelerates to a TOF of 171 h^{-1}. Interestingly, the molecular weight dropped to a third of the calculated theoretical molecular weight for Table 5, entry 14, while the $Đ$ remained narrow. Although the structure of the produced polymer was not fully investigated, the formation of cyclic products could diminish the molecular weight. Another possibility can be the formation of a dormant species facilitated by the second anchor at the ligand backbone, which would then act as a kind of shuttling agent.

In the case of the copolymerization of PO with NA the difference between the TOFs of the reactions with and without the employment of PPNCl with cat. 4 was found to be even more significant. If PPNCl is employed (Table 6, entry 6) a decent TOF of 185 h^{-1} was observed. In the absence of an additional cocatalyst the TOF was debased to only 73 h^{-1}

(Table 6, entry 7). However, the drop in molecular weight was not as pronounced in the PO/NA copolymerization as in the PO/PA copolymerization.

3.2.3.3 Cocatalyst Effect on PO/PA & PO/NA ROCOP

Besides the employed metal complex, the cocatalyst plays an important role in the discussed catalyses. PPNCl is widely used as cocatalyst and proved itself to be efficient in the copolymerization of PO and CO_2 and in the copolymerizations of anhydrides and epoxides, as well. Still, there might be unrecognized potential in this reaction system. Hence, two other cocatalysts were synthesized using 2,4-dinitrophenolate as a constant counter anion. PPN(DNP) and TBA(DNP) were both tested in the ROCOPs of PO/PA and PO/NA (Table 5, entry 3 & 4, Table 6, entry 2 & 3). The phosphino ammonium cocatalysts, PPNCl and PPN(DNP), showed not only much higher activity, but produced also higher molecular weight polymers compared to TBA(DNP) (Fig. 38). An overview of the calculated turnover frequencies is provided in Fig. 38. When TBA(DNP) is employed as a cocatalyst a strong broadening of *Đ* in PO/NA copolymerization (Table 6, entry 3) was observed, which can be attributed to transesterification. The large difference in activity can be rationalized by the lower steric demand near the electrophilic center of the PPN cocatalysts compared to TBA. Exchanging chloride in PPNCl by 2,4–dinitrophenolate allowed to elucidate the effect of the cocatalyst counter anion. As the chloride anion is exchanged by the stronger base 2,4-dinitrophenolate the TOF increases significantly in both ROCOP reactions. Interestingly, the exchange of the anion has a significantly stronger effect on the PO/PA ROCOP than on the PO/NA copolymerization. The PO/NA copolymerization is accelerated only by 23 % while the PO/PA copolymerization is accelerated by 54 %.

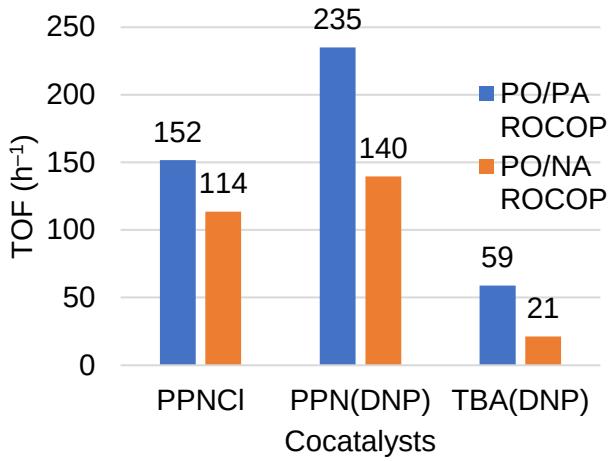

*Fig. 38: Comparison of TOF of PO/PA & PO/NA ROCOP with **1** and cocatalyst variation. Data from (Table 5, entries 1, 3, 4 & Table 6, entries 1-3).*

Thus, all catalyst and cocatalyst components are of mayor importance for fine tuning of the reaction. This represents an example of a mayor impact of a minor change in the reaction system. The exchange of the anion in the context of salen complexes was partly covered in related reaction systems for the copolymerization of CO_2 and epoxides.[55-57, 66, 87] However, systematic anion exchange in the catalyst or the cocatalyst are not well investigated in the literature.

3.2.3.4 Kinetic Investigation of PO/PA ROCOP

In order to obtain a better picture of the whole reaction system, the polymerization kinetics were investigated with complex **2**, as catalysts with fully aromatic backbones are currently widely used in the literature in ROCOP polyester synthesis. Since the general reaction mechanisms for the complexes **1**,**2** and **3** are expected to be similar, the study focused only on complex **2** in order to obtain a general trend. For the kinetic analysis the rate constants were calculated for the first 20 % conversion using the linear part after the induction period.

The copolymerization of phthalic anhydride and propylene oxide was considered as test reaction and the progress was followed by *in situ* IR spectroscopic measurements. While the reaction conditions were kept constant, the amount of employed anhydride was varied in a range between 100 and 1000 equivalents. The obtained rate constants are plotted in Fig. 39.

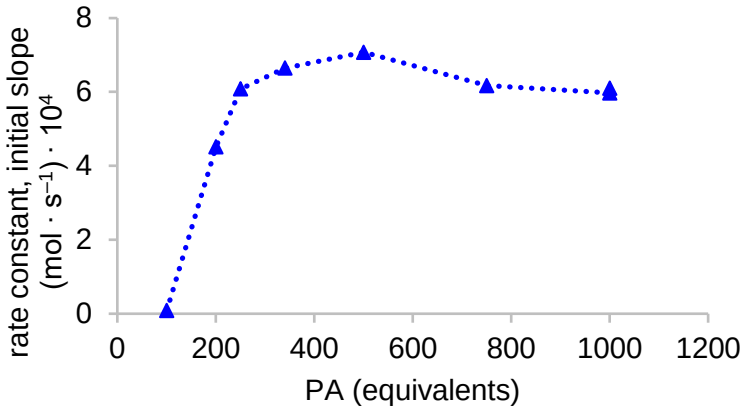

Fig. 39: Reaction rates of first 20 % PA conversion with variation of PA concentration, [cat]/[PPNCl]/[PO] = 1/1/5000, 50 °C, 50 vol% toluene, reactions were performed with React IR setup, reaction progress was followed by in situ IR spectroscopic measurement under Ar atmosphere. [cat]: ***2****. The dotted line is a guide for the eye.*

The reaction rate generally increases with increasing amount of phthalic anhydride. Compared to a rate of $8.4 \cdot 10^{-6}$ mol · s^{-1} with 100 equivalents of PA, the rate increases drastically by two orders of magnitude at 200 equivalents of PA. Increasing the amount of substrate further resulted only in a moderate increase of the rate. The highest rate of $7.1 \cdot 10^{-4}$ mol · s^{-1} was observed at 500 equivalents of PA. Interestingly, the kinetics change when the concentration of PA is further increased. While in the first branch the kinetic behavior appears to be linear (up to 250 equiv PA), which corresponds to first order kinetics, the second part of the curve (250 equiv to 1000 equiv) reaches a saturation regime which corresponds to a zero-order reaction kinetic. Increasing the amount of anhydride equivalents above 500 even tends to decrease the observed reaction rates, which results from substrate inhibition. A potential substrate inhibition effect was already observed in PO/MA ROCOP and will be addressed in this context in detail below. Nevertheless, for clarification further experimental data needs to be collected. With respect to the obtained data all polymerization experiments were performed using 500 equivalents of anhydride.

3.2.3.5 Sequential Addition: PO/PA and PO/NA ROCOP

Thanks to the broad general substrate scope of the salen complexes there is a high potential for a variation of material properties, which is made possible by the synthesis of (block) polyesters and the post–polymerization modification thereof. In order to investigate the catalyst system's behavior in the classical strategy of a sequential monomer addition to generate block terpolymers the anhydrides were first tested separately. As a model system the ROCOP of PO and PA was investigated in 1:1 and 1:2 ratios of the sequential additions. Subsequently, the investigation of sequential addition was expanded to NA and the mixed addition of both anhydrides.

In this context the effect of the aromatic backbone in complex **2** was also tested in the ROCOP of PO and PA. A summary of the performed copolymerizations can be found in Table 7. Interestingly in a 1:1 addition, the initial reaction rates increase with both catalysts (Table 7 entry 1 & 2) after the first portion of anhydride is consumed (Fig. 40). If complex **2** is employed in catalysis, the reaction time to consume 250 equivalents of PA in the second portion is 16 % shorter than for the first portion of the reaction (Table 7, entry 1, Fig. 40, **B**). The initial reaction rate for the respective second portion, however, is nearly identical. Hence, the efficiency of the (re)initiation of the polymerization reaction is the same for the 2nd portion of PA as for the first, but an acceleration takes place in the course of the reaction with the second batch of PA.

Table 7: Reaction rates of PO/PA and PO/NA ROCOP at sequential anhydride addition.

Entry[a]	Cat.	Anhydride	equiv Anhydride[b]	t (h) 1st/2nd run	k_{init} (mol · s^{-1})[c]
1	2	PA	250/250	2.15/1.85	6.08/6.13
2	1	PA	250/250	1.98/1.90	9.12/9.18
3	1	PA	250/500	1.83/4.66	8.98/2.48
4	1	NA	250/500	2.90/5.42	3.45/2.61

[a][cat]/[PPNCl]/[PO] = 1/1/5000, 47 °C, 50 vol% toluene, reactions were performed with React IR setup, reaction progress was followed by in situ react IR spectroscopic measurement under Ar atmosphere. [b]Equivalents of the respective anhydride employed sequentially. [c]Reaction rate for first 20 % of anhydride conversion.

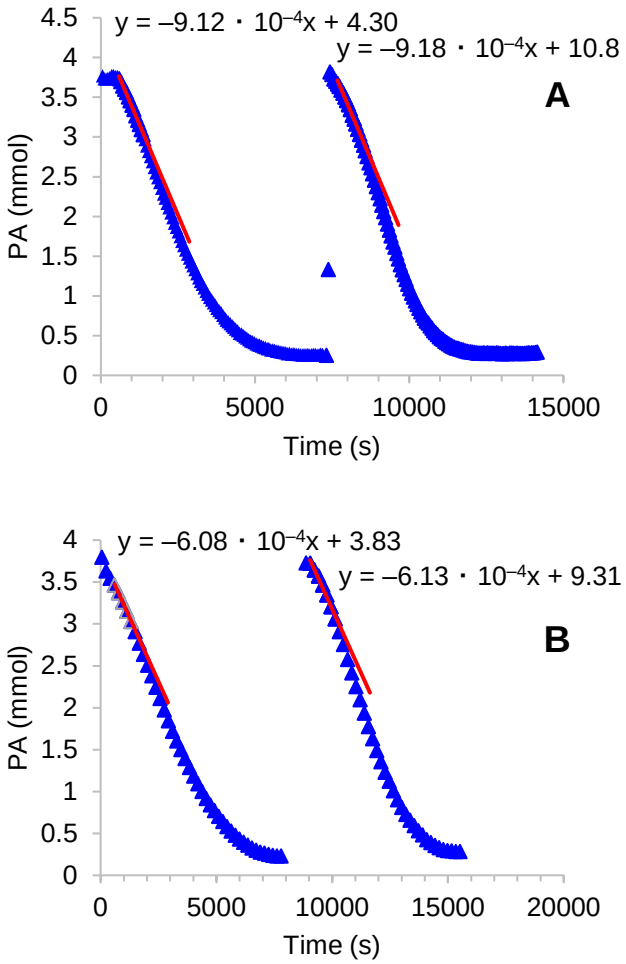

*Fig. 40: **A**: Kinetic measurement of PO/PA copolymerization with **1**/PPNCl as catalyst system and sequential anhydride addition (Table 7, entry 2), cat. **B**: Kinetic measurement of PO/PA copolymerization with **2**/PPNCl as catalyst system and sequential anhydride addition (Table 7, entry 1).*

This observation can also be made with complex **1** (Table 7, entry 2, Fig. 40, **A**). Here, the acceleration of the second reaction step is not as pronounced as in entry 1. Different observations can be made when 500 equivalents of PA are employed in the second reaction step. Instead of an acceleration of the reaction, which would be in agreement with the previous results and the kinetic investigation of the copolymerization of PO and PA, the initial reaction rate is debased by 73 % for PO/PA (Table 7, entry 3) and 24 % for PO/NA (Table 7, entry 4) copolymerizations (see Fig. 41). Considering Table 7 entry 3, the first portion of the anhydride was consumed according to the previous observations. After the addition of another 500 equivalents of PA to the reaction system, the polymerization starts significantly slower, but accelerates during the reaction as more and more anhydride is consumed (Fig. 41, **A**). A similar acceleration effect can be observed for Table 7 entry 4 (Fig. 41, **B**). Fig. 41 shows the reaction progress as observed by *in situ* IR spectroscopy.

The reaction rates for the marked regions were obtained from the slope of the linear regression (see Table 7, entry 3). While the conversion rate slows down towards the end of the first part of the reaction, the rate of conversion increases during the second part of the reaction. As a result, the linear part of the reaction can be found in the last 20 % of conversion, indicating the fastest rate (Fig. 41, **A**). Although the reaction rate increases during the consumption of the second portion of anhydride, the rate does not reach the reaction rate of the first sequence. To emphasize the difference of the slopes between the different regimes, they are marked in Fig. 41 **A** and Fig. 41 **B**.

Although not exactly the same catalyst was investigated in the kinetic study (Fig. 39), similar kinetics are anticipated for the complex **1**. Thus, the reaction rate should decrease with a decreasing amount of anhydride, according to the observed pseudo-first-rate behavior.

As shown earlier, the concentration of reactants in the reaction solution has a strong impact on the reaction kinetics. To exclude an impact on the reaction kinetics because of the consumption of PO, a 20-fold excess of PO was employed in the first reaction part in all discussed experiments. After the first part of the reaction was completed, still a 9.5-fold excess of PO with respect to anhydride was present at the second monomer addition. Therefore, the overall concentration increase in the PO solution was considered not significant. However, instead the anticipated reaction progress, such as in Fig. 40, a substrate inhibition behavior was observed (Fig. 41). The already active polymerization in combination with free unreacted anhydride blocked the coordination of PO at the active site of the catalyst. As the anhydride cannot homopolymerize, the rate of polymerization increases as the cobalt center becomes more accessible for the PO when the excess of employed PO is reduced during the reaction.

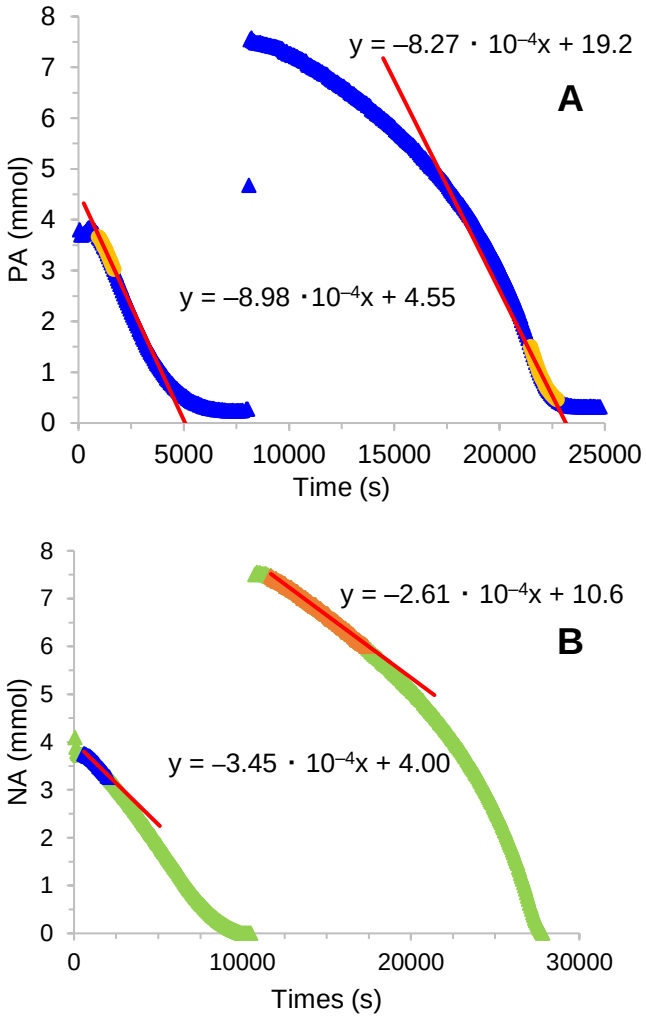

*Fig. 41: **A**: Reaction progress of PO/PA ROCOP with sequential addition of PA of 250 equiv. and 500 equiv., catalyzed by **1**/PPNCl, Table 7, entry 3. **B**: Kinetic measurement of PO/NA copolymerization with **1**/PPNCl as catalyst system and sequential anhydride addition (Table 7, entry 4). The line represents the linear regression for the marked region. The different regions are marked to emphasize differences in reaction progress.*

A kinetic investigation with a similar Al salen complex was performed by *Coates* and coworkers who observed a zero-order dependence of the reaction rate on the employed anhydride and a first order dependence with respect for the epoxide.[158] In *Coates'* studies a two to five fold excess of butene oxide over carbic anhydride with about 1 % catalyst loading with respect to anhydride was employed.

Moreover, *Coates'* group showed in the same study that a 1:1 ratio of anhydride and epoxide did not lead to any reaction beyond the formation of the initiating bis(alkoxide) complex species. *Coates* rationalizes this observation with the low concentration of Al-bis(alkoxide) complex. Additional polymerization experiments with a 1:1:100:100 ratio of IIIb:PPNCl:butene oxide:carbic anhydride showed a prolonged initiation phase which was discussed by *Coates* to support the above mentioned observations. This finding would

support the observation of a potential substrate inhibition by the anhydride, hypothesized herein, because the reaction rate increases with decreasing anhydride concentration. However, the data, shown in this study, adds an additional aspect to the studies of *Coates*. That is, the rate of polymerization steadily increases with the consumption of anhydride in the second part of the reaction. This acceleration of the reaction can indeed be observed in Fig. 41. Nevertheless, it is important to note that as soon as the concentration of anhydride should reach the concentration level of the first part of the reaction, the rates of polymerization should be equal. This is not strictly the case as seen in Fig. 41. This observed difference between the first and the second part of the polymerization reactions should be subject to further investigations to exclude the observation to be an artefact caused by modelling operations in the IR spectrometer software.

3.2.3.6 Sequential Addition: PO/NA/PA ROCOP

As next step towards the synthesis of block terpolymers the sequential addition of two anhydrides was investigated. In the sequence, first 250 equivalents of NA with respect to the catalyst were employed. After complete consumption of NA, another 500 equivalents of PA were added to the reaction system. In contrast to previous observations in the sequential anhydride addition, no inhibition behavior can be observed in this case (Fig. 42). The consumption of phthalic anhydride begins directly after addition and is, as anticipated, faster than that of the norbornene anhydride.

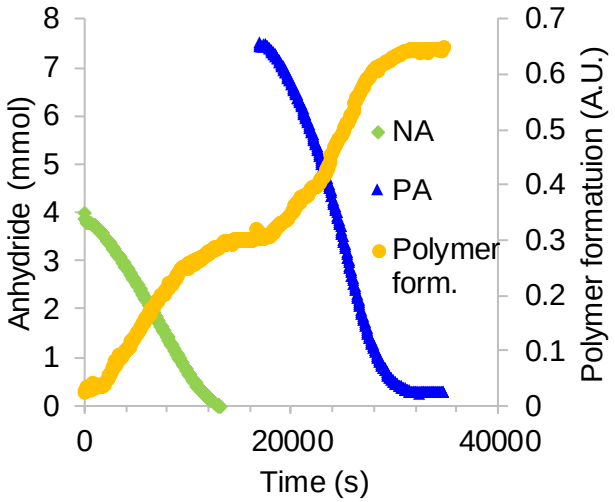

*Fig. 42: Consumption of cis-endo-5-norbornene-2,3-dicarboxylic anhydride (NA), phthalic anhydride (PA) and polymer formation. [cat]/[PPNCl]/[PO]/[PA]/[NA] = 1/1/5000/500/250, 40 °C, 50 vol% toluene, reactions were performed in React IR setup, reaction progress was followed by in situ IR spectroscopic measurements under Ar atmosphere. [cat]: **1**/PPNCl.*

The formation of the carbonyl bands of the respective polymer segments can be distinguished as the reaction progress was followed by *in situ* IR spectroscopy (Fig. 43). A further deconvolution also reveals overlapping IR bands. This is particularly important for the investigation of anhydride consumption when two anhydrides are added simultaneously. The polyester carbonyl band of the NA-PO polyester can be observed at about 1745 cm^{-1} while the polyester carbonyl band of the PA-PO segments arise after PA addition at about 1730 cm^{-1} (Fig. 43).

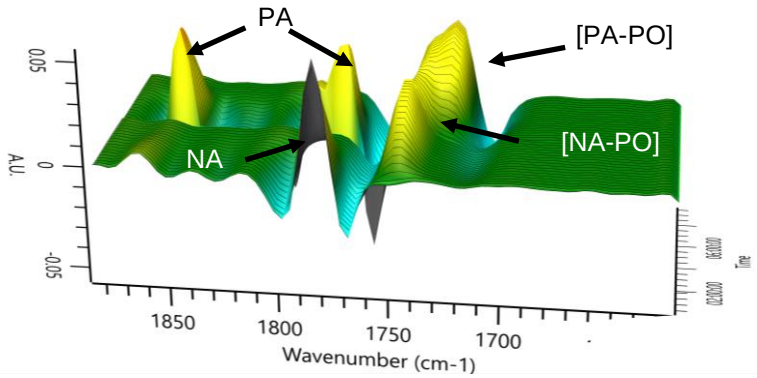

Fig. 43: Deconvoluted 3D plot of sequential anhydride addition of NA followed by PA, [cat]/[PPNCl]/[PO]/[PA]/[NA] = 1/1/5000/500/250, 40 °C, 50 vol% toluene, reaction progress was followed by in situ IR spectroscopic measurement under Ar atmosphere. [cat]: ***1****.*

The strategy of a sequential addition of monomers and thereby to synthesize block polymers is on the one hand simple and powerful, but, on the other hand, can bear the problem of connectivity. If the active chain ends are terminated in the process of a sequential addition and the formation of a new chain is entropically favored compared to a chain propagation, the resulting polymer is a blend of two polymers instead of a block polymer. In that case the material properties might not be the targeted ones. An NMR spectroscopic analysis of the sequential anhydride addition (reactions shown in Fig. 42 & Fig. 43) proves the block architecture of the polymer. The 1:2 ratio of the anhydrides should clearly allow to distinguish in DOSY NMR spectra if the blocks of the two formed polyesters are connected. ^{1}H–NMR spectra suggest a block architecture, because the methylene signals are well separated (Fig. S7). Additionally, the DOSY NMR spectrum (Fig. S8) shows a single trace, which proves the connectivity. Moreover, considering the low UV activity of the PO-NA segments compared to PO-PA, a polymer blend with large difference in molecular weight should be easily distinguishable in a GPC trace with triple detection and an additional UV/Vis detector. Instead, a strong UV response can be found throughout the whole distribution (Fig. S38 vs. Fig. S39). Based on these results further investigations were performed on the preference of incorporation of the two anhydrides in a one-pot

reaction system. However, in this case transesterification might cause the UV response throughout the whole molecular weight distribution.

3.2.3.7 Direct Addition: PO/NA/PA ROCOP

As it was shown in the previous section, stepwise addition is a convenient strategy for the formation of block polyesters. However, a stepwise addition can be an additional complication in terms of continuous processes. Therefore, self-controlling systems where a single catalyst is capable to incorporate different analogues of a monomer, with one monomer being incorporated preferentially before the other, would be a step towards more versatile polymerization systems.

Here, a ternary system of PA, NA and PO was investigated regarding the preferential incorporation of one anhydride. For that, all monomers were combined right from the beginning and the mixture was then heated to 43 °C. The incorporation probability of the respective anhydride was plotted over the course of the reaction, taking into account the rate of consumption of each anhydride using the deconvoluted collected data (Fig. 44) from *in situ* IR measurements. The consumption of anhydride was divided into linear parts from which the rate constant was calculated. The analysis was performed with a 1:2 and a 1:1 ratio of NA and PA. At an initial 1:1 ratio of the anhydrides (Fig. 44 **A**) NA is incorporated with a probability of 28 % which increases to a probability of 53 % at a PA conversion of 76 %. As the PA is converted faster than the NA, the probability of NA incorporation reaches the highest probability of 95 % at 98 % conversion of PA. Hence, at a high conversion of PA the probability of an incorporation of PA remains at 5 %. Because of the differences in reaction rates, a gradient-like polymer architecture is formed in the course of the reaction. Additionally, it is noteworthy that the reaction rate of the consumption of norbornene anhydride increases, once 50 % of the phthalic anhydride is consumed. This causes a step in the probability plot, because of the faster consumption rate of NA and the simultaneously decelerating consumption of PA.

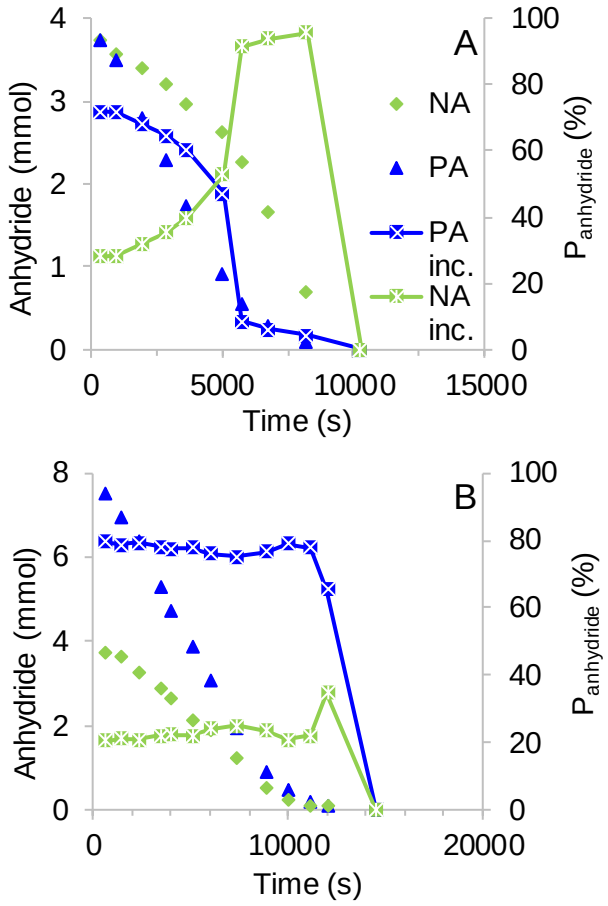

*Fig. 44: Anhydride consumption at simultaneous addition of PA/NA and incorporation probability of the respective anhydride. **A**: PA/NA = 250/250, **B**: NA/PA = 250/500, [cat]/[PPNCl]/[PO] = 1/1/5000, 43 °C, 50 vol% toluene, reaction progress was followed by in situ React IR spectroscopic measurement under Ar atmosphere. [cat]: 1/PPNCl.*

As the amount of phthalic anhydride is increased the consumption of the anhydrides proceeds in a different fashion. When a 1:2 ratio of NA and PA is employed, a constant incorporation of PA, as well as, of NA is observed (Fig. 44 **B**). The consumption rate is constant leading to a constant incorporation of NA and PA in a ratio of around 24:76. Just before the conversion of PA is completed, the probability of NA incorporation exhibits a spike. This is because the concentration PA lies below the concentration of NA. This leads to a brief increase in incorporation probability of NA, just before all anhydride is consumed.

All in all, a different polymer architecture can be produced by changing the initial ratio of the two anhydrides. While at a 1:1 ratio a gradient, triblock, structure is formed, a 1:2 ratio leads to a random distribution of PO-NA segments along the PO-PA polyester chain. Fig. 45 illustrates the monomer consumption as a sum of the IR spectroscopic signals of the respective repeating units in the polymer formation. Fig. 45 **A** illustrates the offset of the polymer formation with the predominant formation of poly(phthalic acid propyl)ester in the beginning of the polymerization, followed by poly(norbornene dicarboxylic acid

propyl)ester formation later in the reaction progress. Fig. 45 **B** illustrates the simultaneous formation of both polymer segments with a faster carbonyl signal growth of the PO-PA repeating units. Additional evidence for the structural change with increasing molecular weight is provided by the overlay of the GPC chromatogram and the intrinsic viscosities Fig. 46. The retention time of a polymer fraction is dependent on the hydrodynamic volume which correlates with the molecular weight. A strong step in the intrinsic viscosity is evident with increasing molecular weight (i.e. shorter retention times) at the transition to the main polymer fraction (Fig. 46, black box). This change in intrinsic viscosity indicates structural alteration due to an increasing amount of incorporated PO-NA segments. Naturally, a change is observable in PO/PA copolymers with increasing molecular weight, as well, as the polymer structure in solution is also dependent on the molecular weight. However, this change is not as pronounced as the introduction of another monomer into the polymer structure.

The isolated polymer from Fig. 44 B with its constant composition shows a constant trend in intrinsic viscosity, as well. The mentioned GPC trace is provided in Fig. S41 in the appendix.

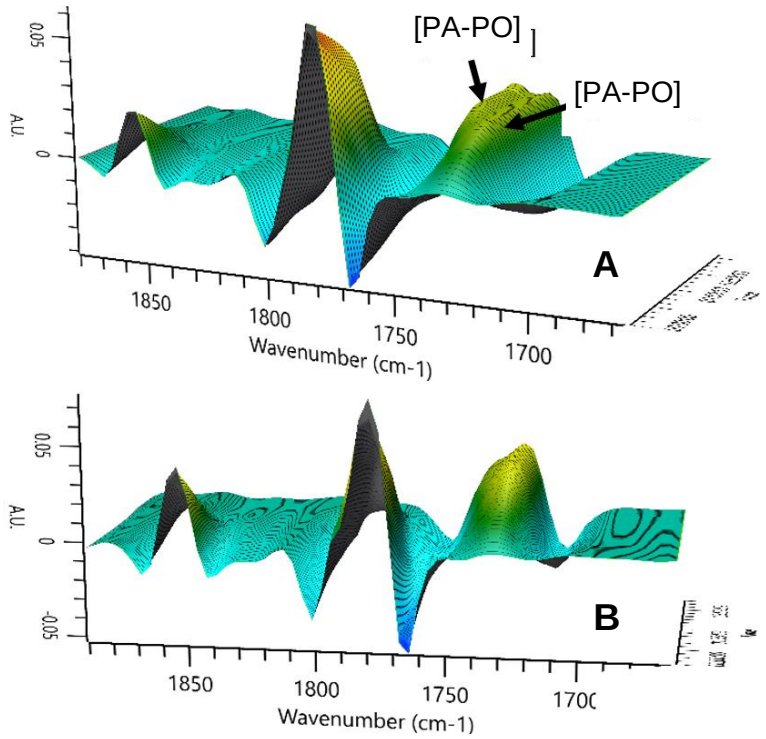

*Fig. 45: Deconvoluted 3D plots of direct addition of PA & NA. **A**: PA/NA = 250/250, **B**: PA/NA = 250/500. [cat]/[PPNCl]/[PO] = 1/1/5000, 43 °C, 50 vol% toluene, reaction progress was followed by in situ IR measurement under Ar atmosphere. [cat]: **1**/PPNCl.*

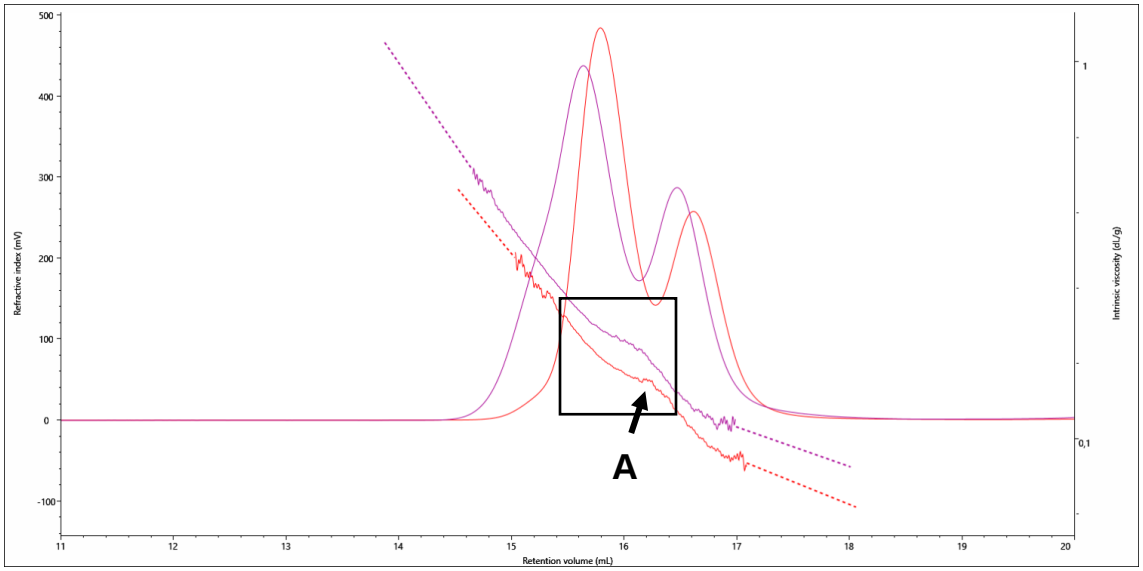

*Fig. 46: Representative GPC trace of PO/PA/NA terpolymer with **1**/PPNCl as catalyst system and direct anhydride combination (250 equiv. PA and 250 equiv. NA) (red) vs. GPC trace of PO/PA copolymer (purple). Intrinsic viscosity (IV) of the terpolymer progresses with a step transition **A** between the modes while IV of the PO/PA copolymer shows a smooth transition.*

3.2.3.8 ROCOP of PA/PO and NA/PO under CO_2 Atmosphere

Co salen complexes are not only known to catalyze the copolymerization of anhydrides and epoxides, they also catalyze the ring–opening copolymerization of epoxides with CO_2. As a consecutive step for the synthesis new materials, such as polyester carbonates, the influence of a CO_2 atmosphere on the ROCOP of anhydrides and epoxides was tested. To elucidate the potential of combined polyester/polycarbonate synthesis with the discussed catalyst system, the discussed copolymerization and terpolymerization systems were tested under CO_2 atmosphere.

As a first step, each polyester synthesis was performed separately under CO_2 atmosphere. Fig. 47 provides an overview of the PA consumption, the polyester formation and the polycarbonate formation. Fig. 49 depicts the corresponding deconvoluted 3D plot of the *in situ* IR measurement. The formation of polyester appears to proceed faster at very low conversions than the formation of polycarbonate. At a PA conversion of about 12 % the formation of polycarbonate appears to overcome an induction period and continues slightly faster than the formation of polyester. The delay of the onset of the polycarbonate formation should strongly depend on the speed and quality of the agitation and consequently on the concentration of CO_2 in solution. The impact of this relationship was not investigated in this study.

Although the formation of the ester and the carbonate segments seems to proceed almost with equal rates in the steady state, the incorporation was probably not strictly alternating. A comparison with reaction rates of the polymer formation of the individual polyesters and polycarbonates revealed that both bond formations, the ester and the carbonate, proceed significantly faster separately than in the reaction illustrated in Fig. 47. A detailed comparison of the change of the polymer formation rates for the polymerization with and without the CO_2 atmosphere can be found in Fig. 48. The copolymerization of PO and PA, catalyzed by **1**/PPNCl in the absence of CO_2, proceeds rapidly, followed by the copolymerization of PO and CO_2. When all monomers are combined in a terpolymerization process the formation of carbonate proceeded faster than the formation of polyester. This is indicative for a competitive coordination of the monomers to the catalyst, strongly slowing down all reactions. Again, the block architecture can be conveniently distinguished from random incorporation by NMR spectroscopy (see Fig. S14 & Fig. S15 vs. Fig. S16 for comparison).

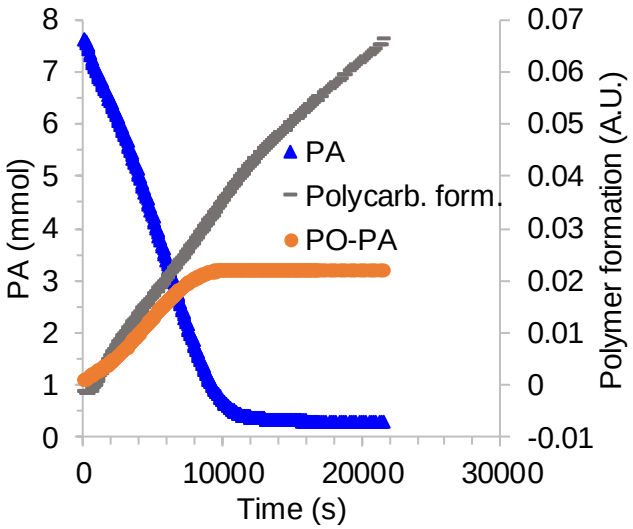

*Fig. 47: Consumption of PA and formation of polypropylene carbonate (Polycarb.) and PO-PA segments. [cat]/[PPNCl]/[PO]/[PA] = 1/1/5000/500, 40 °C, 50 vol% toluene, reaction progress was followed by in situ react IR spectroscopic measurement under CO_2 (10 bar) atmosphere, [cat]: **1**/PPNCl. The data for the PO-PA formation was graphically corrected due to a measurement artifact.*

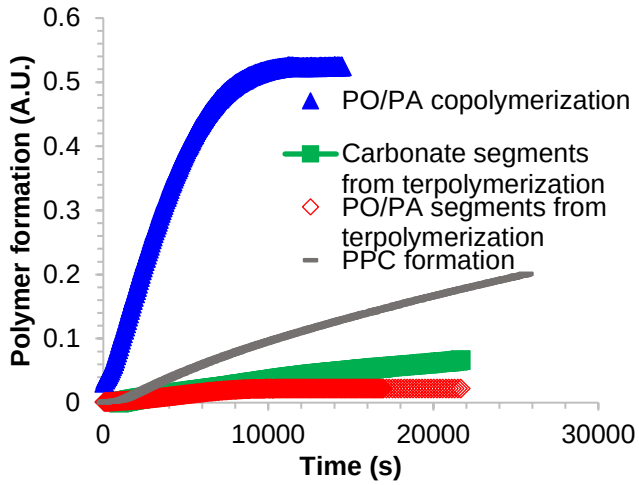

*Fig. 48: Comparison of reaction progresses of the formation of different polymers. Terpolymerizations are recorded from PO/PA copolymerizations under CO_2 atmosphere. [cat]: **1**/PPNCl.*

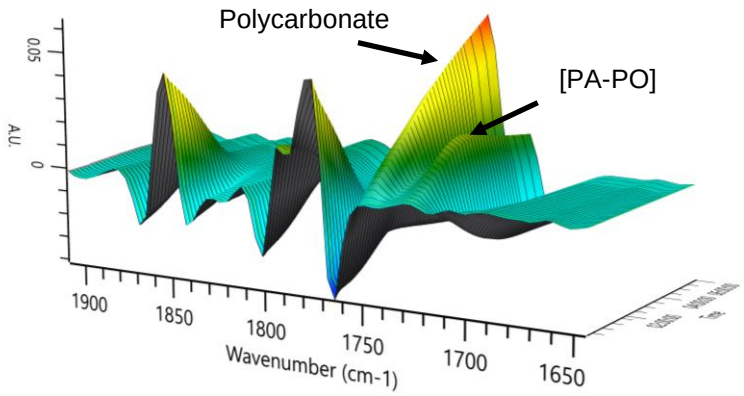

*Fig. 49: Deconvoluted 3D plot of the ROCOP of PO & PA under CO_2 (10 bar) atmosphere, [cat]/[PPNCl]/[PO]/[PA] = 1/1/5000/500, 50 °C, 50 vol% toluene. [cat]: **1**/PPNCl.*

Thus, despite the fact of an apparent correlation of the formation rates, a comparison of the ^{13}C–NMR spectra of the respective polyester, polycarbonate and the polymer obtained by sequential PO/PA and PO/CO_2 polymerization (Fig. S14) do support a rather random distribution of the carbonate segments in the polymer chain.

In contrast to the polymerization of PO and PA under CO_2 atmosphere, the copolymerization of NA and PO under CO_2 atmosphere proceeds completely different (Fig. 50). While in the former case carbonate and ester bonds are formed simultaneously, here NA is consumed almost completely before the polycarbonate formation starts. Unfortunately, the polycarbonate formation continues comparably slow. Moreover, only a small amount of about 15 % polycarbonate was detected in the polymer according to ^{13}C–NMR signals of the ester and carbonate moieties. This indicates the strong affinity of the polyester chain end to the catalyst, blocking the trajectory for a CO_2 insertion. This

difference in coordination affinity is one successful step towards self-controlling systems and the production of block polyester carbonates.

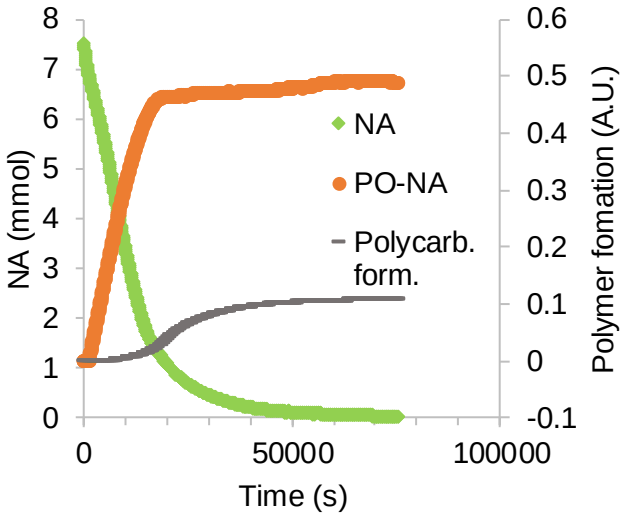

*Fig. 50: Consumption of NA and formation of polypropylene carbonate (Polycarb.) and PO-NA segments. [cat]/[PPNCl]/[PO]/[NA] = 1/1/5000/500, 40 °C, 50 vol% toluene, reaction progress was followed by in situ IR spectroscopic measurement under CO_2 (10 bar) atmosphere. [cat]: **1**/PPNCl.*

Consequently, the next step was to investigate a four-component system in the copolymerization behavior of PO, PA and NA under CO_2 atmosphere.

The reaction progress with anhydride consumption and polymer formation is depicted in Fig. 51. As observed in the direct combination of PA and NA in one polymerization reaction (see Fig. 44), a clear preference of PA incorporation over NA was observed. Unfortunately, we were not able to fully deconvolute the respective bands of the *in situ* IR spectroscopic measurement due to its complexity and strong superposition of the IR bands. A formal calculation of incorporation probabilities similar to in Fig. 44 **A** was performed, as well (Fig. 52). The incorporation behavior of the anhydrides was found to be similar to that observed in Fig. 44 **A**. At low conversions PO/PA segments are formed almost exclusively. As the PA conversion approaches 60 %, 60 % NA and 40 % PA incorporation are predicted. Overall, a similar segmentation as presented in Fig.44 **A** but with a less pronounced separation was observed. However, in this experiment the immanent influence of the CO_2 atmosphere was revealed by a pressure release and a subsequent atmosphere purge to replace CO_2 by Ar. The consumption of NA accelerated rapidly after CO_2 was replaced by argon, while consumption of PA remained approximately constant. Unlike the PO/PA/NA reaction presented in Fig. 44, NA was consumed faster than PA just before conversion was complete. This leads to a second reversal in the incorporation probability with PA being incorporated preferentially at the beginning and at the end of the polymerization (Fig. 52).

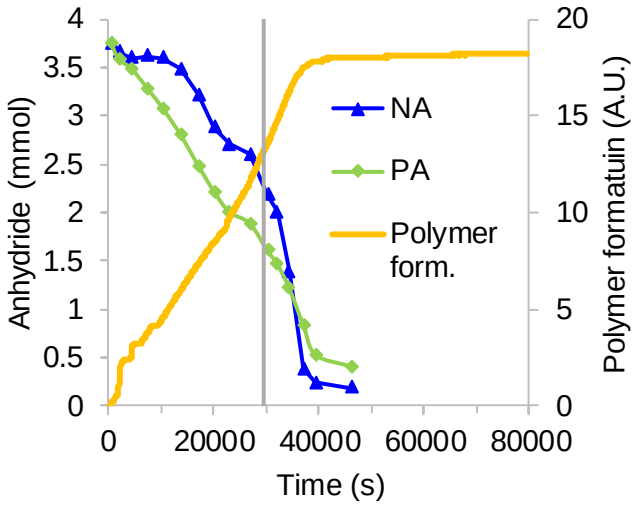

*Fig. 51: Consumption of NA, PA and formation of polymer. The polymer formation represents the superimposed polymer carbonyl signals of both ester and the carbonate repeating units. The vertical line represents the replacement of CO_2 by an Ar atmosphere. [cat]/[PPNCl]/[PO]/[PA]/[NA] = 1/1/5000/250/250, 50 °C, 50 vol% toluene, reaction progress was followed by in situ IR spectroscopic measurement under CO_2 (10 bar) atmosphere. [cat]: **1**/PPNCl.*

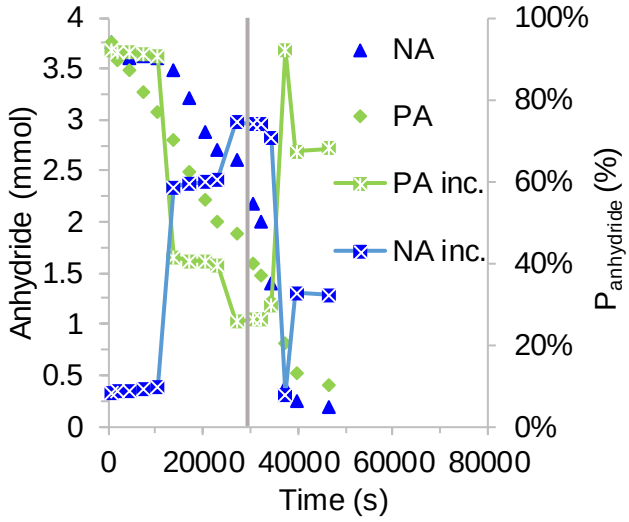

*Fig. 52: Anhydride consumption in the simultaneous addition of PA and NA and incorporation probability of the respective anhydride under CO_2 atmosphere and **1**/PPNCl as catalyst system. The vertical line marks CO_2 pressure release.*

Interestingly, the nature of the reaction mixture has a strong impact on the incorporation of propylene oxide in the polymer backbone. Considering the carbonyl and the methine signals in the ^{13}C–NMR spectra, no preference of one PO enantiomer over the other by the catalyst can be observed, anymore (see Fig. S19), indicating that stereodifferentiation of PO incorporation proceeds via chain end control rather than enantiomorphic site control. The strong decrease of enantioenrichment in all representative regions in the ^{13}C–NMR spectrum argues against a significant polymer block formation. Additionally, exclusively

head-to-tail (HT) connectivity for the polycarbonate was detected with an enantioenrichment of the opposite PO enantiomer compared to the PO/PA polyester produced by **1/**PPNCl. Moreover, the carbonate signal is significantly shifted, pointing towards a change in the environment in close proximity, which emphasizes the preference of **1**/PPNCl for the copolymerization of PO with anhydrides over the formation of polypropylene carbonate. Thus, chain end control could favor insertion of (*R*)-PO in case of the less sterically demanding carbonate end group, while (*S*)-PO is preferred for the PO-anhydride segments. Altogether, this could point towards an alternating incorporation of carbonate and anhydride-based segments in the polymer backbone.

Because the ROCOP of PO with anhydrides prefers (*S*)-PO, the steric demand of the chain end might have a stronger effect on the selection of the PO enantiomer than the steric demand of the catalyst. As the steric demand of the chain end is lower in the case of carbonate formation, the stereo information of the catalyst backbone determines the PO enantiomer selection in the carbonate formation. This leads to a selection of (*R*)-PO for the formation of the carbonate segments. The alternating incorporation of CO_2 and anhydrides in this system could thus be favored because racemic PO was used.

Certainly, more experiments would be necessary to understand the presented system in depth.

3.3 Post Polymerization Modification

The worlds energy demand is growing.[163] So is the necessity to substitute the conventional energy production by environmentally benign energy production methods as the global warming shows the tendency to accelerate rather than to slow down. Thus, a complementary mix of energy production based on renewable energy is a goal to strive for. Next to wind or tidal energy, photovoltaic energy plays an important role in this energy mix. As solar energy is the most abundant energy source and, hence, can be accessed almost everywhere, photovoltaic devices have the unique potential of being employed locally. As silicon based photovoltaic cells are comparatively heavy and the usability on flexible surfaces is limited, organic solar cells gained much attention since *Grätzels* first findings in 1991.[164] Since these first findings tremendous research work has been done in the field of organic photovoltaics. Several types of organic solar cells with different architectures exhibiting increasing power conversion efficiencies (PCE) were developed since then,[165-169] among which dye sensitized organic solar cells take an increasingly prominent role. However, some challenges have to be faced when dyes are considered as photosensitizers. One major issue is the electron transport. As incident light causes a

charge separation in the sensitizer, the charges must be mobile enough to reach the load. If the charge mobility is hampered for any reason either a charge recombination or the formation of a molecular exciton follows, which leads to lower efficiencies. Another challenge is the adjustment of the LUMO level of the sensitizer, which has to be high enough for the excited electrons to relax into the conduction band of TiO_2 (in the case of bulk heterojunction (BHJ) cells) or to relax into a corresponding level at a acceptor, which in its turn directs the electron to the electrode.[170-172] This electron transport mechanism is a key aspect in the development of organic solar cells. However, another aspect which should not be underestimated, especially in the context of larger π-systems as sensitizers, is the aggregation of the sensitizing molecules. Particularly if a small molecule sensitizer comprises both moieties, acceptor and donor, an unordered aggregation of two molecules would destroy the dipole moment and quench the photoactivity.[173] One approach is to introduce the photoactive layer as a polymer, which is a synthetic challenge compared to polyester syntheses.[166] Another approach is the introduction of aliphatic substituents, which increase the steric demand.[169, 174] Thus, the molecular packing shows a certain impact on the efficiency of dye sensitized organic solar cells (DSSC). A different approach is to provide the dye sensitizer a rigid, but amorphous polymer scaffold to avoid the aggregation mentioned. Here we present first investigations on the synthesis of such a scaffold. Poly(norbornene dicarboxylic acid propyl) ester was used as a model polymer system with a modifiable aliphatic scaffold. Furthermore, phthalic acid propyl ester segments were introduced to investigate the effect of “double bond dilution” on the polymer modification. In this context the post polymerization modification was performed *via* double bond metathesis with styrene, modified fluorescein derivatives and modified nile red.

3.3.1 Stability of Polymers at light irradiation

As a first orientation regarding the polymer stability at irradiation, base polymers were irradiated in the solid state. For that, a polymer sample was divided into three parts and the samples were irradiated with 254 nm UV light (Phillips G15T8) over the duration of 1, 2 and 3 weeks. The samples were contained in sealed glass vials. The vials consisted of common borosilicate glass, which transmittance is significant in the UV-A region (315 nm to 400 nm) but block shorter wavelengths. The employed UV lamp provides several wavelengths between 300 and 550 nm in addition to the main wavelength of 254 nm according to the manufacturer. Although the intensity of the additional available wavelengths is below 10% of the maximum light intensity, this simple experiment could still provide a first orientation with respect to polymer stability at light irradiation.

Nevertheless, this experiment needs to be verified by using explicitly quartz glass equipment, which was not available at the time of the study. The samples were characterized by GPC analysis after the respective illumination time elapsed. In this first investigation the two polyesters of pure poly(propyl phthalate) or poly(norbornene dicarboxylic acid propyl)ester were tested. Terpolymers were not covered thus far in this study. After the first week of illumination poly(propyl phthalate) does not show significant changes in the obtained GPC data. Even after three weeks of illumination neither the molecular weight changed nor a change in the *Đ* could be measured (Fig. 53, Table 8). Moreover, the constant increase in intrinsic viscosity with molecular weight suggests a unchanged structure of the polymer samples in solution.

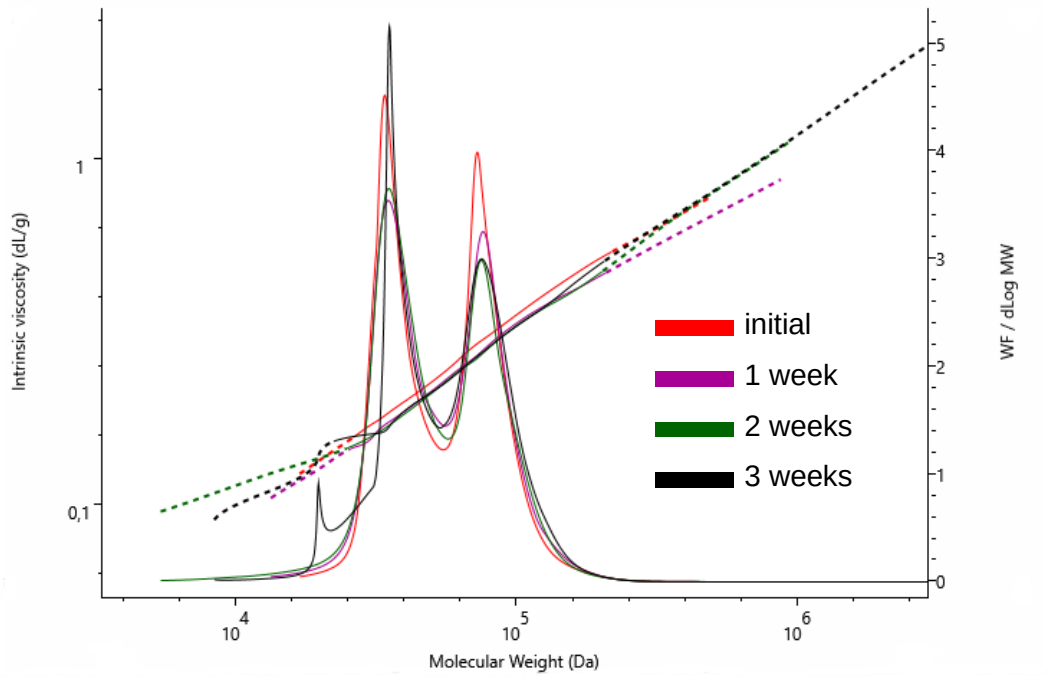

Fig. 53: Distribution plot and intrinsic viscosity plot overlay of poly(propyl phthalate) samples illuminated with a 15 W, 256 nm UV lamp after 0 to 3 weeks of illumination.

Table 8: Summary of obtained GPC data from UV stability experiments with poly(propyl phthalate).

Entry	Illumination time (weeks)	M_n (kg · mol^{-1})[a]	*Đ*
1	0	49.1	1.22
2	1	48.7	1.24
3	2	45.8	1.29
4	3	49.5	1.26

[a]*Determined by GPC calibrated with polystyrene standards employing triple detection.*

Contrary to the observations made for the semiaromatic polyester, the PO/NA copolymer is significantly affected by the UV irradiation. After one week of irradiation the weight averaged molecular weight increased by 50 % which leads to a *Đ* of 1.85. From week 1 to week 2 the M_w increased further by 63 % with a *Đ* of 2.42. From week 2 to week 3, however, no significant change could be observed. Overall, the molecular weights of both averaged values, M_n and M_w, strongly increased. After three weeks of irradiation the M_n increased by 26 % while the M_w increased by 210 % accompanied by a respective increase in *Đ* (Fig. 54, Table 9).

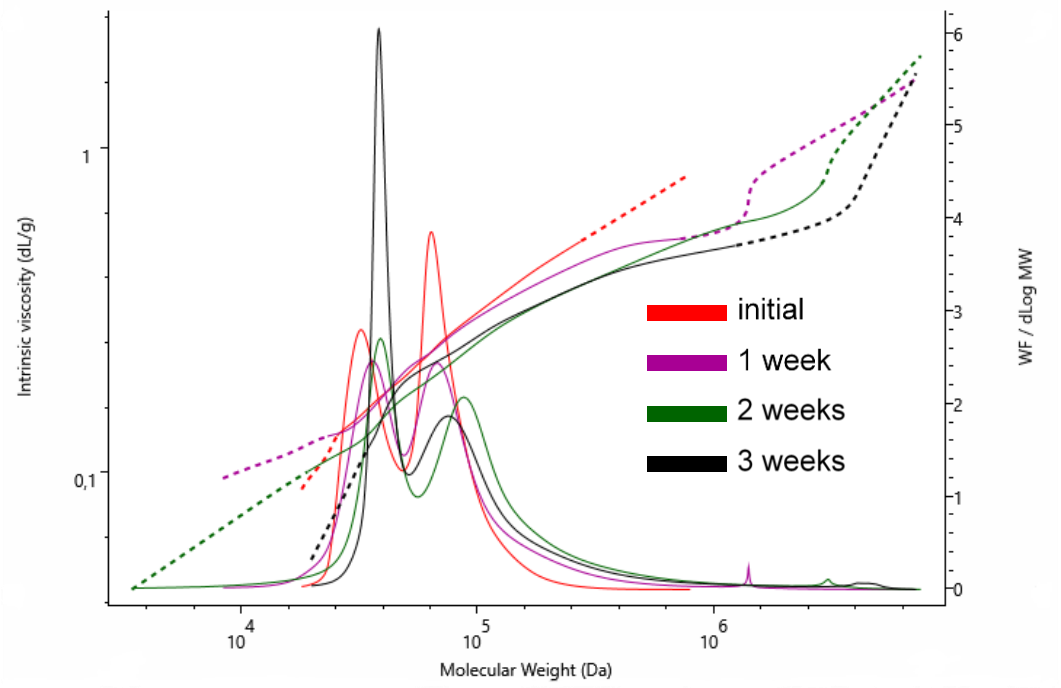

Fig. 54: Distribution plot and intrinsic viscosity plot overlay of poly(norbornene dicarboxylic acid propyl)ester samples illuminated by 15 W, 256 nm UV light after 0 to 3 weeks of illumination.

Another interesting aspect is the shape change of the particles in solution. As already discussed above the *Mark-Houwink* parameter α provides insight into the shape of polymer particles in solution. For the PO/NA copolymer an α of 0.63 was found which points towards strongly swollen polymer spheres. After three weeks of irradiation α decreased to 0.44 which translates to a development to a more compact sphere. This fact can be read out from Fig. 54 if the respective (black) line is followed. At the major weight fraction of the polymer the slope of the intrinsic viscosity curve is comparatively steep and shows a bent at the transition to the higher molecular weights. As the intrinsic viscosity is reciprocal to the density, this curve can be interpreted as a strong decrease in polymer density with increasing molecular weight in the lower molecular weight main fraction and a slower density decrease in the higher molecular weight fraction. At the same time none of the two

slopes match the slopes of the initial polymer. This additionally emphasizes the structural change of the polymer in the course of the UV irradiation.

Table 9: Summary of obtained GPC data from UV stability experiments with poly(norbornene dicarboxylic acid propyl)ester.

Entry	Illumination time (weeks)	M_n (kg · mol^{-1})[a]	*Đ*
1	0	49.1	1.26
2	1	50.5	1.85
3	2	62.8	2.42
4	3	62.0	2.53

[a]*Determined by GPC calibrated with polystyrene standards employing triple detection.*

The structural changes are were hypothesized to be attributed to UV mediated crosslinking at the double bond moieties in the polymer backbone. It can be assumed that shorter chains with a low degree of entanglement are crosslinked leading to an increase in *Đ*. As shorter polymer chains naturally cannot be strongly entangled with other chains, they can partly align which leads to a higher density. Although this alignment is not strong enough to form crystallites the smaller possible void volume leads to a higher density. This weak alignment is apparently increased by crosslinking. As the chain lengths of the polymer increases with molecular weight, the potential entanglement increases alike leading to larger void volumes. This strong entanglement was already observed in DSC measurements of the parent polymer (see Fig. S50). Since the irradiation of the polymer was performed in solid state, the chain conformations were frozen. Therefore, the already entangled polymer chains were linked in the course of the reaction. The crosslinking is, thus, beneficial for preserving the voids. In sum, this leads to a strong intrinsic viscosity (IV) increase, and thus, to a decrease in density of the polymer with increasing molecular weight compared to the unirradiated parent polymer. This development is indeed well observable in Fig. 54.

Additional experiments, such as thermo-analyses or tensile strength tests could lead to useful information regarding the thermal and mechanical properties of the material, which is believed to improve by a higher degree of crosslinking.

All in all, no degradation of neither of the polymers could be observed, which should be observable by a significant decrease of molecular weight. Instead, the M_n of the poly(norbornene dicarboxylic acid propyl)ester even increased after irradiation, giving an optimistic outlook towards the stability of the polymer in further irradiation experiments, which are necessary to be conducted.

3.4 Postmodification

As very first modification experiments and to proof the viability of the postmodification route *via* double bond metathesis, styrene was employed in the post polymerization modification reactions. Styrene provides a useful molecular probe to verify a functioning incorporation mechanism. When styrene is grafted to the polymer backbone a strong UV response should be detectable in the UV/VIS GPC trace at the exact retention time of the polymer sample.

As a second step, model dyes for the post–polymerization modification of the synthesized polymers should be grafted. Two cheap, readily available and non-toxic dyes, namely fluorescein and nile red, were selected. As double bond metathesis was chosen as mechanistic base for the modification of the polymers, the dyes had to be modified to provide the necessary reactivity. The synthetic work and the catalytic modification reactions were carried out in close collaboration with Christian Markl and are additionally a topic of his master thesis.[175] Thus, the synthetic procedures will not be discussed in detail in the experimental section. Also additional sample characterization can be found in his thesis. However, the synthetic pathway will be provided in a brief fashion, herein.

3.4.1 Synthetic Pathway for Dye Synthesis

Two complications have to be taken into account when considering the structure of the two chosen model dyes together with the aimed post–polymerization modification by double bond metathesis. First, the dyes as such (Fig. 55) have no suitable double bond moieties that can undergo double bond metatheses. Second, the presence of hydroxy groups might deactivate the Grubbs-Hoveyda 2nd generation catalyst. Hence, the targeted dyes were modified accordingly.

To introduce the required reactive double bonds, fluorescein was reacted with allyl bromide under basic conditions to cap the hydroxy or carboxylic acid groups. The allyl moieties were believed to be suitable to undergo a metathesis reaction with the double bond of the norbornene groups in the polymer backbone. The modification of nile red, on the other hand, is not as straight forward as the modification reaction of fluorescein. As nile red does not bear a hydroxy group which could be modified in a similar fashion, a hydroxy group was introduced first. The synthetic pathway of the respective dye modification will be briefly described below.

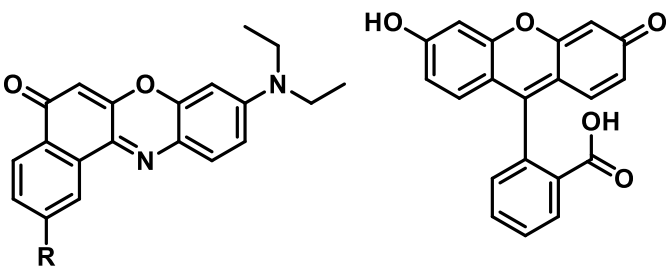

R = H: Nile Red
R = OH: Hydroxy nile red

Fluorescein

Fig. 55: Nile red and fluorescein.

The synthetic procedure to modify fluorescein comprises only the allylation for the compound already bears a hydroxy and a carboxylic acid moiety. The allylation reaction was performed according to literature reactions (Scheme 29).[176]

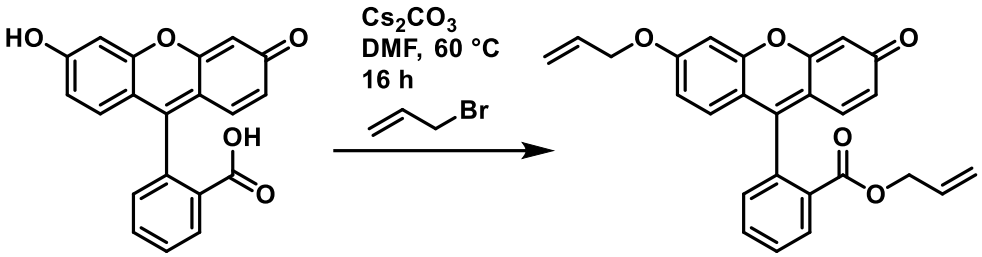

Fluorescein **32 %** **Bisallyloxy fluorescein**

Scheme 29: Allylation reaction of fluorescein to bisallyloxy fluorescein.

The synthetic procedure for the hydroxy modified nile red was adapted from *Higgings* and coworkers (Scheme 30).[177]

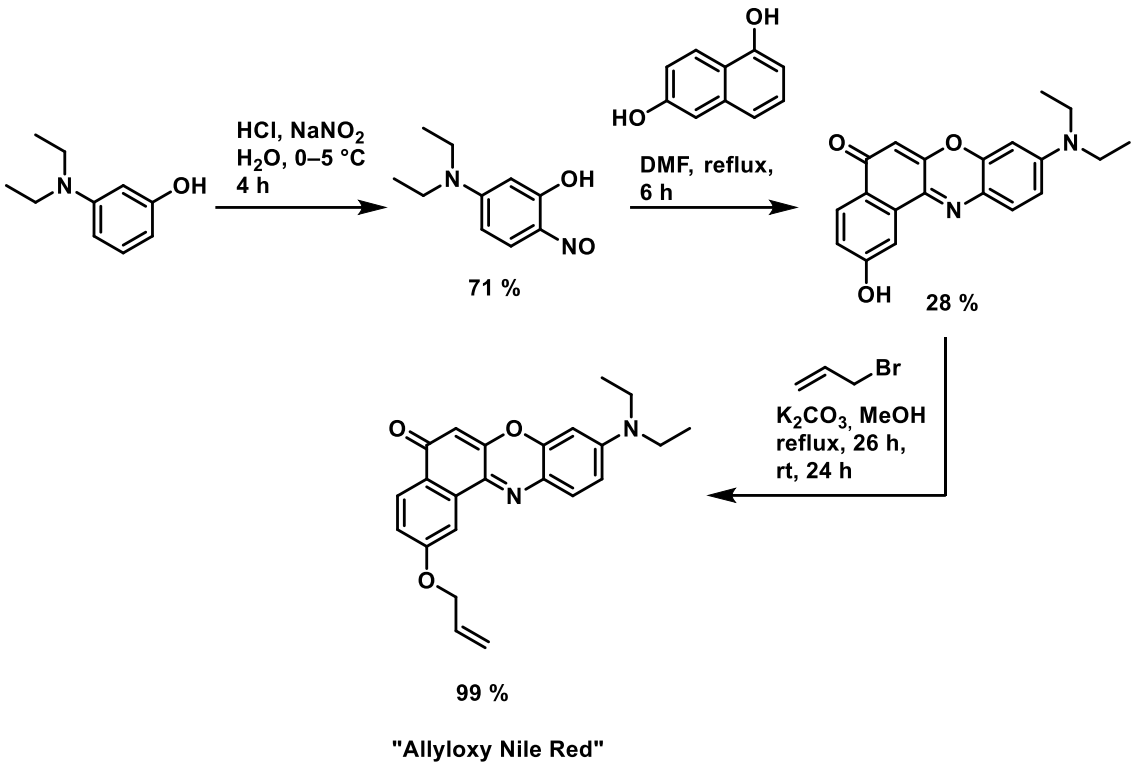

Scheme 30: Synthetic pathway to "Allyloxy Nile Red".

The first step of the synthesis is the *ortho* substitution of the 3-diethylamino phenol. This simple nitrosylation gives an isolated yield of 71 % of the respective nitrosophenol. The second step comprises the ring closure to "hydroxy nile red". This step presents itself as very challenging. Although the reaction procedure is comparatively simple, only moderate yields were achieved. A variety of by products were formed in accordance to the literature.[177] However, the separation of the desired product from the byproducts *via* column chromatography failed in our hands. However, the product was crystallized from an ethanol/toluene mixture to give 28 % yield after another recrystallization step. While the procedure has not been thoroughly optimized, it should be noted that the mother liquor contained additional product. The allylation step, on the other hand, was carried out with almost quantitative yield.

3.5 Modified Polymers

3.5.1 Styrene Modification

To investigate the principle viability of the planned post–polymerization procedure, the grafting of styrene to the polymer was tested first (Scheme 31). To do so, the amounts of

double bonds of the polymer were calculated based on the mass of the employed sample divided by the molecular weight of one repeating unit of the polymer. The Grubbs-Hoveyda 2nd generation catalyst was employed in 0.01 mol%, 0.1 mol%, 1 mol% and 3 mol% with respect to the number of double bonds. Styrene was employed accordingly with one equivalent with respect to the number of double bonds.

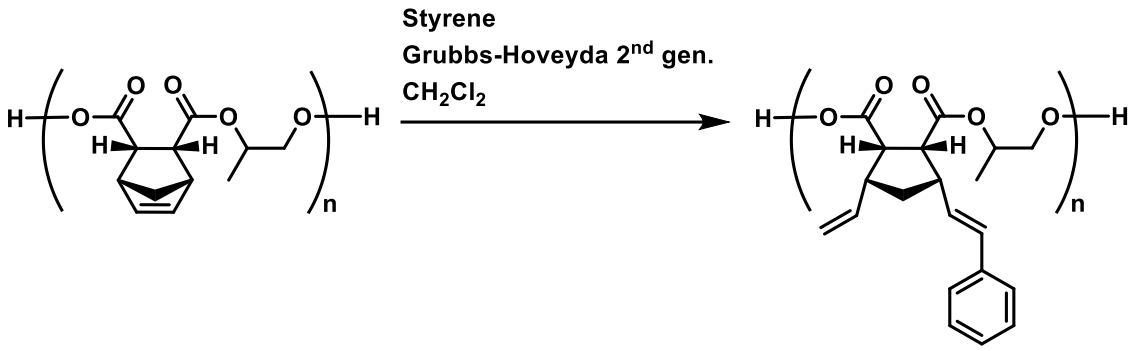

Scheme 31: Post–polymerization modification of poly(norbornene dicarboxylic acid propyl ester) with styrene.

The procedure for the reaction setup has proven to be crucial from earlier experiments. That is, the solvent and its amount, the soaking time and the order of addition are crucial to the reaction outcome.

To address these difficulties, all reactions were carried out in CH_2Cl_2 maintaining identical reaction volumes and a soaking time of the polymer of 2 h under continuous stirring before the addition of the metathesis catalyst. The polymer was soaked in the respective mixtures of styrene and CH_2Cl_2. The reaction time in each case were set to 16 h. After the reaction time the polymers were worked up similarly to all polymers discussed so far in this thesis by precipitation into methanol. Die GPC data of the isolated polymer is summarized in Table 10.

Table 10: GPC data of post modification reactions of poly(norbornene dicarboxylic acid propyl ester) with styrene.

Entry	mol% catalyst[a]	M_n (kg · mol^{-1})[b]	$Đ^b$	Styrene inc. %
1[c]	/	33.3	1.26	/
2	0.01	36.9	1.41	2
3	0.1	135.9	3.21	16
4	1	152.9	3.22	15
5	3	690.4	2.14	16

[a]With respect to the number of double bonds. Styrene: 1 equivalent, solvent: CH_2Cl_2, soaking time: 2 h, reaction time: 16 h. [b]Determined by GPC calibrated with polystyrene standards employing triple detection. [c]Parent polymer.

The homometathesis of the polymer and of the styrene are expected side reactions in the grafting reaction, leading to stilbene and crosslinking in the polymer. Within this model study the extend of stilbene formation was not of major importance and was not further investigated. Regarding the crosslinking reaction within the polymer, increasing the amount of the metathesis catalyst had a strong impact. Fig. 56 provides the molecular weight distribution plots of the isolated styrene modified polymers.

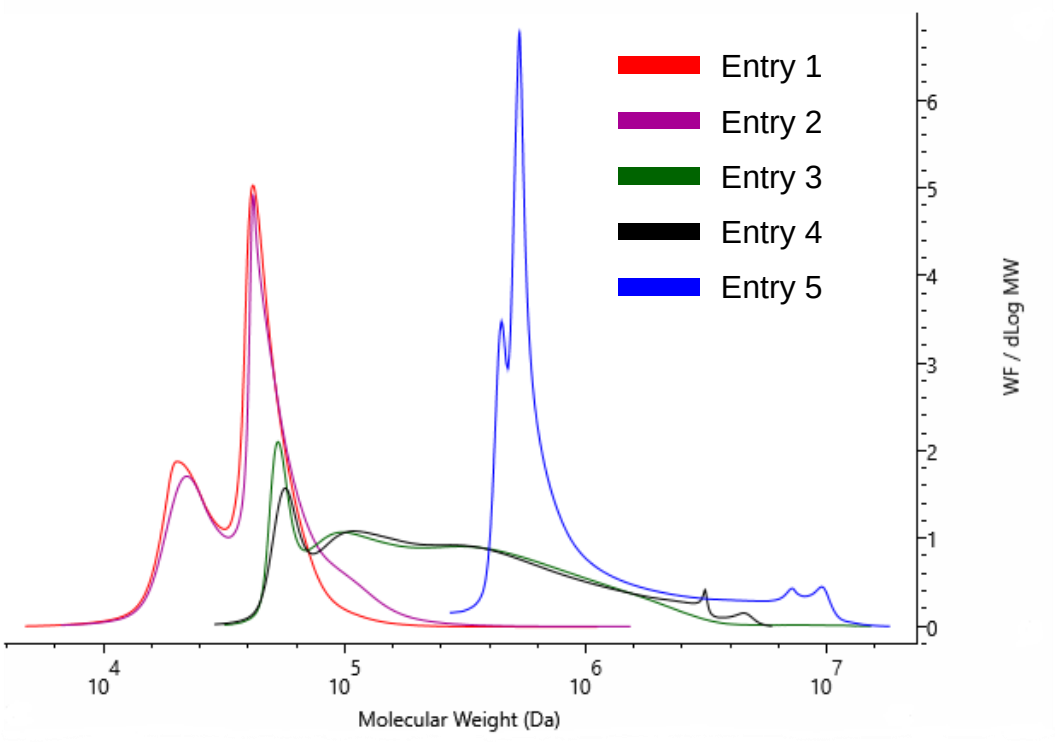

Fig. 56: Overlay of molecular weight distribution plots from the isolated polymers of Table 10.

While Table 10, entry 2 showed only a slight increase in molecular weight, it still showed some styrene incorporation. Fig. 57 shows a comparison of the ^{1}H–NMR spectra of the two polymers from in Table 10 entries 1 and 2 with an insert depicting the aromatic region. The parent polymer does not contain any aromatic moieties and the detected aromatic signals originate solely from the employed styrene. DOSY experiments were performed to prove the success of the modification of the polymer and disprove the possibility that the aromatic signals originate from free unbound styrene or stilbene. The DOSY spectrum (Fig. 58) clearly provides only one trace of polymer signals comprising the respective aromatic signals. Free styrene or stilbene was not detected in the sample. A comparison of polymer integrals and the integrations of the aromatic signals gives a styrene/polymer ratio of 2:100.

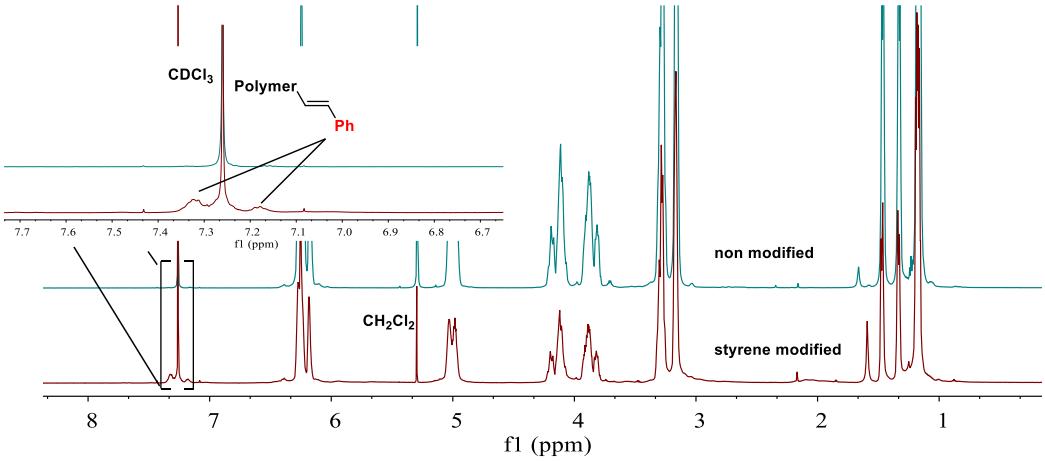

Fig. 57: Comparison of styrene–modified and unmodified poly(norbornene dicarboxylic acid propyl)ester. Non–modified: Table 10, entry 1, styrene–modified: Table 10, entry 2.

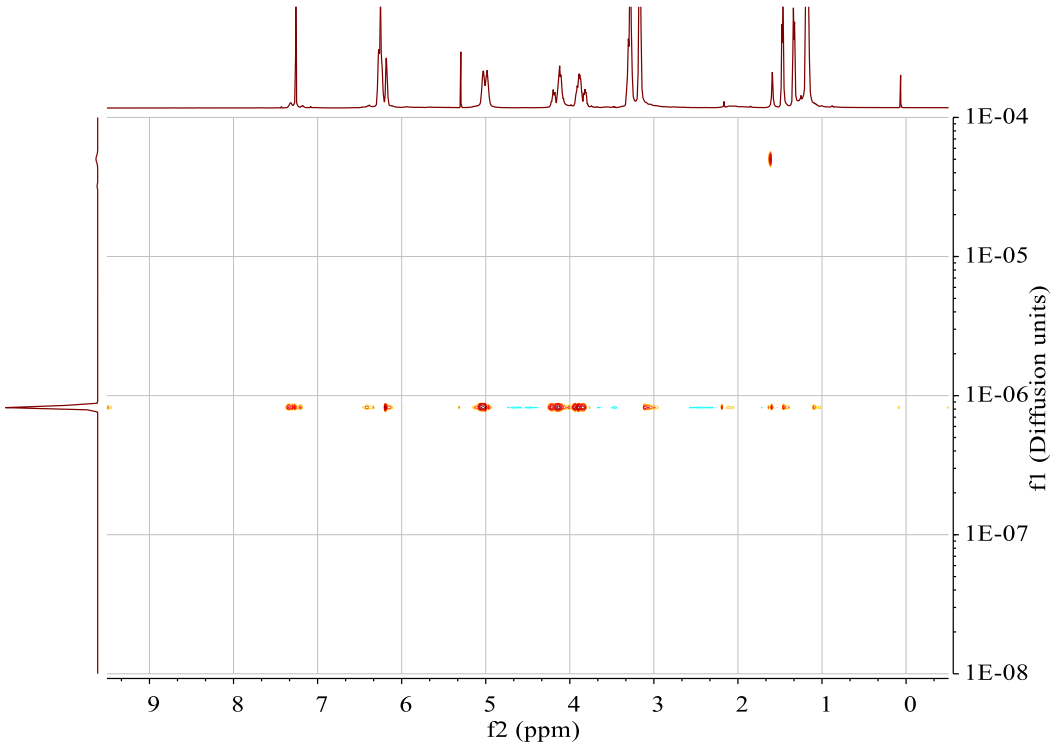

Fig. 58: ^{1}H–DOSY NMR spectrum of the styrene-modified polymer sample from Table 10, entry 2. Diffusion units: $cm^2 \cdot s^{-1}$.

A further increase in catalyst loading to 0.1 mol% led to a strong increase in molecular weight and *Đ*. At this point a threshold seems to have been reached, as 1 mol% catalyst loading did not significantly affect the molecular weight or *Đ*. A comparatively small increase from 1 mol% to 3 mol% in catalyst loading leads to a fourfold increase of M_n. All of the polymers from entry 3 to 5 exceed the upper detection limits of the UV detector in

the GPC instrument. However, NMR spectroscopy indicated 15 % styrene content in the polymer of entry 3. No free styrene could be detected in DOSY NMR spectroscopic analysis. However, a certain uncertainty in integration of the ^{1}H–NMR spectrum must be mentioned as the respective signals are broadened due to the highly crosslinked structure of the polymer. Therefore, the styrene content could be overestimated to some extent. The same is true for the polymers of Table 10 entries 4 and 5. Thus, the possible degree of modification is only dependent on the catalyst loading to a small extent in that regime. The incorporation of styrene into the polymer is possibly rather limited by the simultaneous accessibility of the norbornene double bonds and styrene to the metathesis catalyst. One could hypothesize that only the surface of the polymer particles are modified with styrene and that the core of the particles is inaccessible for styrene and the metathesis catalyst explaining a threshold in modification. This would also mean that the homomethathesis of the norbornene double bond predominantly occurs on the particles surface, as well. This would additionally explain the decreasing *Đ* in entry 5 for a fraction of polymer particles is cured during the reaction, which leads to a strong increase of M_w of the polymer sample.

3.5.2 Allyloxy Nile Red Modification

The incorporation of nile red, an abundant and non-toxic model system, was investigated first. However, as mentioned before, a nile red analogue needed to be synthesized to be suitable for further reactions. That is, the toxicity of the produced compound might be evaluated separately. The synthetic procedure to enable double bond metathesis at the dye molecule is described in Scheme 30. The procedure for polymer modification with allyloxy nile read (see Scheme 31) was maintained identical to the styrene polymer modification. Within this set of experiments both the effect of varying amounts of the nile red dye and the “dilution” of the double bond moieties within the polymer were investigated. Initially, tests with 1 and 2 equivalents of dye with respect to the number of double bonds were employed with a poly(norbornene dicarboxylic acid propyl)ester and a 1/1 and 2/1, (PA/NA) terpolymer from direct anhydride addition (see section 3.2.3.7). An overview of the modified and isolated polymers of this reaction set is provided in Table 11. To minimize the error in handling and variation of conditions the reaction set was performed all at once. After the reaction time had elapsed, the solvent was evaporated and the residue was washed with methanol to remove catalyst and unbound dye in order to verify whether a simple washing procedure is potentially sufficient for purification. The resulting polymer samples were dried in high vacuum. This procedure was applied to Table 11, entries 5–7 and 9. DOSY NMR spectroscopic analysis indicated, as anticipated, the presence of large

amounts of free dye. However, ^{1}H–NMR signals of nile red with the same diffusion coefficient as the polymer were detected, as well. Because the degree of dye incorporation could not be properly determined in a sample with free dye, the respective polymer samples were reprecipitated from CH_2Cl_2 into methanol.

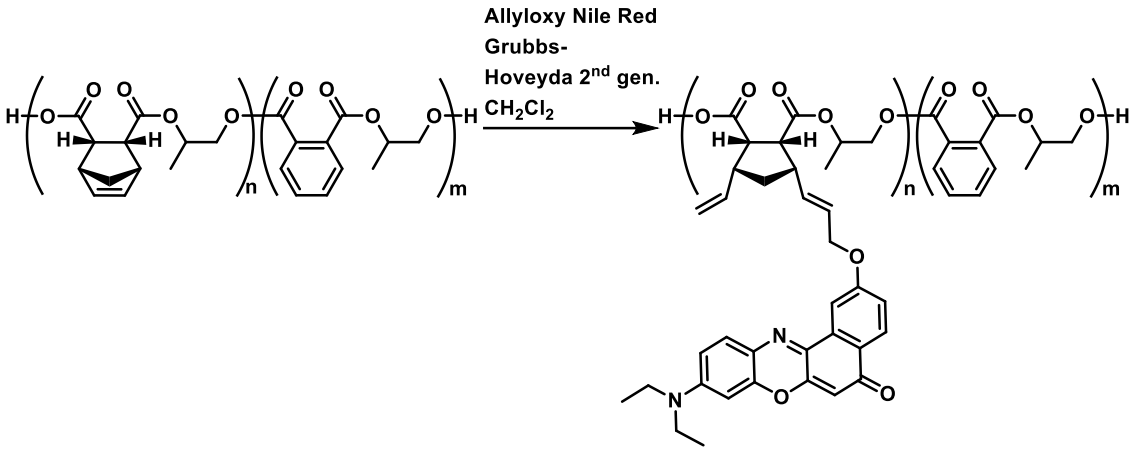

Scheme 32: Post–polymerization modification of PA/NA/PO co- and terpolymers with allyloxy nile red. The respective reactions are summarized in Table 11.

Table 11: Polymer modification with allyloxy nile red.

Entry	Parent Polymer (PA/NA)[a]	Dye equivalents[b]	M_n (kg · mol^{-1})[c]	*Đ*[c]
1[d]	0/1	/	32.4	1.27
2[d]	1/1	/	29.3	1.25
3[d]	2/1	/	36.8	1.21
4	0/1	1	87.7	2.31
5	0/1	2	97.7	2.71
6	1/1	1	48.0	1.45
7	1/1	2	53.1	2.45
8	2/1	1	49.8	1.15
9	2/1	2	42.5	1.71

[a]Repeating unit ratio in the parent polymer. PA: phthalic acid propyl ester segments in the employed polymer, NA: norbornene dicarboxylic acid propyl ester segments in the employed polymer. [b]Equivalents with respect to double bond moieties in the employed polymer. [c]Determined by GPC calibrated with polystyrene standards employing triple detection. [d]Parent polymer. Catalyst: Grubbs-Hoveyda 2nd generation, 0.1 mol% with respect to amount of double bonds. The catalyst was added from a 1.59 · 10^{-3} mol/L stock solution. CH_2Cl_2 was added to a total volume of 4 mL.

The precipitated polymer was dried and analyzed by NMR spectroscopy. Contrary to the previous measurements, no free dye could be detected in the DOSY NMR spectra.

Unfortunately, the signals for the bound dye disappeared, as well. This discrepancy can be attributed to an encapsulation of the dye into polymer capsules, which remain intact upon dissolution in chloroform. The same procedure was carried out for the all polymer samples of Table 11, no dye incorporation was detected by NMR spectroscopic analysis, despite of the fact that the polymer samples were all colored.

Interestingly, a color change could be observed over time, in the prepared NMR samples of the modified polymers. Whereas fresh NMR samples had a pink color, the sample color changed to blue after 24 h. In order to exclude a simple degradation of the dye in air, an NMR sample of the synthesized allyloxy nile red was prepared in the same manner, but no color change was observed after 24 h. Nile red is known to have solvatochromic properties. Thus, the color change could indicate a conformational change of the modified polymer in solution such that the polar groups are encapsuled by the less polar polymer backbone. During that process the dye moieties can be expected to organize themselves according to dipole–dipole interactions. This encapsulation appears to exclude the deuterated chloroform from the particles, leading to a color change.

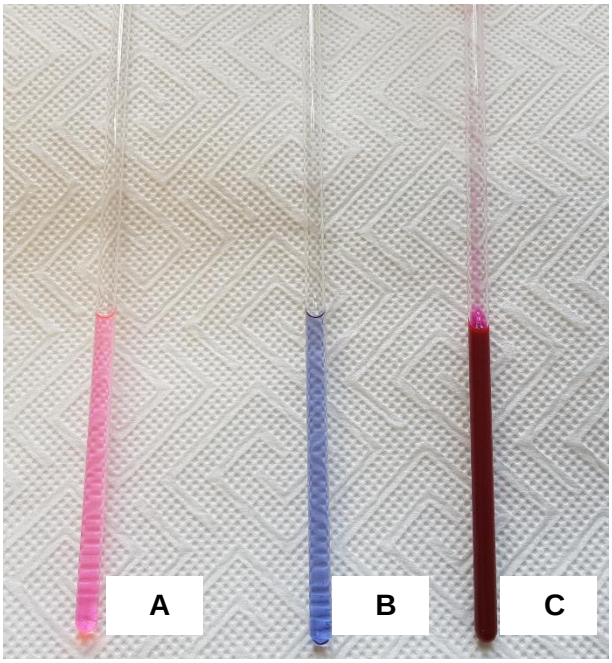

Fig. 59: NMR samples of allyloxy nile red modified polymer. A: freshly dissolved in $CDCl_3$, B: dissolved in $CDCl_3$ after 24 h, C: free allyloxy nile red dissolved in $CDCl_3$ after 24 h.[175]

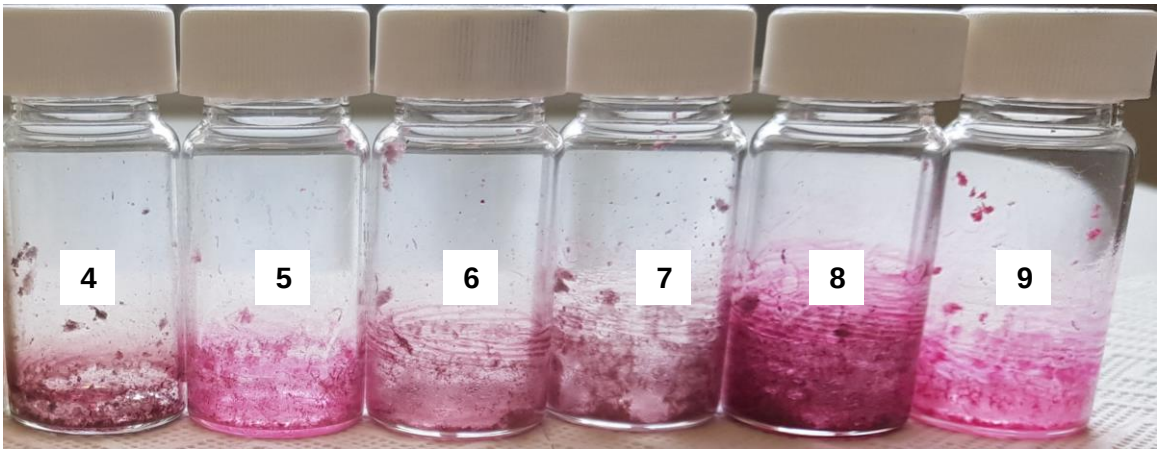

Fig. 60: Isolated polymers from Table 11 after precipitation. The numbering represents the entries in the table.[175]

Although no bound or free dye was detected by NMR spectroscopic analysis, the presence of the modified nile red in the samples is readily visible. Thus, additionally UV/Vis spectra were recorded by in–line GPC measurements. For classical off–line visible light measurements see Christian Markl's master thesis.[175]

The GPC results show a clear dependence between the double bond concentration in the polymer and the crosslinking. Samples with a 100 % norbornene content (Table 11, entries 4 & 5) show a very strong crosslinking with accordingly increased M_n, as well as, a strongly broadened *Đ*. In comparison to the parent polymer (M_n of 32.4 kg/mol, *Đ* = 1.27) the molecular weights of the modified polymers tripled. As the concentration of norbornene units is decreased to 50 % (Table 11, entry 6 & 7) the increase was found to be less strong with 29.3 kg/mol (*Đ* = 1.25) (Table 11, entry 2) for the parent polymer and 48 to 53 kg/mol after the modification reaction. This trend continues as the concentration or norbornene units is further decreased to 33 % (Table 11, entry 8 & 9), where the modified polymers had only a slightly increased molecular weights of 49.8 and 42.5 kg/mol, respectively, compared to the parent polymer (M_n of 36.8 kg/mol, *Đ* = 1.21). Interestingly, in the whole reaction series the reactions with 2 equivalents of dye showed a significantly higher polydispersity compared to with only one equivalent. Rationally, the higher dye concentration should slow down polymer crosslinking reactions. Instead, the second equivalent appears to promote crosslinking. The higher dye concentration should accelerate the dye homometathesis, which is an expected side reaction. The dye homocoupling overall appears to be privileged compared to the polymer-dye coupling and the dye incorporation was found to be generally poor. Thus, after the majority of the allyloxy nile red is homocoupled, the residual active catalyst can perform a small quantity of polymer-dye couplings, and after consumption of allyloxy nile red, the catalyst can facilitate

polymer crosslinking. Altogether, this rationale would explain the poor incorporation and the higher polydispersity when a higher amount of dye is present.

The incorporation of nile red, a fluorescent dye, can be visualized by irradiation of the samples by UV light at 366 nm. Fig. 61 shows the fluorescence of the irradiated solid polymer samples. The respective parent polymers do not show such a strong UV response (Fig. 62). The fluorescence of sample 1 in that figure might be due to a small amount of residual catalyst, and the corresponding UV-GPC trace does not exhibit a UV response at 366 nm. Although only in low concentration, the polymer samples clearly contain the covalently bound nile red.

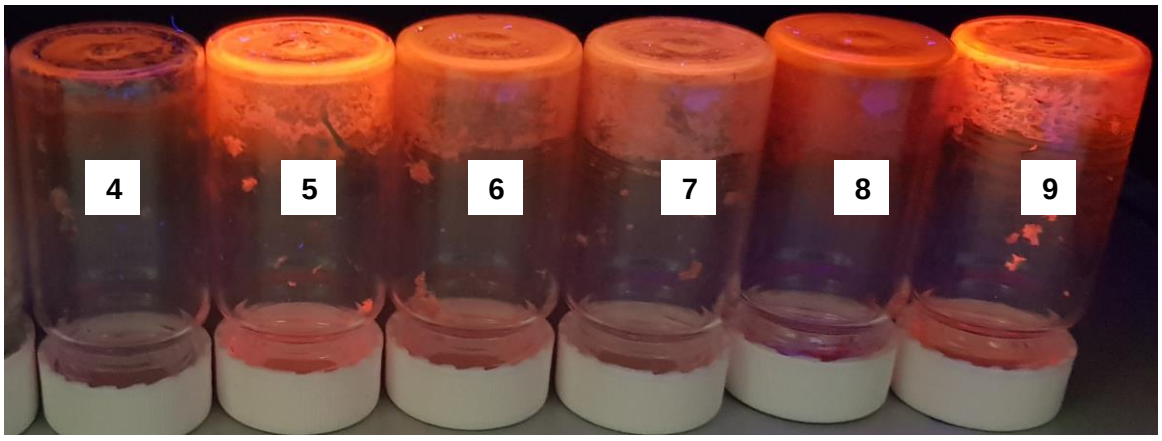

Fig. 61: Polymer samples from Fig. 60 under 366 nm light. Note: The differences in fluorescence intensity might partly be attributed to a not fully homogeneous light distribution and differences in sample thickness.[175]

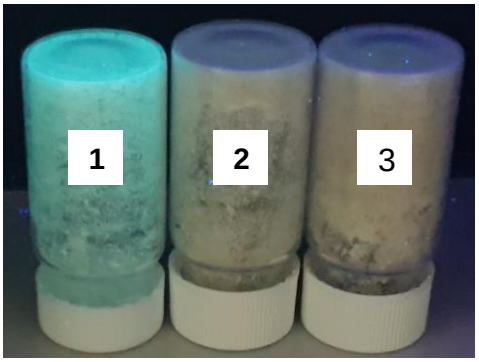

Fig. 62: Parent polymers for post–polymerization modification with allyloxy nile red and bisallyloxy fluorescein under 366 nm UV light. 1: Poly(norbornene dicarboxylic acid propyl)ester, Table 11 entry 1; 2: Poly(norbornene dicarboxylic acid propyl)ester polypropylene phthalate terpolymer 1/1, Table 11, entry 2; 3: Poly(norbornene dicarboxylic acid propyl)ester polypropylene phthalate terpolymer 1/2, Table 11, entry 3.[175]

3.5.3 Bisallyloxy Fluorescein Modification

As additional model system the already discussed bisallyloxy fluorescein was employed. As bisallyloxy fluorescein bears two allyl moieties (see Scheme 29), the scope of the dye addition was expanded. In principle, the two allyl moieties can lead to the formation of fluorescein bridges between different polymer chains as well as within the same polymer chain. The GPC results are summarized in Table 12. As far as the crosslinking side reaction is concerned, throughout the whole reaction series the crosslinking reaction remained insignificant. Except for small variations in *Đ* in Table 12 entries 4 and 6, the molecular weights and polydispersities remained within the error range of the values for the parent polymers. There are two possible explanations for this observation. Either the catalyst was inactive, or, the catalyst is fully selective towards the homocoupling of the bisallyloxy fluorescein.

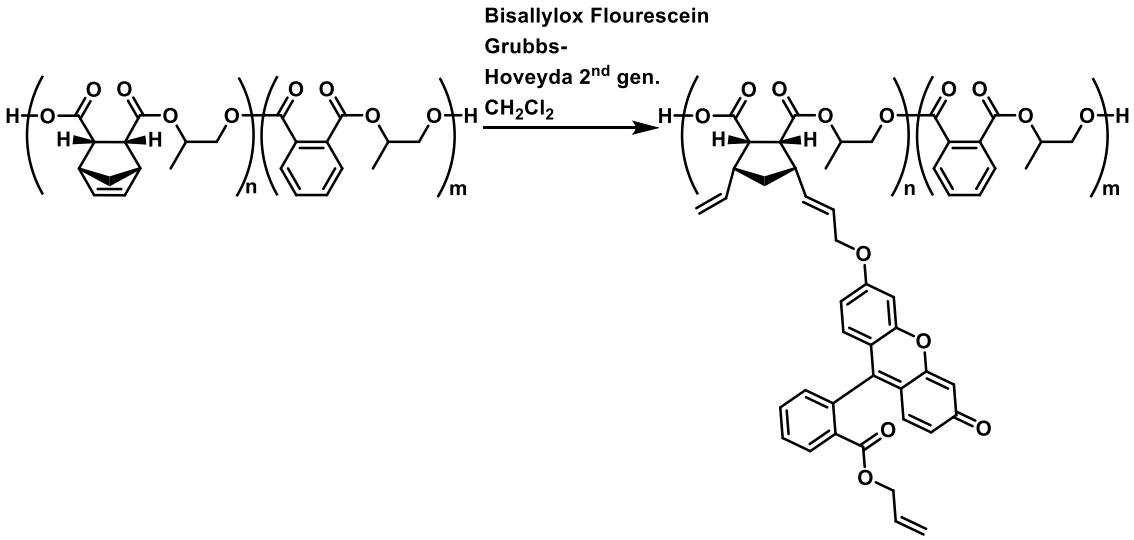

Scheme 33: : Post–polymerization modification of PA/NA/PO co- and terpolymers with bisallyloxy fluorescein. The respective reactions are summarized in Table 12.

Table 12: Polymer modification with bisallyloxy fluorescein.[175]

Entry	Parent Polymer (PA/NA)[a]	Dye equivalents[b]	M_n (kg · mol^{-1})[c]	$Đ$[c]
1[d]	0/1	/	32.4	1.27
2[d]	1/1	/	29.3	1.25
3[d]	2/1	/	36.8	1.21
4	0/1	0.5	34.7	1.54
5	0/1	1	31.1	1.39
6	0/1	2	34.4	1.57
7	1/1	0.5	28.7	1.32
8	1/1	1	28.0	1.34
9	1/1	2	28.5	1.28
10	2/1	0.5	38.4	1.26
11	2/1	1	35.1	1.24
12	2/1	2	37.7	1.28

[a]Repeating unit ratio in the parent polymer. PA: phthalic acid propyl ester segments in the employed polymer, NA: norbornene dicarboxylic acid propyl ester segments in the employed polymer. [b]Equivalents with respect to double bond moieties in the employed polymer. [c]Determined by GPC calibrated with polystyrene standards employing triple detection. [d]Parent polymer. Catalyst: Grubbs-Hoveyda 2nd generation, 0.1 mol% with respect to amount of double bonds. The catalyst was added from a 1.59 · 10^{-3} mol/L stock solution. CH_2Cl_2 was added to a total volume of 4 mL.

The former possibility can be verified utilizing the UV/VIS traces of the GPC eluogram. If the catalyst was inactive in this reaction system, no fluorescein signals would be detectable at the polymer retention time. However, from the molecular weight data it can be anticipated that, if any, only a low signal intensity will be found. Indeed, the isolated polymers show a color change from off white to yellow (Fig. 63) Similar to the allyloxy nile red modified polymers.

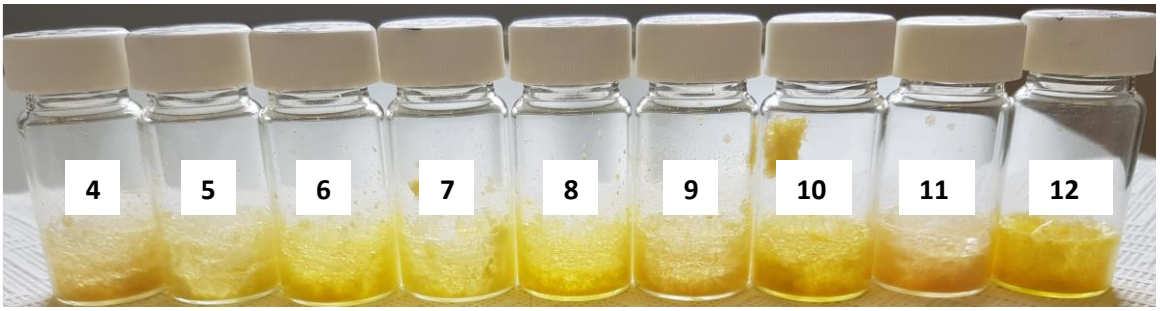

Fig. 63: Isolated polymers from Table 12. The numbering represents the entries in the table.[175]

Fig. 65 provides exemplary UV/VIS GPC traces of modified poly(norbornene dicarboxylic acid propyl)ester with bisallyloxy fluorescein. As anticipated, the incorporation of the

bisallyloxy fluorescein is found to be very low. Although at this point the incorporation cannot be quantified, it was found to be very low considering the already low UV response measured for the parent polymer (Fig. 65, **1**). Interestingly, the incorporation decreases further with increasing amount of added dye. While the catalyst is active for metathesis in this reaction system, the catalyst appears to favor the homocoupling of bisallyloxy fluorescein. With a decrease of the relative amount of norbornene units in the polymer the incorporation decreases further (Table 12, entry 7–12). However, similarly to the allyloxy nile red modified polymer samples, the bisallyloxy fluorescein samples provide a significant response to UV irradiation (Fig. 64). Unfortunately, incorporation of bisallyloxy fluorescein was too low for a proper quantification *via* NMR spectroscopic analysis in this case as well.

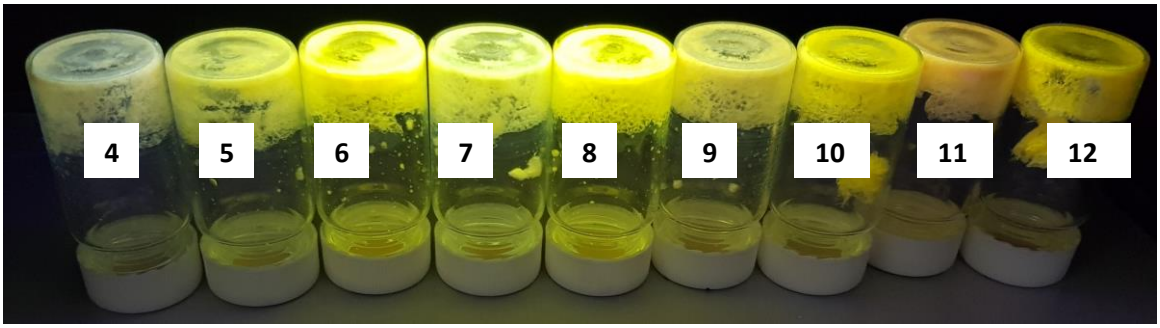

Fig. 64: Polymer samples from Fig. 63 under 366 nm light. Note: The differences in fluorescence intensity might partly be attributed to an inhomogeneous light distribution and differences in sample thickness.[175]

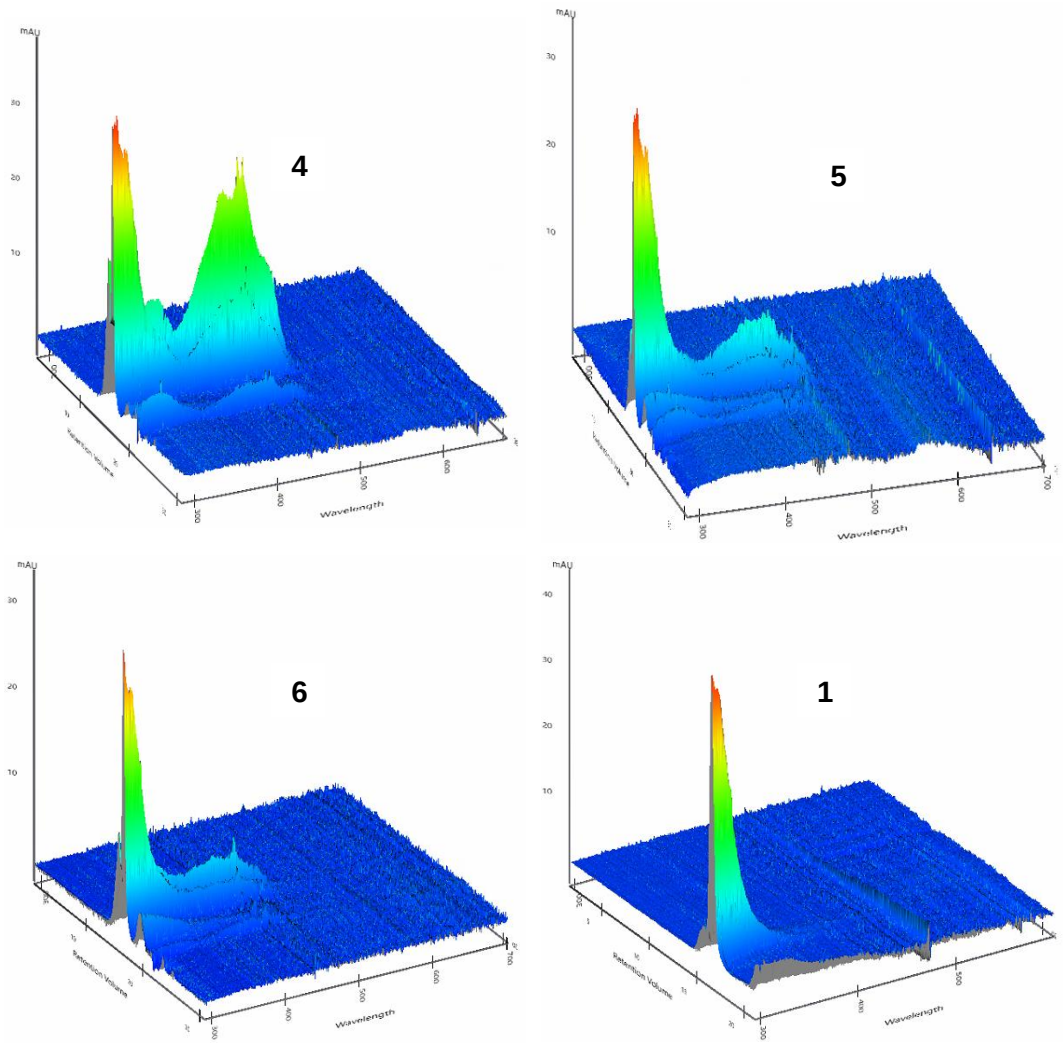

Fig. 65: UV/Vis GPC traces of polymers from Table 12. The numbering represents the entries in the table.[175]

Overall, incorporation of the modified dyes studied herein was limited small amounts under the conditions applied. However, it could be successfully shown that a covalent polymer modification with modified polar dyes is possible by double bond cross metathesis. As mentioned in the introduction of this section, such incorporation is promising in the context of light harvesting applications. However, the investigated system can be seen as a proof of concept and certainly would benefit from further investigations with respect to the employed dyes and modification conditions to improve the dye incorporation. Further spectroscopic investigations on these and other systems is reported in the master thesis of Christian Markl with whom this study was performed in close cooperation.[175]

4 Summary & Conclusion

In this work the synthesis of potentially biobased and degradable polyesters and the post–polymerization modification thereof was investigated. In this context, the copolymerization of phthalic anhydride with propylene oxide and the copolymerization of *cis*-5-norbornene-endo-2,3-dicarboxylic anhydride with propylene oxide was investigated towards their reaction kinetics. Subsequently, the two copolymerization systems were mixed to yield terpolymers with a structure controlled by the kinetics of the incorporation of the respective anhydride monomer. Here, the ratio of the employed anhydrides was found to be crucial, leading either to block polymers with gradient block transition or random incorporation. In addition to that these reaction systems were exposed to CO_2 atmosphere and equally investigated. In the course of these investigations additionally the effect of ligand variations on the catalysis of the mentioned systems was investigated. Altogether, these investigations contribute to the understanding of the ring–opening copolymerization catalyzed by Co-salen type complexes. A deeper understanding of these systems can lead to the synthesis of a variety of biobased and degradable polyester materials mediated by simple homogeneous base metal catalysts, providing novel materials with a minimized environmental footprint and a maximum functionality.

Aiming to show the potential of such produced polymers, first investigations on the post–polymerization modification were carried out. For that the post–polymerization modification of norbornene containing polyesters with three substrates, namely styrene, allyloxy nile red and bisallyloxy fluorescein, *via* ring opening/cross metathesis was considered. Although, incorporation of the substrates could not be achieved quantitatively, a covalent binding of the substrates to the polymer backbone could be shown. Further investigations should concentrate on the improvement of the incorporation of the dye molecules. In a long-term perspective, the scaffolding of the polymer backbone for the attached dye moieties together with a self–organization thereof, the crystallization problem in the field of organic solar cells could be addressed.

Because of the high potential of the investigated reaction systems, a further expansion with respect to the monomer scope in the basic polymer synthesis should be investigated. The substitution of the aromatic phthalic anhydride by aliphatic dicarboxylic anhydrides is highly desirable in the context of degradability of the materials by microorganisms at the end of their lifetime.

5 Experimental Section

5.1 Materials

All air and moisture sensitive reagents were kept in a glovebox under Ar atmosphere. Air and moisture sensitive reactions were either carried out in a glovebox under Ar atmosphere or at a Schlenk line under argon atmosphere using standard Schlenk techniques. Propylene oxide was dried over NaH overnight, distilled prior to use and stored over 3 Å molecular sieves at –30 °C. Solvents that were used for synthesis, but not catalysis, were purified by an MBraun SPS 800 solvent purification system and stored, if possible, over a sodium mirror under Ar atmosphere. Solvents which cannot be stored over a sodium mirror were stored over molsieves under Ar atmosphere in a Schlenk flask. MeOH and acetonitrile were purchased in HPLC grade, degassed and dried over 3 Å molecular sieves prior to use. Ethyl acetate and heptanes were distilled before use. All anhydrides were dissolved, hot filtered and recrystallized twice from chloroform. The recrystallized anhydrides were dried directly after recrystallization for at least 4 h in high vacuum. Subsequently, the purified anhydrides were kept at room temperature in a glovebox under Ar atmosphere. Bis(triphenylphospine)iminium chloride was dissolved in CH_2Cl_2 and crystallized by ether addition. The precipitate was dried under high vacuum und kept in a glovebox under Ar atmosphere at room temperature. THF and toluene were dried over Na/benzophenone, distilled and kept in a storage flask equipped with a sodium mirror in a glovebox under Ar atmosphere.

5.2 Measurements

^{1}H– and $^{13}C\{^{1}H\}$–NMR spectra were either recorded on a Bruker AV III 400 MHz or on an AV III 600 MHz spectrometer. DOSY NMR–spectra were recorded on an AV III 600 MHz spectrometer at 25 °C. The recorded ^{1}H–NMR spectra were referenced to the residual proton signals of the deuterated NMR solvent. $^{13}C\{^{1}H\}$–NMR spectra were referenced to the ^{13}C signal of the used NMR solvent.[178]

Gel permeation chromatography measurements were performed on a Malvern Instruments OmniSec, equipped with triple detection and a UV/Vis detector, in THF at 35 °C column and detector oven temperature and 25 °C autosampler temperature. T6000 and T2500 chromatography columns a purchased from Malvern Instruments were used.

The flow rate was set to 1 mL/min. The instrument was calibrated with polystyrene standards.

Reaction monitoring was either performed by ^{1}H–NMR spectroscopy with aliquots removed from the reaction mixtures or with a Mettler-Toledo ReactIR 15 spectrometer, which was equipped with a MCT detector and a silver halide DiComp probe.

Differential scanning calorimetry (DSC) measurements were performed on a TA Instruments Discovery DSC under nitrogen flow with a heating rate of 10 °C/min in a range between 0 °C and 300 °C. The glass transition temperatures were determined from the third run. TGA measurements were performed on a TA Instruments Discovery TGA prior to DSC measurements to determine decomposition temperatures. The DSC measurements were performed with a maximum temperature accordingly.

X-ray analyses were performed by DI Alexander Prado-Roller and Natalie Gajic. The X-ray intensity data were measured on Bruker D8 Venture diffractometer equipped with multilayer monochromator, Mo K/α INCOATEC micro focus sealed tube and Oxford cooling system. The structures were solved by *Direct Methods, Charge Flipping and Intrinsic Phasing*. Non-hydrogen atoms were refined with *anisotropic displacement parameters*. Hydrogen atoms were inserted at calculated positions and refined with riding model. The following software was used: *Bruker SAINT software package* using a narrow-frame algorithm for frame integration, *SADABS* for absorption correction, *OLEX2* for structure solution, refinement, molecular diagrams and graphical user-interface, *Shelxle* for refinement and graphical user-interface *SHELXS-2015* for structure solution, *SHELXL-2015* for refinement*, Platon* for symmetry check.

5.3 Synthesis of Salen Ligands

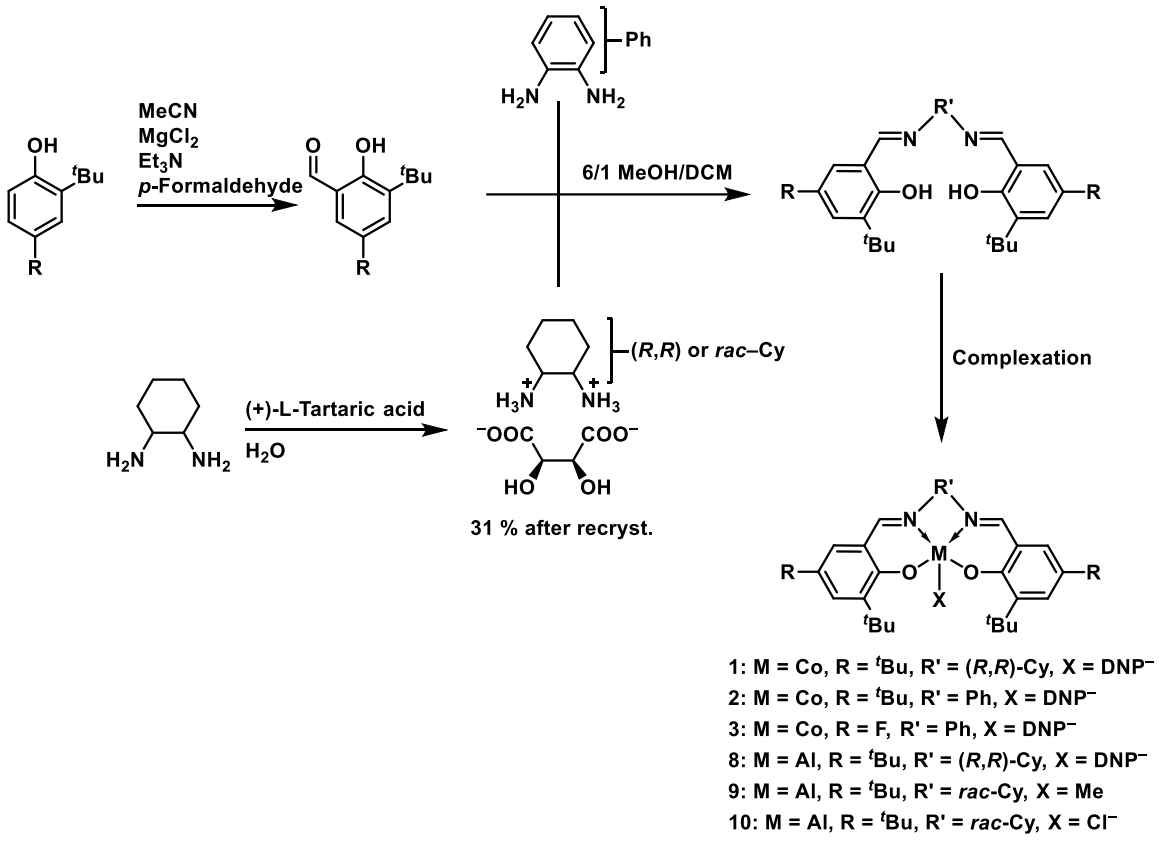

*Scheme S 1: Schematic ligand and complex synthesis of **1–3** and **8–10**.*

5.4 Synthesis of 2,4-Di(*tert*-butyl)salicyl aldehyde[146]

$MgCl_2$ (7.7 g, 81 mmol) was suspended in THF (160 mL) and 2,4-di(*tert*–butyl) phenol (8.24 g, 40 mmol) and *p*-formaldehyde (2.65 g, 88 mmol) were added at ambient temperature. Subsequently, triethylamine (11.5 mL, ρ = 0.73 g·cm^{-3}, 82 mmol) was added slowly. The reaction mixture was stirred for 2 h under reflux conditions and further 16 h at ambient temperature. The reaction mixture was acidified with diluted HCl and extracted with ethyl acetate. The combined organic phases were washed with water and brine and dried over $MgSO_4$. The solvent was evaporated and the crude product was freed of residual starting material by sublimation of the starting material in high vacuum at 50 °C. The product was obtained pure in 75 % (5.5 g, 26 mmol).

^{1}H-NMR (400 MHz, $CDCl_3$): δ 10.85 (s, 1H, O*H*), 9.87 (s, 1H, OC*H*), 7.57 (d, 1H, *J* = 2.5 Hz, Ar*H*), 7.51 (d, 1H, *J* = 2.5 Hz, Ar*H*), 1.43 (s, 9H, *t*Bu), 1.33 (s, 9H, *t*Bu).

5.5 Resolution of (*rac*)-1,2-Diaminocyclohexane

L–(+)-Tartaric acid (52 g, 0.35 mol) was dissolved in 500 mL of deionized water and (*rac*)-1,2-diaminocyclohexane (120 mL, 114 g, 1 mol) was added in a manner to prevent the water from boiling. After the addition a colorless precipitation formed. The suspension was allowed to reach ambient temperature and was further stirred for 2 h. The precipitate was filtered off and washed with MeOH to remove the excess of diamine. The product was recrystallized from water. The product (–)-(*R*,*R*)-1,2-diaminocyclohexane tartrate was obtained in 31 % yield (30 g, 110 mmol) referred to the L–(+)-tartaric acid. The purity was controlled by polarimetry (1 g/100 mL at 25 °C in water at 589 nm, [α]= +11.5) and is in agreement with the literature.[147]

5.6 (*R*,*R*)-*N*,*N*'-Bis(3,5-di-*tert*-butylsalicylidene)-1,2-cyclohexanediamine (L1)[148]

2,4-Di-(*tert*-butyl)salicyl aldehyde (36 mmol,8.45 g) was dissolved in MeOH (200 mL) and (–)-(*R*,*R*)-1,2-diaminocyclohexane L-tartrate (4.75 g, 18 mmol) was added in one portion. Subsequently, K_2CO_3 (72 mmol, 9.95 g) was added. The reaction mixture was stirred for 4 h at reflux conditions. The reaction mixture was allowed to reach ambient temperature and the formed yellow precipitate was filtered off and washed with cold MeOH. The crude product was recrystallized from a 3:1 acetone/MeOH mixture and was obtained pure in 77 % (7.54 g, 13.8 mmol). Spectroscopic data is in agreement with the literature.[148]

^{1}H–NMR (400 MHz, $CDCl_3$): δ 13.70 (s, 2H, O*H*), 8.30 (s, 2H, NC*H*C), 7.31 (d, *J* = 2.4 Hz, 2H, Ar*H*), 6.98 (d, *J* = 2.4 Hz, 2H, Ar*H*), 3.41 – 3.25 (m, 2H, CH_2), 1.95 (m, 2H, CH_2), 1.88 (m, 2H, CH_2) 1.74 (m, 2H, CH_2), 1.47 (m, 2H, CH_2), 1.42 (s, 18H, *t*Bu), 1.24 (s, 18H, *t*Bu).

ESIMS (m/z, M^++H^+): calc: 447.425 found: 447.425

5.7 *N,N*'-Bis(3,5-di-*tert*-butylsalicylidene)-1,2-diaminobenzene (L2)[148]

1,2-phenylene diamine (500 mg, 4.6 mmol) was dissolved in MeOH (150 mL) and 2,4-di-(*tert*-butyl)salicyl aldehyde (2.16 g, 9.20 mmol) was added in one portion. The reaction mixture was refluxed for 2 h and further stirred for 16 h at ambient temperature. The reaction mixture was diluted with CH_2Cl_2 (150mL). The reaction mixture was washed with water and the aqueous phase was extracted with CH_2Cl_2 (3 × 100 mL). The combined organic phases were dried over $MgSO_4$ and the solvent was removed. The crude product was recrystallized by dissolving it in boiling ethanol and slow cooling to 8 °C to give 72 % yield (1.79 g, 3.3 mmol). Spectroscopic data is in agreement to the literature.[148]

^{1}H–NMR (400 MHz, $CDCl_3$): δ 13.52 (s, 2H, O*H*), 8.66 (s, 2H, NC*H*C), 7.44 (d, *J* = 2.4 Hz, 2H, Ar*H*), 7.35 – 7.28 (m, 2H, Ar*H*), 7.25 – 7.15 (m, 4H, Ar*H*), 1.44 (s, 18H, *t*Bu), 1.32 (s, 18H, *t*Bu).

^{13}C{^{1}H}–NMR (151 MHz, $CDCl_3$) δ 164.9 (Ar*C*NAr), 158.7 (Ar*C*), 142.9 (Ar*C*), 140.5 (Ar*C*), 137.3 (Ar*C*), 128.3 (Ar*C*), 127.4 (Ar*C*), 126.9 (Ar*C*), 119.9 (Ar*C*), 118.5 (Ar*C*), 35.3 (*C*$(CH_3)_3$, 34.3 (*C*$(CH_3)_3$, 31.6 (*C*H_3), 29.6 (*C*H_3).

ESIMS (m/z, M^++H^+): calc: 541.3789; found: 541.3770

5.8 *p*-Fluoro-2-(*tert*-butyl)phenol[97, 179]

p-Fluorophenol (5,0 g, 44 mmol) was dissolved in *t*BuOH (9 mL, 94 mmol) and cooled to 0 °C. Concentrated H_2SO_4 (4mL) was added dropwise to the solution. The reaction mixture was allowed to reach ambient temperature (35 °C) and was further stirred for 2 d. The reaction mixture was diluted with CH_2Cl_2 (100 mL) and neutralized with a saturated, aqueous $NaHCO_3$. The phases were separated, and the aqueous phase was extracted with ethyl acetate (3 × 100 mL). The organic phases were combined and dried over $MgSO_4$. The solvents were removed, and the crude product was purified by column chromatography (ethyl acetate/heptane 2–20 %). The product was obtained pure in 70 % yield (5.28 g, 31.4 mmol). The spectroscopic data is in agreement with the literature.[97, 179]

^{1}H–NMR (400 MHz, $CDCl_3$) δ 6.97 (dd, *J* = 10.9, 3.0 Hz, 1H, Ar*H*), 6.74 (ddd, *J* = 8.7, 7.4, 3.1 Hz, 1H, Ar*H*), 6.61 (dd, *J* = 8.7, 4.9 Hz, 1H, Ar*H*), 1.40 (s, 9H, *t*Bu).

5.9 *p*-Fluoro-(*tert*-butyl)salicyl aldehyde[97]

p-Fluoro-2-(*tert*-butyl)phenol (0.428 g, 2.54 mmol) and *p*-formaldehyde (381 mg, 5 eq) were mixed as solids and were placed under an argon atmosphere. 2,6-Lutidine (0.407 g, 1.5 equiv, 3.8 mmol) was added under argon atmosphere and the argon atmosphere was refreshed by several cycles of slight evacuation and refilling. The mixture was suspended in dry toluene (20 mL), cooled to 0 °C and $SnCl_4$ (330 mg, 1.27 mmol) was added to the suspension. The reaction mixture was stirred for 18 h at 90 °C. The reaction was quenched by addition of 1 M aqueous HCl while the mixture was simultaneously vigorously stirred. The mixture was filtered over a celite pad, the phases were separated and the aqueous phase was extracted with diethyl ether. The combined organic phases were dried over $MgSO_4$ and the solvents were evaporated. The crude product was purified by column chromatography with ethyl acetate/heptanes (2–20%). The product was obtained in 41 % yield (201 mg, 1 mmol). The spectroscopic data is in agreement with the literature.[97]

^{1}H–NMR (400 MHz, $CDCl_3$) δ 11.58 (s, 1H, O*H*), 9.82 (s, 1H, OC*H*), 7.30 – 7.26 (m, 1H, Ar*H*), 7.07 (dd, *J* = 7.0, 3.1 Hz, 1H, Ar*H*), 1.42 (s, 9H, *t*Bu).

5.10 *N,N'*-Bis(*tert*-butyl-5-fluorosalicylidene)-1,2-diaminobenzene (L3)[58]

p-Fluoro-2-(*tert*-butyl)salicyl aldehyde (348 mg, 1.77 mmol), and 1,2–phenylene diamine (98.6 mg, 0.91 mmol) were dissolved in dry MeOH (50 mL) under argon atmosphere. The reaction mixture was refluxed for 20 h whereupon an orange solid precipitated. The precipitate was separated from the mother liquor which was concentrated. The resulting precipitate was separated again. The combined solids were dried under high vacuum. The ligand was obtained in 41 % yield (337 mg, 0.73 mmol). The spectroscopic data is in agreement with the literature.[58]

^{1}H–NMR (400 MHz, $CDCl_3$) δ 13.47 (s, 2H, O*H*), 8.59 (s, 2H, NC*H*C), 7.36 (dd, *J* = 5.9, 3.4 Hz, 2H, Ar*H*) 7.26 (m, 2H, Ar*H*), 7.13 (dd, *J* = 10.7, 3.1 Hz, 2H, Ar*H*), 6.93 (dd, *J* = 7.8, 3.1 Hz, 2H, Ar*H*), 1.42 (s, 18H, *t*Bu).

^{13}C{^{1}H}–NMR (151 MHz, $CDCl_3$) δ 163.5 (Ar*C*NAr), 163.5 (Ar*C*NAr), 157.1 (Ar*C*), 156.0 (Ar*C*), 154.4 (Ar*C*), 142.3 (Ar*C*), 140.4 (Ar*C*), 140.4 (Ar*C*), 128.1 (Ar*C*), 119.9 (Ar*C*), 118.6 (Ar*C*), 118.4 (Ar*C*), 114.9 (Ar*C*), 114.7 (Ar*C*), 35.3 ($C(CH_3)_3$, 29.2 (CH_3).

^{19}F–NMR (659 MHz, $CDCl_3$) δ –125.95.

ESIMS (m/z, M^++H^+): calc: 464.2275 found: 465.2347

5.11 2-[[(2-Aminophenyl)imino]methyl]-4,6-bis(1,1-dimethylethyl)phenol[180]

2,4-Di-(*tert*-butyl)salicyl aldehyde (513 mg, 2.2 mmol) and 1,2-phenylen diamine dihydrochloride (793 mg, 4.4 mmol) were dissolved/suspended in dry MeOH (40 mL).To the mixture Et_3N (0.3 mL, ρ = 0.73 g·cm^{-3}, 2.2 mmol) were added. The reaction was stirred for 16 h at ambient temperature. To the reaction mixture sat. aqueous $NaHCO_3$ (40 mL) was added and the aqueous phase was extracted with CH_2Cl_2 (3 × 50 mL). The combined organic phases were dried over $MgSO_4$ and the solvent was evaporated. The crude product was purified by isocratic column chromatography using CH_2Cl_2. The pure product was obtained in 53 % yield (380 mg, 1.17 mmol). Additionally, an 83 % pure (^{1}H–NMR spectroscopy) fraction could be collected. The spectroscopic data is in agreement with the literature.[181]

^{1}H–NMR (400 MHz, $CDCl_3$) δ 13.39 (s, 1H, O*H*), 8.64 (s, 1H, CN*H*C), 7.46 (d, J = 2.5 Hz, 1H, Ar*H*), 7.24 (d, J = 2.4 Hz, 1H, Ar*H*), 7.14 – 7.03 (m, 2H, Ar*H*), 6.83 – 6.77 (m, 2H, Ar*H*), 4.40 (s, br, 2H, N*H*$_2$), 1.48 (s, 9H, *t*Bu), 1.34 (s, 9H, *t*Bu).

5.12 4-*tert*-butyl-methoxybenzene (S1)[104]

Anhydrous K_2CO_3 (38.6 g, 280 mmol) was suspended in acetone (400 mL) and 4-*tert*-butylphenol (30.04 g, 200 mmol) was added to the suspension. Iodomethane (30.92 mL, ρ = 2.28 g·cm^{-3}, 500 mmol) was subsequently added. The reaction mixture was stirred until crude ^{1}H-NMR spectroscopic measurement showed full conversion. An aqueous (10 %) NaOH solution (50 mL) was added to the reaction mixture. The major part of the acetone was evaporated and the residual aqueous phase was extracted with diethyl ether (3 × 100 mL). The combined organic phases were dried over $MgSO_4$ and the solvent was evaporated. The product was obtained as an orange oil in 32.8 g (99 %).

The spectroscopic data is according to the expected signal changes based on the literature. [104]

^{1}H–NMR (400 MHz, $CDCl_3$) δ 7.33 (d, *J* = 8.8 Hz, 2H, Ar*H*), 6.86 (d, *J* = 8.8 Hz, 2H, Ar*H*), 3.81 (s, 3H, OCH_3), 1.32 (s, 9H, *t*Bu).

5.13 2-Iodo-1-methoxy-4-*tert*-butyl benzene (S2)[182]

4-(*tert*-butyl)methoxy benzene (32.8 g, 199 mmol) was dissolved in MeCN (300 mL). Subsequently, I_2 (101.39 g, 393 mmol) was added. 27 % $H_2O_{2(aq)}$ (27.8 mL) and of 38 % of aqueous HCl solution (3.8 mL) were added. The biphasic system was stirred for 16 h at reflux. After letting the mixture reach ambient temperature, the solution was poured into a saturated aqueous solution of $Na_2S_2O_5$ (300 mL). The acetonitrile was evaporated. At this point the formation of SO_2 is possible if a high excess of I_2 was employed. The residual aqueous phase was extracted with CH_2Cl_2 (3 × 150 mL) and the combined organic phases were dried over $MgSO_4$. After evaporation of the solvent the product was obtained in 58.0 g (99 %). The spectroscopic data is in agreement with the literature.)[182]

^{1}H–NMR (400 MHz, $CDCl_3$) δ 7.77 (d, *J* = 2.4 Hz, 1H, Ar*H*), 7.32 (dd, *J* = 8.6, 2.4 Hz, 1H, Ar*H*), 6.76 (d, *J* = 8.6 Hz, 1H, Ar*H*), 3.86 (s, 3H, OCH_3), 1.29 (s, 9H, *t*Bu).

5.14 3-(5-(*tert*-butyl)-2-methoxyphenyl)prop-2-yn-1-ol (S3)[183]

$Pd(PPh_3)_2Cl_2$ (140.4 mg, 0.2 mmol) and CuI (38 mg, 0.2 mmol,) were dissolved in dry MeCN (9 mL) and triethylamine (0.65 mL, 472 mg, ρ = 0.73 g·cm^{-3}, 8 mmol) was added. **S2** (1.06 g, 4 mmol) was added and the solution was stirred for 10 min at ambient temperature. The solution was cooled to 0 °C and 2-propynol (0.65 mL, ρ = 0.948 g·cm^{-3}, 12 mmol) was added. The exothermic reaction could be triggered by heating the mixture gently. The reaction mixture was stirred for 1 h at ambient temperature. The MeCN was evaporated and the dark brown oil was purified by column chromatography (Hept/EtOAc, 12–85 %). The product was obtained as an orange oil in 83 % yield (736 mg, 3.3 mmol).

^{1}H–NMR (400 MHz, $CDCl_3$) δ 7.35 (d, *J* = 2.5 Hz, 1H, Ar*H*), 7.24 (dd, *J* = 8.7, 2.5 Hz, 1H, Ar*H*), 6.75 (d, *J* = 8.7 Hz, 1H, Ar*H*), 4.45 (s, 2H, CH_2), 3.79 (s, 3H, OCH_3), 1.21 (s, 9H, *t*Bu).

ESIMS (m/z, M+Na$^+$): calc: 241.1204, found: 241.1200

5.15 3-(5-(*tert*-butyl)-2-methoxyphenyl)propan-1-ol (S4)

3-(5-(*tert*-butyl)-2-methoxyphenyl)prop-2-yn-1-ol (4.38 g, 20.1 mmol) was dissolved in a heptane/ethanol mixture (4:1, v:v, 50 mL) and 1 mol% of Pd/C (28 mg, 10% loading) was added. The mixture was stirred under 70 bar of H_2 at ambient temperature for 24 h. The product was isolated by filtration over celite and removal of the solvent and was obtained as a yellow oil (4.26 g, 19.2 mmol, 96%). The spectroscopic data is in agreement with the literature.[104]

^{1}H–NMR (400 MHz, $CDCl_3$) δ 7.21 (d, *J* = 2.6 Hz, 1H, Ar*H*), 7.18 (dd, *J* = 5.4, 2.4 Hz, 1H, Ar*H*), 6.80 (d, *J* = 8.3 Hz, 1H, Ar*H*), 3.82 (s, 3H, OCH_3), 3.62 (t, *J* = 6.2 Hz, 2H, CH_2), 2.72 (t, *J* = 7.3 Hz, 2H, CH_2), 1.91 – 1.81 (m, 2H, CH_2), 1.30 (s, 9H, *t*Bu).

5.16 2-(3-Bromopropyl)-4-(*tert*-butyl)-methoxybenzene (S5)[104]

3-(5-(*tert*-butyl)-2-methoxyphenyl)propan1-ol (3.6 g, 13 mmol) was dissolved in toluene (100 mL) and PBr_3 (3.29 mL, 9.37 g, ρ = 2.85 g·cm^{-3}, 34.6 mmol) was added. The reaction was stirred under reflux for 2 h and further overnight at ambient temperature. Afterwards, the reaction mixture was quenched with a sat. aqueous solution of $NaHCO_3$ (100 mL). The organic phase was separated and the aqueous phase was extracted with ethyl acetate (3 × 100 mL). The combined organic phases were dried over $MgSO_4$ and the solvent was evaporated. The crude product was purified by column chromatography using ethyl acetate / heptane (3–30 %). The pure product was obtained in 83 % yield (2.99 g, 10.5 mmol). The spectroscopic data is in agreement with the literature.[104]

^{1}H–NMR (400 MHz, $CDCl_3$) δ 7.18 (dd, *J* = 2.8, 2.2 Hz, 2H, Ar*H*), 6.78 (d, *J* = 8.4 Hz, 1H, Ar*H*), 3.80 (s, 3H, OCH_3), 3.41 (t, *J* = 6.8 Hz, 2H, CH_2), 2.76 (dd, *J* = 8.0, 6.6 Hz, 2H, CH_2), 2.26 – 2.06 (m, 2H, CH_2), 1.30 (s, 9H, *t*Bu).

5.17 7-(3-(5-*tert*-Butyl)-2-(methoxyphenyl)propyl)-1,5,7-triabicyclo[4.4.0]dec-5-ene (S6)[104]

1,5,7-Triabycyclo[4.4.0.]dec-5-ene (4.08 g, 29.3 mmol) was dissolved in degassed, dry THF (50 mL) and NaH (1.7 g, 71 mmol) was added to the solution. The reaction mixture

was stirred for 3 d at room temperature. 2-(3-Bromopropyl)-4-(*tert*-butyl)-methoxybenzene (3.8 g, 13.3 mmol) was added to the deprotonated 1,5,7-triabycyclo[4.4.0.]dec-5-ene and stirred for 2 h. The excess of NaH was quenched by the slow addition of water to the cooled (0 °C) reaction mixture. The phases were separated and the aqueous phase was extracted with CH_2Cl_2 (3 × 50 mL). The combined organic phases were washed with brine (2 x 50 mL) and dried over $MgSO_4$. After evaporation of the solvent the crude product was purified by column chromatography using MeOH/CH_2Cl_2 (0–10 %.) The product was obtained in 3.8 g (11 mmol, 83 %). The spectroscopic data is in agreement with the literature.[104]

^{1}H–NMR (400 MHz, $CDCl_3$) δ 7.25 (d, *J* = 2.5 Hz, 1H, Ar*H*), 7.16 (dd, *J* = 8.5, 2.5 Hz, 1H, Ar*H*), 6.75 (d, *J* = 8.5 Hz, 1H, Ar*H*), 3.78 (s, 3H, CH_3), 3.76 – 3.67 (m, 2H, CH_2), 3.54 (m, 2H, CH_2), 3.30 (m, 6H, CH_2), 2.78 – 2.70 (m, 2H, CH_2), 1.98 (m, 6H, CH_2), 1.28 (s, 9H, *t*Bu).

ESIMS (m/z, M^++H^+): calc: 344.2697, found: 344.2694

5.18 7-(3-(5-*tert*-Butyl)-2-hydroxyphenyl)propyl)-1,5,7-triabicyclo[4.4.0]dec-5-ene (S7)[104]

7-(3-(5-*tert*-Butyl)-2-(methoxyphenyl)propyl)-1,5,7-triabicyclo[4.4.0]dec-5-ene (3.8 g, 12 mmol) was dissolved in dry CH_2Cl_2 (30 mL) and a 1 M solution of BBr_3 in toluene (82 mL) were added to the solution. The reaction mixture was stirred for 16 h (but not more) at room temperature. Significantly longer reaction times were observed to cause a significant amount of side products. The reaction was quenched by the slow addition of saturated $NaHCO_3$ solution. The phases were separated and the aqueous phase was extracted with CH_2Cl_2 (3 × 50 mL). The combined organic phases were dried over $MgSO_4$ and the solvent was evaporated. The product was obtained in 95 % (3.50 g, 11.0 mmol). The spectroscopic data is in agreement with the literature.[104]

^{1}H–NMR (400 MHz, $CDCl_3$) δ 8.93 (br, s, 1H, O*H*), 7.05 (dd, *J* = 8.4, 2.5 Hz, 1H, Ar*H*), 7.00 (d, *J* = 2.5 Hz, 1H, Ar*H*), 6.88 (d, *J* = 8.4 Hz, 1H, Ar*H*), 3.62 – 3.52 (m, 2H, CH_2), 3.51 – 3.42 (m, 2H, CH_2), 3.38 – 3.22 (m, 6H, CH_2), 2.82 – 2.70 (m, 2H, CH_2), 2.08 – 1.79 (m, 6H, CH_2), 1.25 (s, 9H, *t*Bu).

ESIMS (m/z, M^++H^+): calc: 330.254, found: 330.253

5.19 7-(3-(5-*tert*-butyl)-3-(formyl)-2-(hydroxyphenyl)propyl)-1,5,7-triabicyclo[4.4.0]dec-5-ene (S8)[104]

7-(3-(5-*tert*-Butyl)-2-(hydroxyphenyl)propyl)-1,5,7-triabicyclo[4.4.0]dec-5-ene (1.542 g, 4.68 mmol) was dissolved in absolute THF (70 mL) and anhydrous $MgCl_2$ (1.79 g, 18.8 mmol) was added to the solution. To the suspension *p*-formaldehyde (1.07 g, 35.63 mmol) and Et_3N (1.542 mL Et_3N in 20 mL THF, 11.1 mmol) were added. The reaction mixture was stirred for 3 d under reflux conditions. Subsequently, the solvent was evaporated and the residue was dissolved in ethyl acetate (100 mL) and the solution was acidified using an aqueous 4 M HCl until the aqueous phase had about ~ pH 5. The two phases were separated, the acidic aqueous phase was neutralized and extracted with CH_2Cl_2 (3 x 50 mL). The combined organic phases were dried over $MgSO_4$ and the solvent was evaporated. The product was obtained in 52 %. (870 mg, 2.43 mmol) after a purification by column chromatography (MeOH/CH_2Cl_2 0–15 %).

^{1}H–NMR (400 MHz, $CDCl_3$) δ 11.05 (s, br, 1H, O*H*), 9.88 (s, 1H, OC*H*C), 7.64 (d, *J* = 2.5 Hz, 1H, Ar*H*), 7.36 (d, *J* = 2.5 Hz, 1H, Ar*H*), 3.78 (t, *J* = 7.4 Hz, 2H, CH_2), 3.48 (d, *J* = 4.5 Hz, 2H, CH_2), 3.37 – 3.26 (m, 6H, CH_2), 2.87 – 2.79 (m, 2H, CH_2), 2.10 – 1.90 (m, 6H, CH_2), 1.31 (s, 9H, *t*Bu).

ESIMS (m/z, M^++H^+): calc: 358.2490, found: 358.2490

5.20 Synthesis of 2,6-Dibromo-4-(*tert*-butyl) phenol

4-*tert*-butylphenol (1.5 g, 10 mmol) was dissolved in dry CH_2Cl_2 (150 mL) under argon atmosphere. The solution was cooled to 0 °C and Br_2 (2.6 mL, ρ = 3.12 g · cm^{-3}, 50.8 mmol) were dropwise added. The reaction mixture was further stirred for 1.5 h at 0 °C and additional 20 h at room temperature. The residual bromine was quenched by addition of a saturated aqueous $Na_2S_2O_3$ solution (50 mL). The phases were separated and the aqueous phase was extracted with ethyl acetate (3 × 50 mL). The combined organic phases were washed with brine (30 mL), dried over $MgSO_4$ and the solvent was evaporated. The crude product was purified by column chromatography (2–20 %

EtOAc:Hept.). The product was obtained in a yield of 70 % (2.15 g, 0.7 mmol). The spectroscopic data is in agreement with the literature.[185]

^{1}H–NMR (400 MHz, $CDCl_3$) δ 7.43 (s, 2H, Ar*H*), 5.94 (s, br, 1H, O*H*), 1.27 (s, 9H, *t*Bu).

5.21 Synthesis of 2,6-Dibromo-4-methyl phenyl-dimethyl(*tert*-butyl)silyl ether[150]

2,6-Dibromo-4-methyl phenol (1,33 g, 5.00 mmol) and imidazole (1.36 g, 19.98 mmol) were dissolved in dry dichloromethane (30 mL) under argon atmosphere and cooled to 0 °C. Subsequently, a solution of *tert*-butyl-dimethyl-chloro silane (50 % in toluene) (0.75 g, 0.86 mL, 5 mmol) was added dropwise. The reaction mixture was allowed to reach ambient temperature and was additionally stirred under reflux for 18 h. The solvent was evaporated and water (30 mL) and heptanes (80 mL) were added to the residue. The phases were separated and the organic phase was washed with a 0.2 M solution of HCl (30 mL), water (30 mL) and brine (30 mL). The organic phase was dried over $MgSO_4$ and the solvent was evaporated. The crude product was purified by column chromatography (ramp 20%–48% EtOAc:Hept.). The product was obtained pure as colorless liquid in 94 % (1.79 g, 4.7 mmol). The spectroscopic data is in agreement with the literature.[184]

^{1}H–NMR (400 MHz, $CDCl_3$): δ 7.30 – 7.27 (m, 2H, Ar*H*), 2.24 (s, 3H, Me), 1.06 (s, 9H, *t*Bu), 0.35 (s, 6H, Me).

5.22 Synthesis of 3-(*tert*-butyldimethylsilyl)-2-hydroxy-5-methylbenzaldehyde (S9)[150]

2,6-Dibromo-4-methyl phenyl-dimethyl(*tert*-butyl)silyl ether (1.79 g, 4.7 mmol) was dissolved in dry Et_2O (10 mL) and cooled to –78 °C. *n*–BuLi (6.96 mL, 18.8 mmol, 2.7 M in hexanes) was added dropwise to the mixture. The reaction mixture was stirred for further 30 min before allowing the mixture to reach ambient temperature and stirred for additional 1.5 h. The reaction mixture was cooled down again to –78 °C and dry DMF (1.4 mL, ρ = 0.94 $g \cdot cm^{-3}$,18 mmol) was added in one portion. Upon addition the reaction mixture turned slightly yellow. After the addition of DMF the reaction mixture was allowed to warm up to ambient temperature again and was further stirred for 18 h. The reaction was

quenched by addition of $NaHCO_3$ (40 mL) and additional Et_2O (20 mL) were added. The phases were separated and the organic phase was washed with sat. aqueous $NaHCO_3$ solution (30 mL), water (30 mL) and brine (30 mL). After drying the organic phase over $MgSO_4$ the solvent was evaporated and the crude mixture was purified by column chromatography (10%–23% EtOAc:Hept.). The pure product was obtained in 81 % yield (0.955 mg, 3.81 mmol). The spectroscopic data is in agreement with the literature.[150]

^{1}H–NMR (400 MHz, $CDCl_3$): δ 11.11 (s, 1H, OC*H*CO), 9.75 (s, 1H, O*H*), 7.41 (d, *J* = 2.2 Hz, 1H, Ar*H*), 7.31 (d, *J* = 2.1 Hz, 1H, Ar*H*), 2.26 (s, 3H, Me), 0.83 (s, 9H, *t*Bu), 0.25 (s, 6H, Me) ppm.

^{13}C{^{1}H}–NMR (151 MHz, $CDCl_3$) δ 197.0 (Ar*C*O), 164.8 (Ar*C*), 145.3 (Ar*C*), 135.0 (Ar*C*), 128.4 (Ar*C*), 126.5 (Ar*C*), 119.5 (Ar*C*), 29.9 (*C*$(CH_3)_3$) 27.1 (*C*H_3), 20.5 (*C*H_3)–4.74 (Si–*C*H_3).

5.23 Synthesis of 2,6-Dibromo-4-(*tert*-butyl) triphenyl silyl ether[150]

2,6-Dibromo-4-(*tert*-butyl) phenol (2.15 g, 6.98 mmol) and imidazole (1.9 g, 28 mmol) were dissolved in dry CH_2Cl_2 (10 mL) under argon atmosphere and TPSCl (2.26 g, 7.50 mmol) was added. The reaction was stirred for 16 h under reflux conditions. The solvent was removed and hexane (200 mL), CH_2Cl_2 (20 mL) and water (100 mL) were added. After mixing the two phases thoroughly they were separated, and the organic phase was treated with 50 mL of a 0.2 M aqueous HCl solution. The organic phase was washed with water and brine and dried over $MgSO_4$. The solvent was removed and the product was obtained as a white powder in 80 % yield (3.1 g, 5.6 mmol). The spectroscopic data is in agreement with the expected signal changes based on the literature.[150]

^{1}H–NMR (400 MHz, $CDCl_3$) δ 7.74 – 7.67 (m, 6H, Ar*H*), 7.44 – 7.39 (m, 3H, Ar*H*), 7.35 (m, 6H, Ar*H*), 7.32 (s, 2H, Ar*H*), 1.21 (s, 9H, *t*Bu).

5.24 Synthesis of 4-*tert*-butyl-(6-triphenylsilyl) salicylaldehyde (S10)[150]

2,6-Dibromo-4-*tert*–butyl-triphenyl silyl ether (3.1 g, 5.5 mmol) was dissolved dry THF (250 mL) and the solution was cooled to –78 °C. *t*–BuLi (1.7 M in pentane, 13.5 mL,

22.9 mmol) was added dropwise. The reaction mixture was stirred for an additional hour at –78 °C and 1 h at 0 °C. At this stage of the reaction the solution had a deep red color. The reaction mixture was cooled to –78 °C and DMF (1.8 mL, ρ = 0.94 g·cm^{-3}, 22.8 mmol) was added to the mixture, whereupon the color changed to violet and a solid started to form. The reaction mixture was stirred for 1 h at –78 °C and was then allowed to warm up to 0 °C. The mixture turned to a yellow suspension. The reaction was quenched with a sat. NH_4Cl solution (20 mL) and diluted with THF (150 mL). The phases were separated and the aqueous phase was extracted with diethyl ether (3 × 100 mL). The combined organic phases were washed with water (100 mL) and brine (100 mL) and dried over $MgSO_4$. After evaporation of the solvent the product was obtained after recrystallization from methanol in 61 % yield (1.8, 4.27 mmol). The spectroscopic data is in agreement with the literature with the exception of the methyl group. The 4-methyl group. in the literature is exchanged by a *tert*-butyl group in this work.[150]

^{1}H–NMR (400 MHz, $CDCl_3$) δ 11.26 (s, 1H, C*H*CO), 9.92 (s, 1H, O*H*), 7.67 – 7.60 (m, 6H, Ar*H*), 7.56 (dd, *J* = 21.1, 2.6 Hz, 2H, Ar*H*), 7.47 – 7.34 (m, 9H, Ar*H*), 1.17 (s, 9H, *t*Bu).

5.25 Ligand L4

The compound was obtained as product of a transamination reaction which occurred during the purification procedure of **L5**.

7-(3-(5-(*tert*-Butyl)-3-(formyl)-2-(hydroxyphenyl)propyl)-1,5,7-triabicyclo[4,4,0]dec-5-ene (**S8**) (700 mg, 2.18 mmol) and 2-(((2-aminocyclohexyl)imino)methyl)-4,6-di-(*tert*-butyl)phenol (722 mg, 2.18 mmol) were mixed in the solid state and were set under argon atmosphere. The solid mixture was dissolved in CH_2Cl_2 and the solution was stirred for 3 h at ambient temperature. The solvent was evaporated and the crude product was purified by two flash chromatographies over silica using MeOH/CH_2Cl_2 (10–35 % ramp). The compound was obtained in 35 % (600 mg, 0.75 mmol). The spectroscopic data corresponds to the expected signal change from the respective cobalt complex. The ligand was not separately characterized in the literature [104]

^{1}H–NMR (400 MHz, $CDCl_3$) δ 13.26 (s, 2H, O*H*), 8.30 (s, 2H, NC*H*C), 7.31 (d, *J* = 2.4 Hz, 2H), 7.00 (d, *J* = 2.4 Hz, 2H, Ar*H*), 3.71 (m, 4H, CH_2), 3.50 (d, *J* = 9.9 Hz, 6H, CH_2), 3.39 – 3.30 (m, 2H, Cy), 3.27 (t, *J* = 6.1 Hz, 4H, CH_2), 3.19 (m, 4.2 Hz, 6H, CH_2), 2.77 (m,

4H, C*H*$_2$), 1.92 (m, 16H, C*H*$_2$), 1.75 – 1.60 (m, 2H, Cy), 1.53 – 1.41 (m, 2H, Cy), 1.23 (s, 18H, *t*Bu), 1.11 – 0.99 (m, 2H, C*H*N).

ESIMS (m/z, M+2H$^+$): calc: 397.2962, found: 397.2970

5.26 Ligand L5[104]

The synthetic procedure is identical with the synthetic procedure of **L4**. The desired product was obtained as a fraction from chromatographic purification of the described method above in 8 % yield (130 mg, 0.19 mmol). The spectroscopic data is in agreement with the expected signal changes based on the literature.[104]

^{1}H–NMR (400 MHz, $CDCl_3$) δ 13.67 (s, 1H, O*H*), 13.30 (s, 1H, O*H*), 8.30 (s, 1H, NC*H*C), 8.27 (s, 1H, NC*H*C), 7.30 (t, *J* = 2.5 Hz, 1H, Ar*H*), 7.26 (s, 1H, Ar*H*), 6.97 (t, *J* = 2.6 Hz, 2H, Ar*H*), 3.66 (m, 2H, C*H*$_2$), 3.54 – 3.45 (m, 2H, C*H*$_2$), 3.40 – 3.25 (m, 8H, C*H*$_2$), 2.73 (dd, *J* = 9.1, 6.3 Hz, 2H, C*H*$_2$), 2.05 – 1.85 (m, 14H, C*H*$_2$), 1.40 (s, 9H, *t*Bu), 1.23 (s, 9H, *t*Bu), 1.21 (s, 9H, *t*Bu).

ESIMS (m/z, M+H$^+$): calc: 670.5055, found: 670.5053

5.27 Ligand L6[150]

3-(*tert*-Butyl)-dimethylsilyl)-2-hydroxy-5-methylbenzaldehyde (401 mg, 1.6 mmol) was dissolved in methanol (80 mL) and (*R*,*R*)-1,2-diamoniumocyclohexane tatrate (211 mg, 0.8 mmol) was added in one portion. Subsequently, Et_3N (0.33 mL, ρ = 0.726 g · cm^{-3}, 2.4 mmol) was added dropwise to the reaction mixture, whereupon a color change to yellow was observed. The reaction mixture was further stirred overnight at ambient temperature. The solvent was evaporated and the residue was dissolved in dichloromethane (50 mL). The solution was washed with saturated $NaHCO_3$ solution, water and brine (each 50 mL). The organic phase was dried over $MgSO_4$, and the dichloromethane was evaporated and the crude product was purified by column chromatography using a ramp 5–30 % EtOAc/Hept. The product was obtained pure in 38 % (358 mg, 0.62 mmol). The spectroscopic data corresponds to the literature except for in this work the *t*Bu in position 5 is exchanged by a methyl group compared to the literature.[150]

^{1}H–NMR (400 MHz, $CDCl_3$) δ 13.09 (s, 2H, O*H*), 8.15 (s, 2H, C*H*NC), 7.09 (d, *J* = 2.0 Hz, 2H, Ar*H*), 6.86 (d, *J* = 1.8 Hz, 2H, Ar*H*), 2.19 (s, 6H, Me), 2.01 – 1.68 (m, 6H, Cy), 1.38 – 1.18 (m, 4H, Cy), 0.89 (s, 18H, *t*Bu), 0.30 (s, 6H, Me), 0.28 (s, 6H, Me).

ESIMS (m/z, M^++H^+): calc: 579.3797, found: 579.3789

5.28 Ligand L7

2-(((2-aminophenyl)imino)methyl)-4-(*tert*-butyl)-6-(triphenylsilyl)phenol (59.7 mg, 0.11 mmol) and **S10** (51.30 mg, 0.11 mmol) were mixed in the solid state and subsequently dissolved in dried methanol (5 mL) under argon atmosphere. The reaction mixture was further stirred for 16 h at room temperature, then saturated aqueous $NaHCO_3$ solution (10 mL) was added to the reaction mixture. The aqueous phase was extracted with dichloromethane (3 x 15 mL) and the combined organic phases were dried over $MgSO_4$. The solvent was removed to give a yellow solid after column chromatography (2–17 % EtOAc/Hept.) in 99% yield (108 mg, 0.11 mmol).

^{1}H–NMR (400 MHz, $CDCl_3$): δ 13.00 (s, 2H, O*H*), 8.57 (s, 2H, C*H*N), 7.64 (m, 2H, Ar*H*), 7.56 (d, *J* = 6.7 Hz, 12H, Ar*H*)), 7.37 (d, *J* = 14.0 Hz, 4H, Ar*H*), 7.17 (t, *J* = 7.4 Hz, 18H, Ar*H*), 7.10 – 7.04 (m, 2H, Ar*H*), 1.11 (s, 18H, *t*Bu).

ESIMS (m/z, M^++H^+): calc: 945.425, found: 945.426

5.29 Complex Syntheses

5.30 Synthesis of 1[186]

$Co(OAc)_2 \cdot 4\ H_2O$ (498 mg, 2.00 mmol) was dissolved in a dry 6:1 mixture of MeOH and CH_2Cl_2 (70 mL). The mixture was stirred for 20 min. With the following portioned addition of (*R*,*R*)-*N*,*N*'-bis(3,5-di-(*tert*-butyl)salicylidene)-1,2-cyclohexanediamine (**L1**) (504 mg, 0.92 mmol) a brick red solid precipitated out of solution. The solid was filtered of and washed several times with MeOH (20 mL). Subsequently, the solid was dissolved in CH_2Cl_2 (100 mL) and 2,4-dinitrophenol (184 mg, 1 mmol) was added in one portion. The reaction mixture was stirred for an additional 16 h under an oxygen atmosphere. Upon stirring the red colored solution turned first dark green and then almost black. The solution

was filtered, the solvent was evaporated and the residue was washed with cold pentane (5 mL). The complex **1** was dried in high vacuum and was obtained in 77 % yield (561 mg, 0.71 mmol) as a dark green powder. The spectroscopic data is in agreement with the literature.[186]

The complex was also prepared as a racemic mixture in almost quantitative yield (708 mg, 0.9 mmol). Employed substrates: $Co(OAc)_2 \cdot 4\ H_2O$ (490 mg, 1.97 mmol), *rac*-*N*,*N*'-bis(3,5-di-(*tert*-butyl)salicylidene)-1,2-cyclohexanediamine (*rac*-**L1**) (498 mg, 0.91 mmol)

^{1}H–NMR (600 MHz, $(CD_3)_2SO$) δ 8.59 (d, J = 3.2 Hz, 1H, Ar*H*), 7.81 (s, 2H, NC*H*C), 7.77 (dd, J = 9.8, 3.2 Hz, 1H, Ar*H*), 7.46 (dd, J = 16.8, 2.6 Hz, 4H, Ar*H*), 6.30 (d, J = 9.8 Hz, 1H, Ar*H*), 3.61 (m, 2H, Cy), 3.07 (m, 2H, Cy), 2.00 (m, 2H, Cy), 1.92 (m, 2H, Cy), 1.74 (s, 18H, *t*Bu), 1.59 (m, 2H, Cy), 1.30 (s, 18H, *t*Bu).

R,*R*–Complex

^{13}C{^{1}H}–NMR (151 MHz, $(CD_3)_2SO$) δ 170.3 (Ar*C*NO$_2$), 164.6 (Ar*C*NCy), 162.0 (Ar*C*NCy), 141.8 (Ar*C*H), 135.9 (Ar*C*H), 129.2 (Ar*C*), 128.8 (Ar*C*), 127.4 (Ar*C*), 126.5 (Ar*C*), 125.0 (Ar*C*), 118.6 (Ar*C*H), 69.3 (CyN), 35.8 (*C*H$_2$), 33.5 (*C*H$_2$), 31.5 (*C*H$_3$), 30.4 (*C*H$_3$), 29.50 (*C*(CH$_3$)$_3$), 24.3 (*C*(CH$_3$)$_3$).

rac–Complex

^{13}C{^{1}H}–NMR (151 MHz, $(CD_3)_2SO$) δ 170.6 (Ar*C*NO$_2$) 164.7 (Ar*C*NCy), 162.1 (Ar*C*NCy), 141.8 (Ar*C*H), 135.9 (Ar*C*H), 129.3 (Ar*C*), 128.8 (Ar*C*), 127.4 (Ar*C*), 126.6 (Ar*C*), 125.1 (Ar*C*), 118.5 (Ar*C*H), 69.3 (CyN), 35.8 (*C*H$_2$), 33.6 (*C*H$_2$), 31.5 (*C*H$_3$), 30.4 (*C*H$_3$), 29.5 (*C*(CH$_3$)$_3$), 24.3 (*C*(CH$_3$)$_3$).

ESIMS (m/z, M$^+$): calc: 603.3361; found: 603.3345

5.31 Synthesis of 2

$Co(OAc)_2 \cdot 4\ H_2O$ (70.1 mg, 0.28 mmol) was carefully heated with a heat gun (temperature 250 – 300 °C) in dynamic high vacuum while stopping to heat the flask every couple of seconds to avoid decomposition of the cobalt acetate. The flask was heated until the pink color of the substance changed to deep purple. *N*,*N*'-Bis(3,5-di-(*tert*-butyl)salicylidene)-1,2-diaminobenzene (**L2**) (154 mg, 0.28 mmol) was added in solid state and the mixture was dissolved in dry CH_2Cl_2 (20 mL) and MeOH (5 mL). The reaction

mixture was stirred for 2 h at ambient temperature under argon atmosphere and 2,4-dinitrophenol (53 mg, 0.29 mmol) was added to the solution. The argon atmosphere was replaced by O_2 and the reaction solution was stirred for 18 h under oxygen atmosphere. The solvent was evaporated and the residue was washed with cold pentane (2 mL). The complex was obtained in 83 % yield (183 mg, 0.23 mmol). The spectroscopic data is in agreement with the literature.[187]

^{1}H–NMR (600 MHz, $(CD_3)_2SO$) δ 8.93 (s, 2H, NC*H*C), 8.67 – 8.61 (m, 4H, Ar*H*), 8.12 – 8.07 (m, 1H, Ar*H*, DNP), 7.65 (d, *J* = 2.5 Hz, 1H, Ar*H*, DNP), 7.59 – 7.54 (m, 4H, Ar*H*), 6.82 (d, *J* = 9.9 Hz, 1H, Ar*H*, DNP), 1.78 (s, 18H, *t*Bu), 1.35 (s, 18H, *t*Bu).

^{13}C{^{1}H}–NMR (151 MHz, $(CD_3)_2SO$) δ 164.5 (Ar*C*NAr), 161.5 (Ar*C*NAr), 144.6 (Ar*C*), 142.0 (Ar*C*), 136.5 (Ar*C*), 130.9 (Ar*C*H), 129.8 (Ar*C*H), 128.5 (Ar*C*H), 128.0 (Ar*C*H), 117.4 (Ar*C*), 117.3 (Ar*C*), 35.9 ($C(CH_3)_3$), 33.7 ($C(CH_3)_3$), 31.3 (CH_3), 30.3 (CH_3).

ESIMS (m/z, M^+): calc: 597.2891; found: 597.2889
ESIMS (m/z, DNP^-): calc: 183.0042 found: 183.0047

5.32 Synthesis of 3

$Co(OAc)_2 \cdot 4\ H_2O$ (322 mg, 1.29 mmol) was carefully heated with a heat gun (temperature 250 – 300 °C) in dynamic high vacuum while stopping to heat the flask every couple of seconds to avoid decomposition of the cobalt acetate. The flask was heated until the pink color of the substance changed to deep purple. The cobalt acetate was dissolved in dry MeOH (10 mL) and *N*,*N'*-Bis(*tert*-butyl-5-fluorosalicylidene)-1,2-diaminobenzene (**L3**) (596 mg, 1.28 mmol) was added to the solution. The solution changed the color to brown and a brown solid precipitated. Toluene (40 mL) and *o*-difluorobenzene (20 mL) were added, whereupon the solid partially dissolved. The reaction mixture was stirred under reflux conditions for 20 h. The reaction mixture was cooled to ambient temperature, 2,4-dinitrophenol (237 mg, 1.29 mmol) was added, and the mixture was stirred for 3 d under an O_2 atmosphere. The solid was separated from the solution. The filtrate was concentrated to dryness. The desired complex could be obtained as a brown powder in 69 % yield (622 mg, 0.89 mmol). The complex **3** showed poor solubility in chloroform and moderate solubility in dimethyl sulfoxide.

^{1}H–NMR (600 MHz, $(CD_3)_2SO$) δ 8.59 (dd, *J* = 6.3, 3.4 Hz, 2H, NC*H*C), 7.83 – 7.74 (m, 1H, Ar*H*, DNP), 7.63 (dd, *J* = 6.3, 3.2 Hz, 2H, Ar*H*), 7.49 (dd, *J* = 8.5, 3.3 Hz, 2H, Ar*H*), 7.36 (dd, *J* = 10.5, 3.3 Hz, 2H, Ar*H*), 7.29 – 7.11 (m, 1H, Ar*H*, DNP), 6.32 (d, *J* = 9.2 Hz, 1H, Ar*H,* DNP), 1.76 (s, 18H, *t*Bu).

^{13}C{^{1}H}–NMR (151 MHz, $(CD_3)_2SO$) δ 162.6 (Ar*C*NAr), 161.1 (Ar*C*NAr), 152.0 (d, *J* = 230.4 Hz), 144.70 (Ar*C*), 144.5 (Ar*C*), 128.6 (Ar*C*H), 121.9 (Ar*C*H), 121.7 (Ar*C*H), 117.5 (Ar*C*H), 116.8 (Ar*C*), 116.7 (Ar*C*H), 116.5 (Ar*C*H), 116.3 (Ar*C*H), 36.0 (*C*$(CH_3)_3$) 29.81 (*C*H_3).

ESIMS (m/z, M^+): calc: 521.1450 found: 521.1445
ESIMS (m/z, DNP^-): calc: 183.0042 found: 183.0046

^{19}F–NMR (659 MHz, $(CD_3)_2SO$) δ – 129.0 (t, J = 9.2 Hz).

5.33 Synthesis of 4

$Co(OAc)_2 \cdot 4\ H_2O$ (186 mg, 0.75 mmol) was carefully heated with a heat gun (temperature 250 – 300 °C) in dynamic high vacuum while stopping to heat the flask every couple of seconds to avoid decomposition of the cobalt acetate. The flask was heated until the pink color of the substance changed to deep purple. The cobalt acetate was dissolved in dry MeOH (50 mL) and **L4** (600 mg, 0.75 mmol) was added to the solution which turned deep red. The solution was further stirred for 3 h under Ar atmosphere at ambient temperature. 2,4-dinitrophenol (138 mg, 0.75 mmol) were added to the complex solution and the atmosphere was exchanged to oxygen. The reaction mixture was stirred under an O_2 atmosphere for 3 d. The solvent was evaporated and the residue was washed with pentane. The complex **4** was dried in high vacuum and was obtained in 41 % yield (318 mg, 0.31 mmol) as a brown powder. The spectroscopic data is in agreement with expectable signals based on the literature.[104]

^{1}H–NMR (600 MHz, $(CD_3)_2SO$) δ 8.66 (s, 1H, ArH), 8.42 (s, 1H, Ar*H*), 7.98 (s, 1H, Ar*H*), 7.82 (s, 2H, NC*H*C), 7.48 (s, 1H, Ar*H*), 7.37 (m, 1H, Ar*H*), 7.24 (s, 1H, Ar*H*), 6.27 (s, 1H, Ar*H*), 3.58 (m, 4H, CH_2), 3.45 – 3.15 (m, 20H, CH_2), 3.07 (m, 4H, CH_2), 2.31 – 2.09 (m, 2H, CH_2), 2.06 – 1.66 (m, 14H, CH_2), 1.56 (m, 2H, CH_2), 1.31 (s, 9H, *t*Bu), 1.28 (s, 9H, *t*Bu).

$^{13}C\{^{1}H\}$–NMR (151 MHz, $(CD_3)_2SO$) δ 164.1 (Ar*C*NCy), 163.4 (Ar*C*NCy), 149.5 (Ar*C*), 132.9 (Ar*C*), 130.9 (Ar*C*), 128.5 (Ar*C*), 128.2 (Ar*C*), 127.2 (Ar*C*), 117.0 (Ar*C*), 69.2 (CyN), 49.7 (*C*H_2), 47.2 (*C*H_2), 47.0 (*C*H_2), 46.7 (*C*H_2), 46.6 (*C*H_2), 46.3 (*C*H_2), 38.0 (*C*$(CH_3)_3$), 31.2 (*C*H_3), 29.1 (*C*H_2), 27.6 (*C*H_2), 26.4 (*C*H_2), 23.9 (*C*H_2), 20.4 (*C*H_2), 20.1 (*C*H_2), 20.0 (*C*H_2).

ESIMS (m/z, $M^+ + 2H^+$): calc: 283.3865 found: 283.8367

5.34 Synthesis of 5[104]

$Co(OAc)_2 \cdot 4\ H_2O$ (37 mg, 0.2 mmol) was carefully heated with a heat gun (temperature 250 – 300 °C) in dynamic high vacuum while stopping to heat the flask every couple of seconds to avoid decomposition of the cobalt acetate. The flask was heated until the pink color of the substance changed to deep purple. The resulting $Co(OAc)_2$ was dissolved in dry methanol (10 mL) and **L5** (100 mg, 0.14 mmol) was suspended in the solution. The reaction mixture was stirred for 2 h, and then argon atmosphere was exchanged to O_2 and 2,4-dinitrophenol was added (35 mg, 0.2 mmol) to the reaction mixture. The reaction mixture was stirred for 18 h at ambient temperature. The reaction mixture was concentrated and filtered through a 0.45 µm PTFE syringe filter. The solvent was slowly removed under reduced pressure and cool temperatures (~ 15 °C) to prevent the otherwise occurring reduction of the complex. The obtained solid was washed with cold pentane (5 mL) and the product was obtained in 30 % yield (37 mg, 0.04 mmol) as a brown solid. The complex could not be obtained fully pure. The spectroscopic data is in agreement with the literature.[104]

^{1}H–NMR (400 MHz, $(CD_3)_2SO$) δ 8.68 (s, 1H, Ar*H*) 7.95 (s, 1H, Ar*H*), 7.89 (s, 1H, Ar*H*), 7.79 (s, 2H, NC*H*C), 7.53 – 7.40 (m, 2H, Ar*H*), 7.38 (s, 1H, Ar*H*), 6.30 (s, 1H, Ar*H*), 3.62 (m, 2H, CH_2), 3.45 (t, *J* = 7.7 Hz, 2H, CH_2), 3.4 – 3.2 (m, 6H, CH_2), 3.06 (m, 4H, CH_2), 2.1 – 1.8 (m, 10H, CH_2), 1.75 (m, 4H, CH_2), 1.60 (s, 9H, *t*Bu), 1.31 (s, 9H, *t*Bu), 1.30 (s, 9H, *t*Bu).

Note: the integral of the signal 3.4 – 3.2 ppm is assumed, for the signal was superimposed by the residual water signal of $(CD_3)_2SO$.

ESIMS (m/z, $M^+ + H^+$): calc: 363.7113 found: 363.7105

5.35 Synthesis of 6

$Co(OAc)_2 \cdot 4\ H_2O$ (70 mg, 0.28 mmol) was carefully heated with a heat gun (temperature 250 – 300 °C) in dynamic high vacuum while stopping to heat the flask every couple of seconds to avoid decomposition of the cobalt acetate. The flask was heated until the pink color of the substance changed to deep purple. To the dried cobalt acetate **L6** (163 mg, 0.28 mmol) was added as a solid. Subsequently, the solids were dissolved in a 10:1 mixture of dichloromethane and methanol (20 mL CH_2Cl_2 + 2 mL MeOH). The mixture was stirred for 2 h under Ar atmosphere. 2,4-Dinitrophenol (53 mg, 0.29 mmol) was added and the argon atmosphere was purged out with an O_2 atmosphere. The reaction mixture was further stirred for 18 h under oxygen atmosphere. The solvent was removed and the complex was washed with cold heptanes. The complex was obtained as a brownish powder in 96% (220 mg, 0.268 mmol).

^{1}H–NMR (400 MHz, $(CD_3)_2SO$) δ 8.58 (d, *J* = 3.2 Hz, 1H, Ar*H*), 7.76 (dd, *J* = 9.8, 3.2 Hz, 1H, Ar*H*), 7.64 (s, 2H, CN*H*C), 7.49 – 7.36 (m, 4H, Ar*H*), 6.29 (d, *J* = 9.8 Hz, 1H, Ar*H*), 3.54 (d, *J* = 7.7 Hz, 1H, C*H*), 3.00 (d, *J* = 11.8 Hz, 1H, C*H*), 2.29 (s, 6H, *Me*–Ar), 1.94 (dd, *J* = 33.3, 9.1 Hz, 2H, CH_2), 1.58 (d, *J* = 11.0 Hz, 2H, CH_2), 1.38 – 1.19 (m, 4H, CH_2), 1.07 (s, 18H, *t*Bu), 0.67 (s, 6H, *Me*–Si), 0.56 (s, 6H, *Me*–Si).

^{13}C{^{1}H}–NMR (151 MHz, $(CD_3)_2SO$) δ 170.4 (Ar*C*NO_2), 168.6 (CyN*C*Ar), 165.2 (Ar*C*) 164.7 (CyN*C*Ar), 163.2 (Ar*C*NO_2), 143.8 (Ar*C*H), 139.4 (Ar*C*H), 136.9 (Ar*C*H), 133.2 (Ar*C*H), 128.6 (Ar*C*), 127.3 (Ar*C*), 126.5 (Ar*C*H), 122.3 (Ar*C*), 117.9 (Ar*C*), 69.2 (CyN), 29.7 (*C*H_2), 27.5 (*C*H_2), 27.0 (*C*$(CH_3)_3$), 24.2 (*C*H_2), 19.5 (*C*H_3), –2.0 (Si(*C*H_3)), –2.5 (Si(*C*H_3)).

ESIMS (m/z, M^+): calc: 635.2894, found: 635.2896

5.36 Synthesis of 7

$Co(OAc)_2 \cdot 4 \cdot H_2O$ (82 mg, 0.33 mmol) was carefully heated with a heat gun (temperature 250 – 300 °C) in dynamic high vacuum while stopping to heat the flask every couple of seconds to avoid decomposition of the cobalt acetate. The flask was heated until the pink color of the substance changed to deep purple. Subsequently, **L7** (308 mg, 0.33 mmol) was added as a solid. Dried methanol (10 mL) was added to the solids. The reaction mixture was stirred overnight at room temperature under argon atmosphere. The solvent

was removed from the brown solution *in vacuo* and the resulting solid was dried under high vacuum. The residue was redissolved in dry dichloromethane (10 mL) and 2,4-dinitrophenol (61 mg, 0.33 mmol) was added. The reaction mixture was placed under an oxygen atmosphere and was stirred at room temperature for 3 d. The solvent was removed in vacuum. After washing the residue with heptanes (5 mL) the complex was again kept under high vacuum to give complex **7**, which is hardly soluble in chloroform, in 20 % yield (78 mg, 0,066 mmol) as brown powder.

^{1}H–NMR (400 MHz, $(CD_3)_2SO$) δ 7.94 (s, 2H, C*H*NC), 7.90 – 7.83 (m, 12H, Ar*H*), 7.69 (d, *J* = 2.6 Hz, 2H, Ar*H*), 7.49 – 7.40 (m, 18H, Ar*H*), 7.34 (d, *J* = 2.8 Hz, 2H, Ar*H*), 7.18 (d, *J* = 7.4 Hz, 2H, Ar*H*), 7.11 (m, 2H, Ar*H*, DNP), 7.03 (s, 1H, Ar*H*, DNP), 6.91 (t, *J* = 7.5 Hz, 2H), 1.20 (s, 18H, *t*Bu).

^{13}C{^{1}H}–NMR (151 MHz, $CDCl_3$) δ 172.73 (Ar*C*NO_2), 168.67 (Ar*C*NO_2), 156.3 (CyN*C*Ar), 150.4 (Ar*C*H), 146.3 (Ar*C*), 144.6 (Ar*C*H), 138.4 (Ar*C*), 136.5 (SiAr*C*H), 134.9 (Ar*C*), 132.7 (Ar*C*H), 129.4 (Ar*C*), 129.1 (Ar*C*H), 129.0 (Ar*C*H), 128.9 (Ar*C*H), 128.3 (Ar*C*H), 127.8 (Ar*C*), 127.4 (SiAr*C*H), 126.5, (Ar*C*H), 125.5 (Ar*C*H), 116.7 (Ar*C*), 116.6 (Ar*C*), 116.5 (Ar*C*), 113.5 (Ar*C*H), 33.8 (*C*$(CH_3)_3$) 31.34 (*C*H_3).

ESIMS (m/z, $2M^{2+}$+Na): calc: 1197.3449, found: 1197.3404

5.37 Synthesis of 8

L1 (500 mg, 0.9 mmol) was dissolved in dry toluene (40mL) under argon atmosphere and the solution was cooled to –78 °C, Et_2AlCl (119 mg, 0.12 mL, 0.99 mmol) was added dropwise to the cooled solution. After the addition, the reaction mixture was further stirred under cooling for 30 min and was allowed to reach ambient temperature. Subsequently, the reaction mixture was stirred under reflux conditions for 1 h and additional 18 h at ambient temperature. The reaction progress was controlled by ^{1}H–NMR spectroscopy and after complete complexation Na-2,4-dinitrophenolate (Na(DNP)) (207 mg, 1.00 mmol) was added in one portion to the reaction mixture. The suspension was stirred at reflux conditions for 2 h whereupon the morphology of the suspended particles changed, accompanied by a color change of the solution from yellow to orange. The solid was separated from the solution and the solvent of the solution was evaporated *in vacuo*. The desired complex **8** was isolated in 92 % yield (631 mg, 0.835 mmol) as an orange powder.

^{1}H–NMR (600 MHz, $(CD_3)_2SO$) δ 8.58 (s, 1H, Ar*H*), 8.34 (s, 2H, C*H*NC), 7.76 (dd, *J* = 9.8, 3.2 Hz, 1H, Ar*H*), 7.41 (d, *J* = 2.3 Hz, 2H, Ar*H*), 7.38 – 7.31 (d, 2.0 Hz, 2H, Ar*H*), 6.29 (s, 1H, Ar*H*), 2.59 (d, *J* = 11.0 Hz, 2H, CH_2), 1.96 (d, *J* = 7.2 Hz, 2H, C*H*), 1.52 (s, 19H, *t*Bu), 1.47 – 1.40 (m, 4H, CH_2), 1.39 – 1.32 (m, 4H, CH_2), 1.28 (s, 18H, *t*Bu).

^{13}C{^{1}H}–NMR (151 MHz, $(CD_3)_2SO$) δ 164.0 (CyNCAr), 161.6 (CyNCAr), 138.9 (Ar*C*), 136.4 (Ar*C*), 129.1 (Ar*C*H), 128.8 (Ar*C*H), 127.3 (Ar*C*H), 118.9 (Ar*C*), 63.3 (CyN), 35.2 ($C(CH_3)_3$), 33.7 ($C(CH_3)_3$), 31.4 (CH_3), 29.8 (CH_3), 26.9 (CH_2), 23.5 (CH_2).

ESIMS (m/z, M^+): calc.: 571.3839, found: 571.3831
ESIMS (m/z, DNP^-): calc: 183.0042 found: 183.0042

5.38 Synthesis of 9

Racemic **L1** (705 mg, 1.29 mmol) was dissolved in dry toluene (80 mL) and the solution was cooled to –78°C. Subsequently, $AlMe_3$ (2 M solution in toluene, 0.75 mL, 1.44 mmol) was added and the reaction mixture was further stirred for 10 min under cooling. The reaction mixture was allowed to reach room temperature and was stirred under reflux conditions overnight. The solvent was removed *in vacuo* and the remaining yellow solid was kept additional 3 h under high vacuum. The target complex was obtained pure as a yellow powder in near 100% yield (757 mg, 1.29 mmol). The spectroscopic data is in agreement with the literature.[188]

1H NMR (600 MHz, $CDCl_3$) δ 8.29 (s, 1H, C*H*NC), 8.12 (s, 1H, C*H*NC), 7.49 (m, *2*H, Ar*H*), 7.06 (d, J = 2.4 Hz, 1H, Ar*H*), 6.98 (d, J = 2.4 Hz, 1H, Ar*H*), 3.54 (t, J = 10.6 Hz, 1H, C*H*), 3.06 (t, J = 9.8 Hz, 1H, C*H*), 2.58 (m, 1H, CH_2), 2.44 – 2.38 (m, 1H, CH_2), 2.08 (d, J = 11.2 Hz, 2H, CH_2), 1.53 (s, 9H, *t*Bu), 1.52 (s, 9H, *t*Bu), 1.50 – 1.42 (m, 4H, CH_2), 1.32 (s, 9H, *t*Bu), 1.31 (s, 9H, *t*Bu), -1.14 (s, 3H, Al–*Me*).

^{13}C{^{1}H}–NMR (151 MHz, $CDCl_3$) δ 167.8 (CyNCAr), 164.2 (Ar*C*), 162.6 (Ar*C*), 162.2 (Al–CH_3), 141.2 (Ar*C*), 141.1 (Ar*C*), 137.7 (Ar*C*), 137.2 (Ar*C*), 130.8 (Ar*C*), 129.9 (Ar*C*), 127.7 (Ar*C*), 127.3 (Ar*C*), 118.4 (Ar*C*), 118.4 (Ar*C*), 65.8 (CyN), 62.6 (CyN), 35.8 ($C(CH_3)_3$), 35.7 ($C(CH_3)_3$), 34.1 ($C(CH_3)_3$), 34.1 ($C(CH_3)_3$), 31.6 (CH_3), 31.6 (CH_3), 29.9 (CH_3), 29.8 (CH_3), 29.0 (CH_2), 27.4 (CH_2), 24.4 (CH_2), 24.0 (CH_2).

ESIMS (m/z, M^+): calc.: 571.3839, found: 571.3854

5.39 Synthesis of 10

Racemic **L1** (753 mg, 1.4 mmol) was dissolved in toluene (150 mL) and the flask was cooled to –76°C. Et_2AlCl (173 mg, 1.44 mmol) was slowly added and the mixture was stirred for 30 min at –76°C and additional 18 h at ambient temperature. During the reaction a yellow solid precipitated which was filtered off and treated separately. The solid was washed with toluene (5 mL) and dried *in vacuo*. From the filtrate the solvent was removed whereupon a yellow solid remained. NMR analyses proved both solids to be the desired complex. To the combined solids methanol (5 mL) was added and evaporated again to remove residual toluene. The complex was obtained pure in almost quantitative yield (798 mg, 1.3 mmol). The spectroscopic data is largely in agreement with the literature.[189]

^{1}H–NMR (600 MHz, $CDCl_3$) δ 8.38 (s, 1H, C*H*NC), 8.19 (s, 1H, C*H*NC), 7.56 (s, 2H, Ar*H*), 7.11 (s, 1 H Ar*H*), 7.06 (s, 1H, Ar*H*), 3.90 (t, *J* = 8.9 Hz, 2H, CH_2), 3.17 (t, *J* = 10.2 Hz, 2H, CH_2), 2.60 (d, *J* = 9.3 Hz, 2H, CH_2), 2.46 (m, *J* = 9.1 Hz, 1H, Cy), 2.09 (m, 2H, CH_2), 1.54 (s, 18H, *t*Bu), 1.46 (m, 4H, Cy), 1.31 (s, 18H, *t*Bu).

^{13}C{^{1}H}–NMR (151 MHz, $CDCl_3$) δ 168.8 (CyN*C*Ar), 163.9 (CyN*C*Ar), 141.3 (Ar*C*), 139.2 (Ar*C*), 138.7 (Ar*C*), 131.8 (Ar*C*), 130.8 (Ar*C*), 128.0 (Ar*C*), 127.6 (Ar*C*), 118.3 (Ar*C*), 65.9 (CyN), 62.4 (CyN), 35.8 (*C*$(CH_3)_3$), 35.7 (*C*$(CH_3)_3$), 34.2 (*C*$(CH_3)_3$), 31.5 (*C*H_3), 29.9 (*C*H_3), 29.8 (*C*H_3), 28.6 (*C*H_2), 27.4 (*C*H_2), 24.2 (*C*H_2), 23.7 (*C*H_2).

ESIMS (m/z M^+): calc: 571,3844; found: 571.3854

5.40 Synthesis of 11

$Co(OAc)_2 \cdot 4H_2O$ (500 mg, 2 mmol) was carefully heated with a heat gun (temperature 250 – 300 °C) in dynamic high vacuum while stopping to heat the flask every couple of seconds to avoid decomposition of the cobalt acetate. The flask was heated until the pink color of the substance changed to deep purple. **L1** (337 mg ,0.62 mmol) was dissolved in a 6/1 mixture of dried methanol and dichloromethane (40 mL) and the predried cobalt acetate was added in one portion. The reaction mixture was stirred for 18 h under argon atmosphere. The red precipitate was filtered off and was washed with dry methanol (10 mL). The remaining solid was dissolved in dichloromethane (5 mL) and *p*-toluenesulfonic acid (172 mg, 1 mmol) was added to the solution, which was then stirred overnight under oxygen atmosphere. Subsequently, the solution was washed with brine

(20 mL), the aqueous phase was separated and the organic phase was dried over $MgSO_4$. An aliquot was taken for reaction control. The dark green solution was wrapped in aluminum foil and $Ag(OOCCF_3)$ was added (220 mg, 0.99 mmol) and the mixture was stirred for 96 h at room temperature. The solution was filtered, the solvent removed *in vacuo* and the desired complex was isolated in 41 % yield as green solid (272 mg, 0.38 mmol). The spectroscopic data is in agreement with the literature.[190]

^{1}H–NMR (600 MHz, $(CD_3)_2SO$) δ 7.84 (s, 2H, C*H*NC), 7.47 (d, *J* = 2.2 Hz, 2H, Ar*H*), 7.44 (d, *J* = 2.2 Hz, 2H, Ar*H*), 3.60 (m, 2H, Cy), 2.03 (m, 2H, Cy), 2.00 (m, 2H, Cy), 1.87 (m, 2H, Cy), 1.74 (s, 18H, *t*Bu), 1.58 (m, 2H, Cy), 1.30 (s, 18H, *t*Bu).

^{13}C{^{1}H}–NMR (151 MHz, $(CD_3)_2SO$) δ 164.9 (Ar*C*NCy), 162.1 (Ar*C*NCy), 141.8 (Ar*C*), 135.9 (Ar*C*), 129.3 (Ar*C*), 128.8 (Ar*C*), 118.5 (Ar*C*), 69.3 (CyN), 35.8 (CH_2,), 33.6 (CH_2), 31.5 (CH_3), 30.4 (CH_3), 29.5 ($C(CH_3)_3$), 24.3 ($C(CH_3)_3$).

ESIMS (m/z, M^+): calc.: 603.3352, found: 603.3360

5.41 Synthesis of 12

(*R*,*R*)-(−)-*N*,*N*'-Bis(3,5-di-*tert*-butylsalicylidene)-1,2-cyclohexanediamino cobalt(II) (1.31 g, 2.18 mmol) was dissolved in dichloromethane (50 mL) and 2 equiv of acetic acid (261 mg, 0.25 mL) were added to the solution. The reaction mixture showed a color change from deep red into dark green/brown upon stirring under air atmosphere for 48 h. A crude ^{1}H–NMR spectroscopic analysis showed still broad paramagnetic signals. Therefore, the mixture was stirred for additional 2 h under an oxygen atmosphere. The solvent was removed *in vacuo* and the remaining solid product was dried under high vacuum for 24 h. The brown product was obtained in 95 % isolated yield (1.37 g, 2.07 mmol).

Due to probably fluctual behavior of the complex in the NMR solvent, the obtained signals are in parts strongly broadened and superimposed. The signals were assigned according to the literature.[191]

^{1}H–NMR (600 MHz, $(CD_3)_2SO$) δ 7.95 – 7.67 (m, 2H, C*H*NC), 7.50 – 7.19 (m, 4H, Ar*H*), 3.95 (s, 1H, CH_2), 3.59 (s, 1H, CH_2), 3.39 (s, 1H, CH_2), 3.13 – 2.87 (m, 3H, CH_2), 1.99 (s, 3H, OAc), 1.67 (m, 22H, CH_2 + *t*Bu), 1.29 (m, 18H, *t*Bu).

ESIMS (m/z M^+): calc: 603.3361; found: 603.3345

5.42 Synthesis of 13

L1 (299 mg, 0.54 mmol) was dissolved in CH_2Cl_2 and anhydrous $CrCl_3$ (86.6 mg, 0.54 mmol) was added to the solution. To promote the complexation Zn dust (spatula tip) and one drop of a methanolic 4 M HCl solution were added to the mixture. Thereby, the $Cr(III)Cl_3$ is autocatalytically reduced to $Cr(II)Cl_2$ which resulted in complexation observable by a color change to dark red. The reaction mixture was stirred under O_2 atmosphere for 18 h at ambient temperature. Subsequently, the organic phase was washed with saturated NH_4Cl solution (3×40 mL) and brine. The collected organic phases were dried over $MgSO_4$ and the solvent was evaporated to give the product as a brown powder in 70 % yield (240 mg, 0.38 mmol).

Due to the paramagnetic nature of the complex no meaningful NMR spectra could be recorded.

ESIMS (m/z, M^+): calc: 596.3434 found: 596.3415

5.43 Cocatalyst Syntheses

5.44 Bis(triphenylphosphine)ammonium dinitrophenolate (PPN(DNP))

2,4-Dinitrophenol (184 mg, 0.99 mmol) was dissolved in dry THF (50 mL) and NaH (29 mg, 1.2 mmol) was added to the solution. The mixture was stirred for 18 h at ambient temperature under argon atmosphere. To verify full deprotonation, some grains of NaH were added to the reaction mixture to observe potential gas evolution. PPNCl (574 mg, 0.99 mmol) was dissolved in dry THF (50 mL) and both solutions were slowly combined. The reaction mixture was stirred for 3 h at ambient temperature. The formed, white solid was separated and the solvent was evaporated from the solution to give the product as a orange solid in 83 % yield (603 mg, 0.83 mmol).

^{1}H–NMR (600 MHz, $CDCl_3$) δ 8.84 (d, *J* = 3.1 Hz, 1H, Ar*H*, DNP), 7.81 (dd, *J* = 9.7, 3.1 Hz, 1H, Ar*H*, DNP), 7.63 (m, 6H, Ar*H*), 7.49 – 7.39 (m, 24H, Ar*H*), 6.57 (d, *J* = 9.7 Hz, 1H, Ar*H,* DNP).

^{13}C{^{1}H}–NMR (151 MHz, $CDCl_3$) δ 172.4 (Ar*C*NO_2), 136.4 (Ar*C*), 134.0 (Ar*C*), 132.2 (Ar*C*), 129.6 (Ar*C*), 129.1 (Ar*C*), 128.0 (Ar*C*), 127.4 (Ar*C*), 127.4 (Ar*C*), 126.72 (Ar*C*), 126.71 (Ar*C*), 126.4 (Ar*C*).

ESIMS (m/z, M^+): calc: 538.1848 found: 538.1851

5.45 Tetra-*n*-butylammonium-2,4-dinitrophenolate (TBA(DNP))

2,4-Dinitrophenol (920 mg, 4.99 mmol) was dissolved in THF (150 mL) and NaH (144 mg, 6 mmol) was added in small portions under argon atmosphere. The reaction mixture was stirred for additional 16 h at ambient temperature. Subsequently, tetra-*n*-butyl ammonium bromide (1.61 g, 4.99 mmol) was added to the mixture, which was further stirred for 18 h at room temperature. The formed brown solid was separated and the solvent was evaporated from the filtrate to give an orange solid in 76 % yield (1.63 g, 3.83 mmol). The product was isolated as a 2:1 mixture of TBABr and TBA(DNP). As the NMR spectroscopic signals of the two species largely overlap, spectroscopic data comprises both signal sets.

^{1}H–NMR (600 MHz, $CDCl_3$) δ 8.87 (dd, *J* = 10.9, 3.1 Hz, 1H, Ar*H*), 7.87 (td, *J* = 10.3, 3.1 Hz, 1H, Ar*H*), 6.52 (dd, *J* = 9.7, 6.7 Hz, 1H, Ar*H*), 3.28 (q, *J* = 8.7 Hz, 16H, CH_2), 1.64 (h, *J* = 7.6 Hz, 16H, CH_2), 1.42 (hept, *J* = 7.5 Hz, 16H, CH_2), 0.98 (q, *J* = 7.4 Hz, 24H, CH_3).

^{13}C{^{1}H}–NMR (151 MHz, $CDCl_3$) δ 172.1 (Ar*C*NO_2), 136.3 (Ar*C*), 128.2 (Ar*C*), 128.1 (Ar*C*), 127.4 (Ar*C*), 126.3 (Ar*C*), 126.3 (Ar*C*), 59.1 (*C*H_2-N), 24.2 (*C*H_2), 24.2 (*C*H_2), 19.9 (*C*H_2), 13.8 (*C*H_3).

ESIMS (m/z, M^+): calc: 242.2843 found: 242.2846

5.46 DMF catalyzed hydrolysis of (*R*)–propylene oxide[162] and derivatization with (*R*)–Mosher's acid chloride

Propylene oxide (0.5 mL, 415 mg, 7.1 mmol) was loaded under argon atmosphere into vial and dried DMF (51 mg, 54 µL, ρ = 0.94 g·cm^{-3}, 0.7 mmol) was added *via* a microliter syringe. In a second step water (128 mg, 0.13 mL, 7.1 mmol) was added under an argon shower. The vial was sealed stirred for 20 h at 110°C. The reaction was allowed to cool down to ambient temperature and the excess of water was removed by pipette filtration over $MgSO_4$. As the reaction was not aimed to be quantitatively evaluated no reaction yield was determined.

The derivatization of the resulting propylene glycol was kindly performed by Dr. Nawara-Hultzsch according to a general procedure to qualitatively analyze the predominant enantiomer of the propylene glycol.

The alcohol (1–2 mg, ca. 0,01–0.02 mmol) was dissolved in $CDCl_3$ (0.5 mL) in a NMR tube. Hünig's base (8.7 µL, 6 mg, 0,05 mmol) and (R)-Mosher chloride (5.6 µL, 7 mg, 0.03 mmol) were added.

^{19}F–NMR (565 MHz, $CDCl_3$): –71.67.

5.47 Hydrolysis of PA-PO copolymer

A representative PA-PO copolymer (148 mg) was dissolved in 25 mL of EtOH and 25 mL of dichloromethane and NaOH (932 mg) was added. The mixture was stirred for 16 h at reflux conditions. The mixture was allowed to cool down to ambient temperature and was neutralized with 1 M HCl solution. The aqueous phase was extracted with chloroform (8 x 100 mL). The chloroform was evaporated to yield 4 mg of the crude propylene glycol.

1H–NMR (400 MHz, CDCl3) δ 4.01 – 3.86 (m, 1H, OH-C*H*-CH_3), 3.65 (dd, J = 11.0, 3.2 Hz, 1H, CH_2-OH), 3.41 (dd, J = 11.0, 7.7 Hz, 1H, CH_2-OH), 1.18 (d, J = 6.4 Hz, 3H, CH_3).

5.48 General polymerization procedures

5.48.1 Polymerization setup in the glovebox

In a typical polymerization reaction setup $1.5 \cdot 10^{-5}$ mol of the respective catalyst, 1 equivalent of the respective cocatalyst and the respective amounts of anhydrides, typically 500 eq. with respect to the catalyst, were weighed in the glovebox into a predried 20 mL vial, which was soaked in a base bath, an acid bath, washed with water, acetone and ethyl acetate and dried at least overnight at 120 °C, under argon atmosphere. The solids were first dissolved or suspended in toluene or THF (5.2 mL). Subsequently, propylene oxide (5.2 mL, 5000 eq., with respect to the catalyst) was added to the mixture. If reactions were carried out without solvent additive, the solids were directly dissolved in propylene oxide. In those instances, 10000 eq. of propylene oxide were employed. The 20 mL vial was sealed and placed into a preheated aluminum block for the respective reaction time. As the reaction progress was monitored by ^{1}H–NMR spectroscopy the reaction was cooled down to approximately 30 °C to be able to take a small aliquot with a predried Pasteur pipette, which was stored in the same glovebox. Afterwards the vial was sealed and placed back into the aluminum block. After the respective reaction time elapsed, the reaction mixtures were removed from the glovebox and the reaction mixture was quenched by addition of 0.1 M HCl solution in MeOH (100 mL). The precipitated polymer was collected, dissolved in CH_2Cl_2 or acetone (20 mL) and precipitated again in a 0.1 M HCl solution in MeOH (100 mL). The isolated polymers were dried in high vacuum inside a 20 mL vial for storage and analysis.

5.48.2 Polymerization setup with *in situ* IR measurement

Reactions for *in situ* IR spectroscopy experiments were set up in the glovebox. The typically used amounts of catalyst, cocatalyst, solvents and monomers were identical to the previously described typical procedure. The catalyst, cocatalyst and monomers were charged into a flame dried three necked flask. The respective three necked flask was soaked in a base bath, an acid bath, washed with water, acetone and ethyl acetate and dried at least overnight at 120 °C. The solid mixture was dissolved first in toluene and subsequently propylene oxide was added. The reaction mixture was removed from the glovebox and attached to a Schlenk line. The IR probe was introduced under argon counterflow after rinsing the probe with acetone and drying it in warm air. The IR probe was removed, and the reaction mixture was transferred into a beaker and diluted with

CH_2Cl_2 (30 mL) while the reaction flask was rinsed, after full consumption of the anhydrides or after the respective reaction time elapsed. The polymer was precipitated by addition of a 0.1 M HCl solution in MeOH (100 mL). The precipitating polymer was collected, dissolved in a small amount of CH_2Cl_2 (20 mL) and precipitated by addition of a methanolic 0.1 M HCl solution (100 mL). The procedure was repeated until no change in the color of the polymer, before and after precipitation, could be observed. The collected polymer was dried in high vacuum in a 20 mL vial for storage and analysis.

5.48.3 General polymerization procedure under CO_2 atmosphere and *in situ* IR measurement

All reactions comprising CO_2 atmosphere were conducted under 10 bar of CO_2 pressure in a predried 20 mL vial which was placed in a stainless steel Parr beaker autoclave. The autoclave was generally continuously heated in a sand bath at 55 °C. The reactions were prepared as described above and were placed in the preheated autoclave under argon counterflow. The argon was purged out by pressurization and depressurization four times with 10 bars of CO_2. The employed CO_2 gas (99.9 %) was pretreated using an in-line AirLiquide Oxisorb purification cartridge. After the respective reaction time elapsed, the autoclave was cooled down in a water bath and the pressure was slowly released. The remaining workup steps were conducted as already stated above.

5.48.4 Exemplary polymerization of ε-caprolactone

1,5,7-Triazabicyclo[4.4.0]dec-5-en (628 mg, 4.5 mmol) was dissolved in ε-caprolactone (10 mL, 90 mmol) at ambient temperature under air. BnOH (486 mg, 0.47 mL, 0.45 mmol) was added to the reaction solution. After two minutes the magnetic stirring blocked and the highly viscous reaction mixture was further stirred by a glass rod by hand. The reaction was stirred for 15 minutes until no obvious heat development could be observed anymore. The polymer was dissolved in CH_2Cl_2 (10 mL) and precipitated into methanol (40 mL). This procedure was repeated twice. The isolated polymer was dried at 60 °C under vacuum for several hours.

5.48.5 General polymer post modification procedure[175]

The respective polymer (100 mg) was dissolved in CH_2Cl_2. The respective amount of styrene or of the modified dye was added to the polymer (e.g.: 1 eq, with respect to the estimated amount of double bonds of the employed polymer) and CH_2Cl_2 was added so that after the stock solution of the catalyst will be added, a total volume of 4 mL will be reached. The polymer solution was stirred for 2 h under inert atmosphere in the glovebox and the respective amount of Grubbs-Hoveyda 2nd generation catalyst was added *via* a stock solution of a $1.6 \cdot 10^{-3}$ mol/L. The amount of added catalyst stock solution was hereby in the range below 900 µL. The reaction mixture was stirred for 16 h at ambient temperature and was precipitated into methanol after the reaction time elapsed.

More detailed information is given in the master's thesis of Christian Markl with whom the data was generated in cooperation.[175]

6 Representative Polymer NMR Spectra

6.1 Poly(phthalic acid–propyl)ester, (PO-PA)

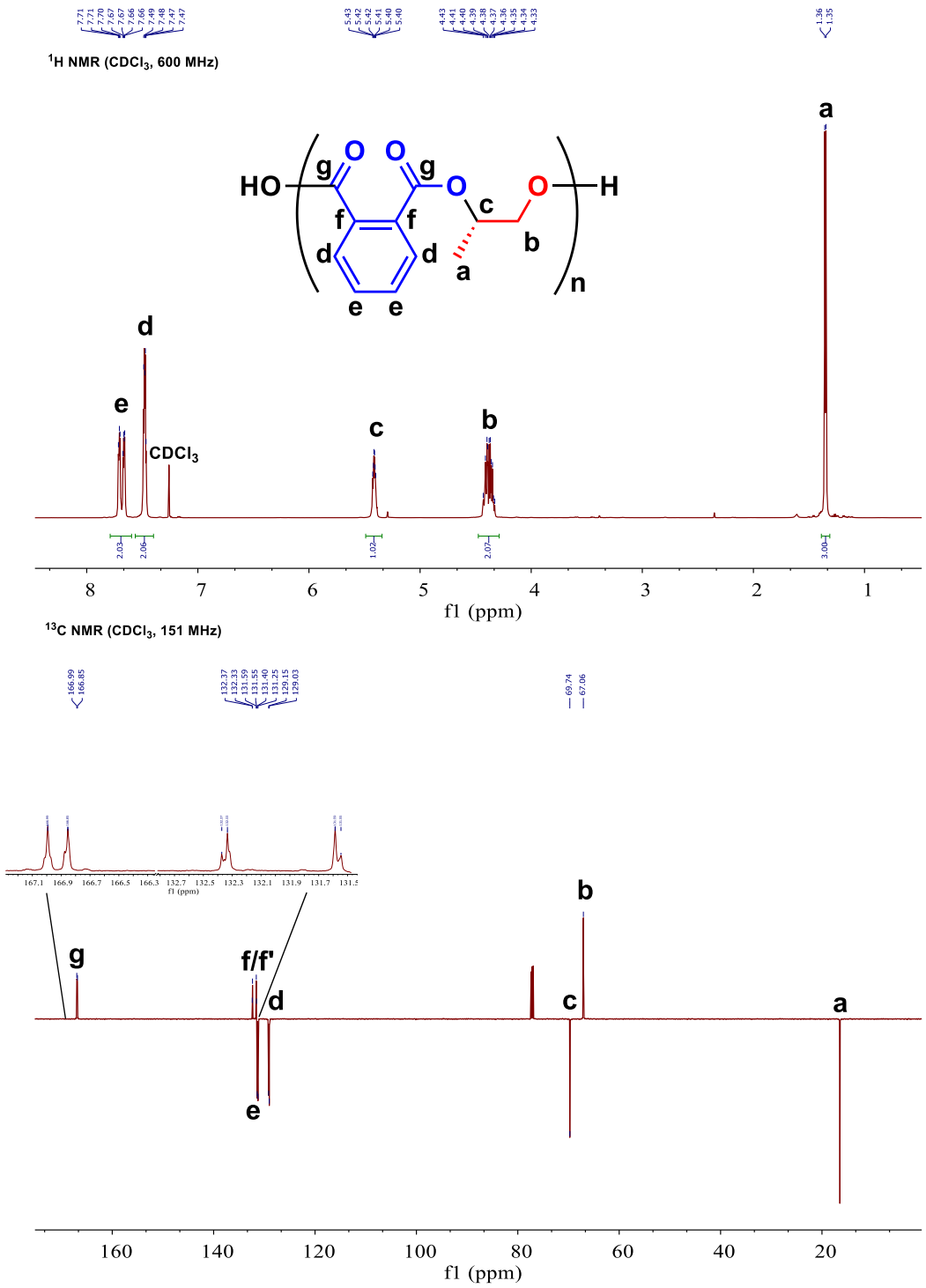

*Fig. S1: ^{1}H–NMR and $^{13}C\{^1H\}$–NMR spectra of enantioenriched (PO-PA) copolymer with **1**/PPNCl as catalyst system.*

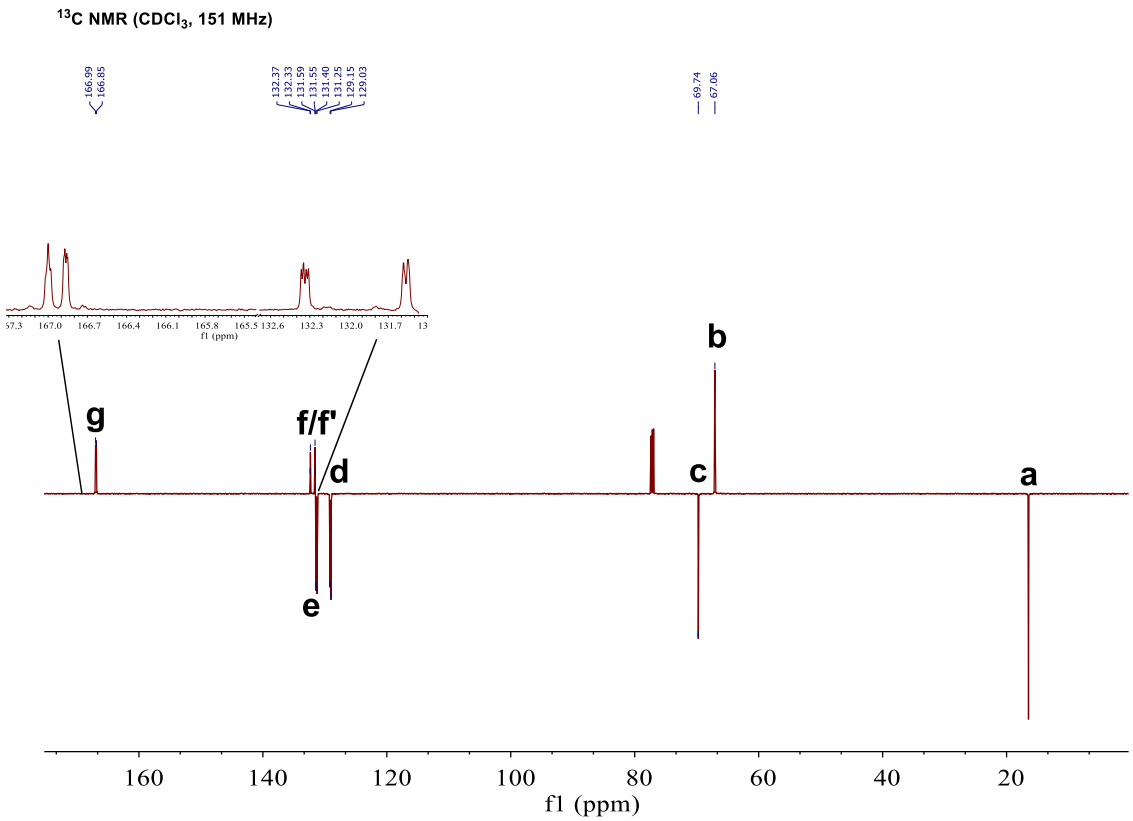

*Fig. S2: $^{13}C\{^{1}H\}$–NMR spectrum of racemic (PO-PA) copolymer with **2**/PPNCl as catalyst system.*

6.2 Poly(norbornene dicarboxylic acid–propyl)ester

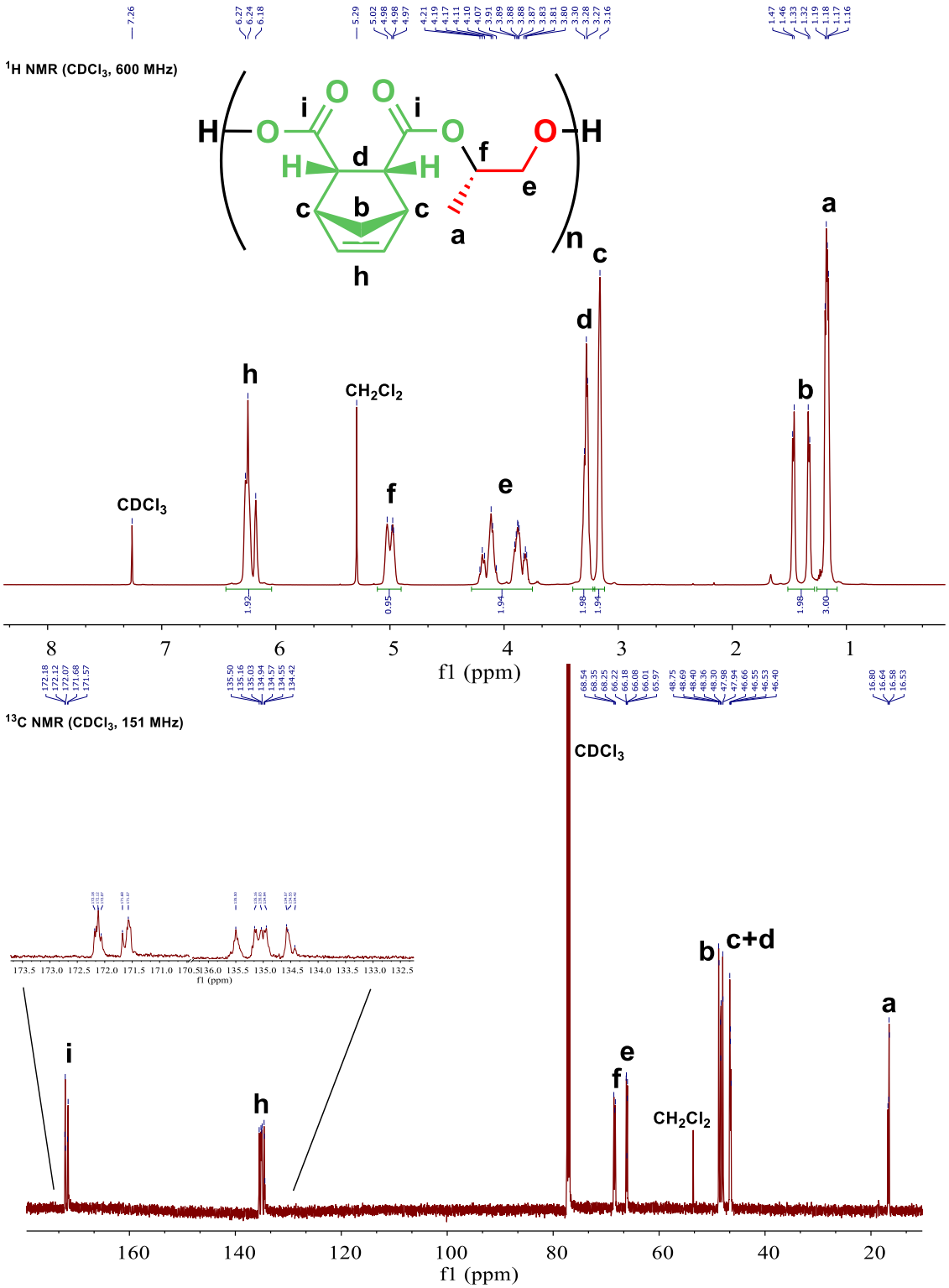

*Fig. S3: ^{1}H–NMR and ^{13}C{^{1}H}–NMR spectra of enantioenriched (PO-NA) copolymer with **1**/PPNCl as catalyst system.*

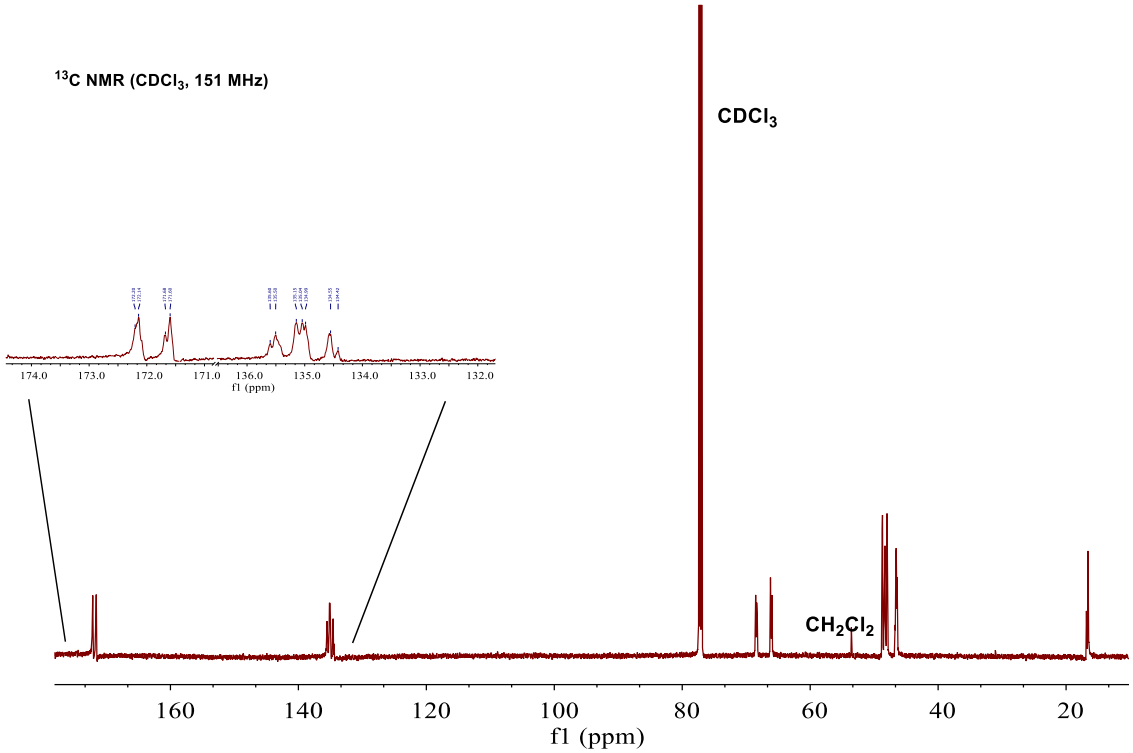

*Fig. S4: $^{13}C\{^1H\}$–NMR spectrum of racemic (PO-NA) copolymer with **2**/PPNCl as catalyst system.*

6.3 Polypropylene carbonate

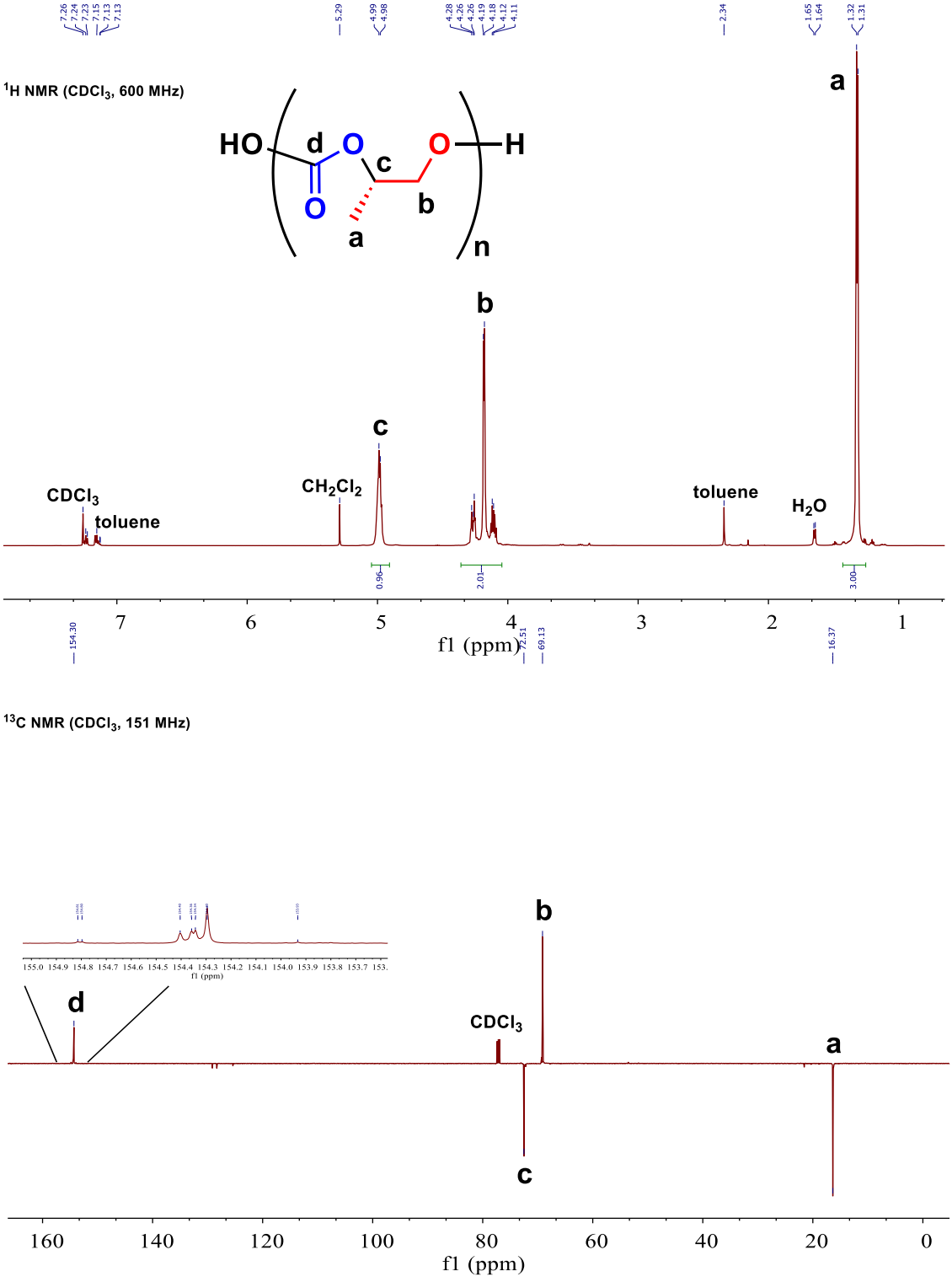

*Fig. S5: ^{1}H–NMR and ^{13}C{^{1}H}–NMR spectra of enantioenriched polypropylene carbonate with **1**/PPNCl as catalyst system.*

6.4 Poly(propyl maleate)

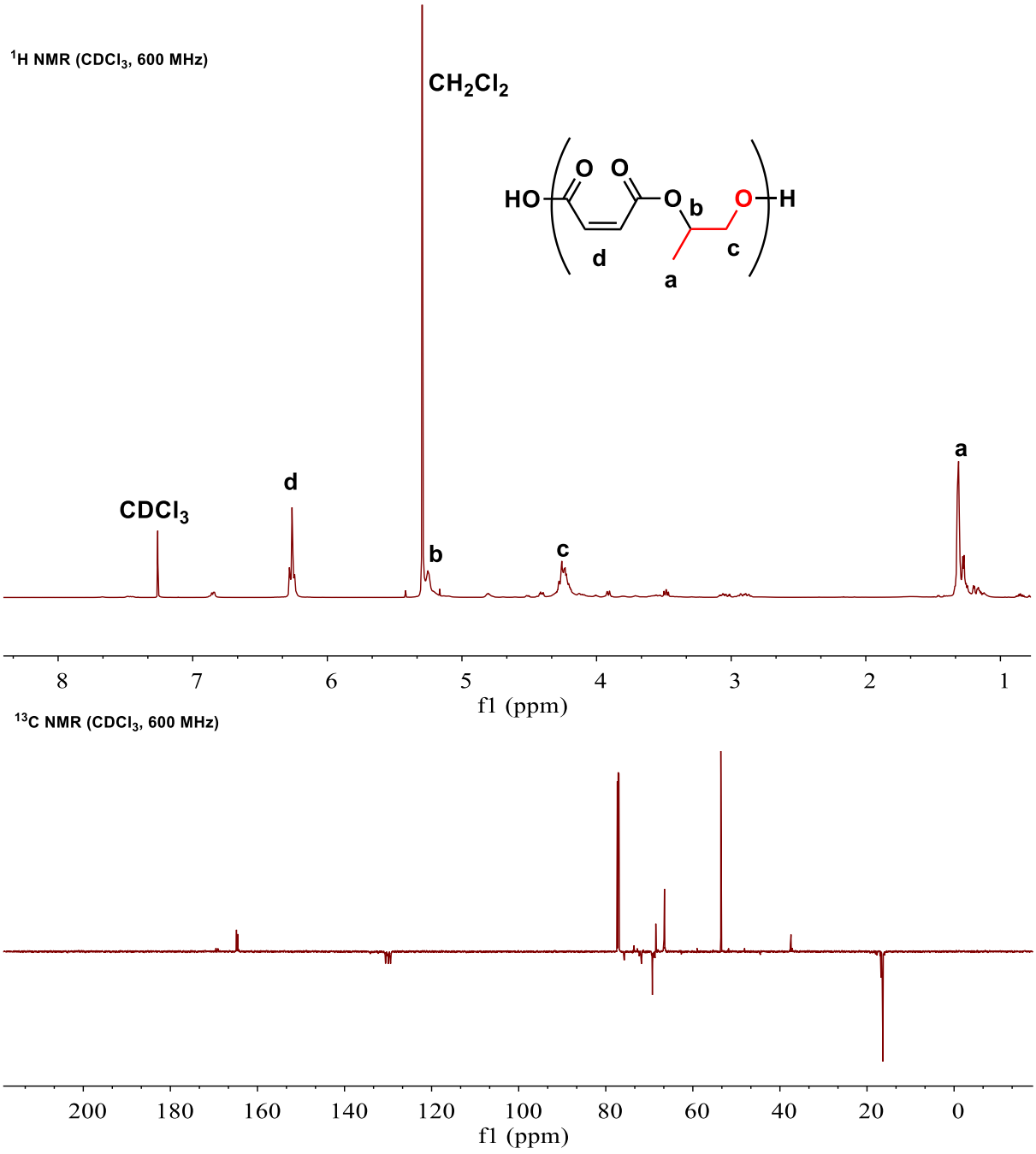

Fig. S6: ^{1}H–NMR and ^{13}C{^{1}H}–NMR spectra of poly(propyl maleate).

6.5 Sequential anhydride addition

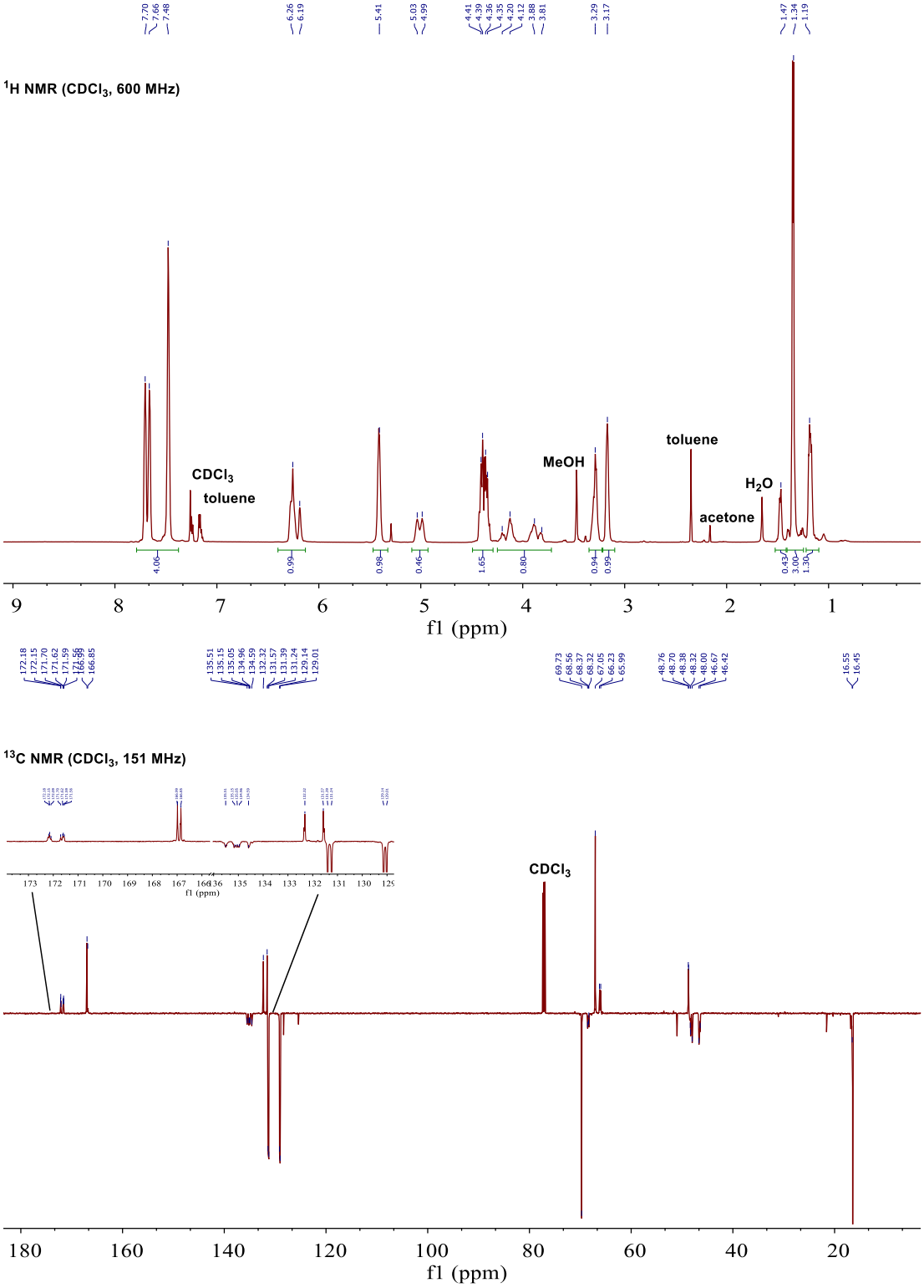

*Fig. S7: ^{1}H–NMR and ^{13}C{^{1}H}–NMR spectra of enantioenriched PO-NA-b-PO-PA block terpolymer synthesized by a sequential addition of 250 equiv of NA and 500 equiv of PA with **1**/PPNCl (1 equiv) as catalyst system.*

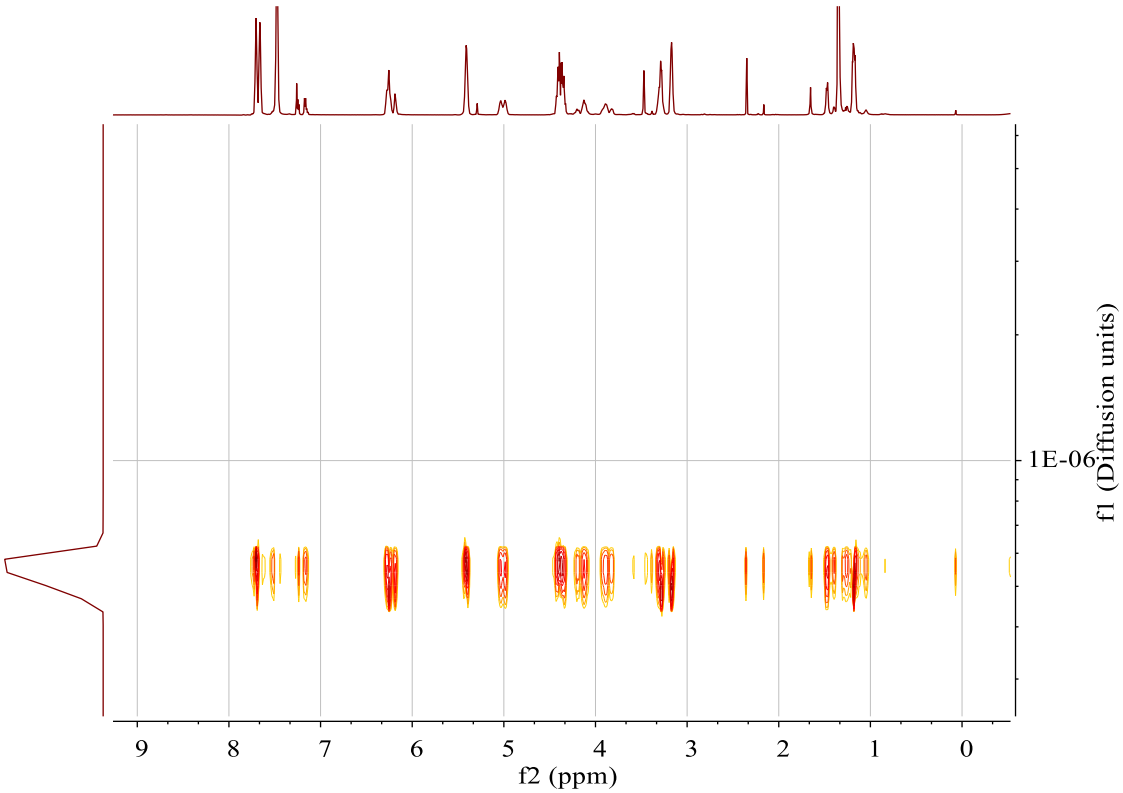

*Fig. S8: DOSY NMR spectrum of enantioenriched [PO-NA]-b-[PO-PA] block terpolymer with a sequential addition of 250 equiv of NA and 500 equiv of PA with **1**/PPNCl (1 equiv) as catalyst system. Diffusion units: $cm^2 \cdot s^{-1}$.*

6.6 Direct anhydride addition

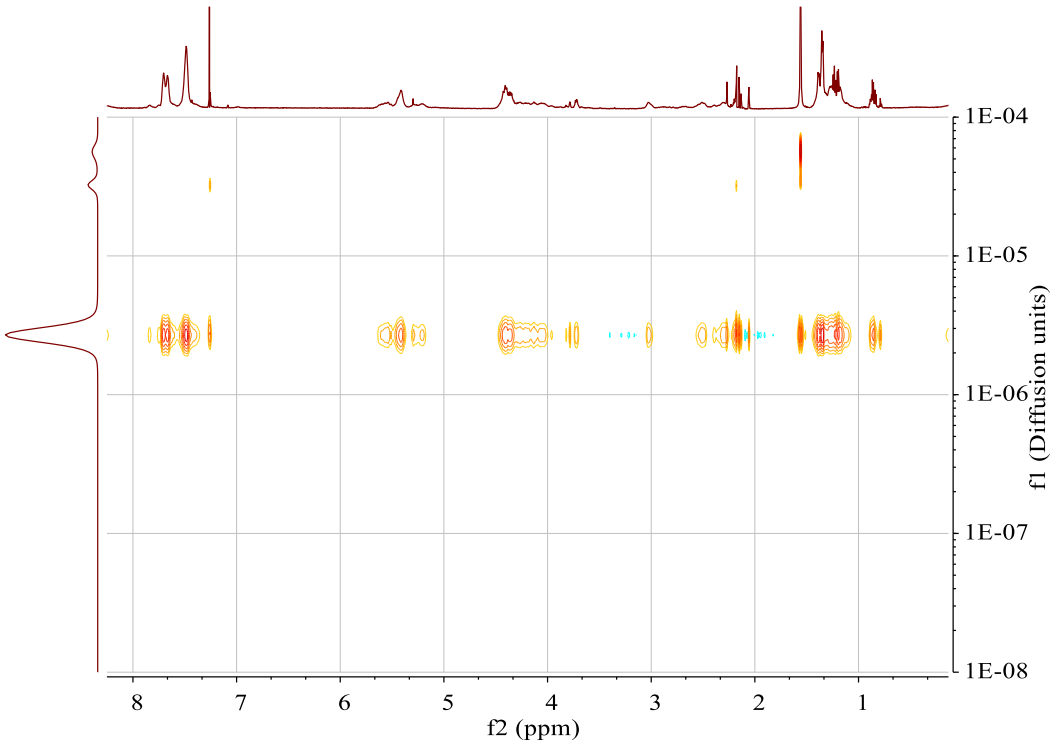

Fig. S9: DOSY NMR spectrum of a poly(propyl tetrahydrotherephthalate)-poly(propyl phthalate) terpolymer from direct terpolymerization with 23 % THPA-PO ester moieties. Diffusion units: $cm^2 \cdot s^{-1}$.

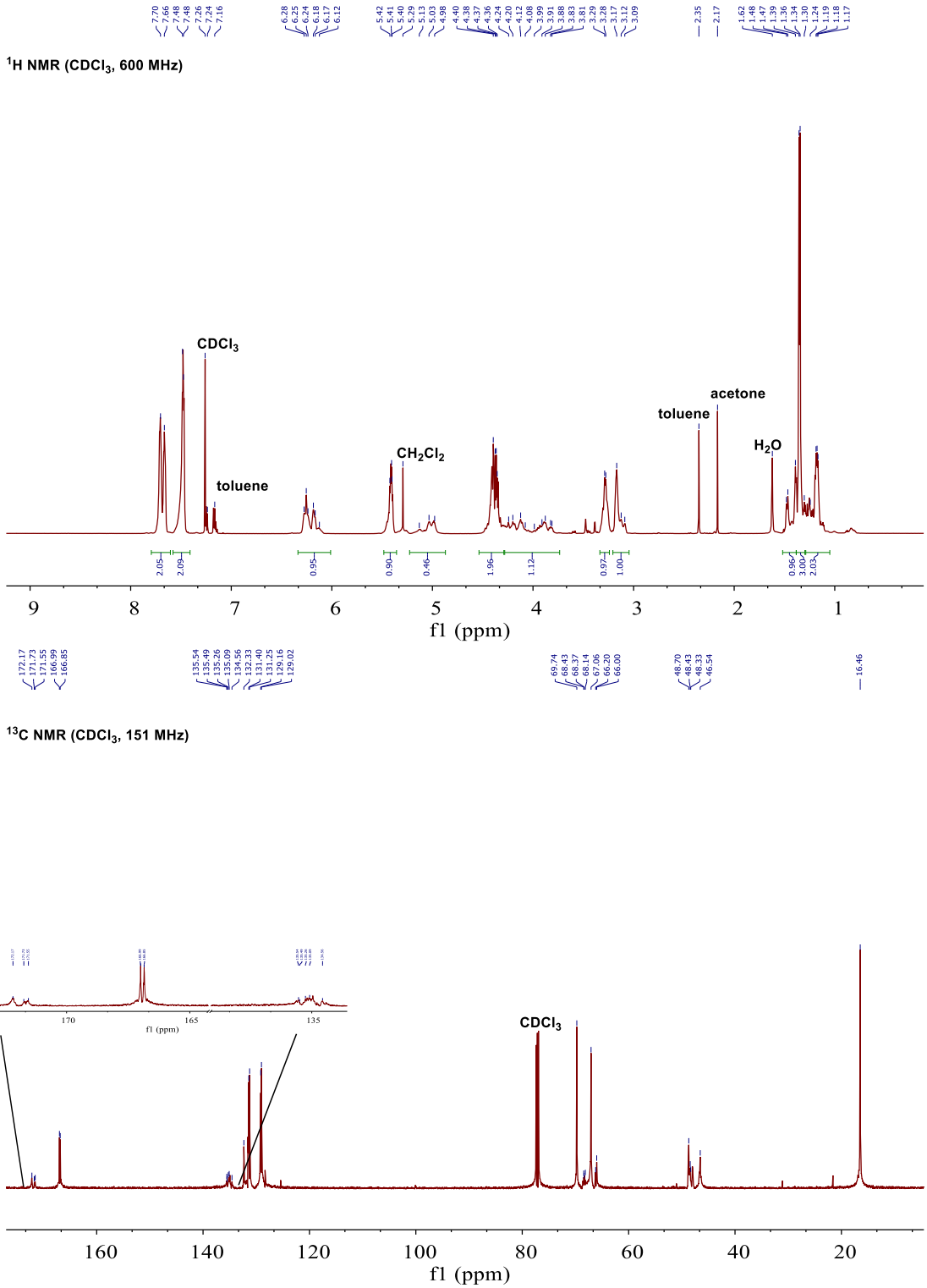

*Fig. S10: ^{1}H–NMR and ^{13}C{^{1}H}–NMR spectra of enantioenriched [PO-PA]/[PO-NA] gradient like terpolymer with a direct combination of 250 equiv of NA and 500 equiv of PA with **1**/PPNCl (1 equiv) as catalyst system (Fig. 44 A).*

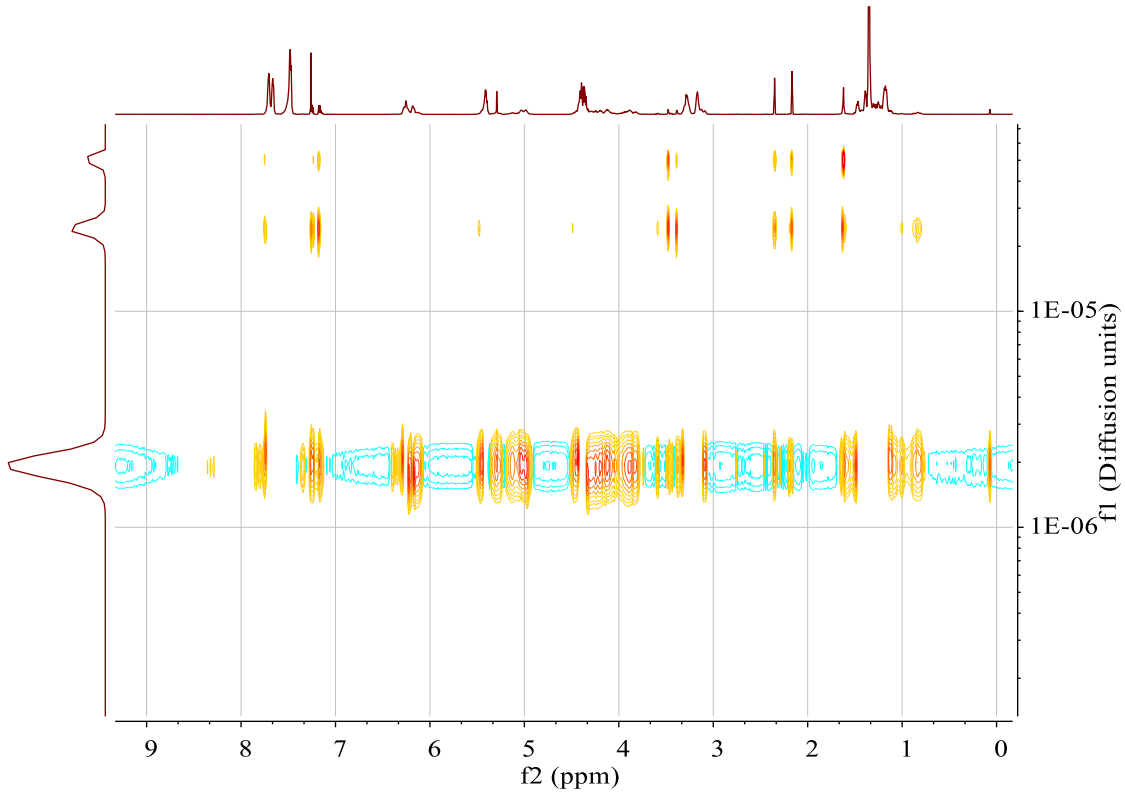

*Fig. S11: DOSY NMR spectrum of enantioenriched [PO-PA]/[PO-NA] gradient like terpolymer with a direct combination of 250 equiv of NA and 500 equiv of PA with **1**/PPNCl (1 equiv) as catalyst system. Diffusion units: $cm^2 \cdot s^{-1}$ (Fig. 44 A).*

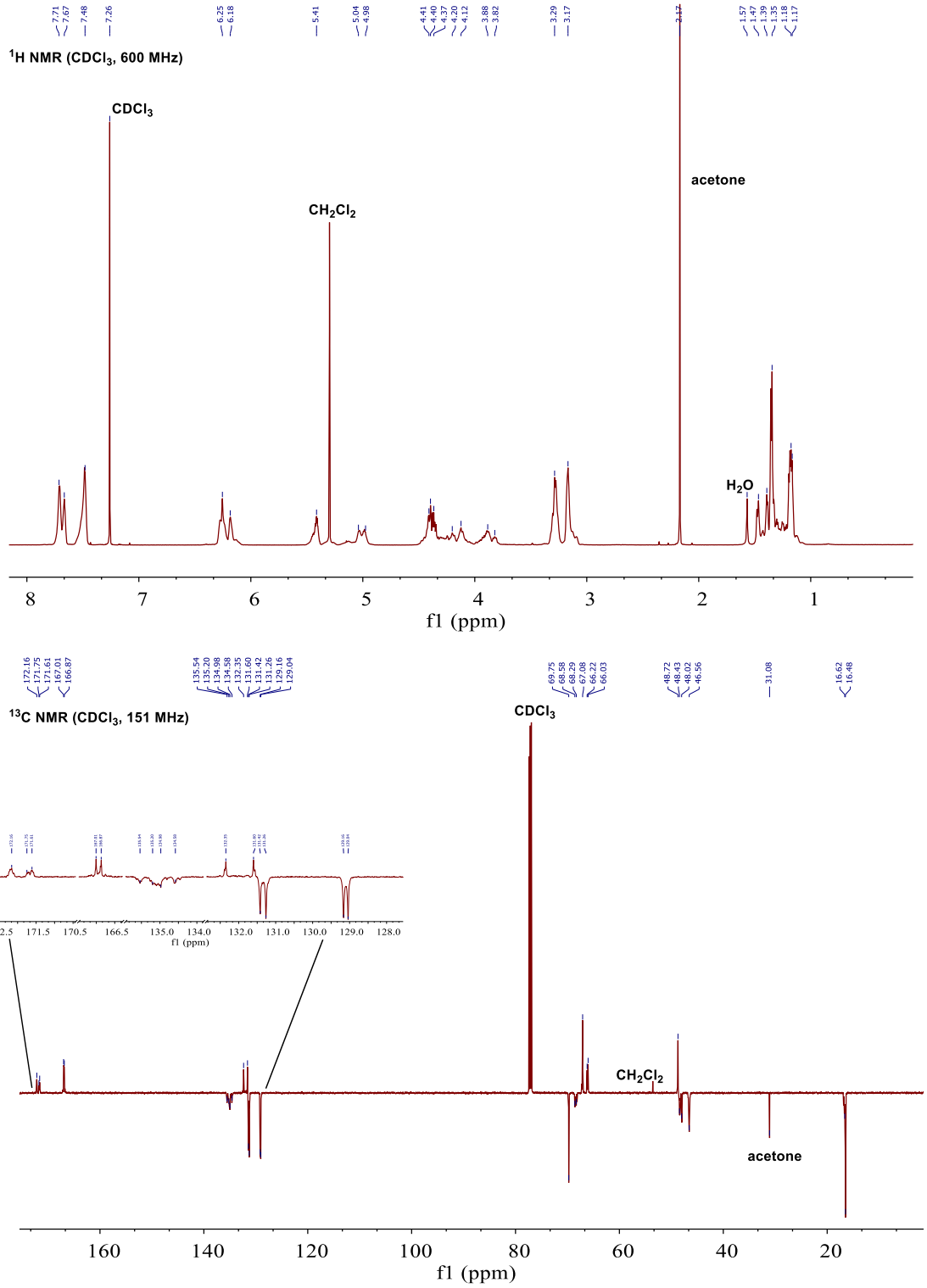

*Fig. S12: ^{1}H–NMR and ^{13}C{^{1}H}–NMR spectra of enantioenriched [PO-PA]/[PO-NA] terpolymer with a direct combination of 250 equiv of NA and 250 equiv of PA with **1**/PPNCl (1 equiv) as catalyst system (Fig. 44, B).*

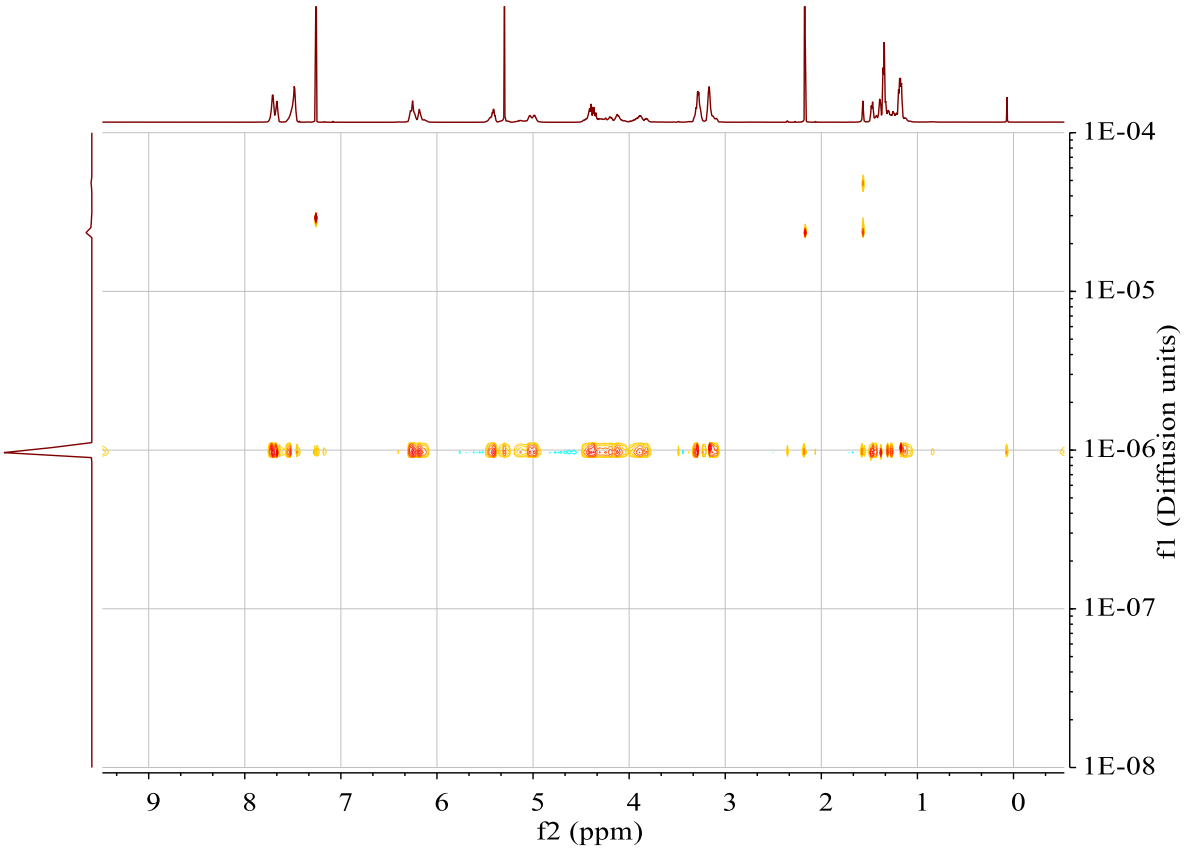

*Fig. S13: DOSY NMR spectrum of enantioenriched [PO-PA]/[PO-NA] terpolymer with a direct combination of 250 equiv of NA and 500 equiv of PA with **1**/PPNCl (1 equiv) as catalyst system. Diffusion units: $cm^2 \cdot s^{-1}$ (Fig. 44, B).*

6.7 ROCOP under CO_2 atmosphere

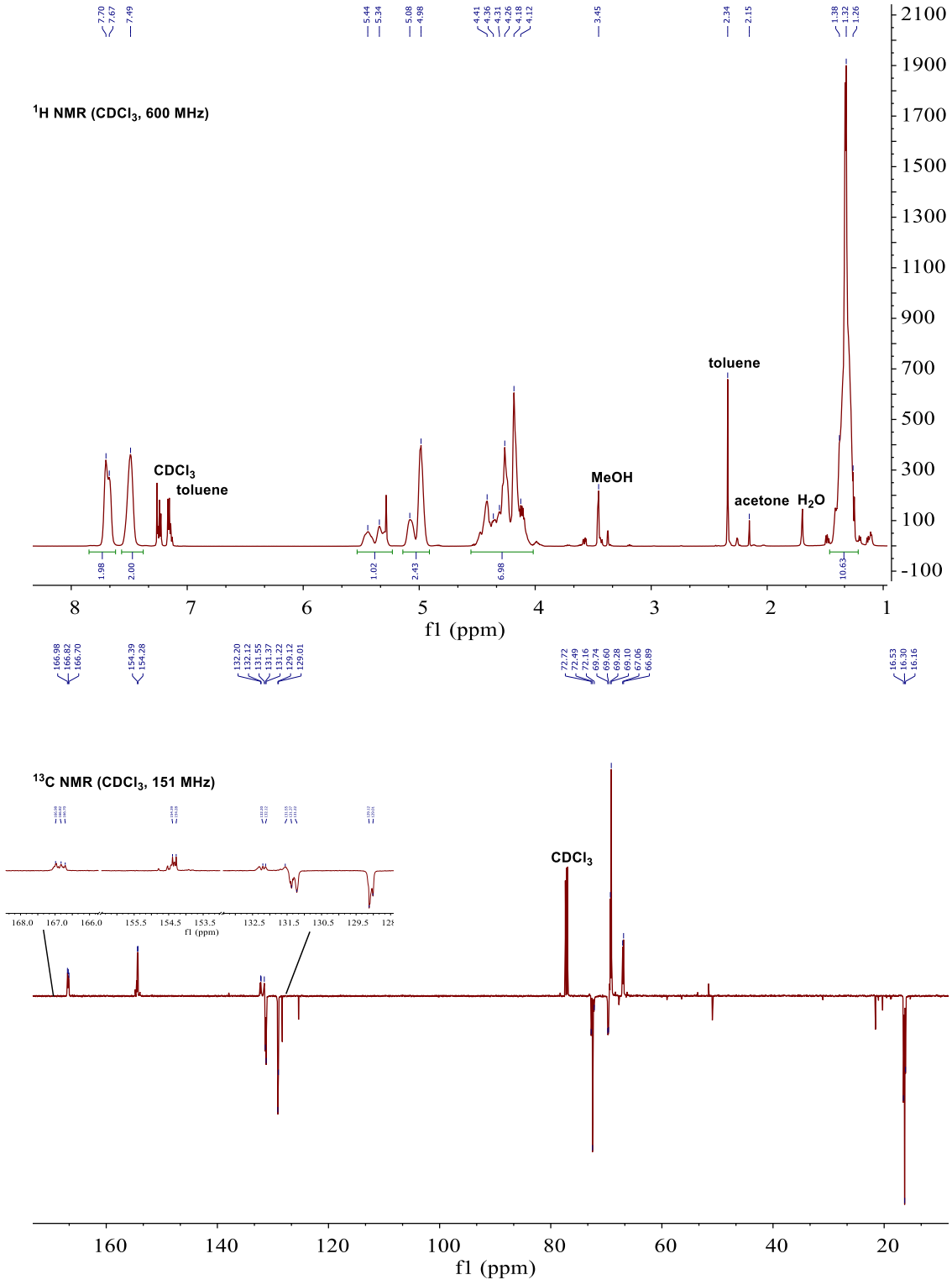

*Fig. S14: ^{1}H–NMR and ^{13}C{^{1}H}–NMR spectra of [PO-PA]/[PPC] terpolymer synthesized by PO/PA ROCOP under CO_2 atmosphere with **1**/PPNCl (1 equiv) as catalyst system (Fig. 47).*

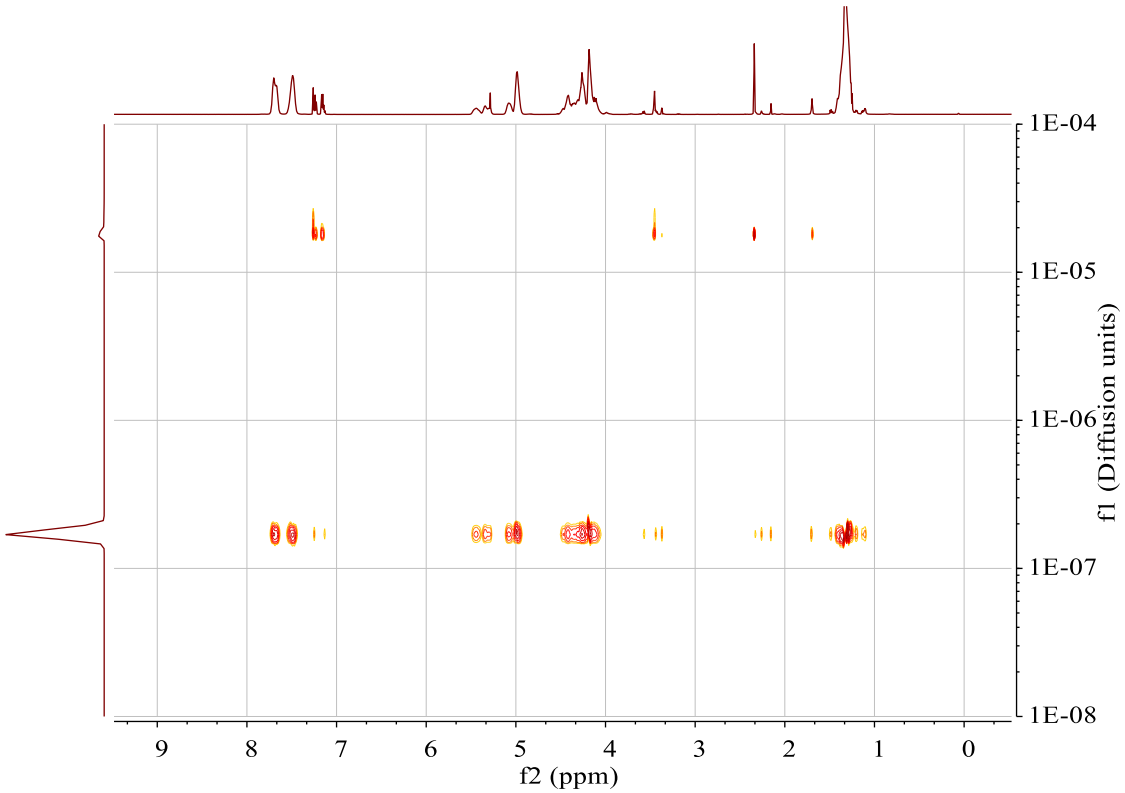

*Fig. S15: DOSY NMR spectrum of [PO-PA]/[PPC] terpolymer synthesized by PO/PA ROCOP under CO_2 atmosphere with **1**/PPNCl as catalyst system. Diffusion units: $cm^2 \cdot s^{-1}$ (Fig. 47).*

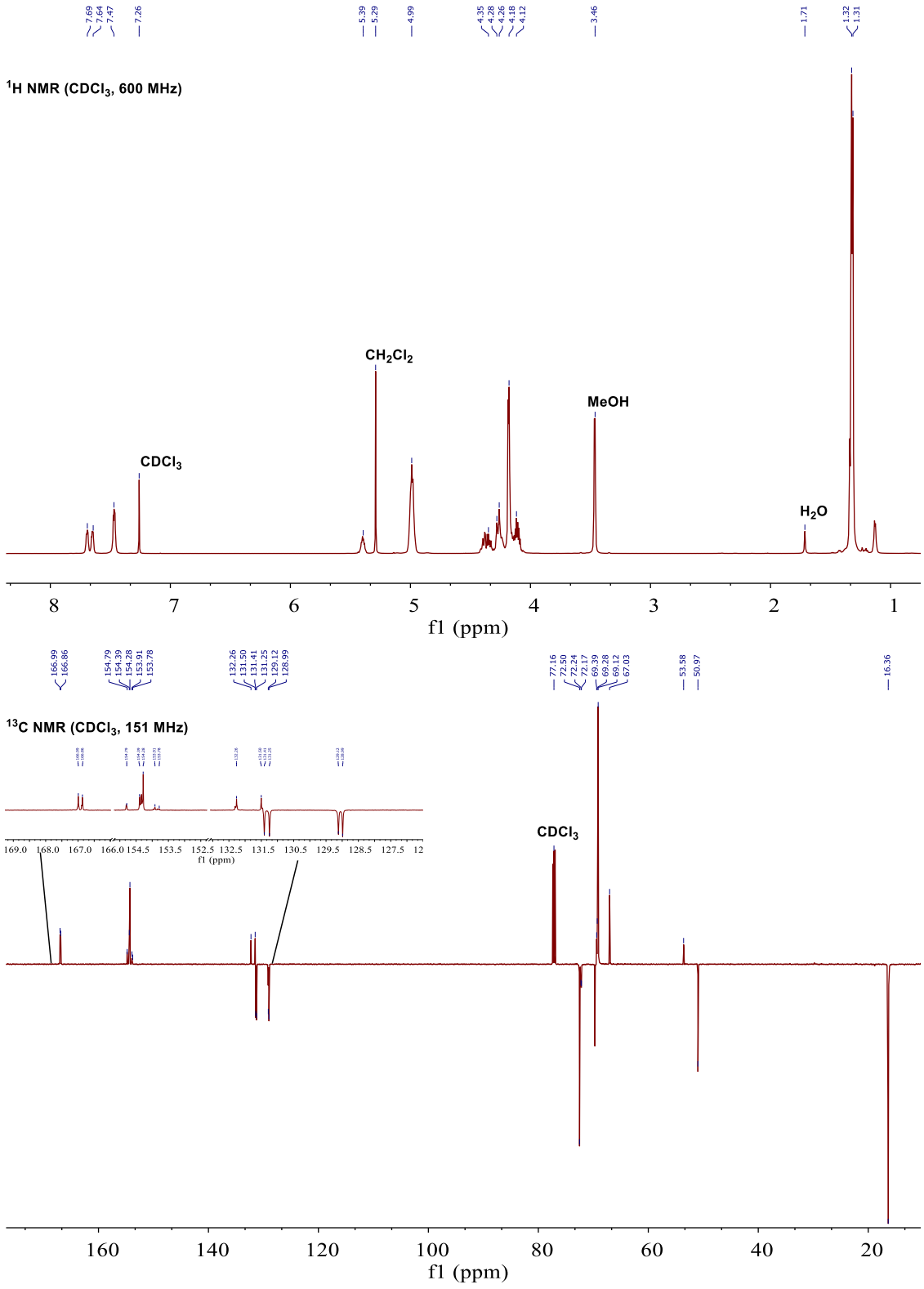

*Fig. S16: ^{1}H– and ^{13}C{^{1}H}–NMR spectra of a PO/PA/PPC block terpolymer from a PO/PA copolymerization with subsequent pressurization with CO_2 and **1**/PPNCl as catalyst system.*

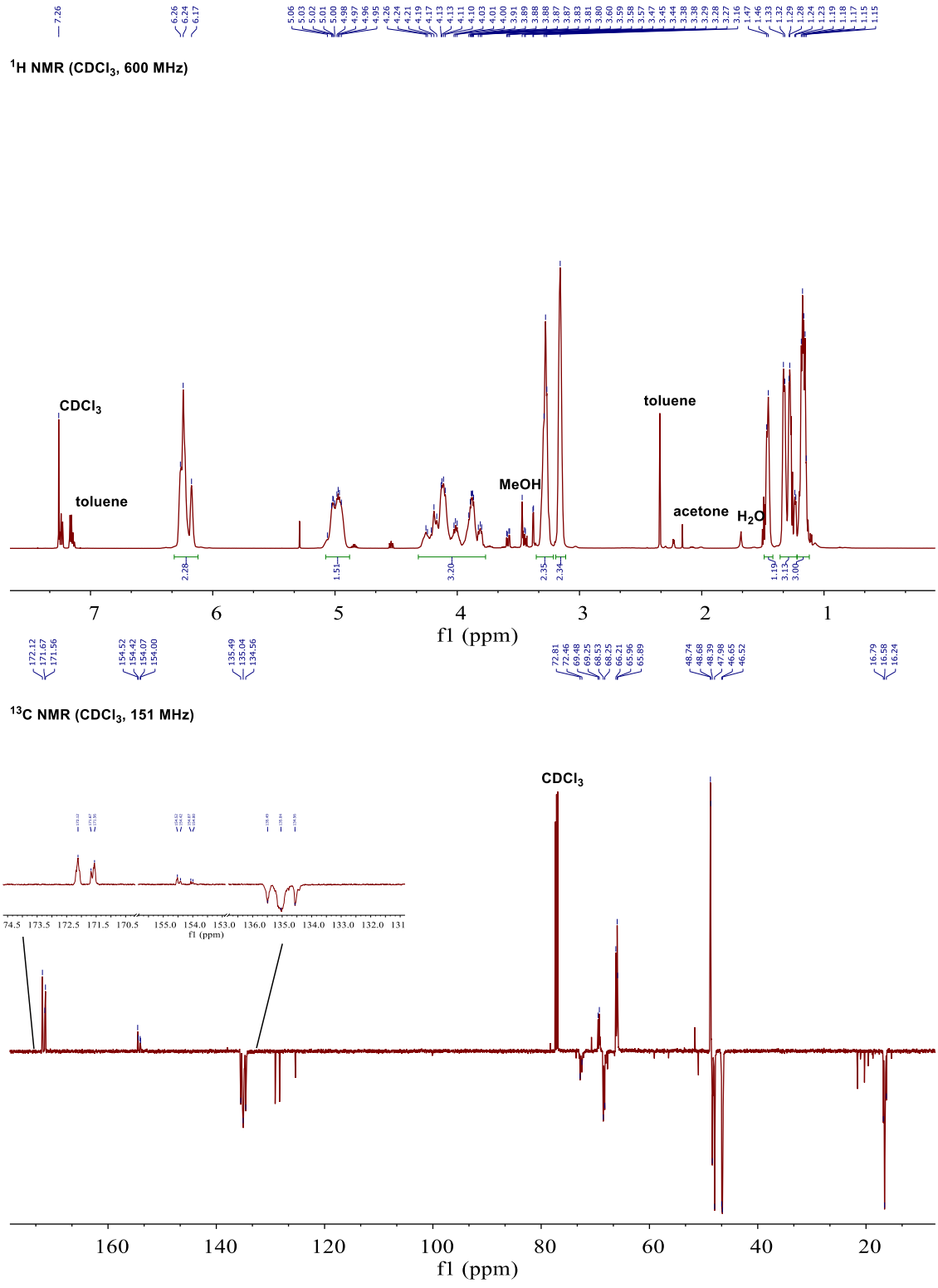

*Fig. S17: ^{1}H–NMR and ^{13}C{^{1}H}–NMR spectra of [PO-NA]/[PPC] terpolymer synthesized by PO/NA ROCOP under CO_2 atmosphere with **1**/PPNCl as catalyst system (Fig. 50).*

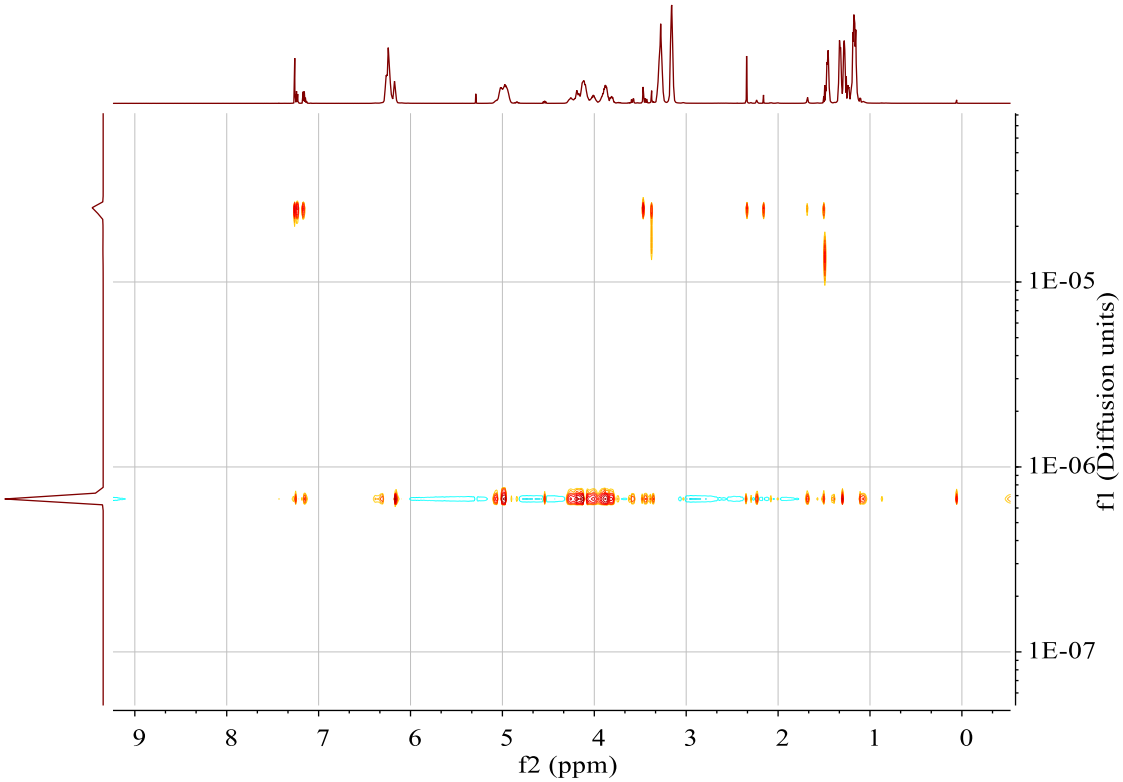

*Fig. S18: DOSY NMR spectrum of PO-NA/PPC terpolymer with **1**/PPNCl as catalyst system (Fig. 14). Diffusion units: $cm^2 \cdot s^{-1}$ (Fig. 50).*

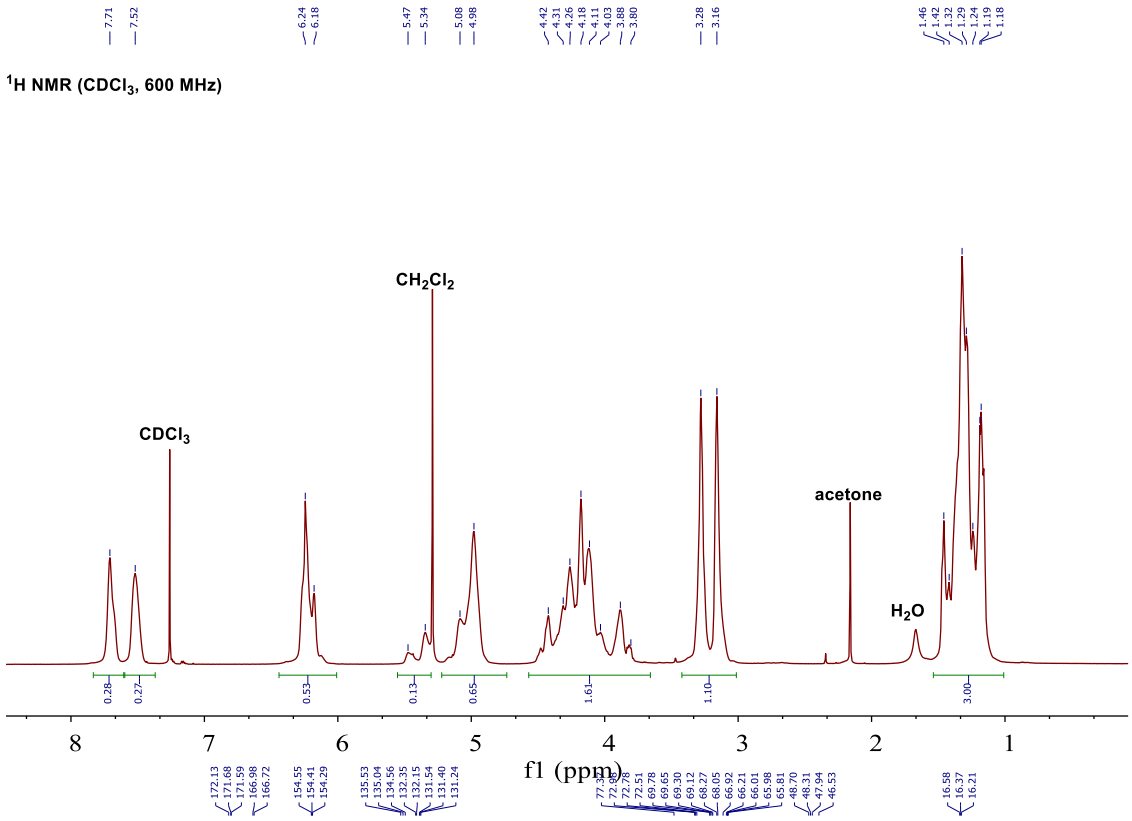

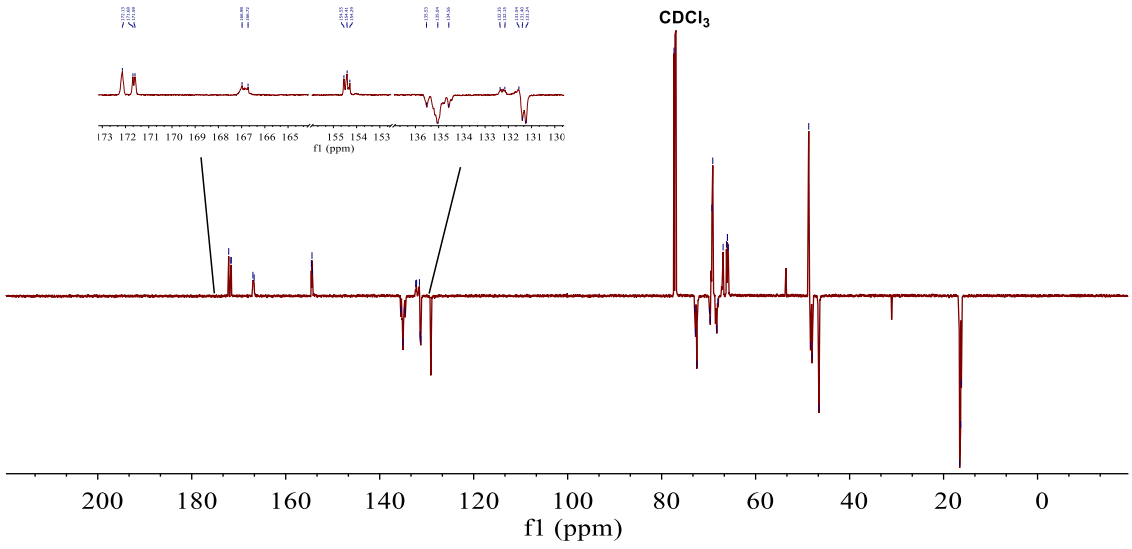

*Fig. S19: ^{1}H–NMR and $^{13}C\{^{1}H\}$–NMR spectra of [PO-PA]/[PO-NA]/[PPC] polymer synthesized by direct anhydride combination and polymerization under CO_2 atmosphere with PA/NA = 250 equiv / 250 equiv and **1**/PPNCl (1 equiv) as catalyst system (Fig. 51).*

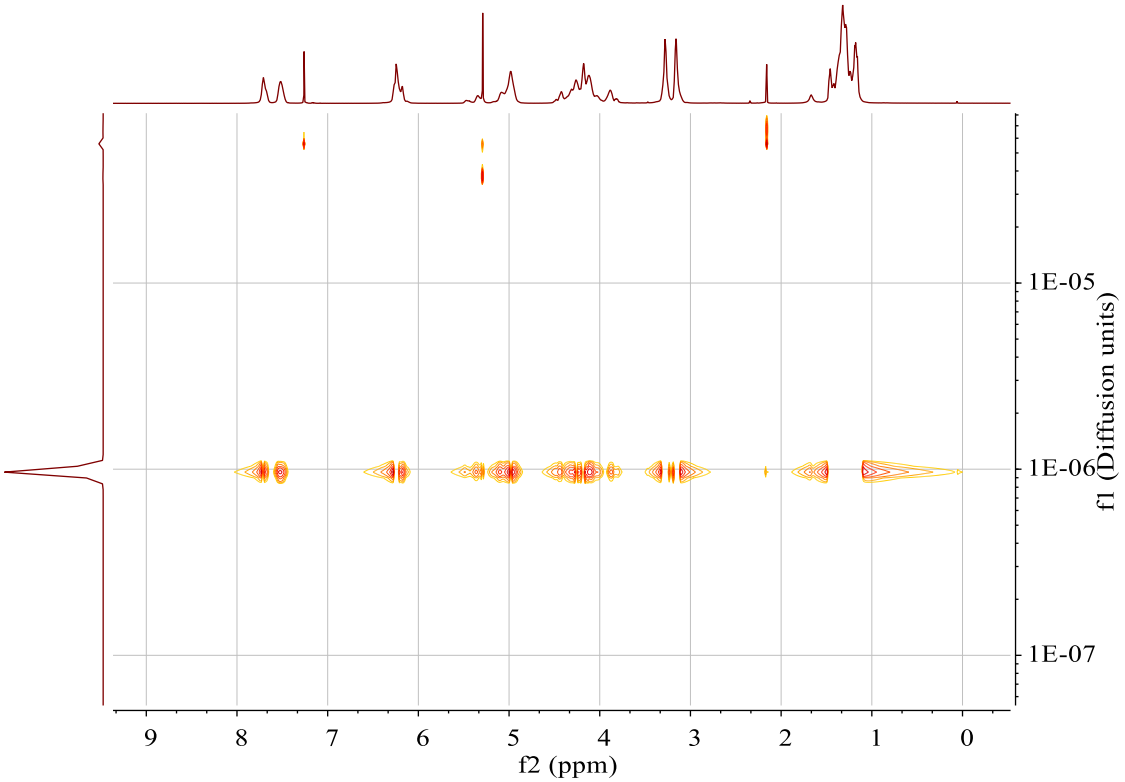

*Fig. S20: DOSY NMR spectrum of [PO-PA]/[PO-NA]/[PPC]polymer with **1**/PPNCl as catalyst system. Diffusion units: $cm^2 \cdot s^{-1}$ (Fig. 51).*

7 Representative NMR Spectra from Polymer Postmodification

7.1 Allyloxy Nile Red

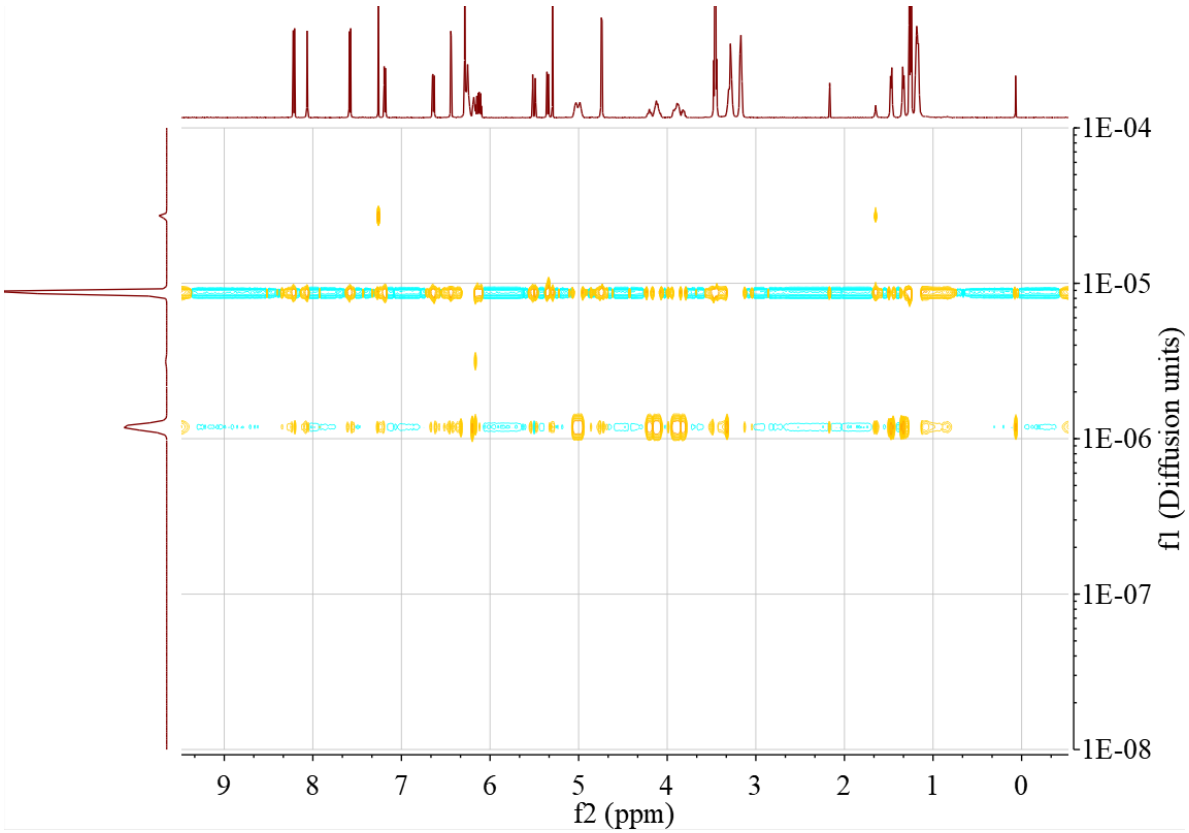

Fig. S21: DOSY spectrum before reprecipitation of the polymer from Table 11, entry 2. Diffusion units: $cm^2 \cdot s^{-1}$

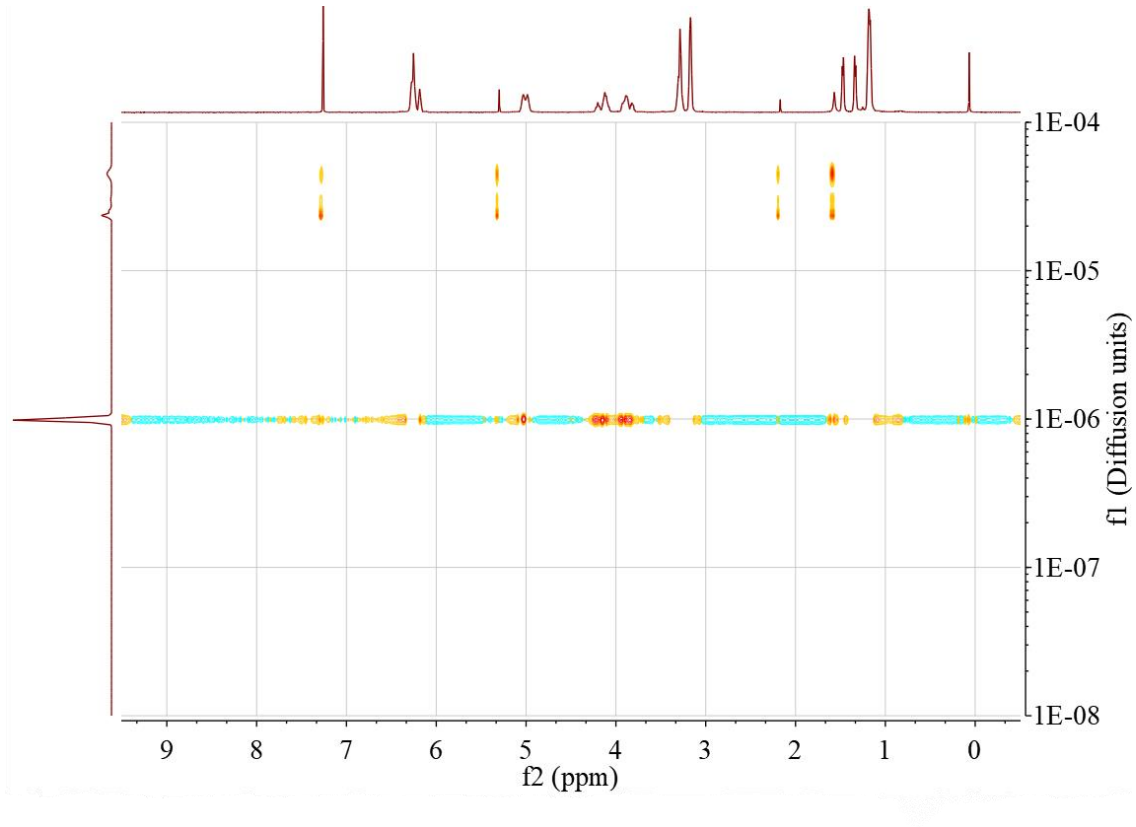

Fig. S22: DOSY spectrum after reprecipitation of the polymer from Table 11, entry 2. Diffusion units: $cm^2 \cdot s^{-1}$.

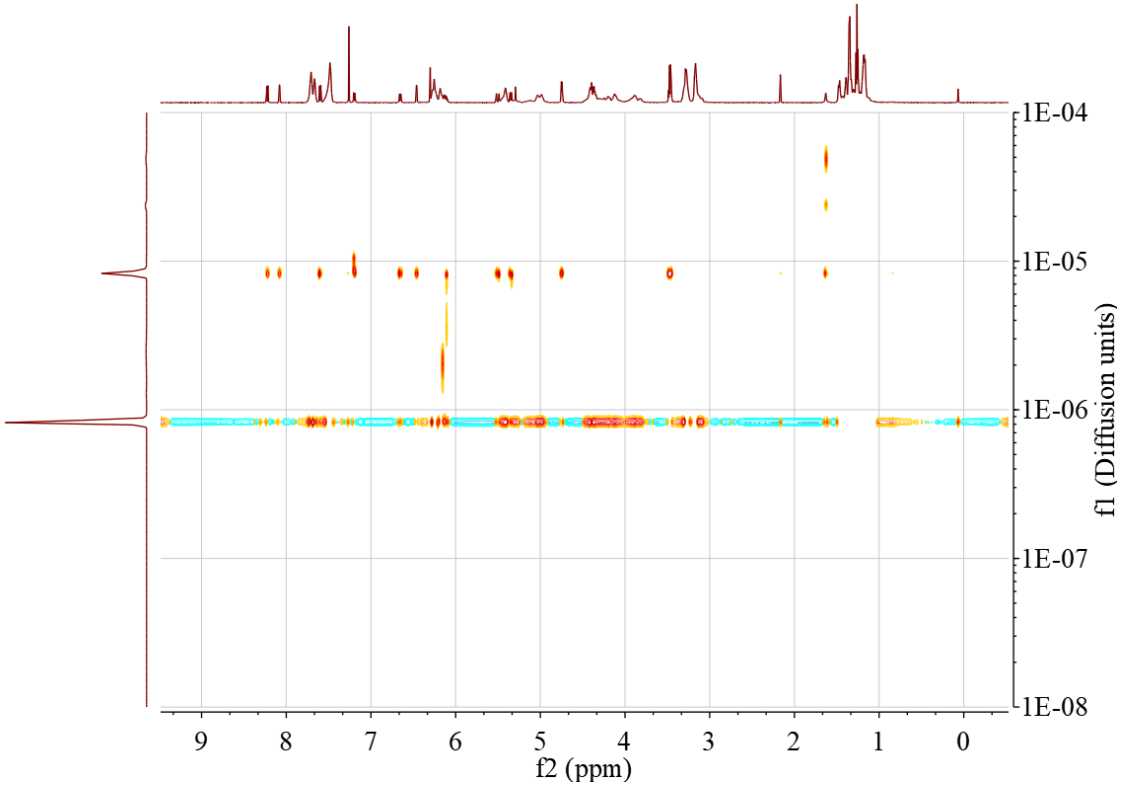

Fig. S23: DOSY spectrum before reprecipitation of the polymer from Table 11, entry 3. Diffusion units: $cm^2 \cdot s^{-1}$.

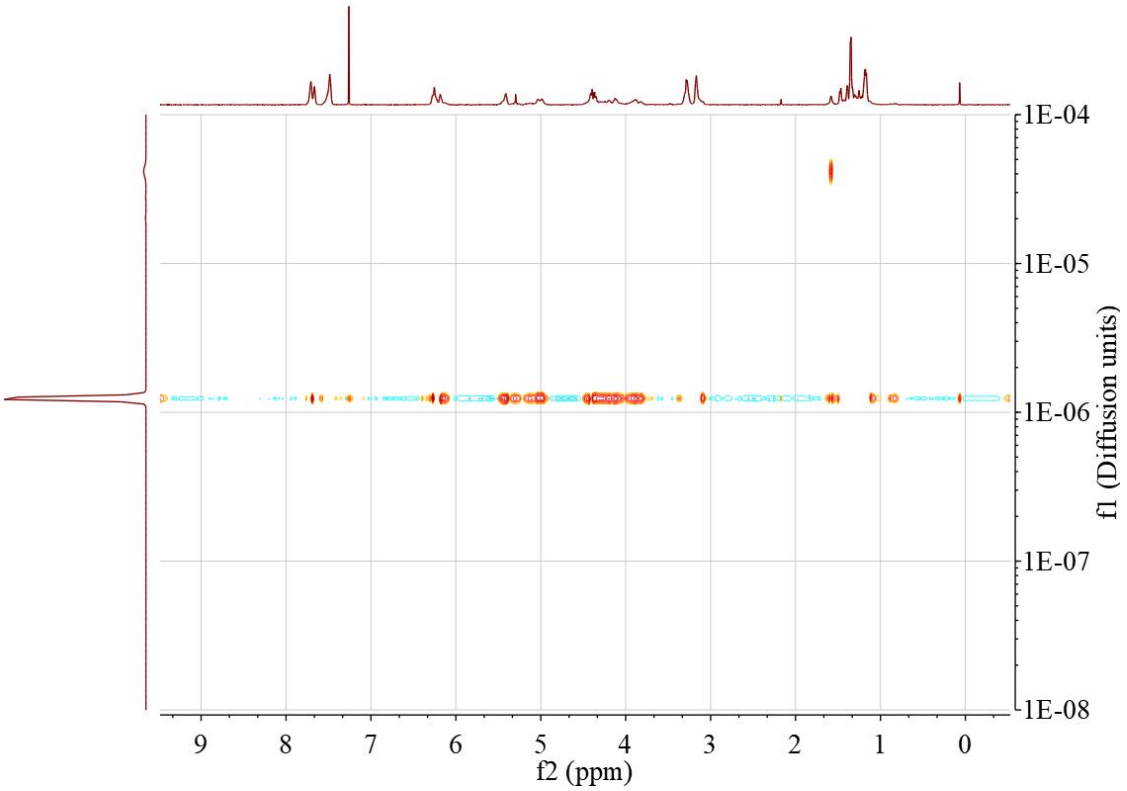

Fig. S24: DOSY spectrum after reprecipitation of the polymer from Table 11, entry 3. Diffusion units: $cm^2 \cdot s^{-1}$.

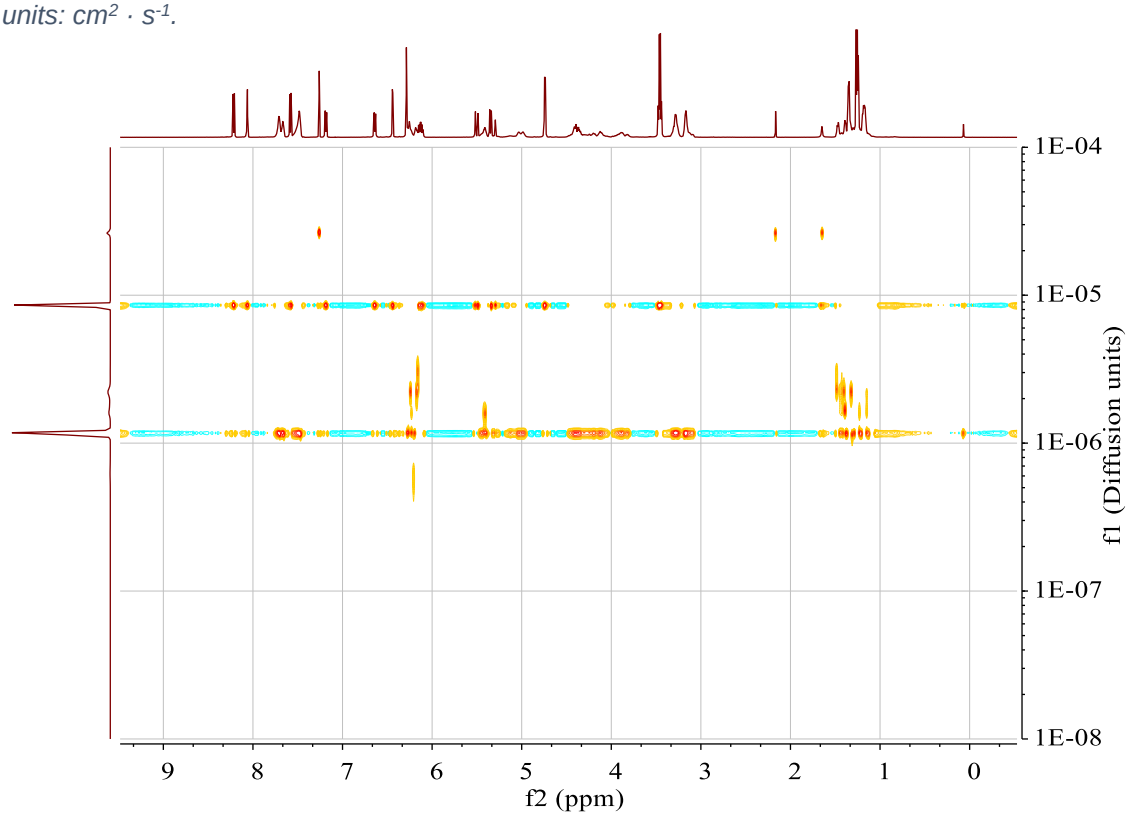

Fig. S25: DOSY spectrum before reprecipitation of the polymer from Table 11, entry 4. Diffusion units: $cm^2 \cdot s^{-1}$.

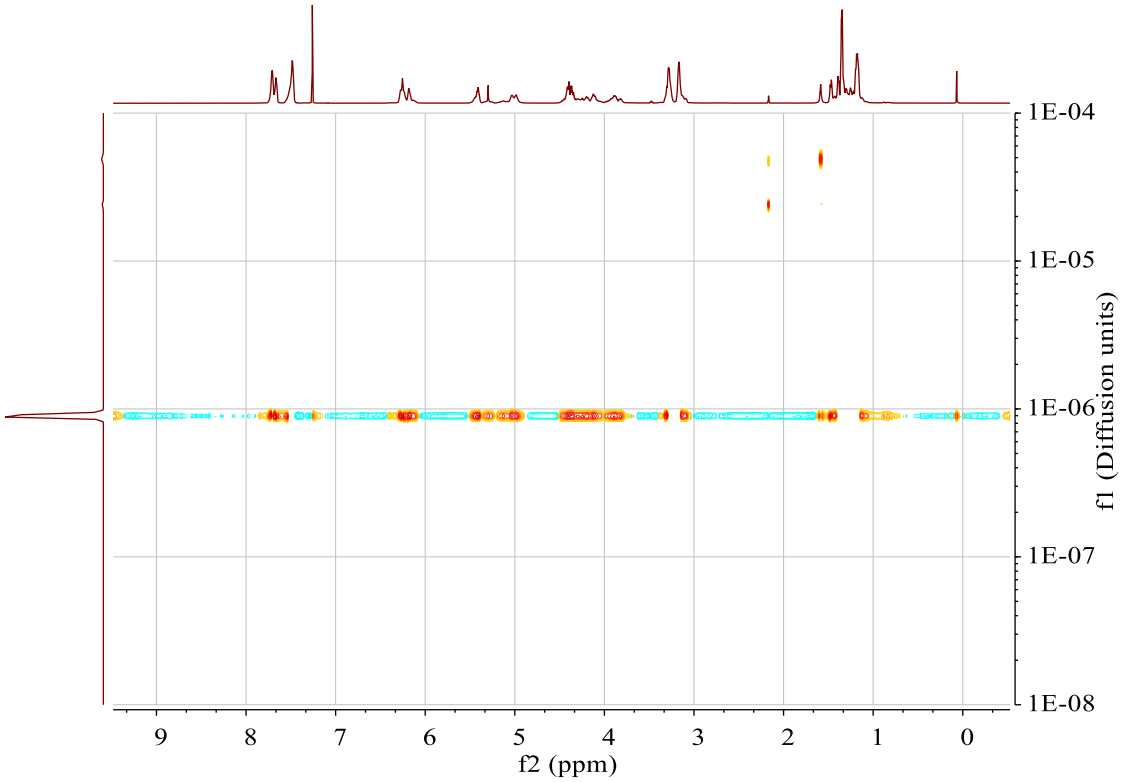

Fig. S26: DOSY spectrum after reprecipitation of the polymer from Table 11, entry 4. Diffusion units: $cm^2 \cdot s^{-1}$.

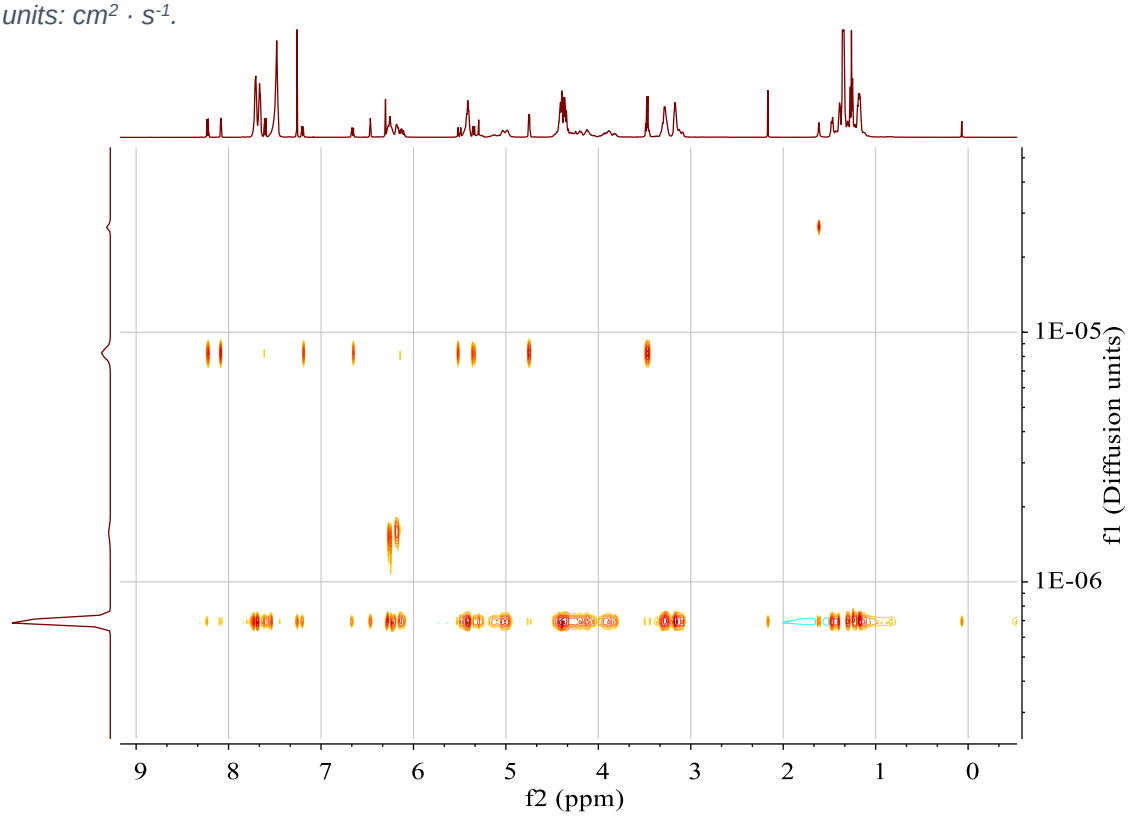

Fig. S27: DOSY spectrum before reprecipitation of the polymer from Table 11, entry 6. Diffusion units: $cm^2 \cdot s^{-1}$.

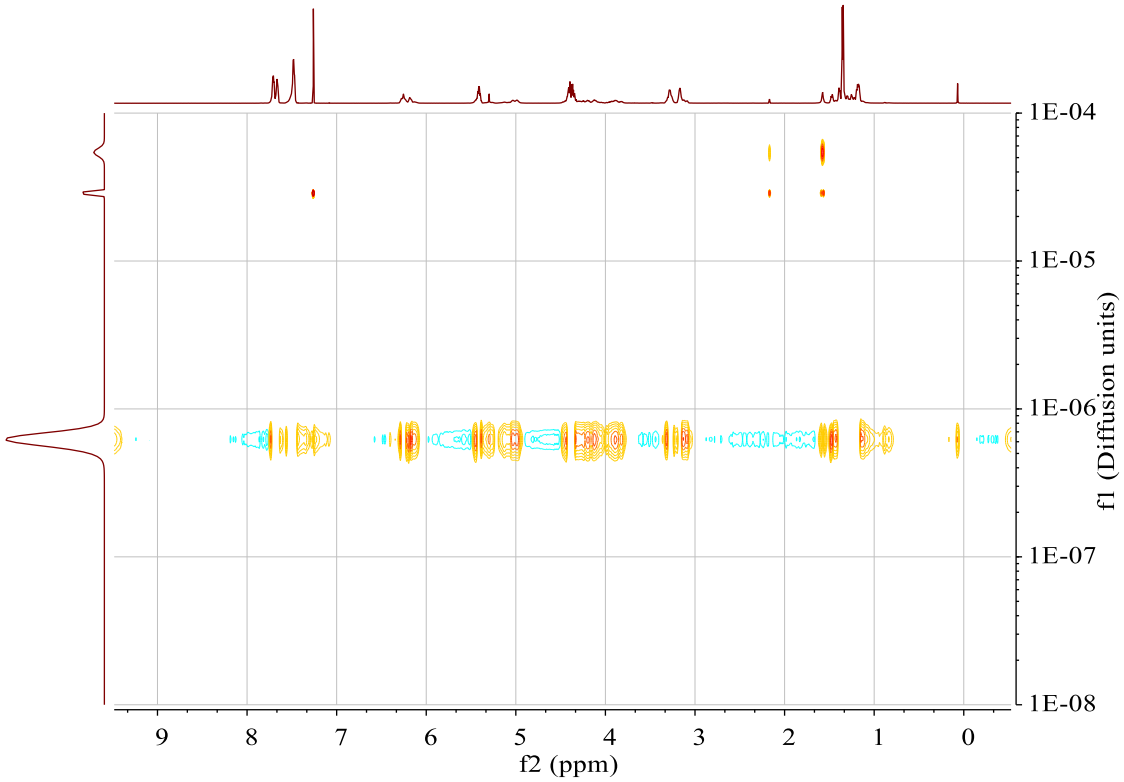

Fig. S28: DOSY spectrum after reprecipitation from Table 11, entry 6. Diffusion units: $cm^2 \cdot s^{-1}$.

7.2 Bisallyloxy Fluorescein

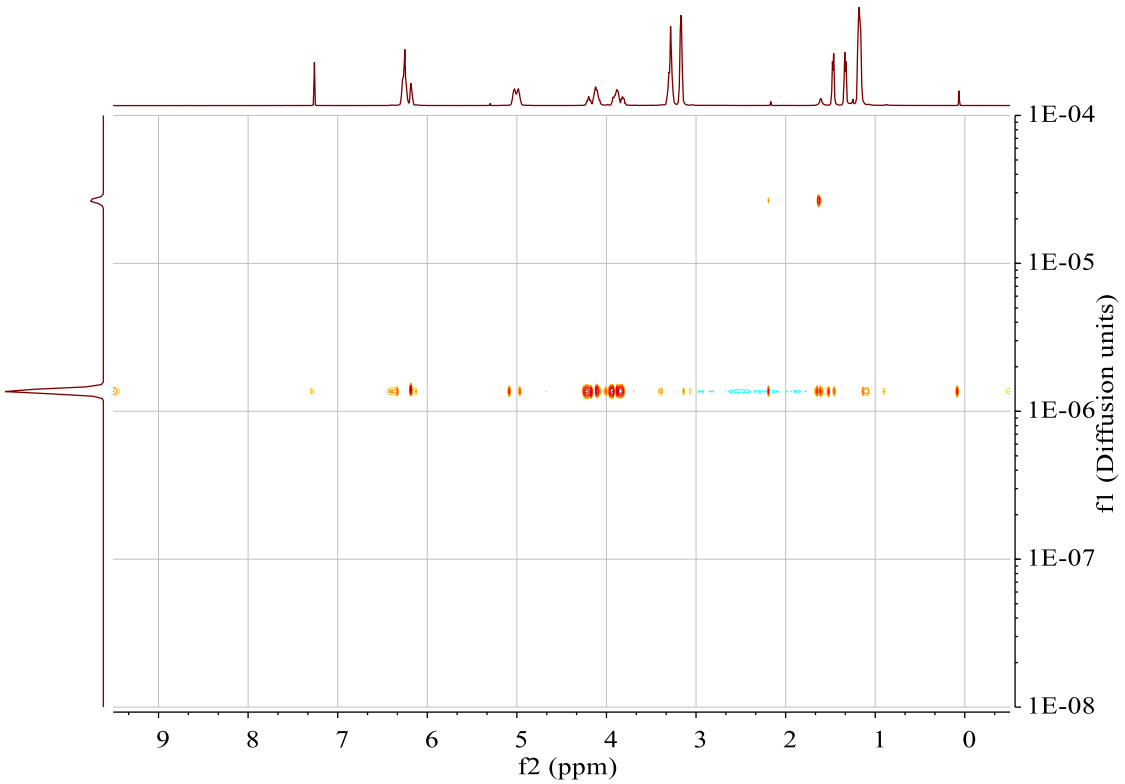

Fig. S29: DOSY spectrum of the polymer from Table 12, entry 4. Diffusion units: $cm^2 \cdot s^{-1}$.

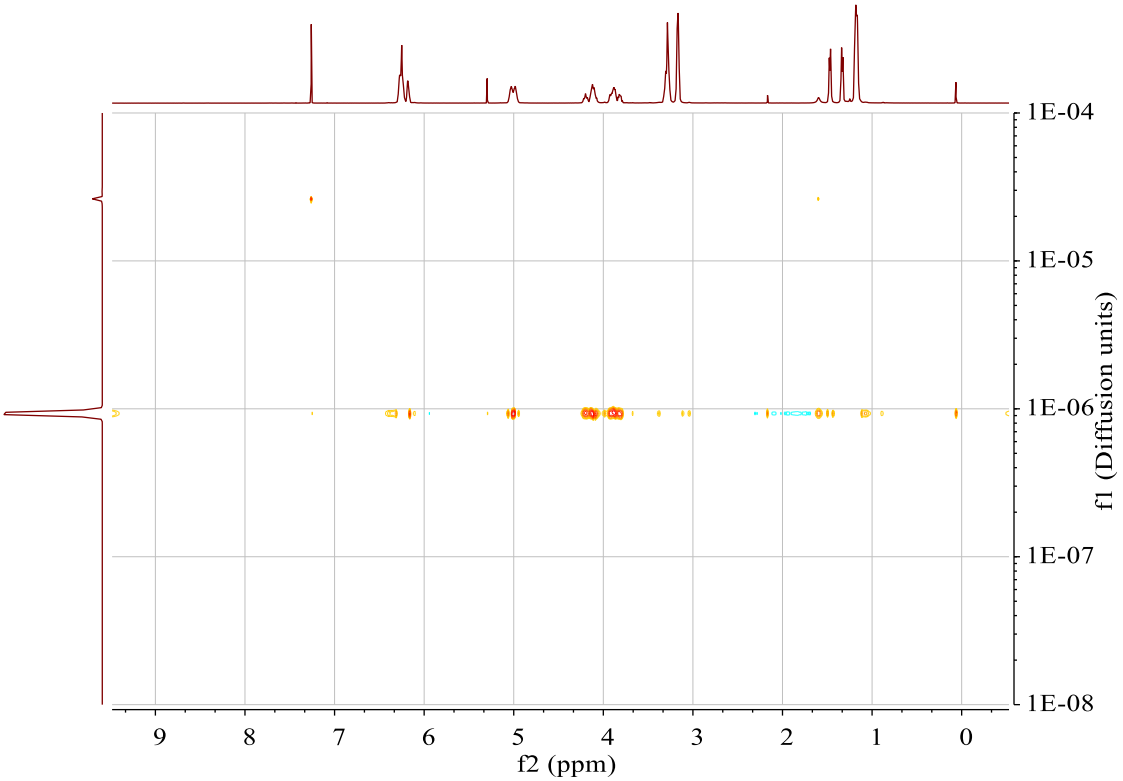

Fig. S30: DOSY spectrum of the polymer from Table 12, entry 5. Diffusion units: $cm^2 \cdot s^{-1}$.

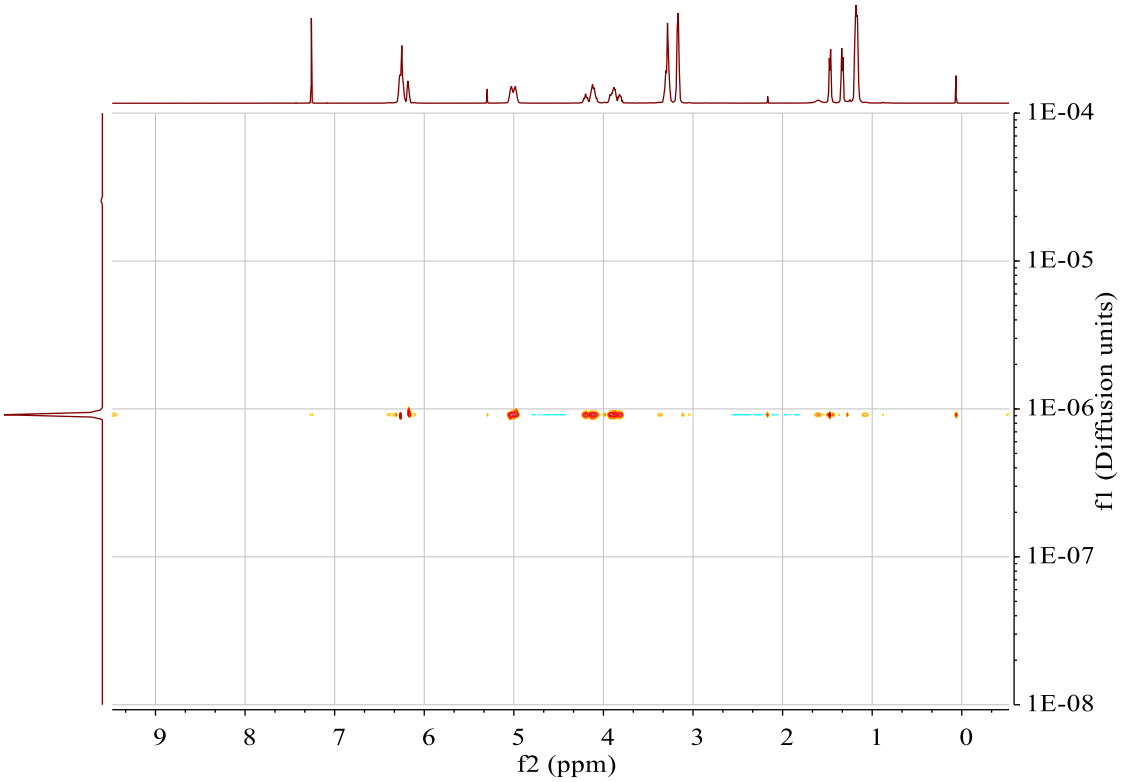

Fig. S31: DOSY spectrum of the polymer from Table 12, entry 6. Diffusion units: $cm^2 \cdot s^{-1}$.

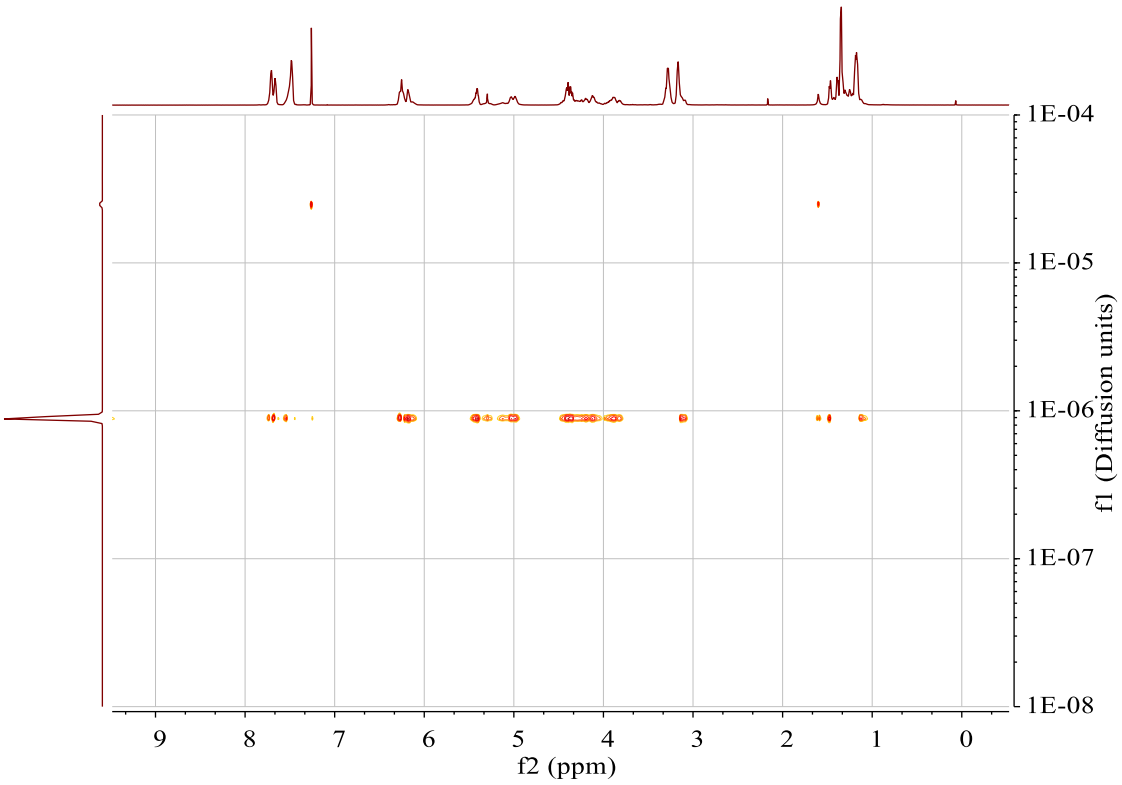

Fig. S32: DOSY spectrum of the polymer from Table 12, entry 7. Diffusion units: $cm^2 \cdot s^{-1}$.

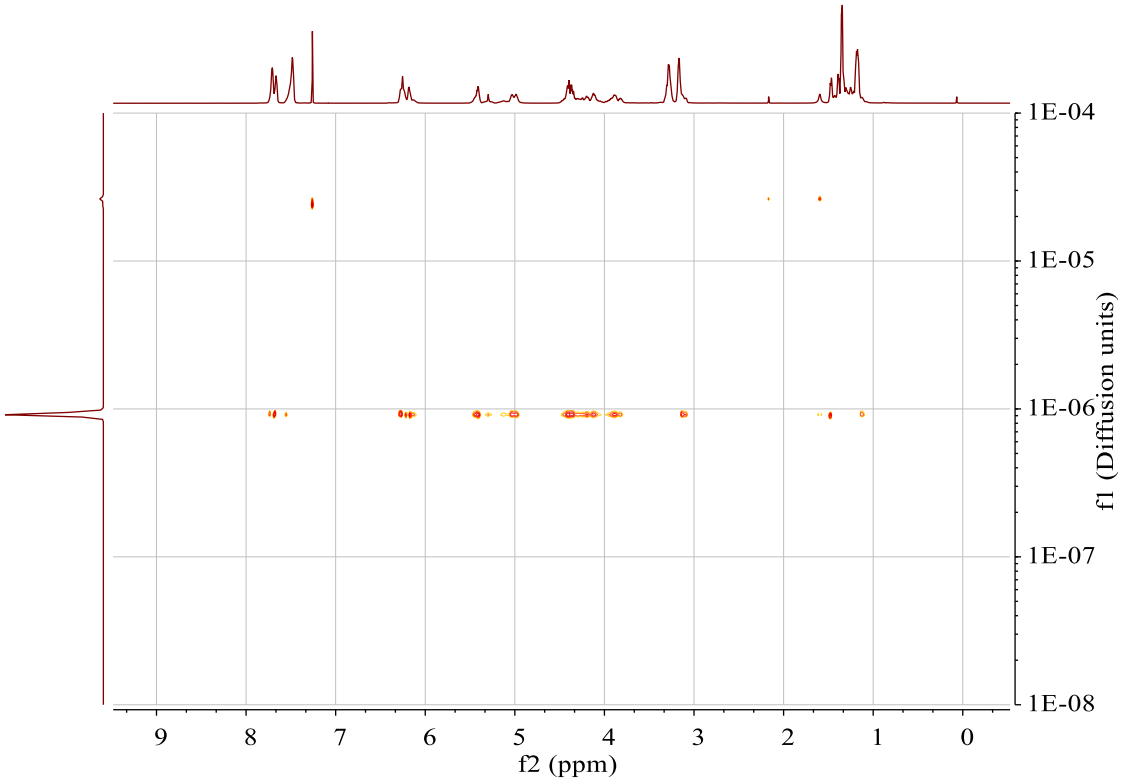

Fig. S33: DOSY spectrum of the polymer from Table 12, entry 8. Diffusion units: $cm^2 \cdot s^{-1}$.

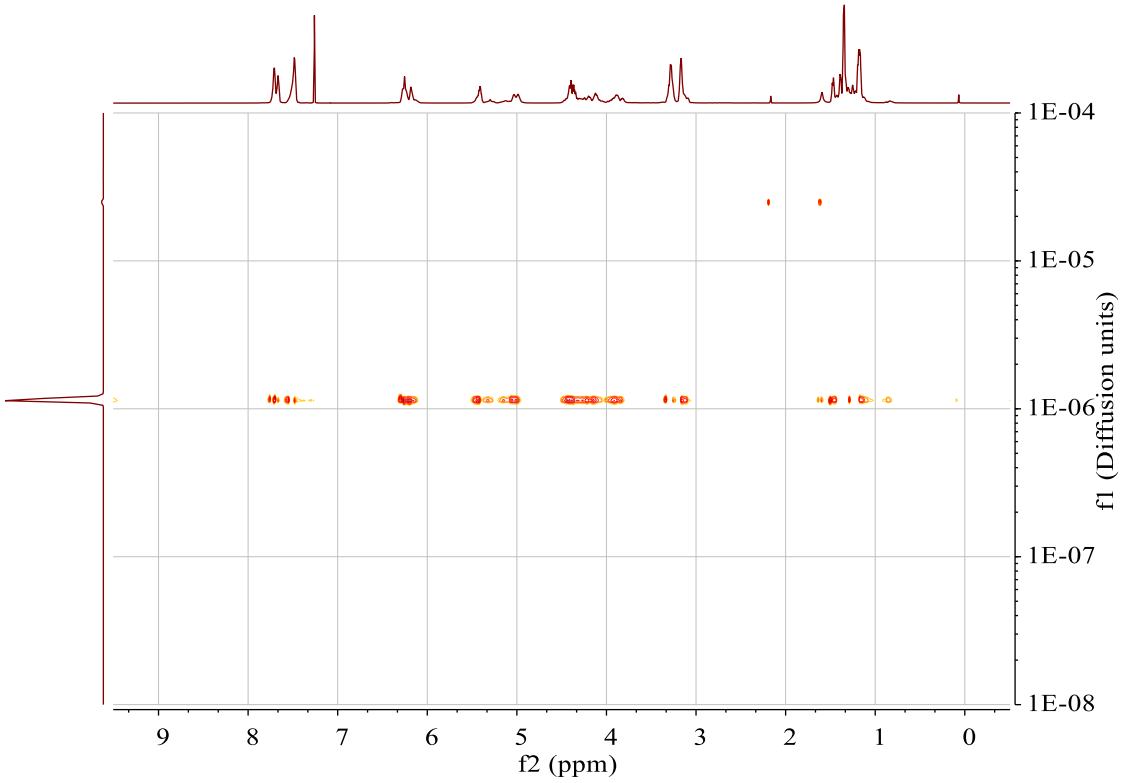

Fig. S34: DOSY spectrum of the polymer from Table 12, entry 9. Diffusion units: $cm^2 \cdot s^{-1}$.

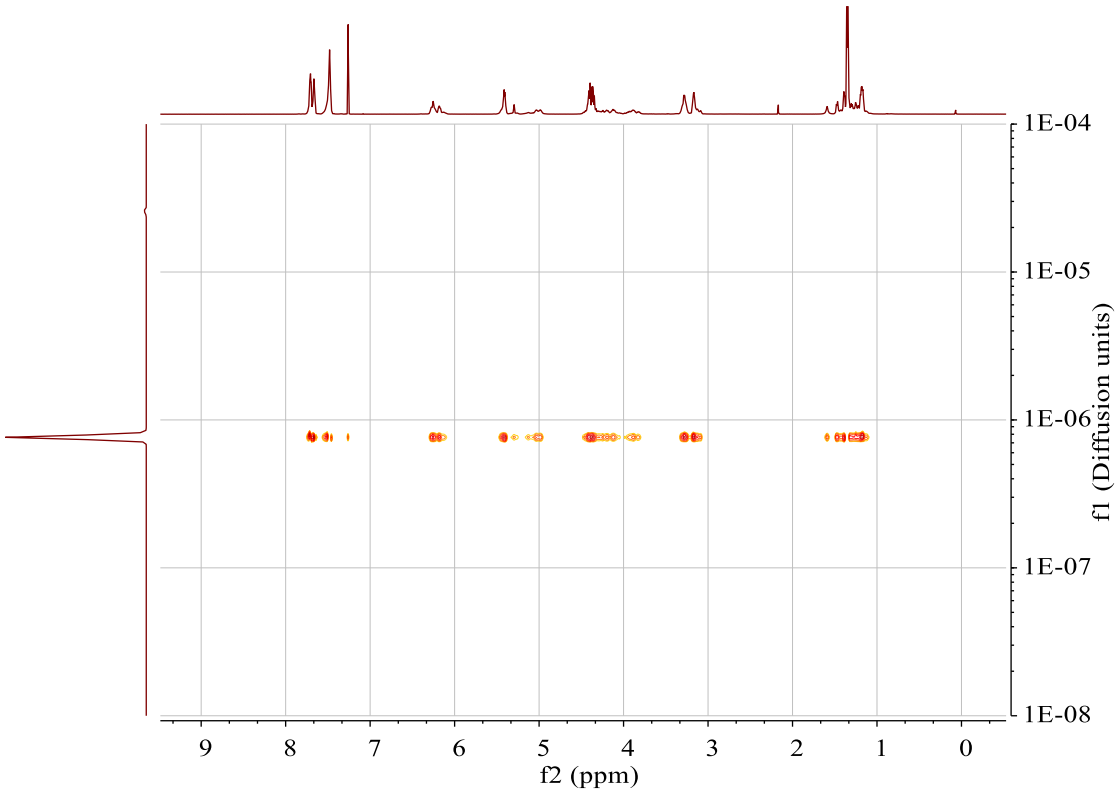

Fig. S35: DOSY spectrum of the polymer from Table 12, entry 10. Diffusion units: $cm^2 \cdot s^{-1}$.

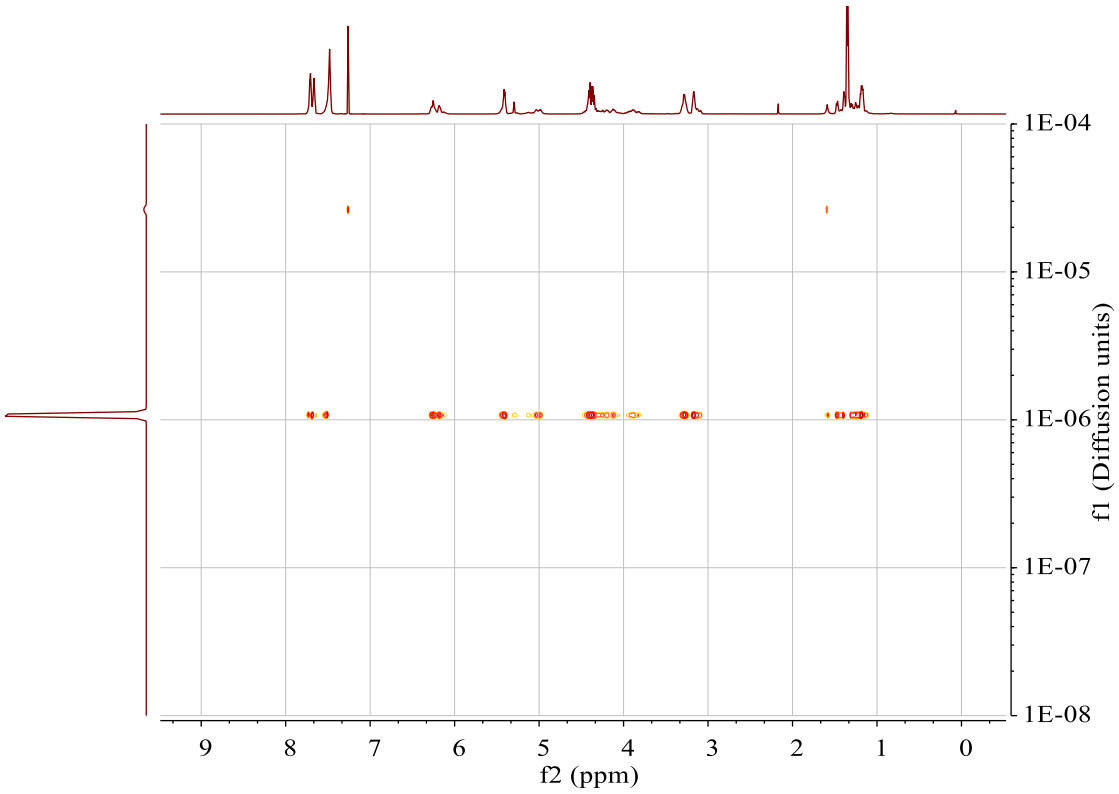

Fig. S36: DOSY spectrum of the polymer from Table 12, entry 11. Diffusion units: $cm^2 \cdot s^{-1}$.

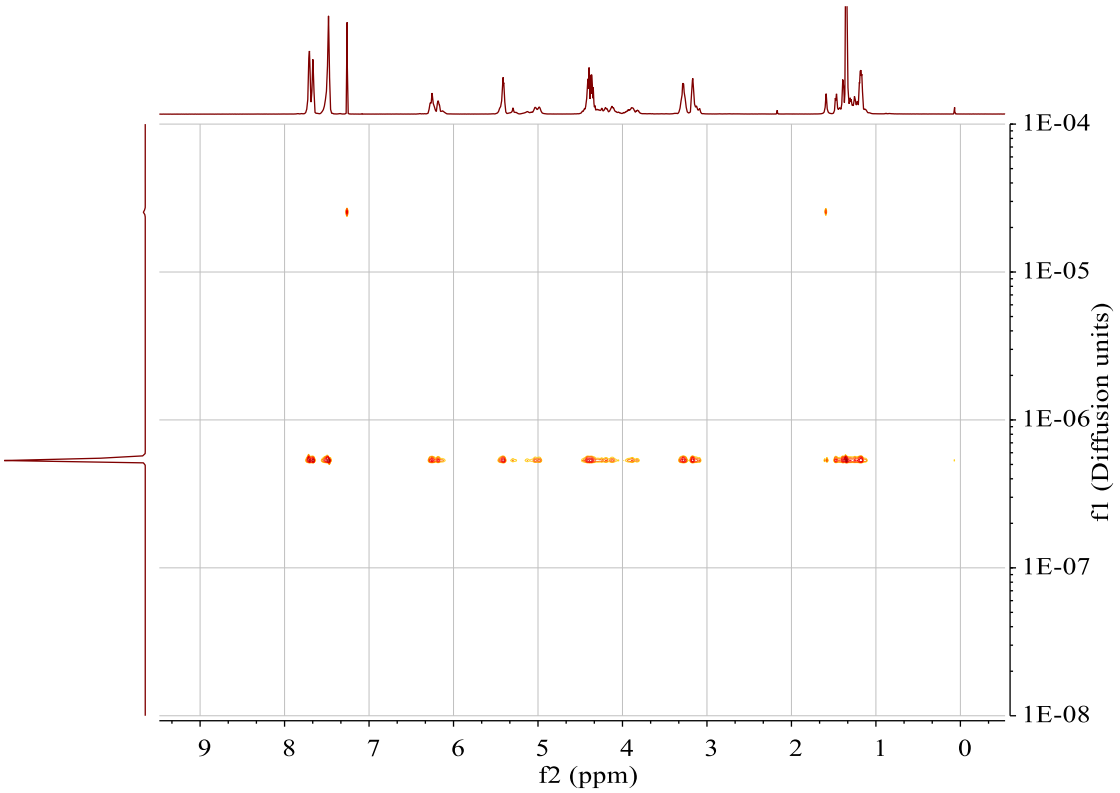

Fig. S37: DOSY spectrum of the polymer from Table 12, entry 12. Diffusion units: $cm^2 \cdot s^{-1}$.

8 GPC Data

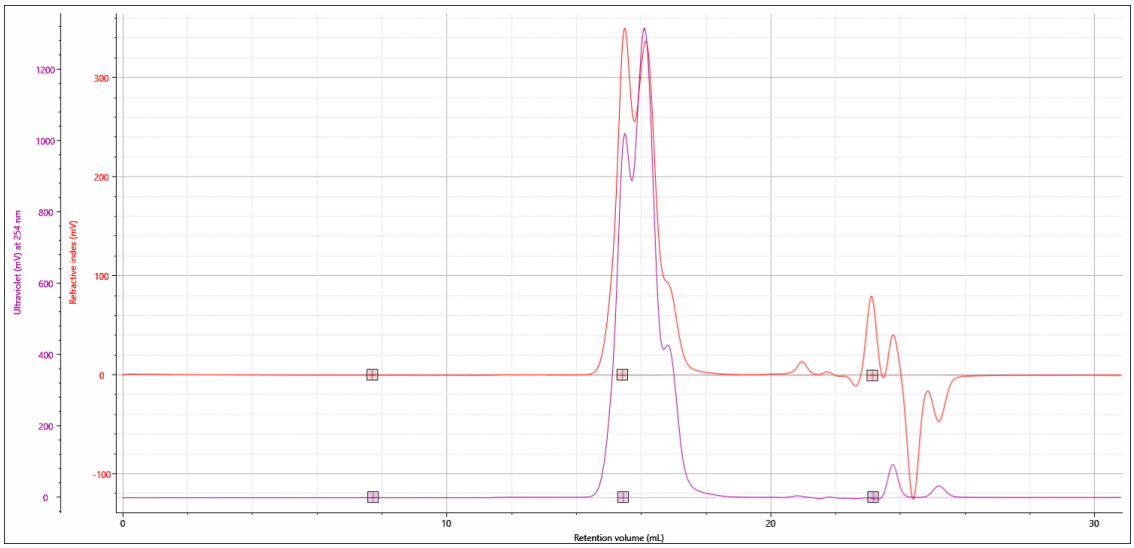

*Fig. S38: Representative GPC trace of PO/NA/PA terpolymer with **1**/PPNCl as catalyst system and sequential anhydride addition of 250 equiv of NA and 500 equiv of PA (Fig. 42).*

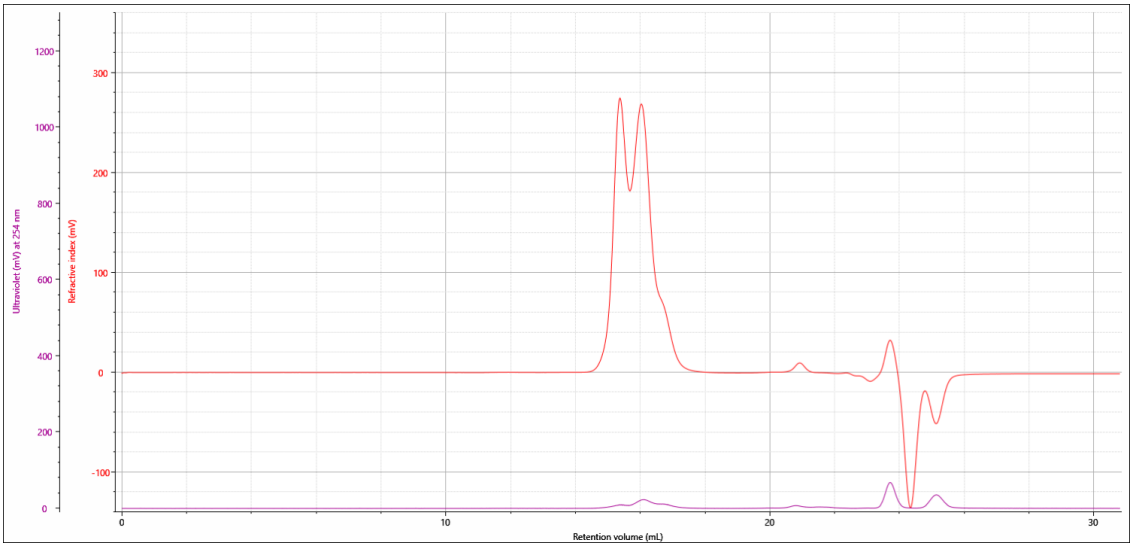

*Fig. S39: Representative GPC trace of PO/NA copolymer with **1**/PPNCl as catalyst system and sequential NA addition of 250 equiv and 500 equiv (Table 7, entry 4).*

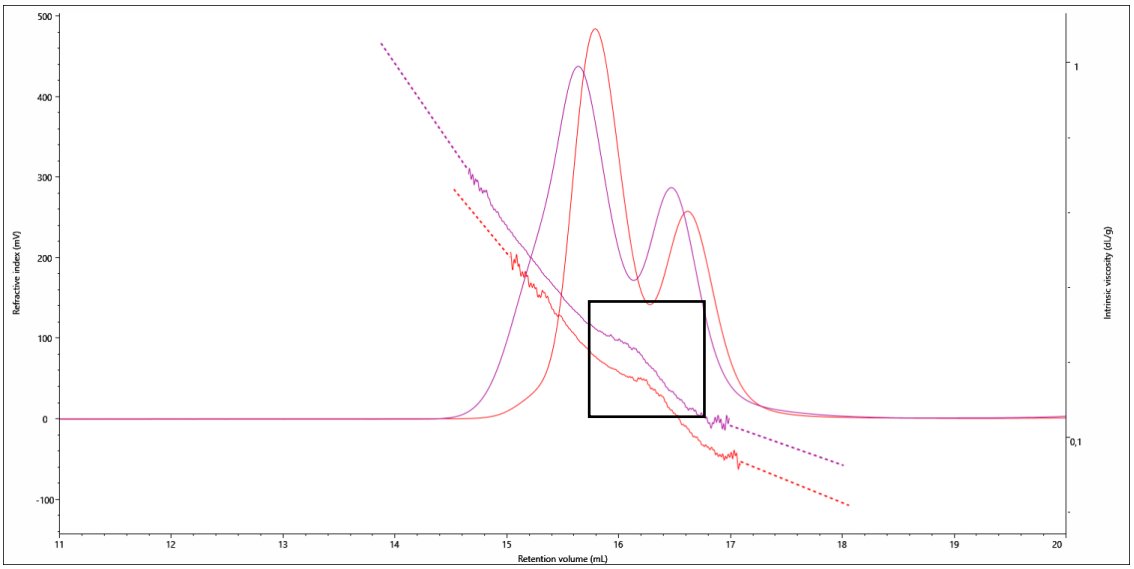

*Fig. S40: Representative GPC trace of PO/PA/NA terpolymer with **1**/PPNCl as catalyst system and direct anhydride combination (250 equiv PA & 250 equiv NA) (red) vs. GPC trace of PO/PA copolymer (purple). Intrinsic viscosity (IV) of the terpolymer progresses with a step transition between the modes while IV shows a smooth transition (Fig. 44 A).*

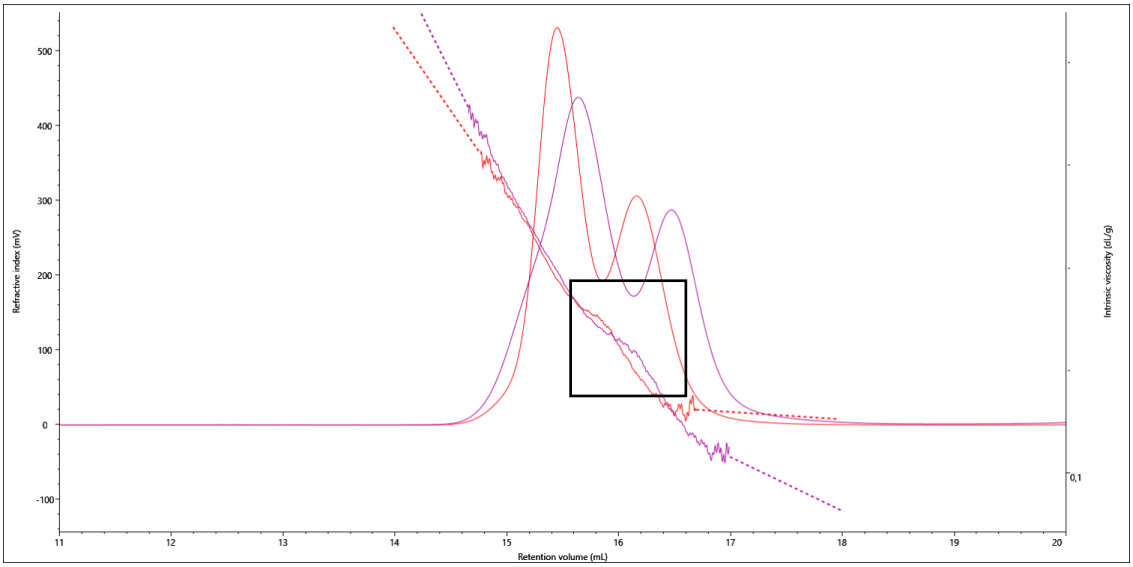

*Fig. S41: Representative GPC trace of PO/PA/NA terpolymer with **1**/PPNCl as catalyst system and direct anhydride combination (500 equiv PA & 250 equiv NA) (red) vs. GPC trace of PO/PA copolymer (purple). Intrinsic viscosity (IV) progresses with a smooth transition between the modes (Fig. 44 B).*

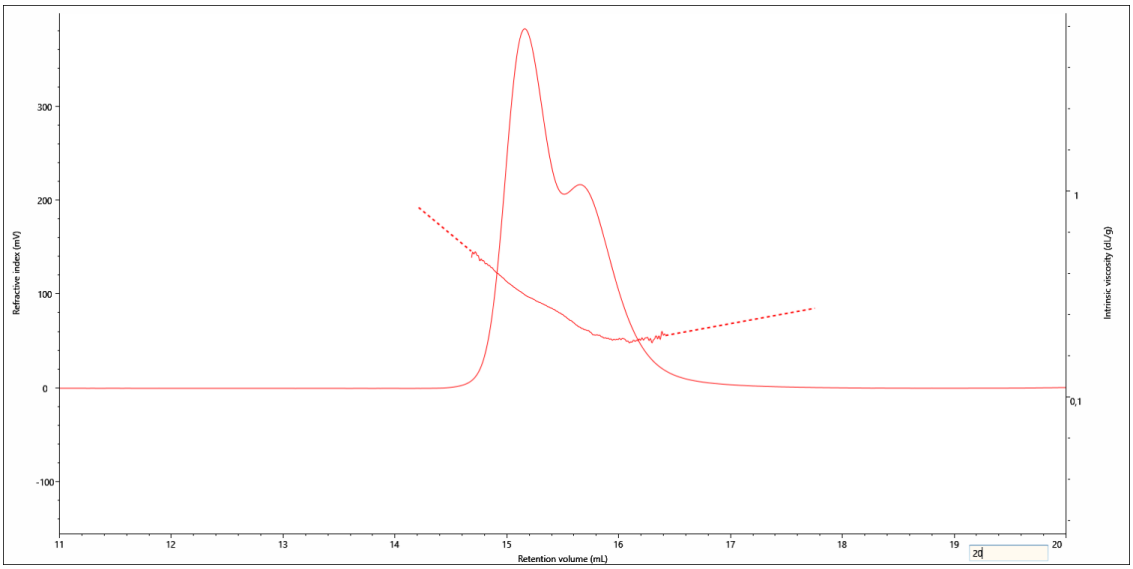

*Fig. S42: Representative GPC trace of a PO/PA copolymer, synthesized under CO_2 atmosphere with **1**/PPNCl as catalyst (Fig. 47).*

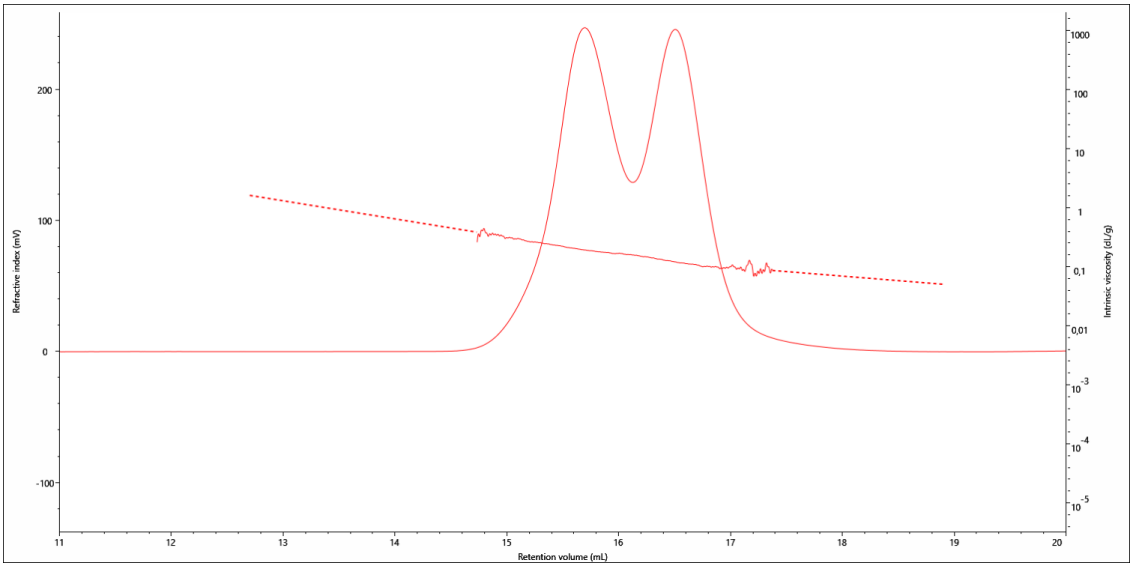

*Fig. S43: Representative GPC trace of a PO/NA copolymer, synthesized under CO_2 atmosphere with **1**/PPNCl as catalyst (Fig. 50).*

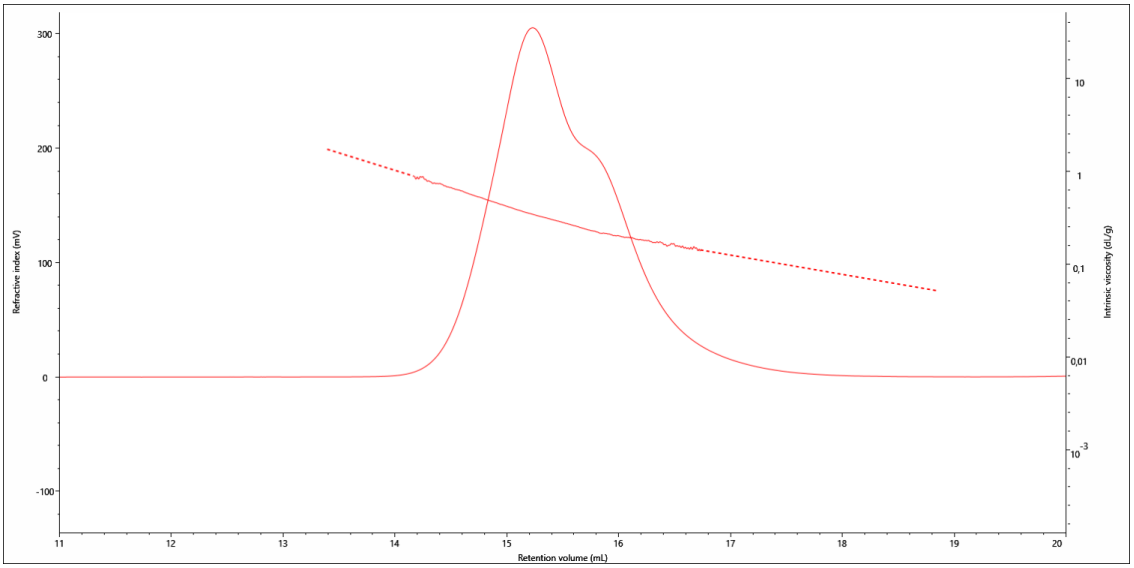

*Fig. S44: Representative GPC trace of a PO/NA/PA terpolymer, synthesized under CO_2 atmosphere with **1**/PPNCl as catalyst (Fig. 51).*

Entry	Equivalents of anhydrides (PA/NA)[a]	CO_2 (bar)	t(h)	M_n (kg · mol^{-1})[b]	PDI	Additional data
1	500/250[c]	/	4.5+4.5[d]	32.4	1.49	Fig. S38
2	0/(250+500)	/	2.9+5.4[d]	33.0	1.40	Fig. S39
3	250/250[e]	/	2.9	33.3	1.23	Fig. S40
4	500/250[e]	/	3.7	46.6	1.23	Fig. S41
5	500/0	10	6	53.0	1.19	Fig. S42
6	0/500	10	20	36.5	1.32	Fig. S43
7	250/250[e]	10	23	43.8	1.51	Fig. S44

*Table S1: Summary of polymer analysis data obtained from PO/PA/NA terpolymers synthesized under Ar and CO_2 atmosphere and **1**/PPNCl (1 equiv) as catalyst. [a]Equivalents with respect to catalyst. [b]Determined by GPC calibrated with polystyrene standards employing triple detection. [c]First lot NA, second lot PA. [d]Reaction time for consumption of first anhydride lot + reaction time for consumption of second anhydride lot. [e]Directly mixed monomers.*

9 3D-IR spectra of polymerizations under CO_2 atmosphere

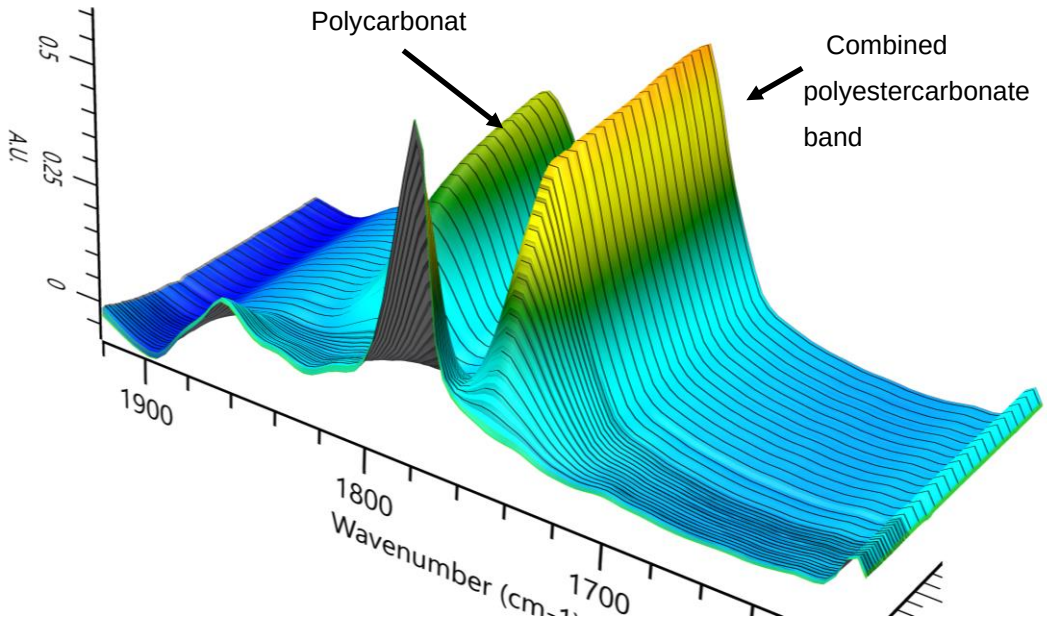

*Fig. S45: 3D plot of the ROCOP of PO & NA under CO_2 atmosphere with **1**/PPNCl as catalyst (Fig. 50, Fig. S41, Table S1, entry 6).*

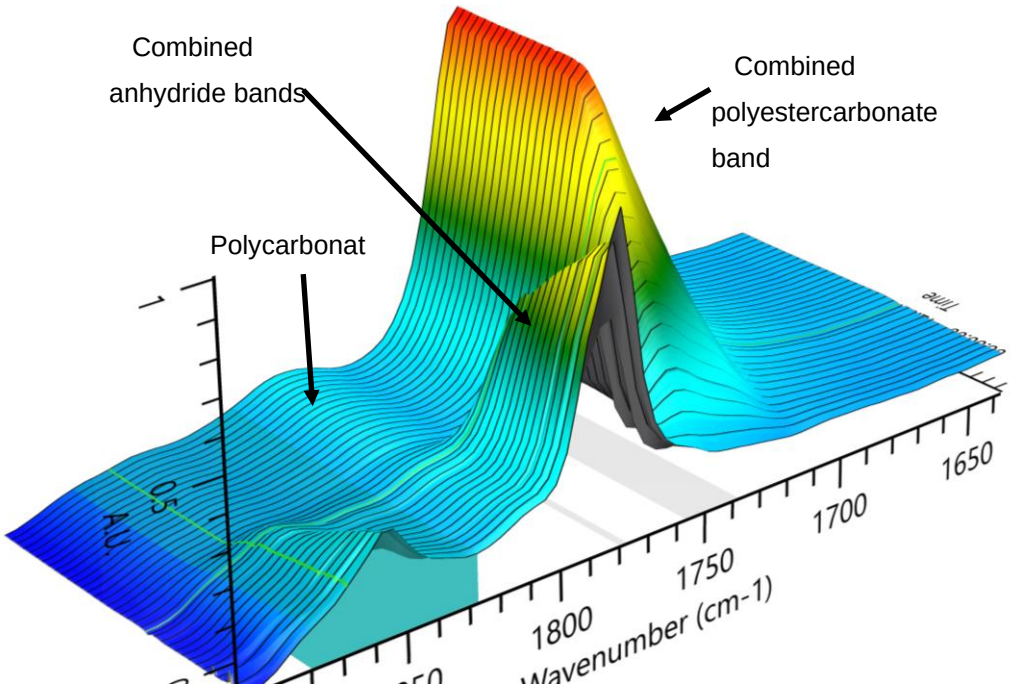

*Fig. S46: 3D plot of the ROCOP of PO, NA & PA under CO_2 atmosphere with **1**/PPNCl as catalyst (Fig. 52, Fig. S44 , Table S1, entry 7).*

10 Representative DSC Measurements

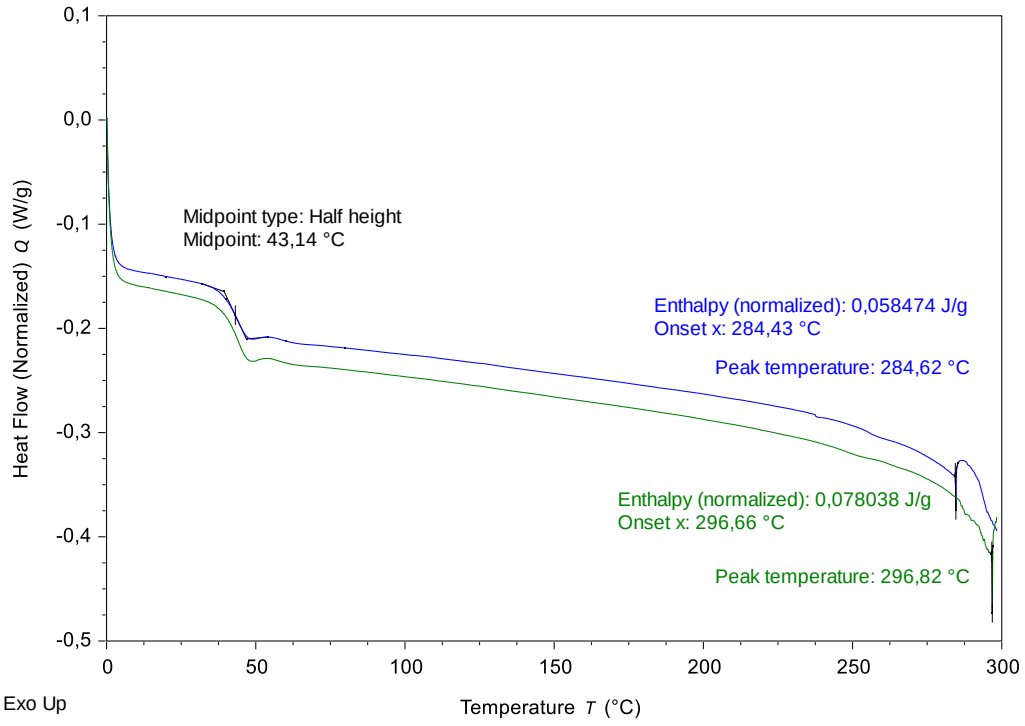

Fig. S47: 2nd and 3rd DSC cycle of a poly(propyl tetrahydrotherephthalate)-poly(propyl phthalate) terpolymer from direct terpolymerization with 23 % THPA-PO ester moieties.

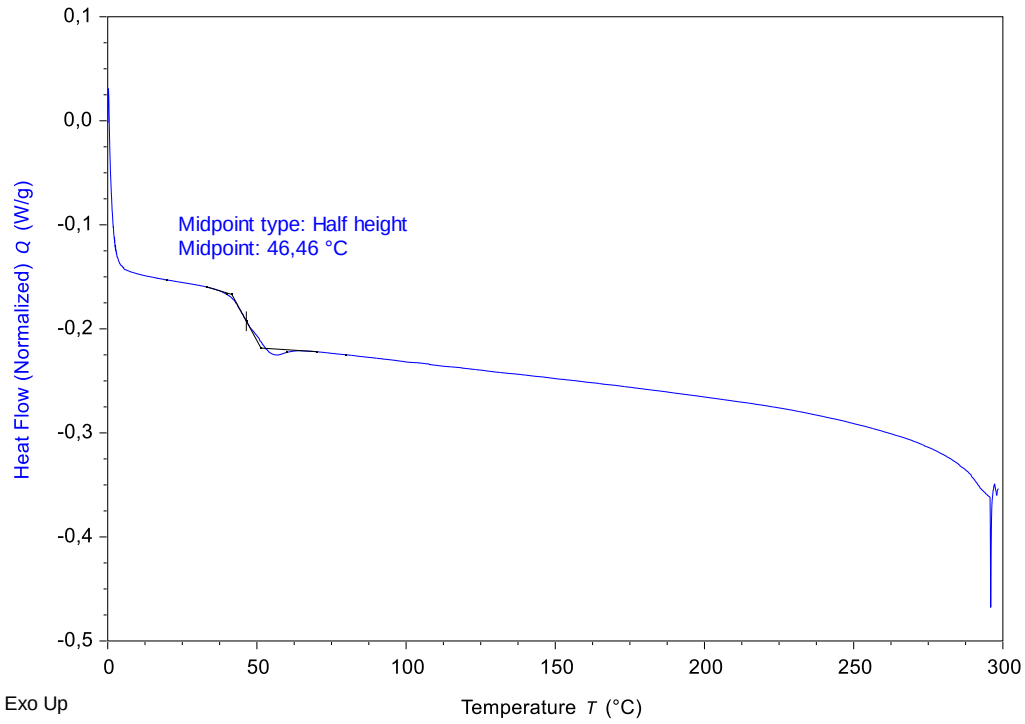

Fig. S48: DSC curve of an enantioenriched poly(phthalic acid propyl)ester (Table 5, entry 2).

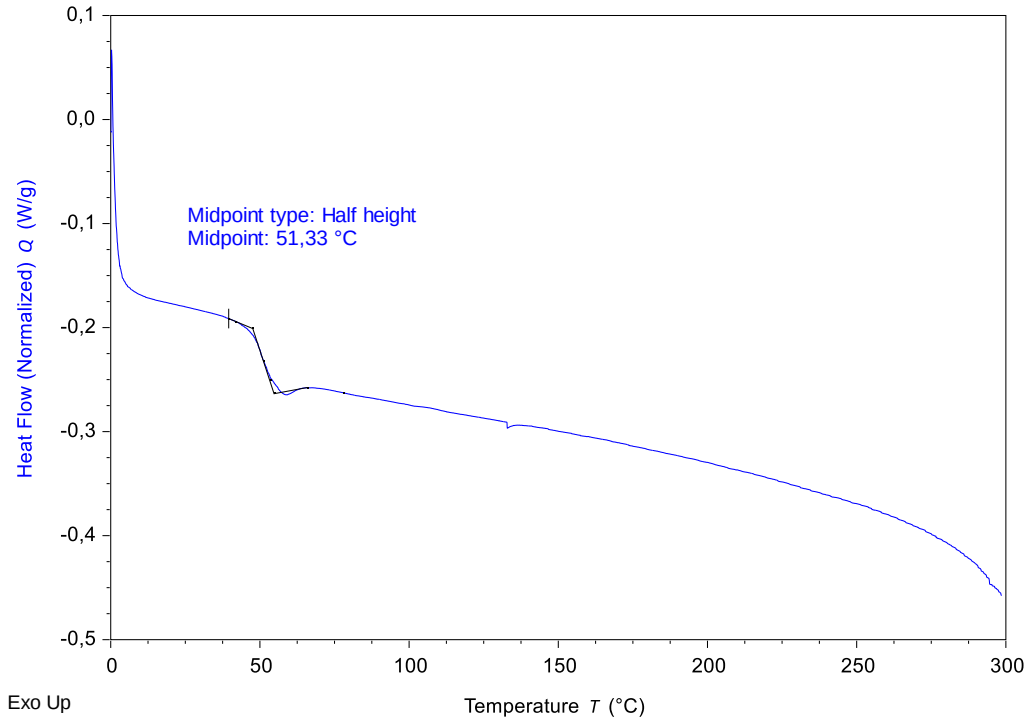

Fig. S49: DSC curve of a racemic poly(phthalic acid propyl)ester (Table 5, entry 10).

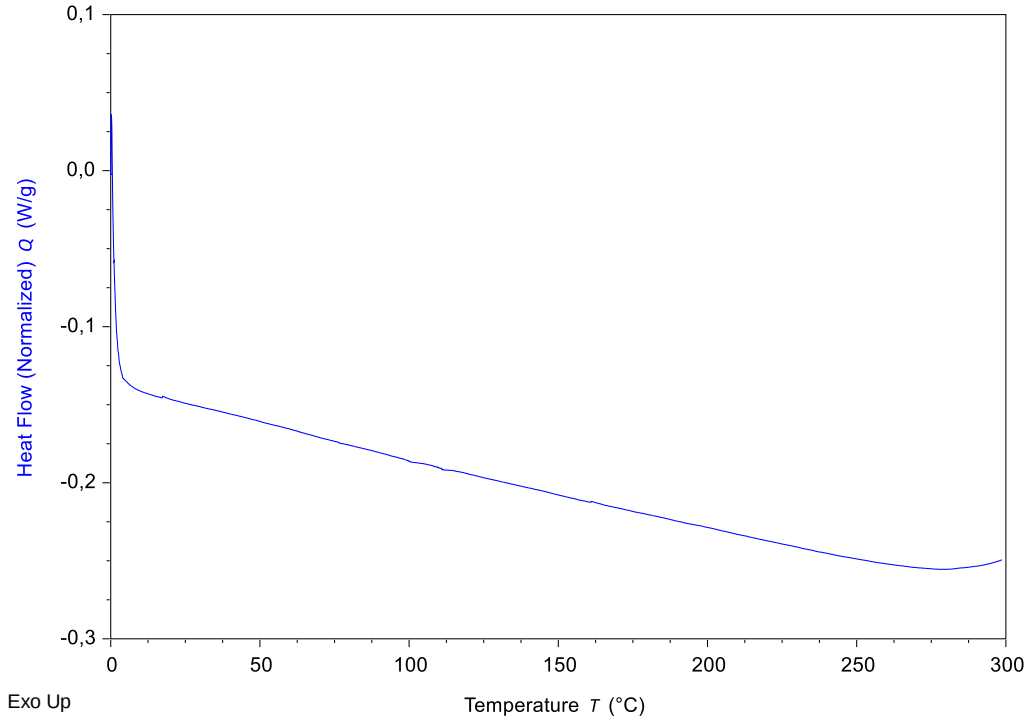

Fig. S50: DSC curve of an enantioenriched poly(norbornene dicarboxylic acid propyl)ester (Table 6, entry 1).

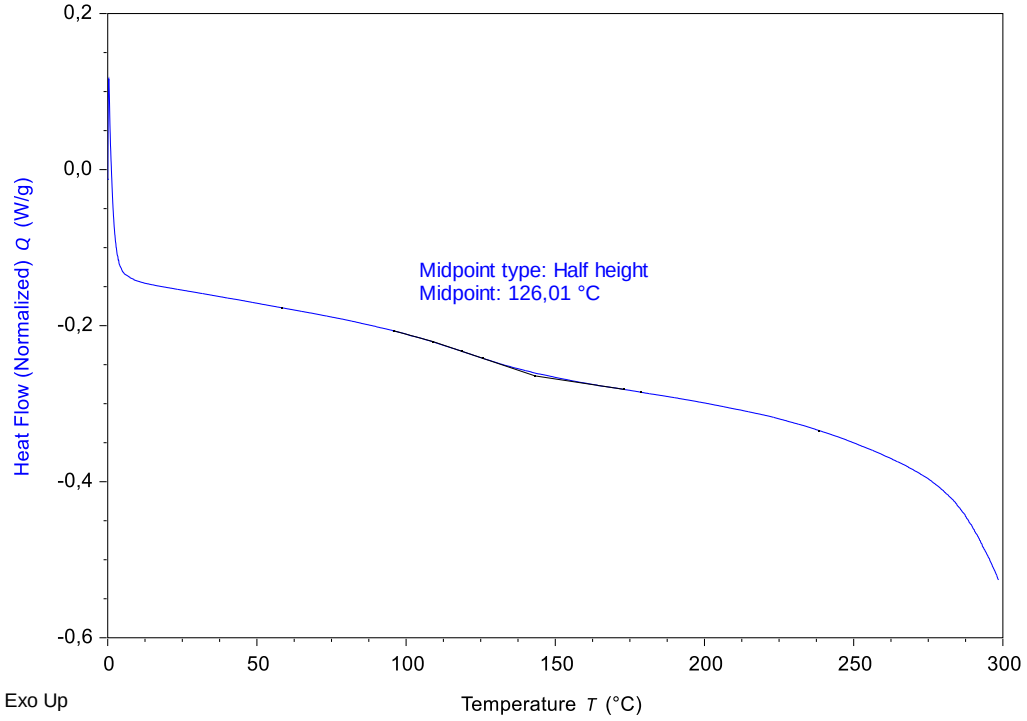

Fig. S51: DSC curve of an racemic poly(norbornene dicarboxylic acid propyl)ester (Table 6, entry 4).

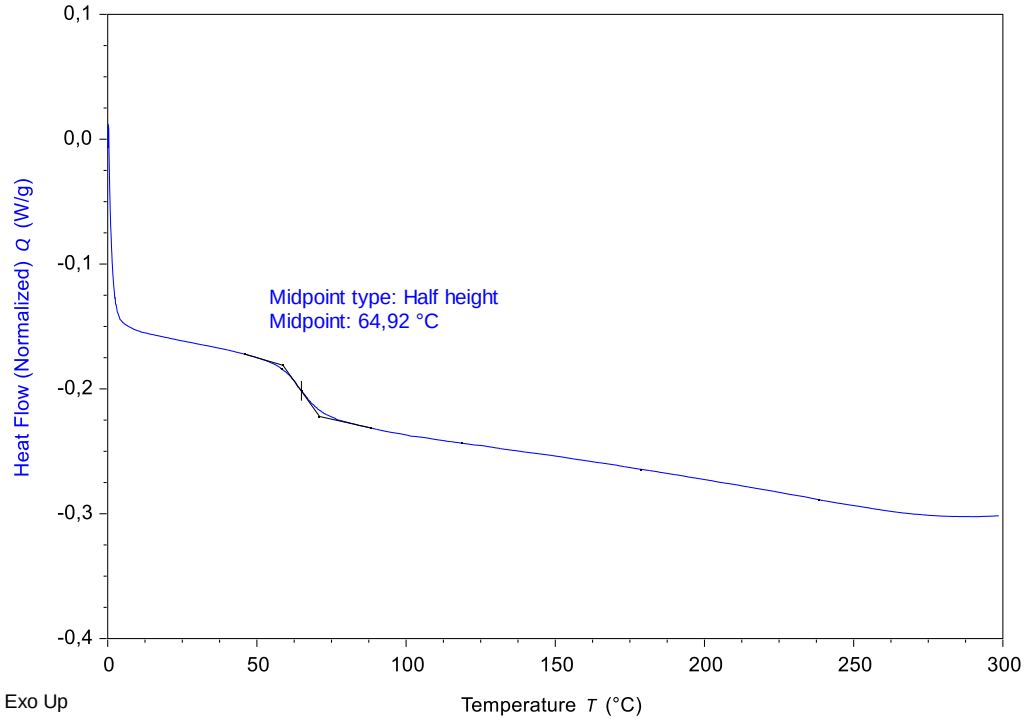

*Fig. S52: DSC curve of a PO/PA/NA terpolymer with an anhydride ratio of PA/NA of 250 equiv / 250 equiv with respect to **1**/PPNCl (1 equiv) (Fig. 44, A).*

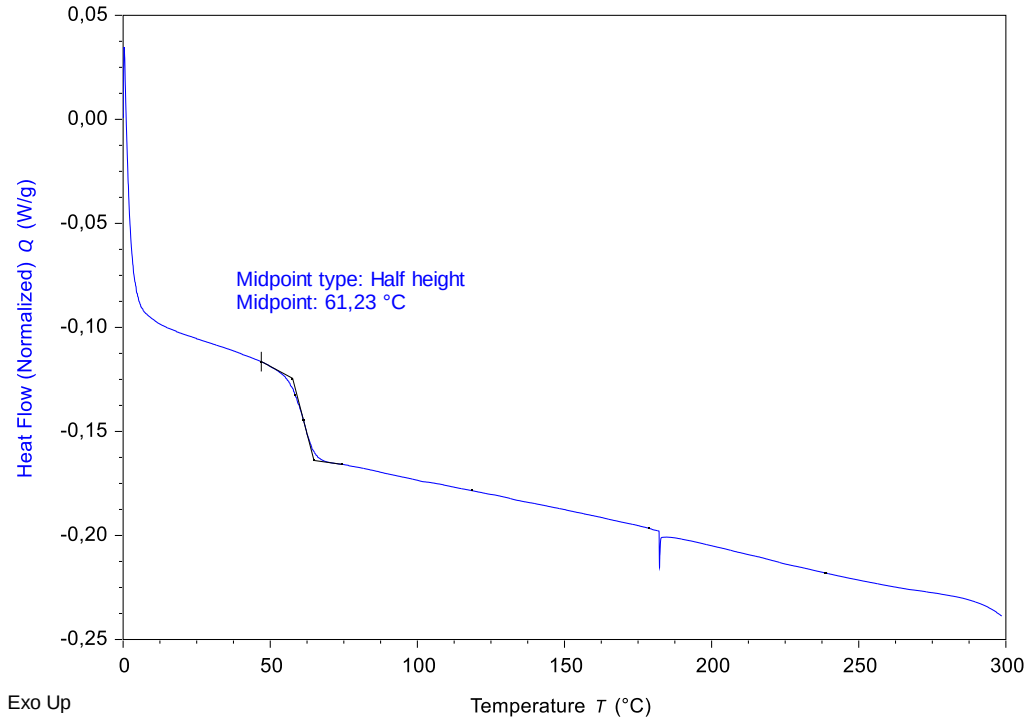

*Fig. S53: DSC curve of a PO/PA/NA terpolymer with an anhydride ratio of PA/NA of 500 equiv / 250 equiv equivalents with respect to **1**/PPNCl (1 equiv) (Fig. 44, B).*

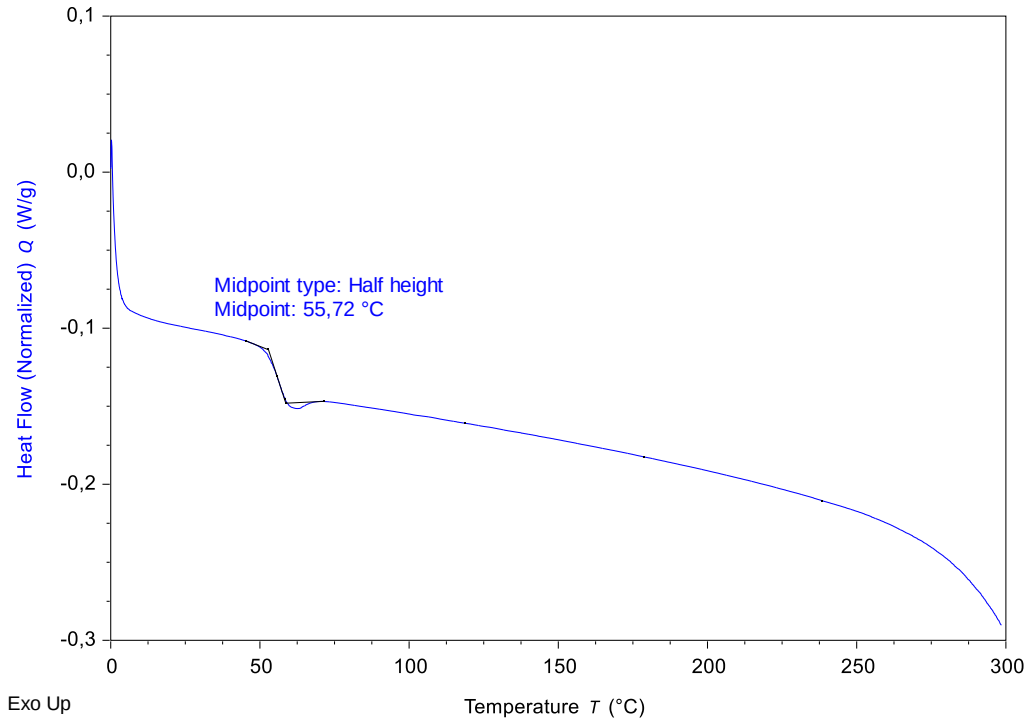

*Fig. S54: DSC curve of a PO/PA based polyestercarbonate with **1**/PPNCl (1 equiv) as catalyst system (Fig. 47).*

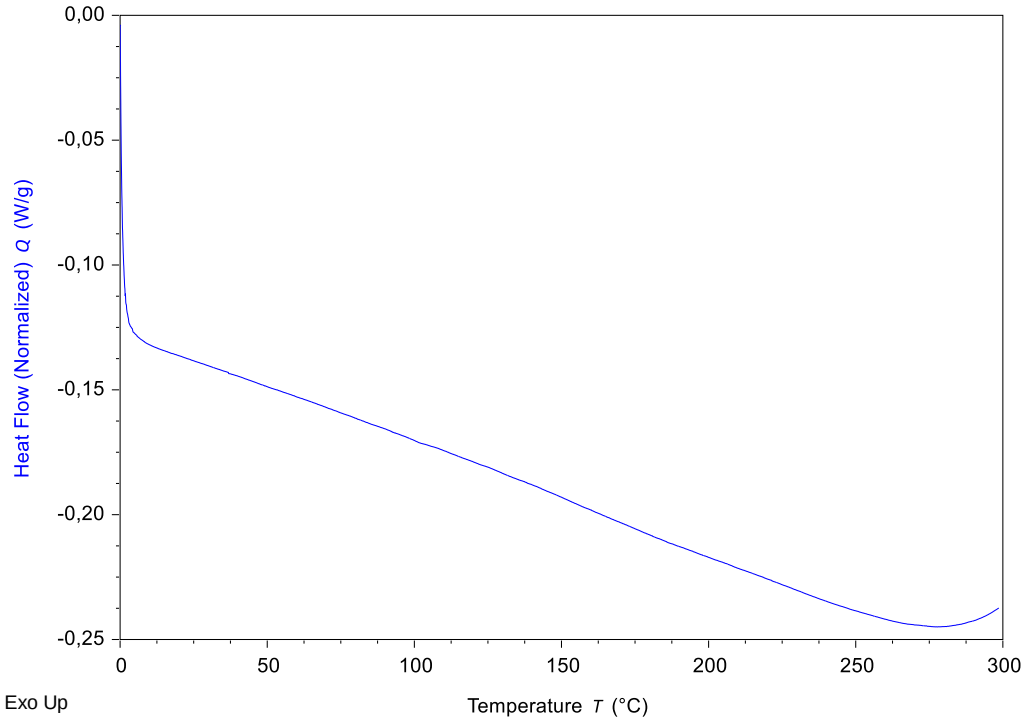

*Fig. S55: DSC curve of a PO/NA based polyestercarbonate with **1**/PPNCl (1 equiv) as catalyst system (Fig. 50).*

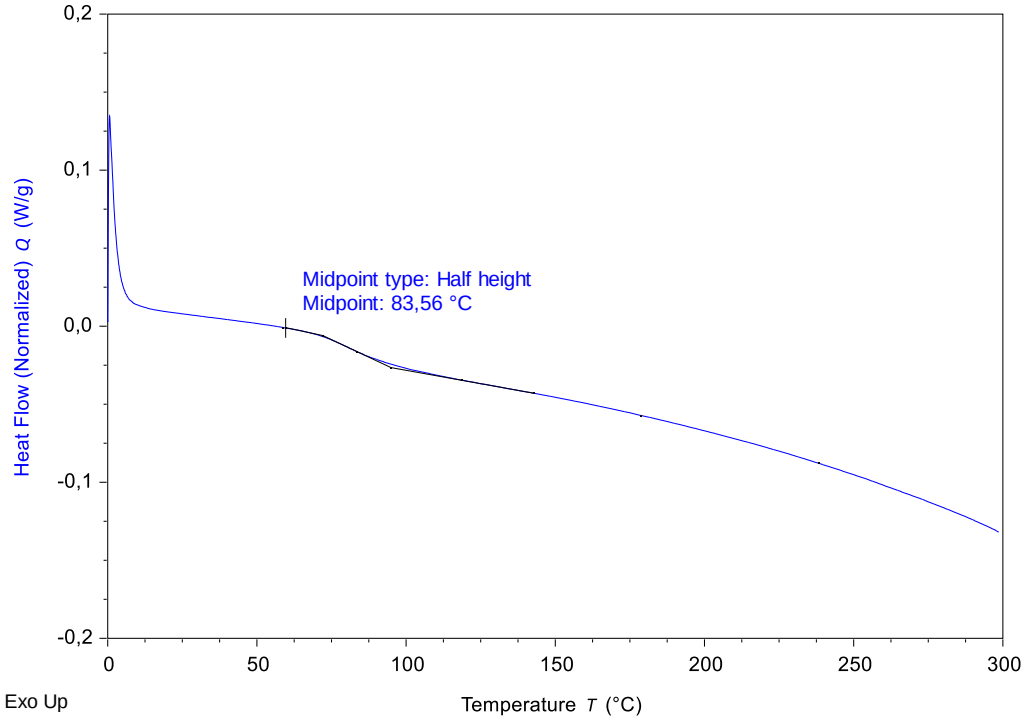

*Fig. S56: DSC curve of a PO/NA/PA (NA: 250 equiv, PA: 250 equiv) based polyestercarbonate with **1**/PPNCl (1 equiv) as catalyst system (Fig. 52).*

11 Additional Metal Complex Spectra

11.1 Complex 6

COSY:

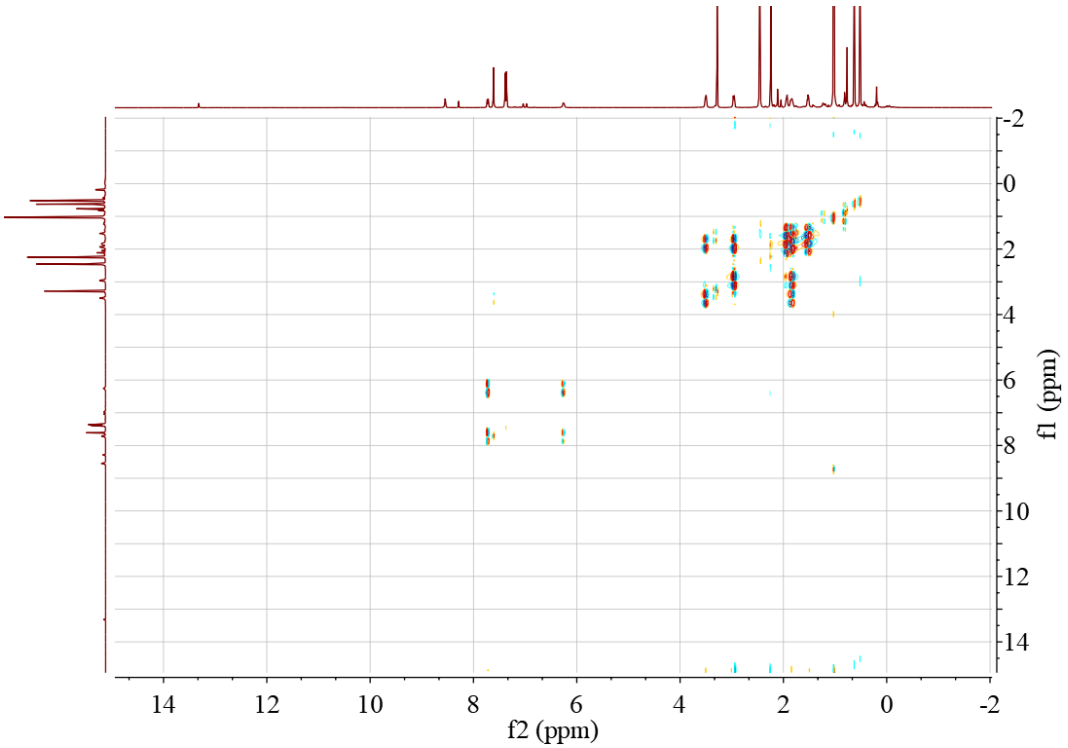

HSQC:

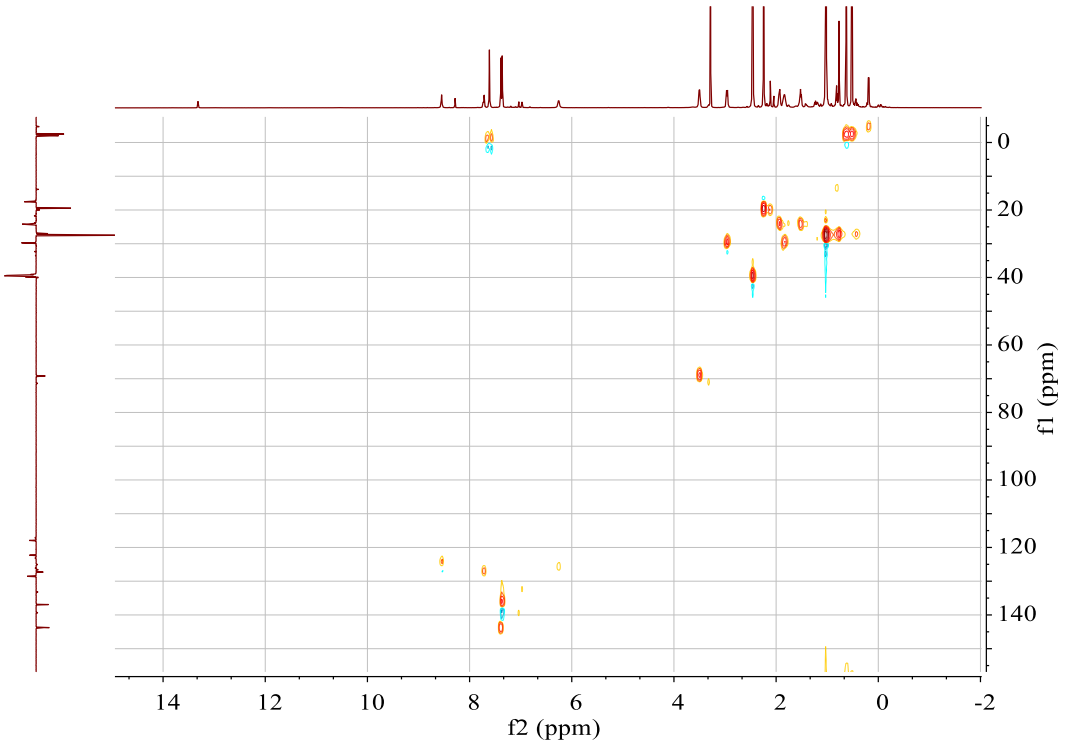

HMBC:

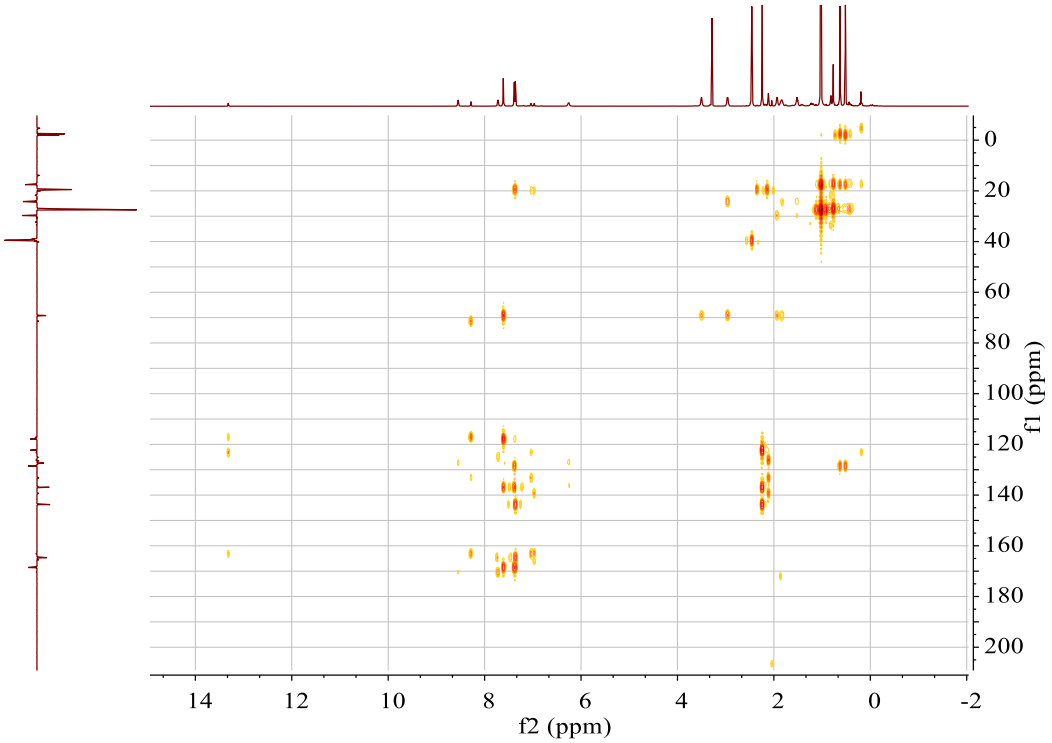

11.2 Complex 7

COSY:

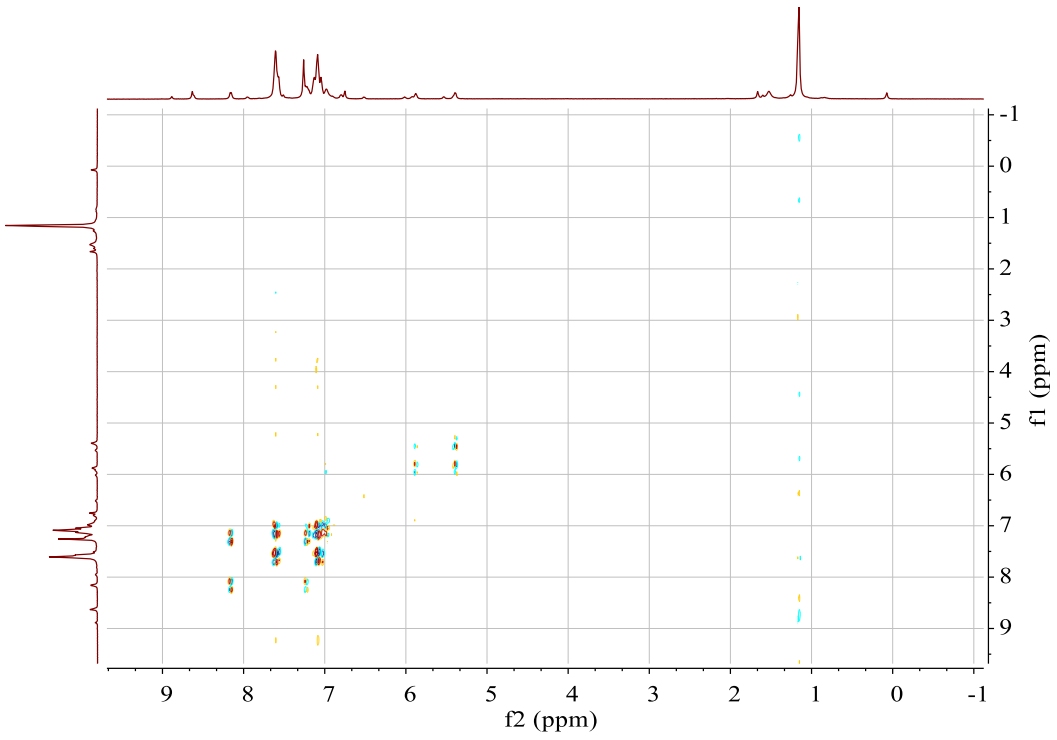

HSQC:

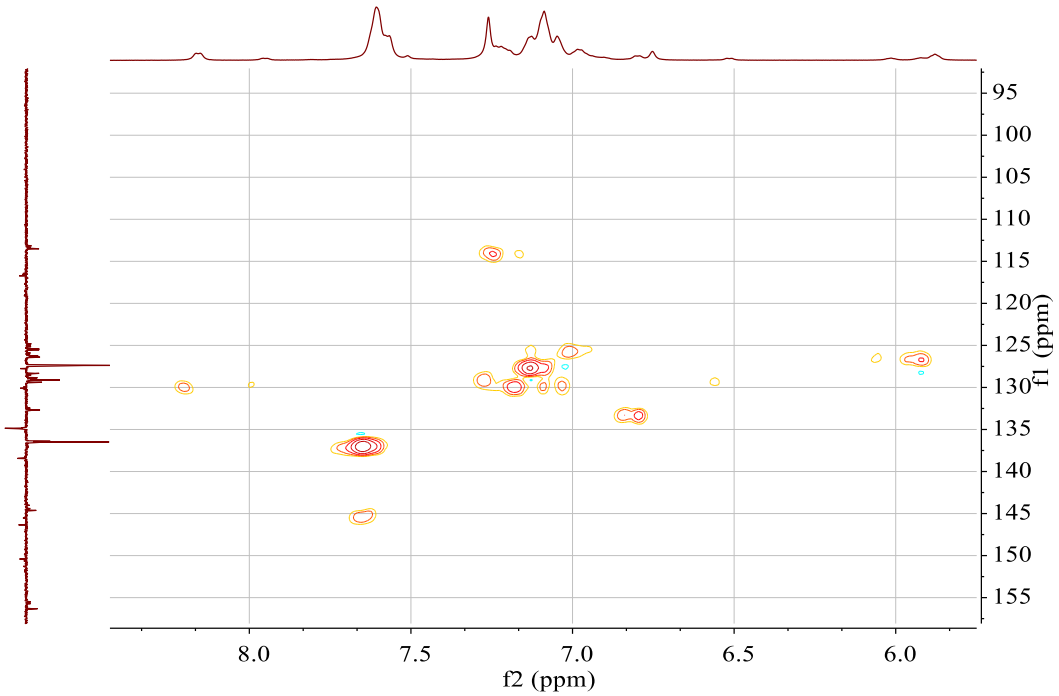
95
100
105
110
115
120
125
130
135
140
145
150
155
f1 (ppm)
8.0
7.5
7.0
6.5
6.0
f2 (ppm)

HMBC:

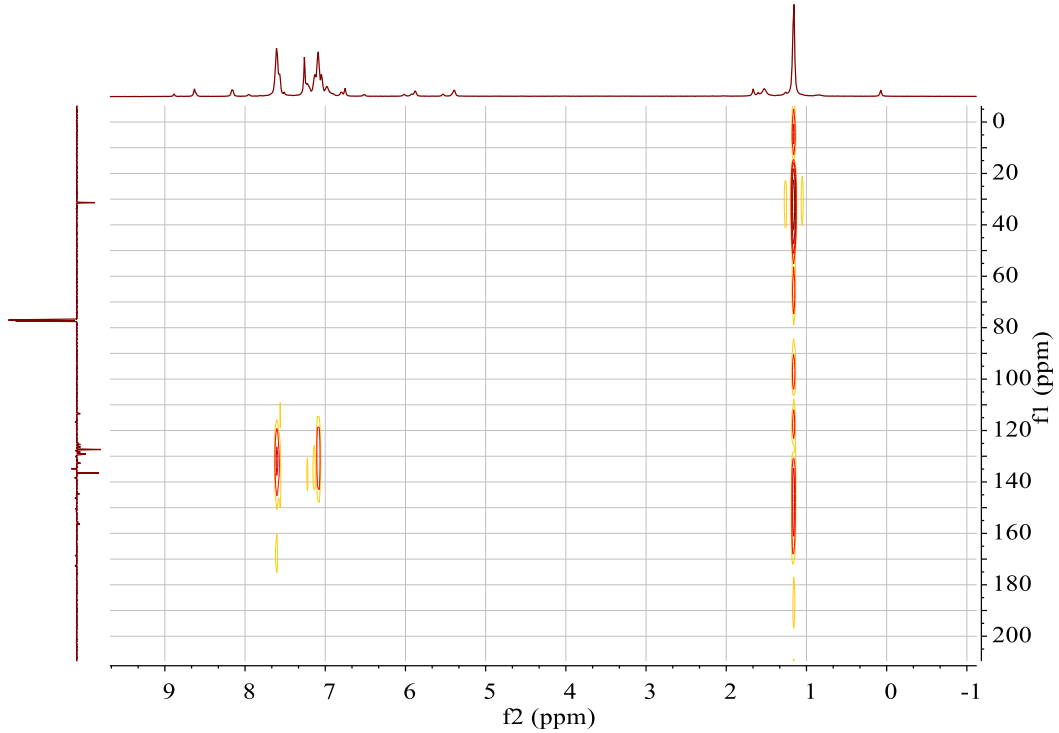
0
20
40
60
80
100
120
140
160
180
200
f1 (ppm)
9
8
7
6
5
4
3
2
1
0
-1
f2 (ppm)

11.3 Complex 8

COSY:

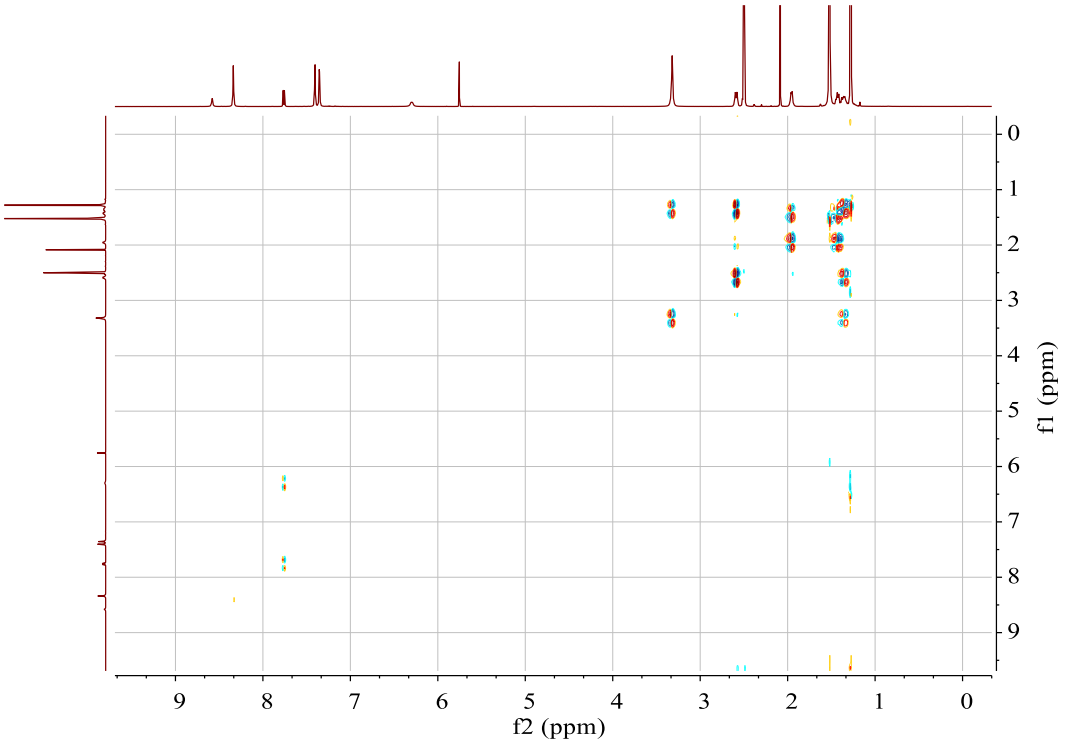

HSQC:

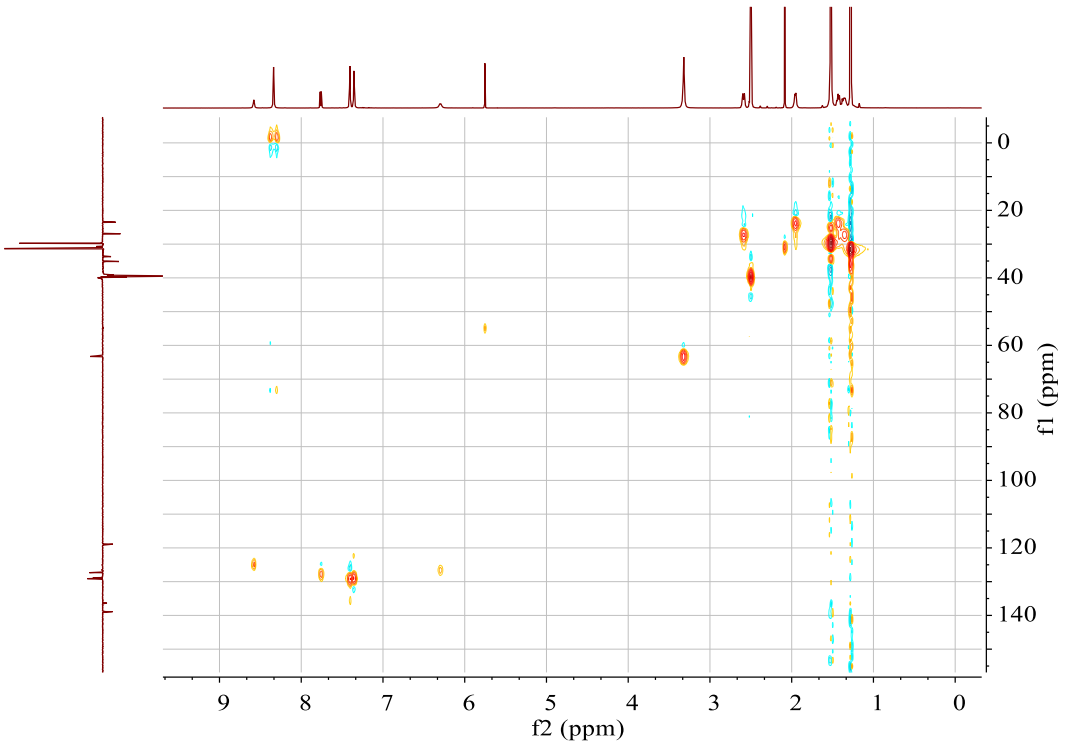

HMBC:

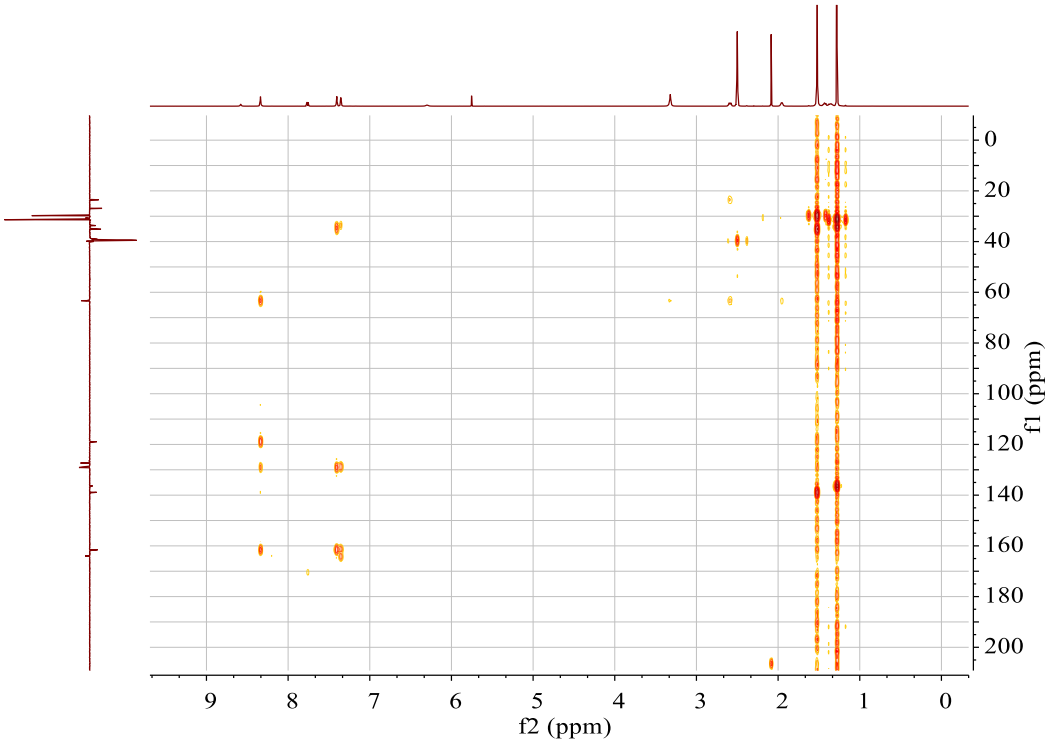
0
20
40
60
80
100
120
140
160
180
200
f1 (ppm)
9
8
7
6
5
4
3
2
1
0
f2 (ppm)

NOESY:

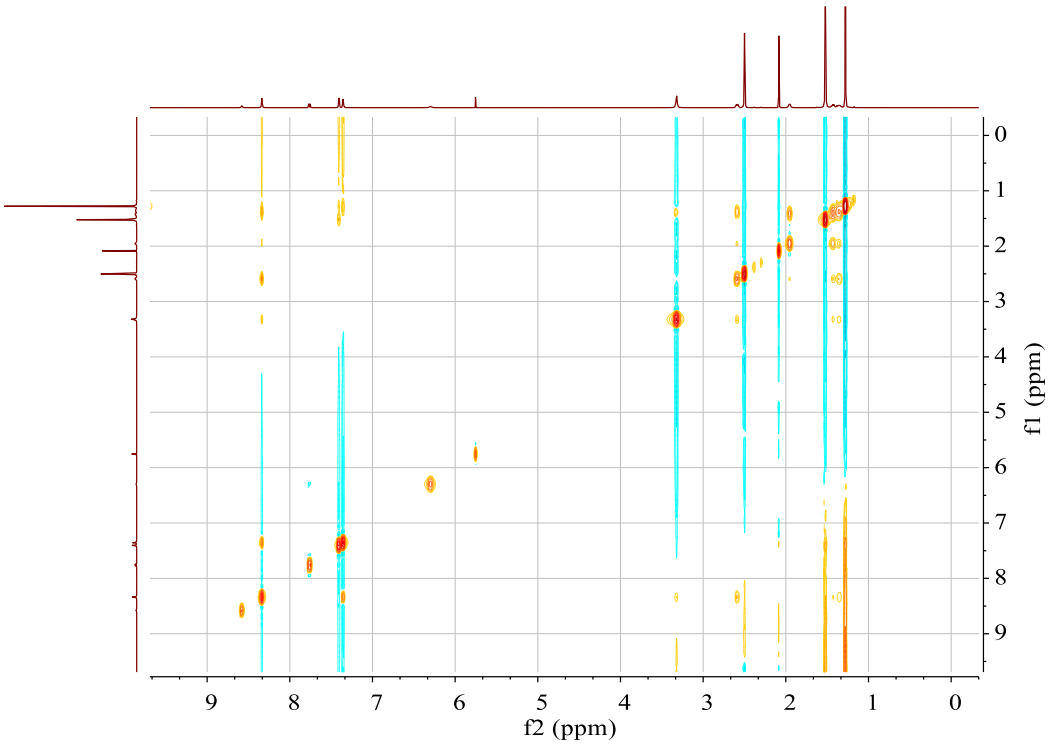
0
1
2
3
4
5
6
7
8
9
f1 (ppm)
9
8
7
6
5
4
3
2
1
0
f2 (ppm)

11.4 Complex 9

COSY:

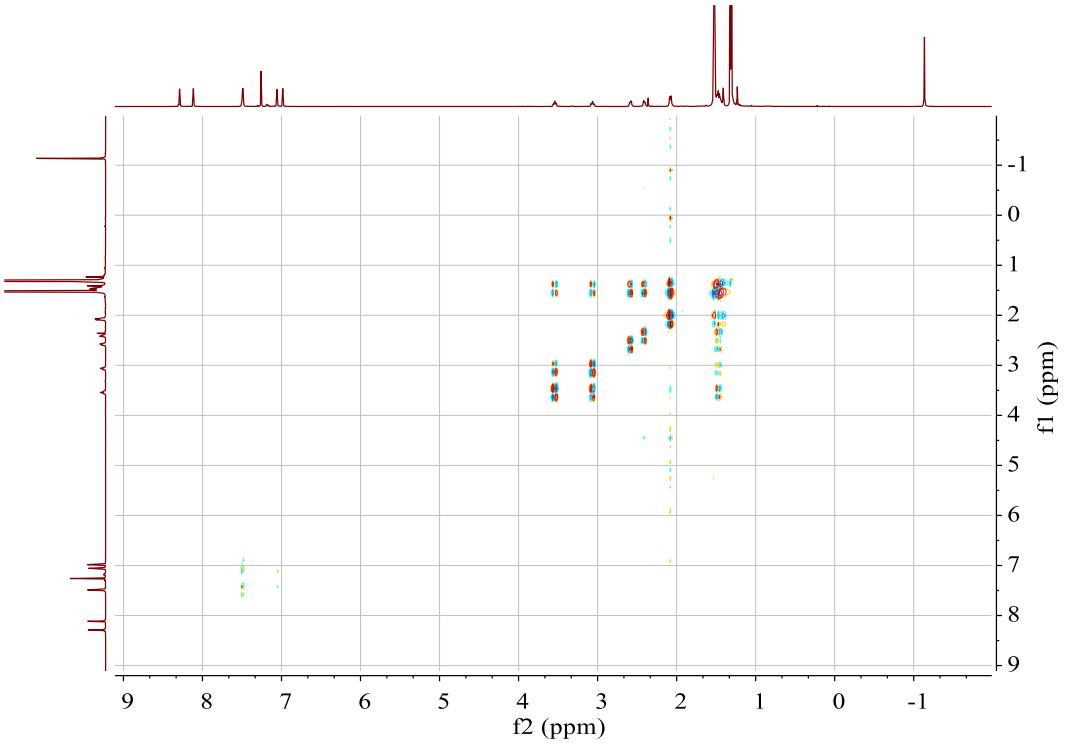

HSQC:

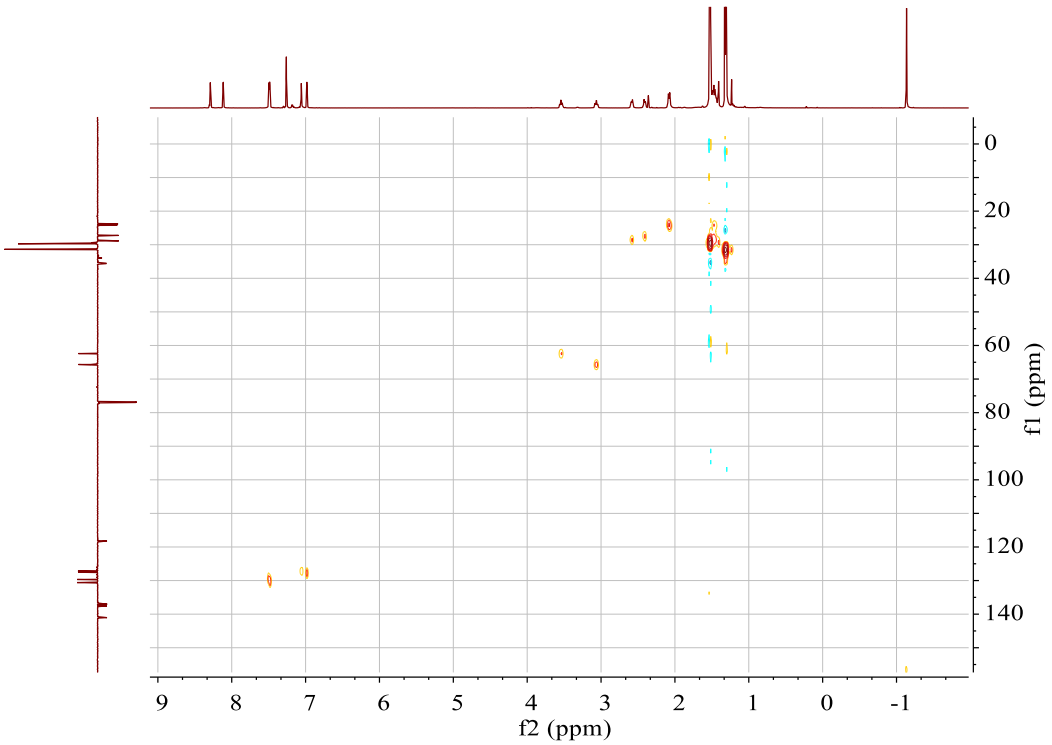

HMBC:

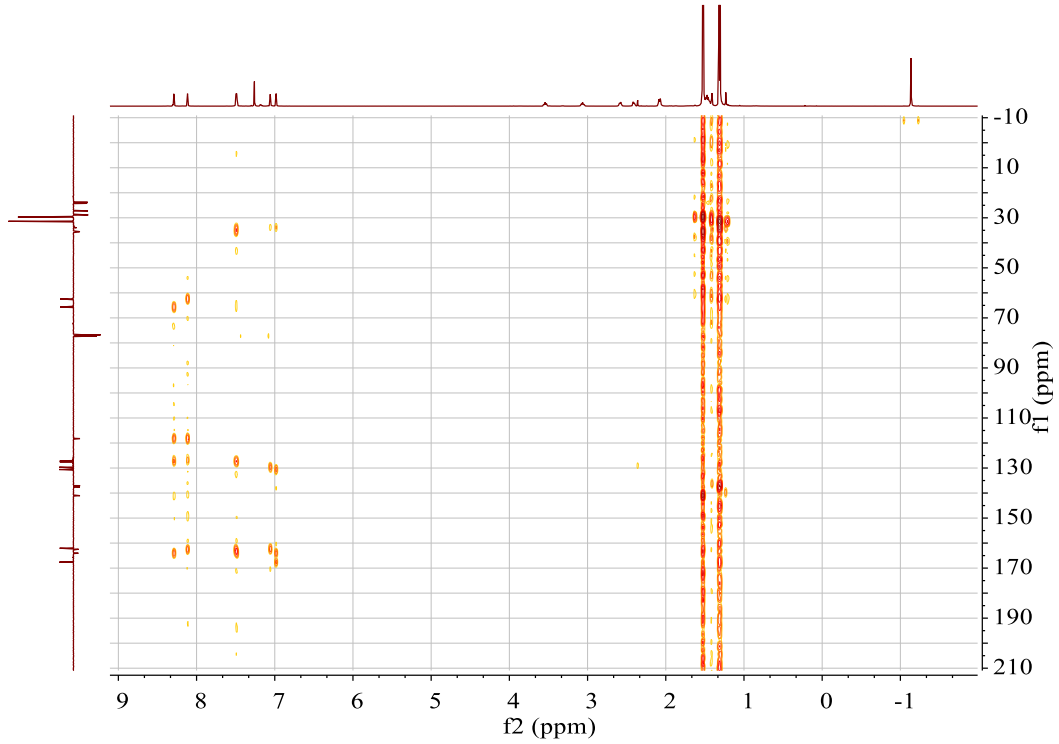

11.5 Complex 10

COSY:

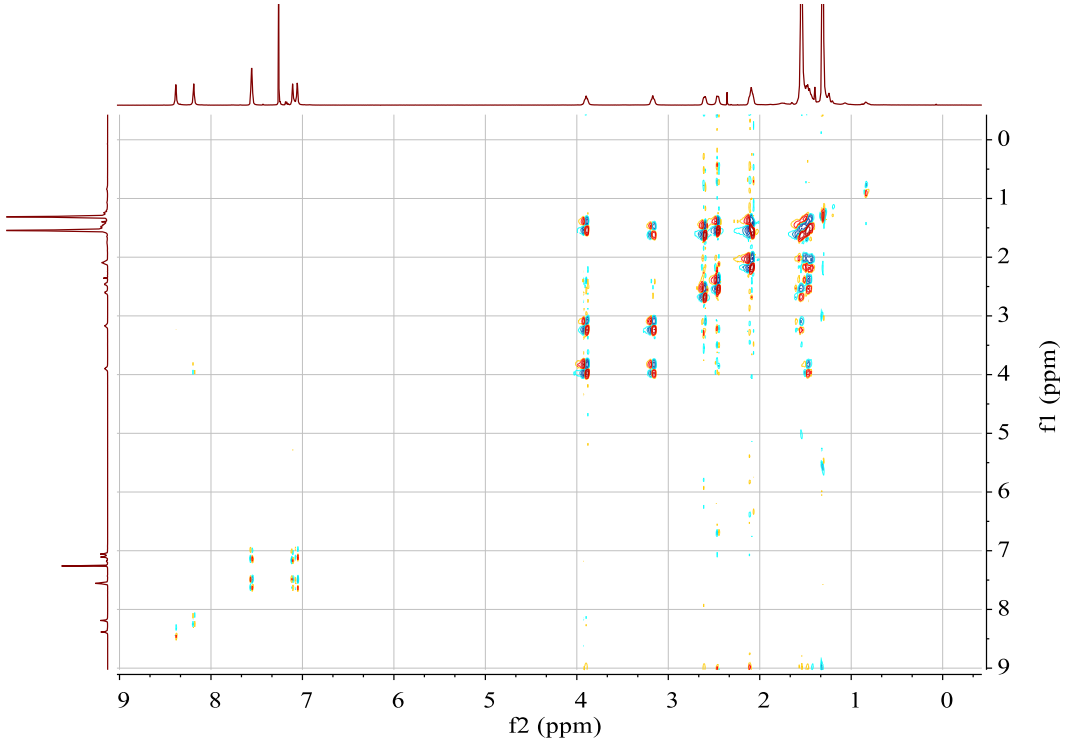

HSQC:

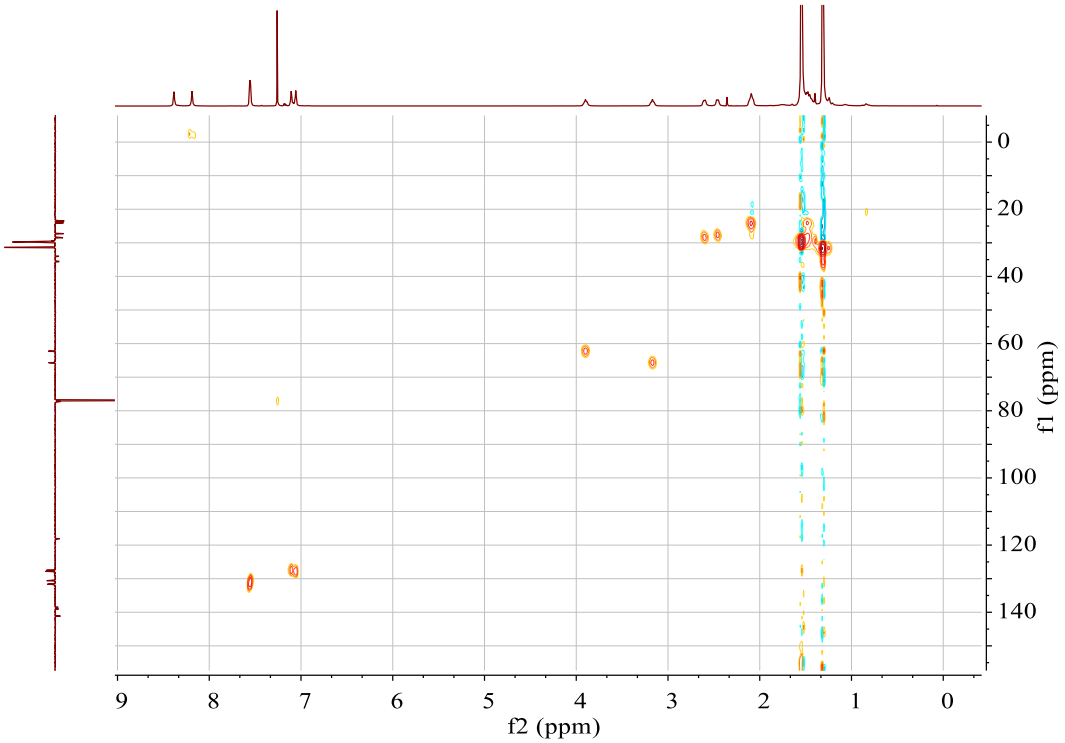
0
20
40
60
80
100
120
140
f1 (ppm)
9
8
7
6
5
4
3
2
1
0
f2 (ppm)

HMBC:

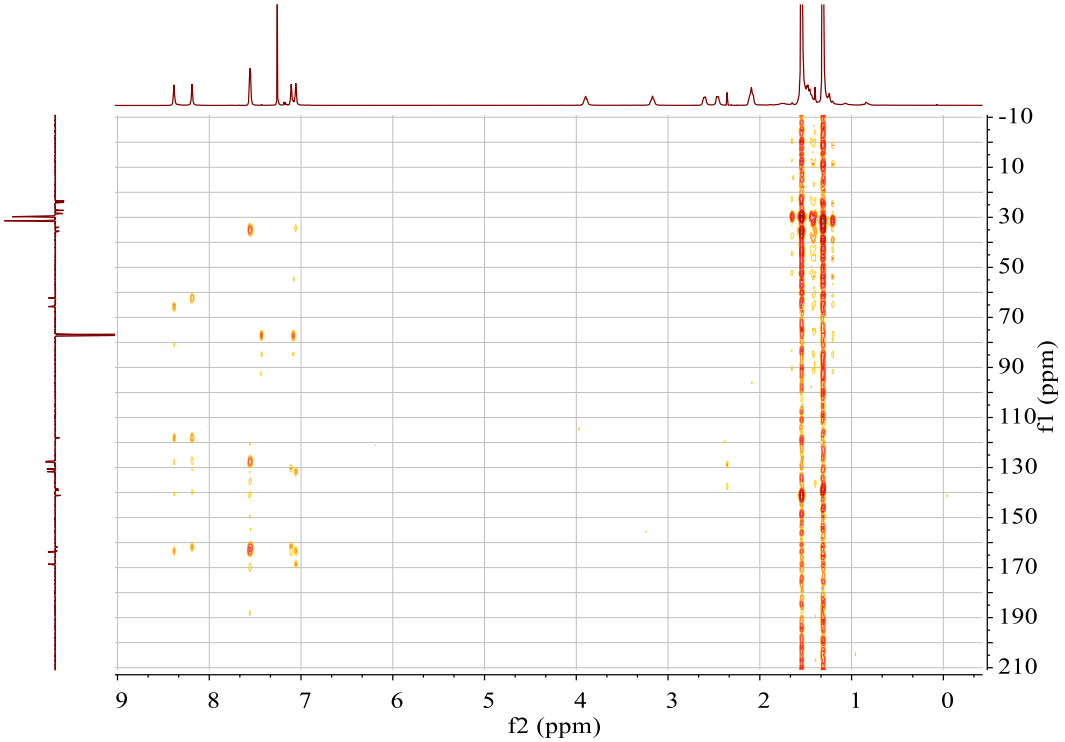
-10
10
30
50
70
90
110
130
150
170
190
210
f1 (ppm)
9
8
7
6
5
4
3
2
1
0
f2 (ppm)

11.6 Complex 12

COSY:

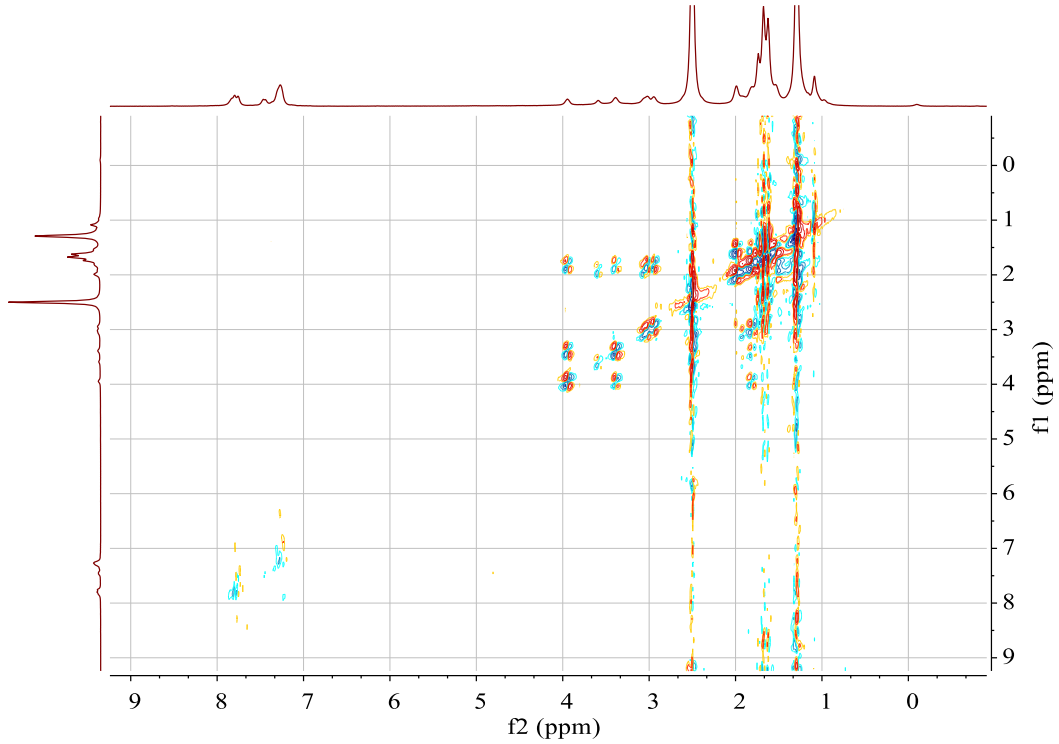

HSQC:

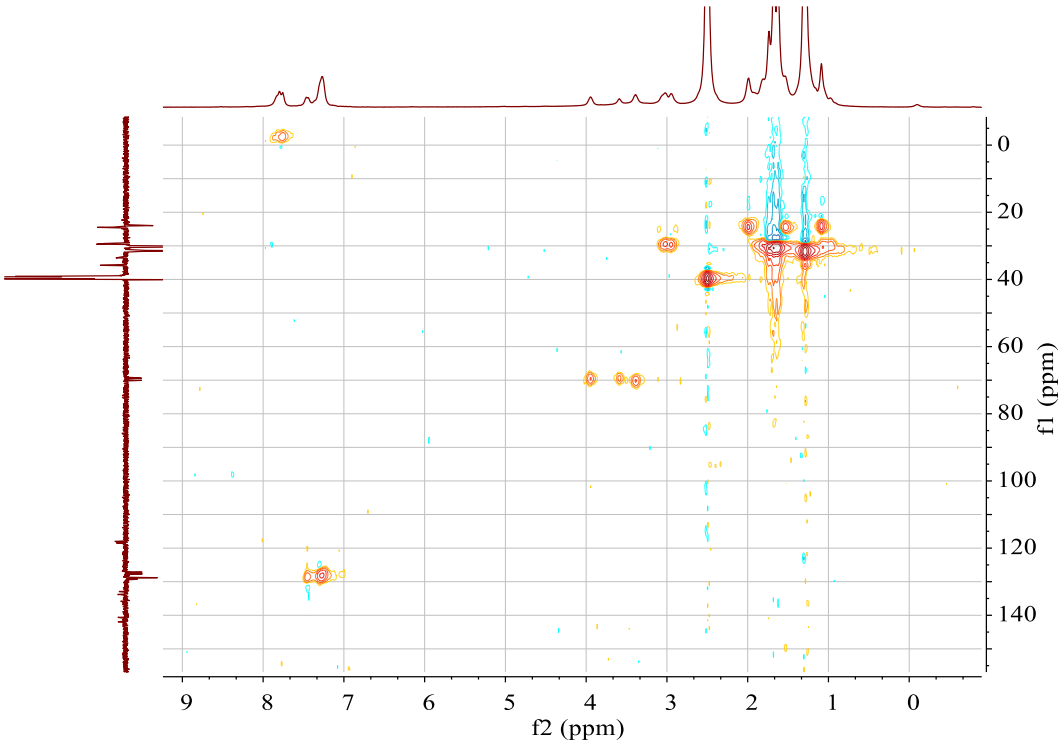

HMBC:

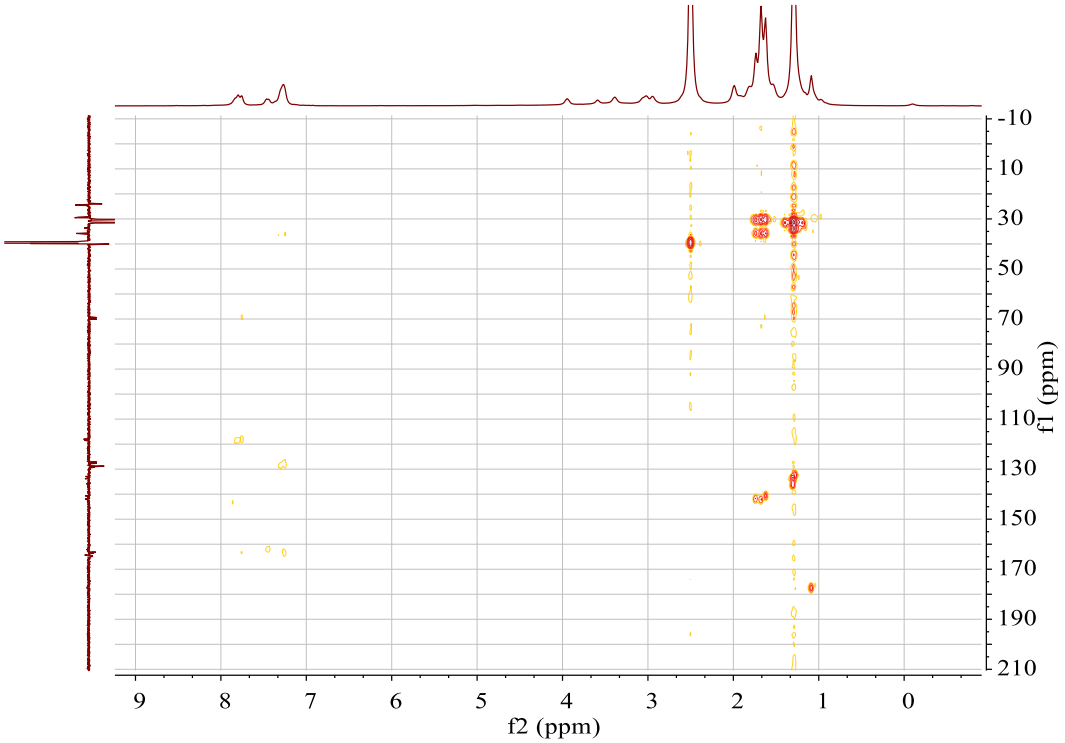

11.7 Complex 13

HR-MS:

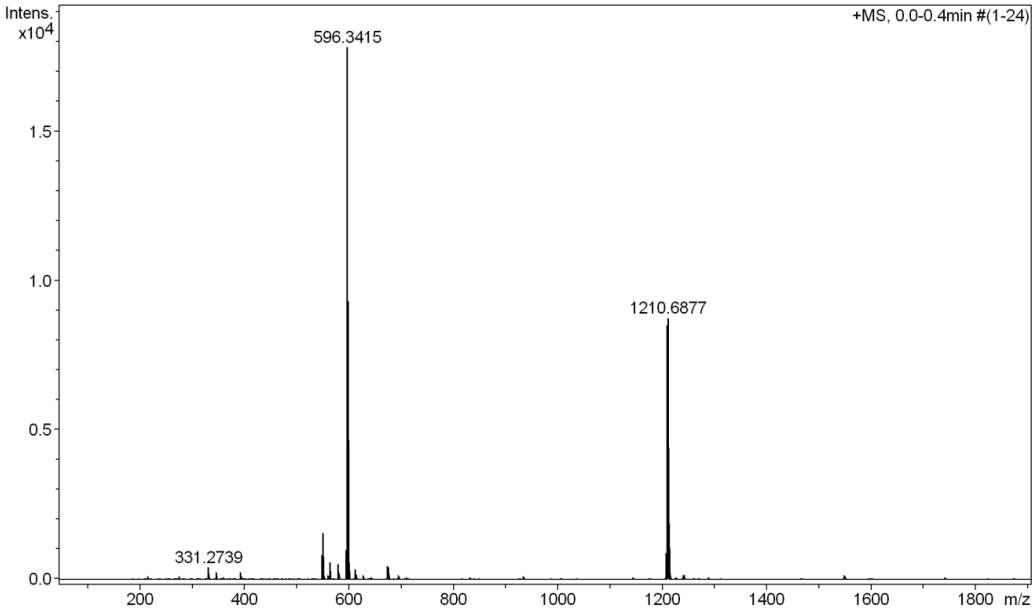

12 Obtained Crystal Structures

12.1 Bis(triphenylphosphino)ammonium-2,4-dinitrophenolate

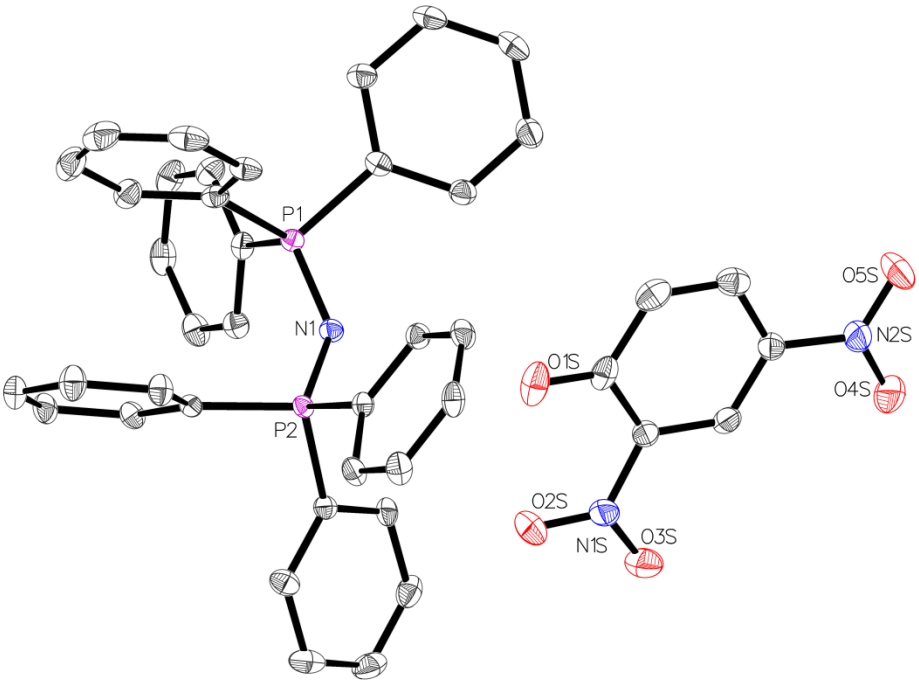

Fig. S57: Crystal structure, drawn with 50% displacement ellipsoid. Hydrogen atoms omitted for clarity. The bond precision for C-C single bonds is 0.0023Å.

Radiation [Å]	Mo Kα (λ = 0.71073)	Z	2	Measurement method	\f and \w scans
Crystal habit	clear yellow block	a [Å]	10.7730(4)		
Crystal size [mm^3]	0.18 × 0.15 × 0.15	b [Å]	12.7932(5)	Abs. correction type	multiscan
Empirical formula	C42H33N3O5P2	c [Å]	14.6241(8)	Abs. correction Tmin	0.6931
Formula weight [g/mol]	721.65	α [°]	64.476(2)	Abs. correction Tmax	0.7460
Temperature [K]	100.0	β [°]	89.206(2)	Density (calculated) [g/cm^3]	1.351
Crystal system	triclinic	γ [°]	78.221(2)	Absorption coefficient [mm^{-1}]	0.174
Space group	P-1	Volume [$Å^3$]	1774.23(14)	F (000) [e^-]	752.0

Table S2: Sample and crystal data.

2Θ range for data collection [°]	3.098 to 60.08	Index ranges		Goodness-of-fit on F^2	0.994
Reflections collected	38661	h	-15 ≤ h ≤ 15	Diff. peak and hole [$e^-Å^{-3}$]	0.45/-0.37
Data / restraints / parameters	10250/0/469	k	-17 ≤ k ≤ 17		
Refinement method	direct methods	l	-20 ≤ l ≤ 20	Function minimized	$\Sigma w (F_o^2 - F_c^2)^2$
		all data	R1 = 0.0614, wR2 = 0.1097	Weighting scheme	where
		I>2σ(I)	R1 = 0.0423, wR2 = 0.0999	$w=1/[\sigma^2(Fo^2) + (0.958P)^2]$	$P=(F_o^2+2F_c^2)/3$

Table S3: Data collection and structure refinement.

12.2 2,2'-[1,2-phenylenebis(nitrilomethylidyne)]bis[6-(1,1-dimethylethyl)]-4-fluorophenol (L3)

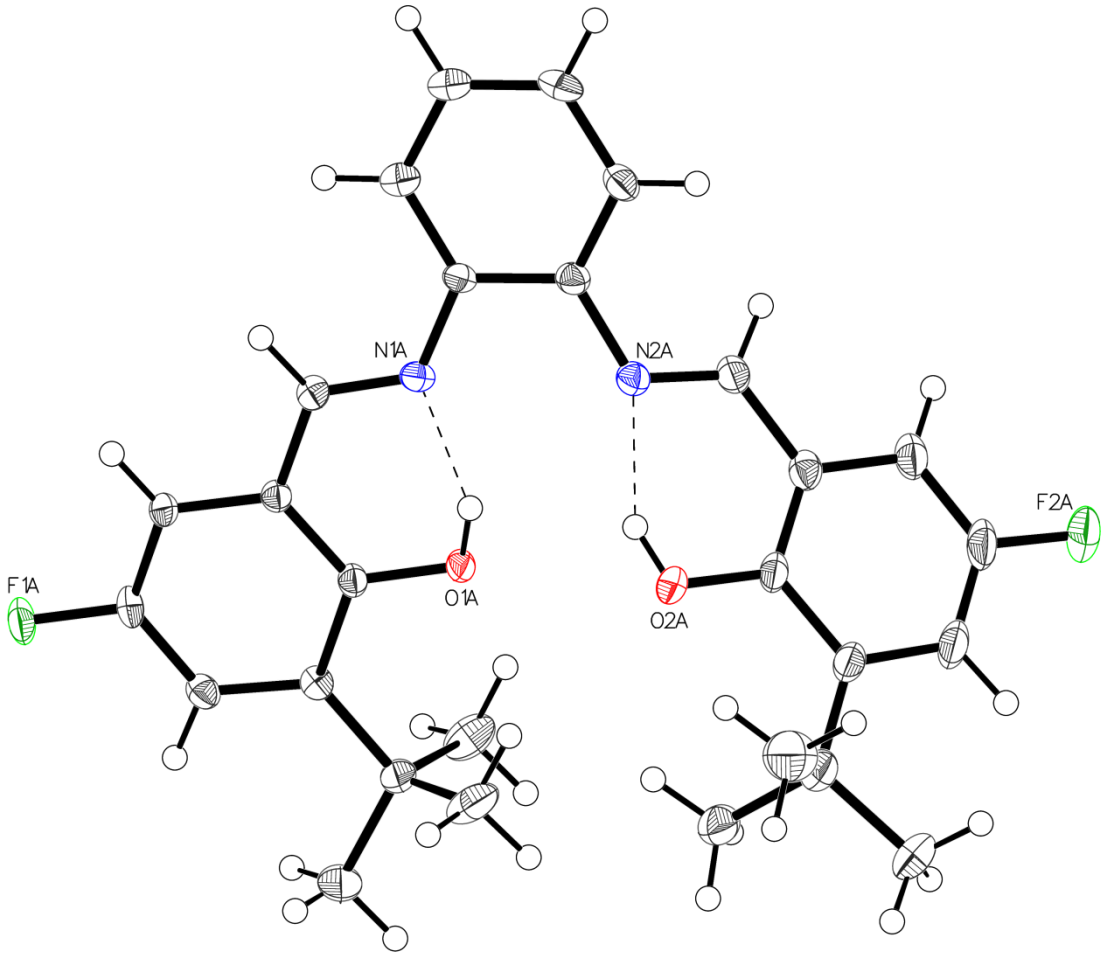

Fig. S58: Crystal structure, drawn with 50% displacement ellipsoid. Because of high disorder only part I is shown, part II omitted for clarity. Main Residue Disorder 79%. The bond precision for C-C single bonds is 0.0027Å.

Radiation [Å]	MoKα (λ = 0.71073)	Z	4	Measurement method	\f and \w scans
Crystal habit	clear orange block	a [Å]	6.7051(2)		
Crystal size [mm^3]	0.6 × 0.4 × 0.4	b [Å]	12.5696(4)	Abs. correction type	multiscan
Empirical formula	C28H30F2N2O2	c [Å]	28.6002(10)	Abs. correction Tmin	0.5982
Formula weight [g/mol]	464.54	α [°]	90	Abs. correction Tmax	0.7460
Temperature [K]	100.0	β [°]	89.9980(13)	Density (calculated) [g/cm^3]	1.280
Crystal system	monoclinic	γ [°]	90	Absorption coefficient [mm^{-1}]	0.091
Space group	P21/n	Volume [$Å^3$]	2410.44(13)	F (000) [e^-]	984.0

Table S4: Sample and crystal data.

2Θ range for data collection [°]	4.314 to 60.126	Index ranges		Goodness-of-fit on F^2	1.169
Reflections collected	44950	h	-9 ≤ h ≤ 9	Diff. peak and hole [$e^-Å^{-3}$]	0.45/-0.55
Data / restraints / parameters	7068/0/551	k	-17 ≤ k ≤ 17		
Refinement method	direct methods	l	-40 ≤ l ≤ 40	Function minimized	$\Sigma w (F_o^2 - F_c^2)^2$
		all data	R1 = 0.0937, wR2 = 0.1739	Weighting scheme	where
		I>2σ(I)	R1 = 0.0745, wR2 = 0.1631	$w=1/[\sigma^2(Fo^2) + (0.958P)^2]$	$P=(F_o^2+2F_c^2)/3$

Table S5: Data collection and structure refinement.

12.3 2,4-dinitrophenolato[[2,2'-[(1,2-phenylene)bis[(nitrilo-κ*N*)methylidyne]]bis[6-(1,1-dimethylethyl)-4-fluorophenolato-κ*O*]](2-)]-cobalt (3)

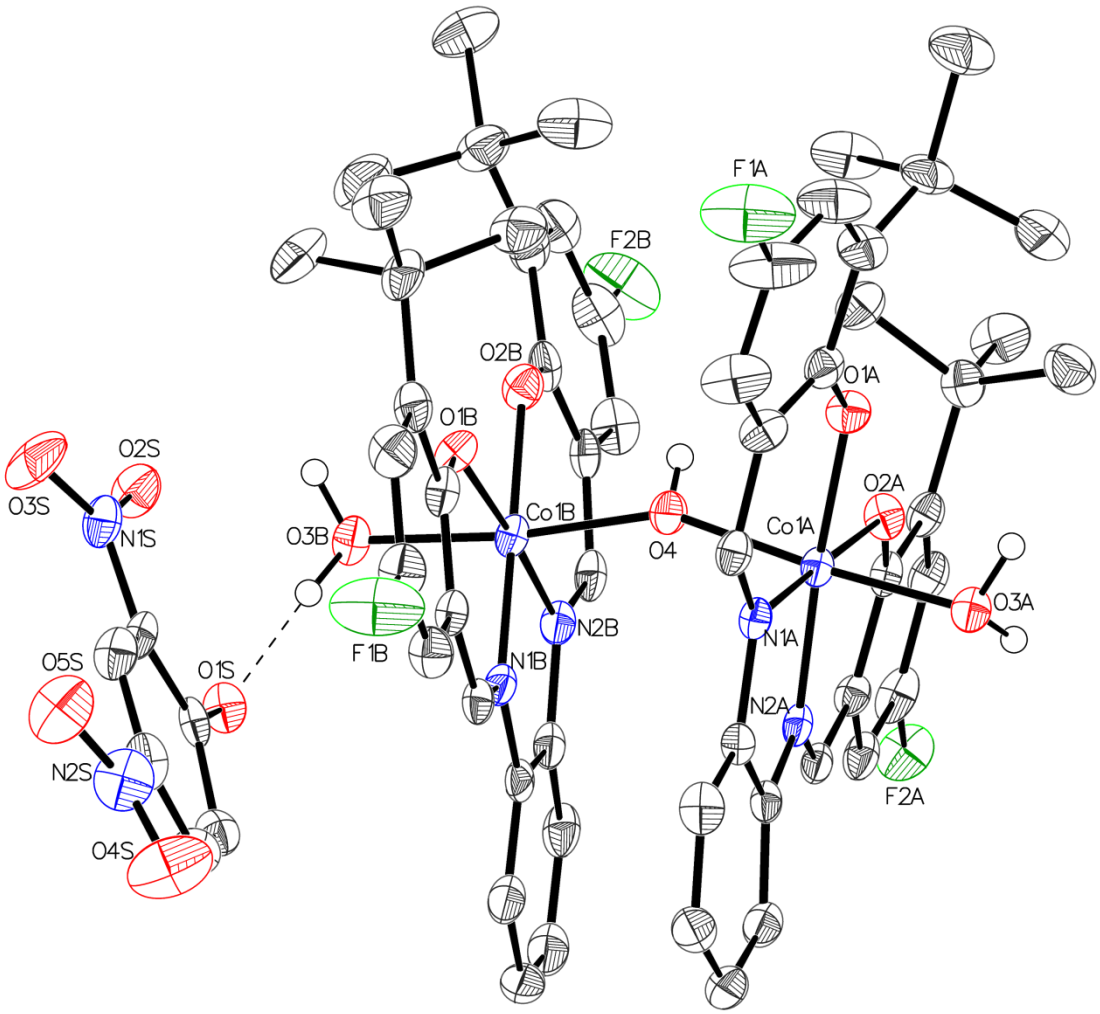

Fig. S59: Crystal structure, drawn with 50% displacement ellipsoid. Hydrogen atoms omitted for clarity. The bond precision for C-C single bonds is 0.0065Å. %. The terminating O3A and O3B are modelled as water. O4 is interpreted as OH^-. Squeeze was used because high degree of disorder on solvent molecules. According voids contain 1532.3Å^3 with 266.8 e^-.

Radiation [Å]	MoKα (λ = 0.71073)	Z	2	Measurement method	\f and \w scans
Crystal habit	clear red block	a [Å]	16.5852 (8)		
Crystal size [mm^3]	0.06 × 0.05 × 0.04	b [Å]	16.6965 (7)	Abs. correction type	multiscan
Empirical formula	C124H124Co4F8N12O24	c [Å]	24.8173 (11)	Abs. correction Tmin	0.6068
Formula weight [g/mol]	2554.06	α [°]	90	Abs. correction Tmax	0.7460
Temperature [K]	100.0	β [°]	101.252 (2)	Density (calculated) [g/cm^3]	1.258
Crystal system	monoclinic	γ [°]	90	Absorption coefficient [mm^{-1}]	0.563
Space group	P21/n	Volume [Å^3]	6740.2(5)	F (000) [e$^-$]	2648.0

Table S6: Sample and crystal data.

2Θ range for data collection [°]	4.49 to 50.696	Index ranges		Goodness-of-fit on F^2	1.011
Reflections collected	97827	h	-19 ≤ h ≤ 19	Diff. peak and hole [e$^-$Å^{-3}]	0.72/-0.94
Data / restraints / parameters	12316/0/781	k	-20 ≤ k ≤ 20		
Refinement method	Charge Flipping	l	-29 ≤ l ≤ 29	Function minimized	Σ w (F_o^2 - F_c^2)^2
		all data	R1 = 0.0990, wR2 = 0.1526	Weighting scheme	where
		I>2σ(I)	R1 = 0.0604, wR2 = 0.1357	w=1/[σ^2(Fo^2) + (0.958P)^2]	P=(F_o^2+2F_c^2)/3

Table S7: Data collection and structure refinement.

12.4 2,2'-[(1R,2R)-(1,2-cyclohexanediyl)bis[(*E*)nitrilomethylidyne]]bis[4,6-bis(1,1-dimethylethyl)]-phenol (L1)

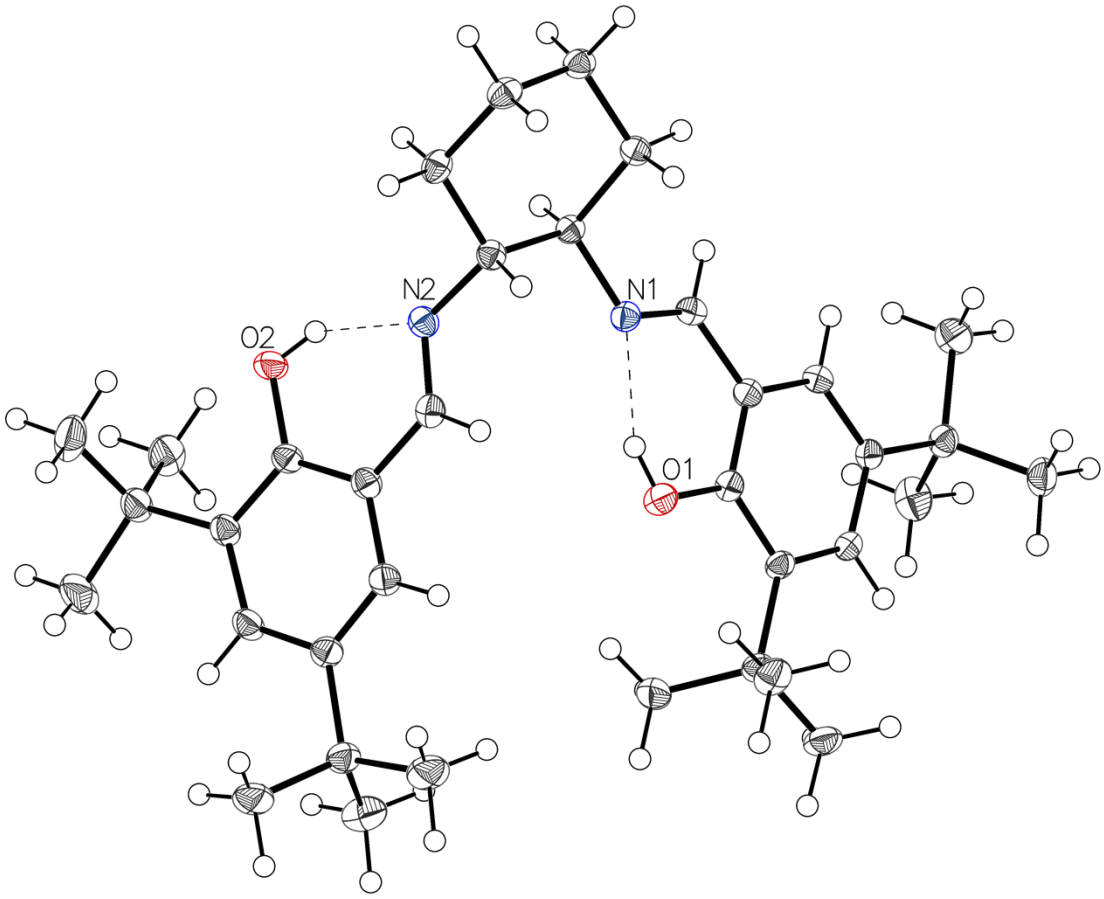

Fig. S60: Crystal structure, drawn with 50% displacement ellipsoid. The bond precision for C-C single bonds is 0.0027Å.

Radiation [Å]	MoKα (λ = 0.71073)	Z	4	Measurement method	\f and \w scans
Crystal habit	clear colourless block	a [Å]	27.275(2)		
Crystal size [mm^3]	0.09 × 0.06 × 0.03	b [Å]	6.7022(5)	Abs. correction type	multiscan
Empirical formula	C36H54N2O2	c [Å]	18.1183(17)	Abs. correction Tmin	0.7063
Formula weight [g/mol]	546.81	α [°]	90	Abs. correction Tmax	0.7460
Temperature [K]	120.0	β [°]	90	Density (calculated) [g/cm^3]	1.097
Crystal system	orthorhombic	γ [°]	90	Absorption coefficient [mm^{-1}]	0.067
Space group	P212121	Volume [$Å^3$]	3312.0(5)	F (000) [e^-]	1200.0

Table S8: Sample and crystal data.

2Θ range for data collection [°]	4.738 to 60.22	Index ranges		Goodness-of-fit on F^2	1.058
Reflections collected	188774	h	-38 ≤ h ≤ 38	Diff. peak and hole [$e^-Å^{-3}$]	0.20/-0.20
Data / restraints / parameters	9750/0/375	k	-9 ≤ k ≤ 9		
Refinement method	Intrinsic Phasing	l	-25 ≤ l ≤ 25	Function minimized	$\Sigma w (F_o^2 - F_c^2)^2$
		all data	R1 = 0.0520, wR2 = 0.1023	Weighting scheme	where
		I>2σ(I)	R1 = 0.0427, wR2 = 0.0970	$w=1/[\sigma^2(Fo^2) + (0.958P)^2]$	$P=(F_o^2+2F_c^2)/3$

Table S9: Data collection and structure refinement.

13 References

1. Geyer, R.; Jambeck, J. R.; Law, K. L., *Sci. Adv.* **2017,** *3*, e1700782.
2. Shen, M.; Song, B.; Zeng, G.; Zhang, Y.; Huang, W.; Wen, X.; Tang, W., *Environ. Pollut.* **2020,** *263*, 114469.
3. Lechner, M. D., Nordmeier E. H., Gehrke K., *Makromolekulare Chemie, Ein Lehrbuch für Chemiker, Physiker, Materialwissenschaftler und Verfahrenstechniker*. Springer Spektrum: Berlin, Heidelberg, **2014**.
4. Cowie, J. M. G., & Arrighi, V. , *Polymers: Chemistry and Physics of Modern Materials, Third Edition (3rd ed.)*. 3 ed.; CRC Press: **2007**.
5. Polyester Properties, Production, Price, Market and Uses. https://www.plasticsinsight.com/resin-intelligence/resin-prices/polyester/#polyesterproduction (accessed 03/13/2020).
6. Barot, A.; Panchal, T.; Patel, A.; Patel, C., *Arch. Appl. Sci. Res.* **2019,** *11*, 19.
7. Gubbels, E.; Heitz, T.; Yamamoto, M.; Chilekar, V.; Zarbakhsh, S.; Gepraegs, M.; Köpnick, H.; Schmidt, M.; Brügging, W.; Rüter, J.; Kaminsky, W., *Ullmann's Encyclopedia of Industrial Chemistry* **2018,** 1–30.
8. Lechner, M. D.; Nordmeier, E. H.; Gehrke, K., *Makromolekulare Chemie: Ein Lehrbuch für Chemiker, Physiker, Materialwissenschaftler und Verfahrenstechniker*. 4. überarbeitete und erweiterte Auflage ed.; Basel, **2010**.
9. Künkel, A.; Becker, J.; Börger, L.; Hamprecht, J.; Koltzenburg, S.; Loos, R.; Schick, M. B.; Schlegel, K.; Sinkel, C.; Skupin, G.; Yamamoto, M., *Ullmann's Encyclopedia of Industrial Chemistry* **2016,** 1–29.
10. Ajellal, N.; Carpentier, J.-F.; Guillaume, C.; Guillaume, S. M.; Helou, M.; Poirier, V.; Sarazin, Y.; Trifonov, A., *Dalton Trans.* **2010,** *39*, 8363–8376.
11. Pretula, J.; Slomkowski, S.; Penczek, S., *Adv. Drug Delivery Rev.* **2016,** *107*, 3–16.
12. Huang, B. H.; Dutta, S.; Lin, C. C., 1.39 - Main-Group Catalysts for Lactide Polymerization. In *Comprehensive Inorganic Chemistry II (Second Edition)*, Reedijk, J.; Poeppelmeier, K., Eds. Elsevier: Amsterdam, 2013; pp 1217–1249.
13. Wheaton, C. A.; Hayes, P. G.; Ireland, B. J., *Dalton Trans.* **2009,** 4832–4846.
14. Dusselier, M.; Van Wouwe, P.; Dewaele, A.; Jacobs, P. A.; Sels, B. F., *Science* **2015,** *349*, 78.
15. Schnell, H. B., L.; Krimm, H. (Bayer) Thermoplastic aromatic polycarbonates and their manufacture. 532,543, Oct. 16, 1953.
16. Fukuoka, S.; Fukawa, I.; Adachi, T.; Fujita, H.; Sugiyama, N.; Sawa, T., *Org. Process Res. Dev.* **2019,** *23*, 145–169.
17. Su, W.-F., Ring-Opening Polymerization. In *Principles of Polymer Design and Synthesis*, Springer Berlin Heidelberg: Berlin, Heidelberg, 2013; pp 267–299.
18. Wypych, G., *Handbook of Polymers*. ChemTec Publishing: **2016**.
19. Tyl, R. W., *Seminars in Fetal and Neonatal Medicine* **2014,** *19*, 195–202.
20. Polycarbonate Properties, Production, Price, Market and Uses. https://www.plasticsinsight.com/resin-intelligence/resin-prices/polycarbonate/#process (accessed 03/27/2020).

21. Stadler, B. M.; Wulf, C.; Werner, T.; Tin, S.; de Vries, J. G., *ACS Catal.* **2019,** *9*, 8012–8067.
22. Quadrelli, E. A.; Centi, G.; Duplan, J.-L.; Perathoner, S., *ChemSusChem* **2011,** *4*, 1194–1215.
23. Jacobsen, E. N.; Zhang, W.; Muci, A. R.; Ecker, J. R.; Deng, L., *J. Am. Chem. Soc.* **1991,** *113*, 7063–7064.
24. Latscha, H. P. K., Uli; Klein, Helmut, *Organische Chemie*. Springer Spektrum: **2016**.
25. Brückner, R., *Reaktionsmechanismen*. Springer Spektrum: **2004**.
26. Sharpless, K. B., *Angew. Chem. Int. Ed.* **2002,** *41*, 2024–2032.
27. Wang, Z.-X.; Tu, Y.; Frohn, M.; Zhang, J.-R.; Shi, Y., *J. Am. Chem. Soc.* **1997,** *119*, 11224–11235.
28. Kobe, J. M.; Evans, W. E.; June, R. L.; Lemanski, M. F., Epoxidation – Industrial. In *Encyclopedia of Catalysis*, Horváth, I., Ed. 2002.
29. Russo, V.; Tesser, R.; Santacesaria, E.; Di Serio, M., *Ind. Eng. Chem. Res.* **2013,** *52*, 1168–1178.
30. Schmidt, F. B., Maik; Morell, Heiko; Pascaly, Matthias, *Chim. Oggi* **2014,** *32*, 31–34.
31. Khatib, S. J.; Oyama, S. T., *Catal. Rev.* **2015,** *57*, 306-344.
32. Bernhard, M.; Anton, J.; Schmidt, F.; Sandkaulen, F.; Pascaly, M., *Chemie in unserer Zeit* **2017,** *51*, 198–209.
33. Blanckenberg, A.; Malgas-Enus, R., *Catal. Rev.* **2019,** *61*, 27-83.
34. Machado, P. G.; Walter, A.; Cunha, M., *Biofuels, Bioproducts and Biorefining* **2016,** *10*, 623–633.
35. Keim, W., *Angew. Chem. Int. Ed.* **2013,** *52*, 12492–12496.
36. Hulea, V., *ACS Catal.* **2018,** *8*, 3263–3279.
37. Kuznetsov, A.; Kumar, G.; Ardagh, M. A.; Tsapatsis, M.; Zhang, Q.; Dauenhauer, P. J., *ACS Sustainable Chem. Eng.* **2020,** *8*, 3273–3282.
38. Sun, P.; Liu, S.; Zhou, Y.; Zhang, S.; Yao, Z., *ACS Sustainable Chem. Eng.* **2018,** *6*, 13579–13587.
39. Li, X.; Kant, A.; He, Y.; Thakkar, H. V.; Atanga, M. A.; Rezaei, F.; Ludlow, D. K.; Rownaghi, A. A., *Catal. Today* **2016,** *276*, 62–77.
40. Rodrigues, A.; Bordado, J. C.; dos Santos, R. G., *Energies* **2017,** *10*, 1817.
41. Okoye, P. U.; Hameed, B. H., *Renewable Sustainable Energy Rev.* **2016,** *53*, 558–574.
42. Yu, L.; Yuan, J.; Zhang, Q.; Liu, Y.-M.; He, H.-Y.; Fan, K.-N.; Cao, Y., *ChemSusChem* **2014,** *7*, 743–747.
43. Klingler, F. D.; Ebertz, W., *Ullmann's Encyclopedia of Industrial Chemistry* **2000**.
44. Eberson, L., Landström, L, *Acta Chem. Scand.* **1972,** *26*, 239-249.
45. Pierre, B.; Jean, Z.; Gerard, P.; Jean-Pierre, R., *Heterocycl. Commun.* **1994,** *1*, 13–16.
46. Cott, D. J.; Ziegler, K. J.; Owens, V. P.; Glennon, J. D.; Graham, A. E.; Holmes, J. D., *Green Chem.* **2005,** *7*, 105–110.
47. Mahmoud, E.; Watson, D. A.; Lobo, R. F., *Green Chem.* **2014,** *16*, 167-175.
48. Biermann, U.; Butte, W.; Eren, T.; Haase, D.; Metzger, J. O., *Eur. J. Org. Chem.* **2007,** 3859–3862.
49. Struga, M.; Krawiecka, M.; Kossakowski, J.; Stefańska, J.; Miroslaw, B.; Koziol, A. E., *J. Chin. Chem. Soc.* **2008,** *55*, 1258–1265.
50. Yeung, C. S.; Wang, Y. A., *J. Phys. Chem. C* **2011,** *115*, 7153–7163.

51. Li, D.; Liu, G.; Hu, Q.; Wang, C.; Xi, Z., *Org. Lett.* **2007,** *9*, 5433–5436.
52. Glebov, E. M.; Krishtopa, L. G.; Stepanov, V.; Krasnoperov, L. N., *J. Phys. Chem. A* **2001,** *105*, 9427–9435.
53. Knutson, B. L.; Dillow, A. K.; Liotta, C. L.; Eckert, C. A., Kinetics of a Diels—Alder Reaction in Supercritical Propane. In *Innovations in Supercritical Fluids*, American Chemical Society: 1995; Vol. 608, pp 166–178.
54. Liu, H.; Chen, F.; Liu, B.; Estep, G.; Zhang, J., *Macromolecules* **2010,** *43*, 6058–6066.
55. Longo, J. M.; Sanford, M. J.; Coates, G. W., *Chem. Rev.* **2016,** *116*, 15167–15197.
56. Paul, S.; Zhu, Y.; Romain, C.; Brooks, R.; Saini, P. K.; Williams, C. K., *Chem. Commun.* **2015,** *51*, 6459–6479.
57. Kember, M. R.; Buchard, A.; Williams, C. K., *Chem. Commun.* **2011,** *47*, 141–163.
58. Van Zee, N. J.; Sanford, M. J.; Coates, G. W., *J. Am. Chem. Soc.* **2016,** *138*, 2755–2761.
59. Darensbourg, D. J.; Yeung, A. D., *Polym. Chem.* **2015,** *6*, 1103–1117.
60. Osakada, K., *Organometallic Reactions and Polymerization*. Springer-Verlag Berlin Heidelberg: Heidelberg, New York, Dordrecht, London, **2014**.
61. Coates, G. W., *Chem. Rev.* **2000,** *100*, 1223–1252.
62. Razavi, A., Syndiotactic Polypropylene: Discovery, Development, and Industrialization via Bridged Metallocene Catalysts. In *Polyolefins: 50 years after Ziegler and Natta II: Polyolefins by Metallocenes and Other Single-Site Catalysts*, Kaminsky, W., Ed. Springer Berlin Heidelberg: Berlin, Heidelberg, 2013; pp 43–116.
63. Childers, M. I.; Vitek, A. K.; Morris, L. S.; Widger, P. C. B.; Ahmed, S. M.; Zimmerman, P. M.; Coates, G. W., *J. Am. Chem. Soc.* **2017,** *139*, 11048–11054.
64. Darensbourg, D. J., *Green Chem.* **2019,** *21*, 2214–2223.
65. Huang, J.; Worch, J. C.; Dove, A. P.; Coulembier, O., *ChemSusChem* **2020,** *13*, 469–487.
66. Lu, X.-B.; Darensbourg, D. J., *Chem. Soc. Rev.* **2012,** *41*, 1462–1484.
67. Trott, G.; Saini, P. K.; Williams, C. K., *Phil. Trans. R. Soc. A* **2016,** *374*.
68. Cozzi, P. G., *Chem. Soc. Rev.* **2004,** *33*, 410–421.
69. Hošťálek, Z.; Trhlíková, O.; Walterová, Z.; Martinez, T.; Peruch, F.; Cramail, H.; Merna, J., *Eur. Polym. J.* **2017,** *88*, 433–447.
70. Han, B.; Zhang, L.; Liu, B.; Dong, X.; Kim, I.; Duan, Z.; Theato, P., *Macromolecules* **2015,** *48*, 3431–3437.
71. Kummari, A.; Pappuru, S.; Chakraborty, D., *Polym. Chem.* **2018,** *9*, 4052–4062.
72. Lin, L.; Liang, J.; Xu, Y.; Wang, S.; Xiao, M.; Sun, L.; Meng, Y., *Green Chem.* **2019,** *21*, 2469–2477.
73. Ji, H.-Y.; Wang, B.; Pan, L.; Li, Y.-S., *Green Chem.* **2018,** *20*, 641–648.
74. Zhang, D.; Boopathi, S. K.; Hadjichristidis, N.; Gnanou, Y.; Feng, X., *J. Am. Chem. Soc.* **2016,** *138*, 11117–11120.
75. Kummari, A.; Pappuru, S.; Gupta, P. K.; Chakraborty, D.; Verma, R. S., *Mater. Today Commun.* **2019,** *19*, 306–314.
76. Kou, X.; Li, Y.; Shen, Y.; Li, Z., *Macromol. Chem. Phys.* **2019,** *220*, 1900416.

77. Ji, H.-Y.; Song, D.-P.; Wang, B.; Pan, L.; Li, Y.-S., *Green Chem.* **2019,** *21*, 6123–6132.
78. Pappuru, S.; Chakraborty, D., *Eur. Polym. J.* **2019,** *121*, 109276.
79. Aida, T.; Inoue, S., *J. Am. Chem. Soc.* **1985,** *107*, 1358–1364.
80. Bernard, A.; Chatterjee, C.; Chisholm, M. H., *Polymer* **2013,** *54*, 2639–2646.
81. Robert, C.; Ohkawara, T.; Nozaki, K., *Chem. Eur. J.* **2014,** *20*, 4789–4795.
82. Huijser, S.; Hosseini, N., Elham; Sablong, R.; de Jong, C.; Koning, C. E.; Duchateau, R., *Macromolecules* **2011,** *44*, 1132–1139.
83. DiCiccio, A. M.; Coates, G. W., *J. Am. Chem. Soc.* **2011,** *133*, 10724–10727.
84. Chatterjee, C.; Chisholm, M. H., *The Chemical Record* **2013,** *13*, 549–560.
85. Hosseini Nejad, E.; Paoniasari, A.; Koning, C. E.; Duchateau, R., *Polym. Chem.* **2012,** *3*, 1308–1313.
86. Aida, T.; Sanuki, K.; Inoue, S., *Macromolecules* **1985,** *18*, 1049–1055.
87. Darensbourg, D. J., *Chem. Rev.* **2007,** *107*, 2388–2410.
88. Jeske, R. C.; DiCiccio, A. M.; Coates, G. W., *J. Am. Chem. Soc.* **2007,** *129*, 11330–11331.
89. Moore, D. R.; Cheng, M.; Lobkovsky, E. B.; Coates, G. W., *Angew. Chem. Int. Ed.* **2002,** *41*, 2599–2602.
90. Tokunaga, M.; Larrow, J. F.; Kakiuchi, F.; Jacobsen, E. N., *Science* **1997,** *277*, 936–938.
91. Robert, C.; de Montigny, F.; Thomas, C. M., *Nat. Commun.* **2011,** *2*, 586.
92. Darensbourg, D. J.; Poland, R. R.; Escobedo, C., *Macromolecules* **2012,** *45*, 2242–2248.
93. Hosseini Nejad, E.; van Melis, C. G. W.; Vermeer, T. J.; Koning, C. E.; Duchateau, R., *Macromolecules* **2012,** *45*, 1770–1776.
94. Robert, C.; de Montigny, F.; Thomas, C. M., *Nat. Commun.* **2011,** *2*, 586.
95. Yoon, T. P.; Jacobsen, E. N., *Science* **2003,** *299*, 1691-1693.
96. S, S.; Min, J. K.; Seong, J. E.; Na, S. J.; Lee, B. Y., *Angew. Chem. Int. Ed.* **2008,** *47*, 7306–7309.
97. DiCiccio, A. M.; Longo, J. M.; Rodríguez-Calero, G. G.; Coates, G. W., *J. Am. Chem. Soc.* **2016,** *138*, 7107–7113.
98. Sanford, M. J.; Peña Carrodeguas, L.; Van Zee, N. J.; Kleij, A. W.; Coates, G. W., *Macromolecules* **2016,** *49*, 6394–6400.
99. Sanford, M. J.; Van Zee, N. J.; Coates, Geoffrey W., *Chem. Sci.* **2018,** *9*, 134–142.
100. Hiranoi, Y.; Nakano, K., *Beilstein J. Org. Chem.* **2018,** *14*, 2779–2788.
101. Duan, Z.; Wang, X.; Gao, Q.; Zhang, L.; Liu, B.; Kim, I., *J. Polym. Sci., Part A: Polym. Chem.* **2014,** *52*, 789–795.
102. Jeon, J. Y.; Eo, S. C.; Varghese, J. K.; Lee, B. Y., *Beilstein J. Org. Chem.* **2014,** *10*, 1787–1795.
103. Abel, B. A.; Lidston, C. A. L.; Coates, G. W., *J. Am. Chem. Soc.* **2019,** *141*, 12760–12769.
104. Ren, W.-M.; Liu, Z.-W.; Wen, Y.-Q.; Zhang, R.; Lu, X.-B., *J. Am. Chem. Soc.* **2009,** *131*, 11509–11518.
105. Zhu, Y.; Romain, C.; Williams, C. K., *J. Am. Chem. Soc.* **2015,** *137*, 12179–12182.
106. Thevenon, A.; Garden, J. A.; White, A. J. P.; Williams, C. K., *Inorg. Chem.* **2015,** *54*, 11906–11915.

107. Pilkington, N. H.; Robson, R., *Aust. J. Chem.* **1970,** *23*, 2225–2236.
108. Saini, P. K.; Romain, C.; Zhu, Y.; Williams, C. K., *Polym. Chem.* **2014,** *5*, 6068–6075.
109. Winkler, M.; Romain, C.; Meier, M. A. R.; Williams, C. K., *Green Chem.* **2015,** *17*, 300–306.
110. Garden, J. A.; Saini, P. K.; Williams, C. K., *J. Am. Chem. Soc.* **2015,** *137*, 15078–15081.
111. Romain, C.; Zhu, Y.; Dingwall, P.; Paul, S.; Rzepa, H. S.; Buchard, A.; Williams, C. K., *J. Am. Chem. Soc.* **2016,** *138*, 4120–4131.
112. Romain, C.; Garden, J. A.; Trott, G.; Buchard, A.; White, A. J. P.; Williams, C. K., *Chem. Eur. J.* **2017,** *23*, 7367–7376.
113. Zhu, Y.; Radlauer, M. R.; Schneiderman, D. K.; Shaffer, M. S. P.; Hillmyer, M. A.; Williams, C. K., *Macromolecules* **2018,** *51*, 2466–2475.
114. Stößer, T.; Williams, C. K., *Angew. Chem. Int. Ed.* **2018,** *57*, 6337–6341.
115. Stosser, T.; Mulryan, D.; Williams, C. K., *Angew. Chem., Int. Ed.* **2018,** *57*, 16893–16897.
116. Chen, T. T. D.; Zhu, Y.; Williams, C. K., *Macromolecules* **2018,** *51*, 5346–5351.
117. Saini, P. K.; Fiorani, G.; Mathers, R. T.; Williams, C. K., *Chem. Eur. J.* **2017,** *23*, 4260–4265.
118. Su, Y.-C.; Tsai, C.-Y.; Huang, L.-S.; Lin, C.-H.; Ko, B.-T., *Dalton Trans.* **2019,** *48*, 12239–12249.
119. Su, Y.-C.; Liu, W.-L.; Li, C.-Y.; Ko, B.-T., *Polymer* **2019,** *167*, 21–30.
120. Li, M.-H.; Liu, G.-L.; Su, Y.-C.; Ko, B.-T., *Eur. Polym. J.* **2019,** *120*, 109224.
121. Chang, C.-H.; Tsai, C.-Y.; Lin, W.-J.; Su, Y.-C.; Chuang, H.-J.; Liu, W.-L.; Chen, C.-T.; Chen, C.-K.; Ko, B.-T., *Polymer* **2018,** *141*, 1–11.
122. Yu, C.-Y.; Chuang, H.-J.; Ko, B.-T., *Catal. Sci. Technol.* **2016,** *6*, 1779–1791.
123. Wu, L.-y.; Fan, D.-d.; Lü, X.-q.; Lu, R., *Chin. J. Polym. Sci.* **2014,** *32*, 768–777.
124. Liu, D.-F.; Wu, L.-Y.; Feng, W.-X.; Zhang, X.-M.; Wu, J.; Zhu, L.-Q.; Fan, D.-D.; Lü, X.-Q.; Shi, Q., *J. Mol. Catal. A: Chem.* **2014,** *382*, 136–145.
125. Zhu, L.; Liu, D.; Wu, L.; Feng, W.; Zhang, X.; Wu, J.; Fan, D.; Lü, X.; Lu, R.; Shi, Q., *Inorg. Chem. Commun.* **2013,** *37*, 182–185.
126. Isnard, F.; Carratù, M.; Lamberti, M.; Venditto, V.; Mazzeo, M., *Catal. Sci. Technol.* **2018,** *8*, 5034–5043.
127. Isnard, F.; Lamberti, M.; Pellecchia, C.; Mazzeo, M., *ChemCatChem* **2017,** *9*, 2972–2979.
128. Isnard, F.; Lamberti, M.; Lettieri, L.; D'Auria, I.; Press, K.; Troiano, R.; Mazzeo, M., *Dalton Trans.* **2016,** *45*, 16001–16010.
129. Huang, J.; Xu, Y.; Wang, M.; Duan, Z., *J. Macromol. Sci., Part A: Pure Appl. Chem.* **2020,** *57*, 131–138.
130. Liu, F.-P.; Li, J.; Liu, Y.; Ren, W.-M.; Lu, X.-B., *Macromolecules* **2019,** *52*, 5652–5657.
131. Li, J.; Ren, B.-H.; Chen, S.-Y.; He, G.-H.; Liu, Y.; Ren, W.-M.; Zhou, H.; Lu, X.-B., *ACS Catal.* **2019,** *9*, 1915–1922.
132. Hatazawa, M.; Takahashi, R.; Deng, J.; Houjou, H.; Nozaki, K., *Macromolecules* **2017,** *50*, 7895–7900.
133. Jiang, Y.-J.; Ren, W.-M.; Liu, Y.; Lu, X.-B., *Chin. J. Polym. Sci.* **2019,** *37*, 1200–1204.

134. Duan, R.; Hu, C.; Sun, Z.; Zhang, H.; Pang, X.; Chen, X., *Green Chem.* **2019,** *21*, 4723–4731.
135. Li, X.; Hu, C.; Pang, X.; Duan, R.; Chen, X., *Catal. Sci. Technol.* **2018,** *8*, 6452–6457.
136. Zhou, Y.; Duan, R.; Li, X.; Pang, X.; Wang, X.; Chen, X., *Chem. - Asian J.* **2017,** *12*, 3135–3140.
137. Duan, R.; Qu, Z.; Pang, X.; Zhang, Y.; Sun, Z.; Zhang, H.; Bian, X.; Chen, X., *Chin. J. Chem.* **2017,** *35*, 640–644.
138. Yang, J.; Sun, Z.; Duan, R.; Li, L.; Pang, X.; Chen, X., *Sci. China: Chem.* **2016,** *59*, 1384–1389.
139. Sun, Z.; Duan, R.; Yang, J.; Zhang, H.; Li, S.; Pang, X.; Chen, W.; Chen, X., *RSC Adv.* **2016,** *6*, 17531–17538.
140. Li, X.; Duan, R.; Pang, X.; Gao, B.; Wang, X.; Chen, X., *Appl. Catal., B* **2016,** *182*, 580–586.
141. Sun, Z.; Duan, R.; Zhang, H.; Pang, X.; Wang, X.; Chen, X., *J. Renewable Mater.* **2015,** *3*, 82–90.
142. Pang, X.; Duan, R.; Li, X.; Gao, B.; Sun, Z.; Wang, X.; Chen, X., *RSC Adv.* **2014,** *4*, 22561–22566.
143. Pang, X.; Duan, R.; Li, X.; Chen, X., *Polym. Chem.* **2014,** *5*, 3894–3900.
144. Bester, K.; Bukowska, A.; Myśliwiec, B.; Hus, K.; Tomczyk, D.; Urbaniak, P.; Bukowski, W., *Polym. Chem.* **2018,** *9*, 2147–2156.
145. Proverbio, M.; Galotto Galotto, N.; Losio, S.; Tritto, I.; Boggioni, L., *Polymers* **2019,** *11*, 1222.
146. Hansen, T. V.; Skattebøl, L., *Tetrahedron Lett.* **2005,** *46*, 3829-3830.
147. Mucha, P.; Mlostoń, G.; Jasiński, M.; Linden, A.; Heimgartner, H., *Tetrahedron: Asymmetry* **2008,** *19*, 1600–1607.
148. Tang, X.; Chen, E. Y. X., *Nat. Commun.* **2018,** *9*, 2345.
149. Ciaccia, M.; Cacciapaglia, R.; Mencarelli, P.; Mandolini, L.; Di Stefano, S., *Chem. Sci.* **2013,** *4*, 2253–2261.
150. Thadani, A. N.; Huang, Y.; Rawal, V. H., *Org. Lett.* **2007,** *9*, 3873–3876.
151. Corey, E. J.; Venkateswarlu, A., *J. Am. Chem. Soc.* **1972,** *94*, 6190–6191.
152. Smith, A. B.; Xian, M.; Kim, W.-S.; Kim, D.-S., *J. Am. Chem. Soc.* **2006,** *128*, 12368–12369.
153. Hua, Z.; Qi, G.; Chen, S., *J. Appl. Polym. Sci.* **2004,** *93*, 1788–1792.
154. Liu, Y.; Huang, K.; Peng, D.; Wu, H., *Polymer* **2006,** *47*, 8453–8461.
155. Song, P. F.; Xiao, M.; Du, F. G.; Wang, S. J.; Gan, L. Q.; Liu, G. Q.; Meng, Y. Z., *J. Appl. Polym. Sci.* **2008,** *109*, 4121–4129.
156. Woo, W. H.; Hyun, K.; Kim, Y.; Ryu, J. Y.; Lee, J.; Kim, M.; Park, M. H.; Kim, Y., *Eur. J. Inorg. Chem.* **2017,** *2017*, 5372–5378.
157. Ji, H.-Y.; Wang, B.; Pan, L.; Li, Y.-S., *Green Chem.* **2018**.
158. Fieser, M. E.; Sanford, M. J.; Mitchell, L. A.; Dunbar, C. R.; Mandal, M.; Van Zee, N. J.; Urness, D. M.; Cramer, C. J.; Coates, G. W.; Tolman, W. B., *J. Am. Chem. Soc.* **2017,** *139*, 15222–15231.
159. Impemba, S.; Della Monica, F.; Grassi, A.; Capacchione, C.; Milione, S., *ChemSusChem* **2020,** *13*, 141–145.
160. Koltzenburg, S., Maskos, M., Nuyken, O., *Polymere: Synthese, Eigenschaften und Anwendungen*. 1 ed.; Springer Spektrum, Berlin, Heidelberg: **2014**.
161. Chan, T. C.; Li, H. T.; Li, K. Y., *J. Phys. Chem. B* **2015,** *119*, 15718–15728.
162. Jiang, J. L.; Xiu, Z.; Hua, R., *Synth. Commun.* **2008,** *38*, 232–238.

163. Hanna Ritchie, M. R., Energy. In *Our World in Data*, https://ourworldindata.org/energy, 2020.
164. O'Regan, B.; Grätzel, M., *Nature* **1991,** *353*, 737–740.
165. Tian, H.; Sun, L., 8.16 - Organic Photovoltaics and Dye-Sensitized Solar Cells. In *Comprehensive Inorganic Chemistry II, 2nd Ed.*, Reedijk, J.; Poeppelmeier, K., Eds. Elsevier: Amsterdam, 2013; pp 567–605.
166. Hou, W.; Xiao, Y.; Han, G.; Lin, J.-Y., *Polymers* **2019,** *11*, 143.
167. Cui, C.; Li, Y., *Energy & Environmental Science* **2019,** *12*, 3225–3246.
168. Vogelbaum, H. S.; Sauvé, G., *Synth. Met.* **2017,** *223*, 107–121.
169. Khopkar, S.; Shankarling, G., *Dyes Pigm.* **2019,** *170*, 107645.
170. Brédas, J.-L.; Norton, J. E.; Cornil, J.; Coropceanu, V., *Acc. Chem. Res.* **2009,** *42*, 1691-1699.
171. Fu, Y.; Li, B.; Liu, H.; Xue, B.; Liu, E., *Mater. Chem. Phys.* **2020,** *239*, 121970.
172. Ramki, K.; Venkatesh, N.; Sathiyan, G.; Thangamuthu, R.; Sakthivel, P., *Organic Electronics* **2019,** *73*, 182–204.
173. Würthner, F., *Acc. Chem. Res.* **2016,** *49*, 868–876.
174. Luo, J.-S.; Wan, Z.-Q.; Jia, C.-Y., *Chin. Chem. Lett.* **2016,** *27*, 1304–1318.
175. Markl, C. A. Catalytic copolymerization of anhydrides and epoxides and postmodifications. Wien, 2021.
176. Nekongo, E. E.; Popik, V. V., *J. Org. Chem.* **2014,** *79*, 7665–7671.
177. Martin-Brown, S. A.; Fu, Y.; Saroja, G.; Collinson, M. M.; Higgins, D. A., *Anal. Chem.* **2005,** *77*, 486–494.
178. Fulmer, G. R.; Miller, A. J. M.; Sherden, N. H.; Gottlieb, H. E.; Nudelman, A.; Stoltz, B. M.; Bercaw, J. E.; Goldberg, K. I., *Organometallics* **2010,** *29*, 2176–2179.
179. Nizovtsev, A. V.; Scheurer, A.; Kosog, B.; Heinemann, F. W.; Meyer, K., *Eur. J. Inorg. Chem.* **2013,** *2013*, 2538–2548.
180. Campbell, E. J.; Nguyen, S. T., *Tetrahedron Lett.* **2001,** *42*, 1221–1225.
181. Muñoz-Hernández, M.-A.; Keizer, T. S.; Parkin, S.; Patrick, B.; Atwood, D. A., *Organometallics* **2000,** *19*, 4416–4421.
182. Bedrač, L.; Iskra, J., *Adv. Synth. Catal.* **2013,** *355*, 1243–1248.
183. Tietze, L. F.; Vock, C. A.; Krimmelbein, I. K.; Wiegand, J. M.; Nacke, L.; Ramachandar, T.; Islam, K. M. D.; Gatz, C., *Chem. Eur. J.* **2008,** *14*, 3670–3679.
184. Akai, S.; Ikawa, T.; Takayanagi, S.-i.; Morikawa, Y.; Mohri, S.; Tsubakiyama, M.; Egi, M.; Wada, Y.; Kita, Y., *Angew. Chem. Int. Ed.* **2008,** *47*, 7673–7676.
185. Adimurthy, S.; Ramachandraiah, G.; Bedekar, A. V.; Ghosh, S.; Ranu, B. C.; Ghosh, P. K., *Green Chem.* **2006,** *8*, 916–922.
186. Lu, X.-B.; Shi, L.; Wang, Y.-M.; Zhang, R.; Zhang, Y.-J.; Peng, X.-J.; Zhang, Z.-C.; Li, B., *J. Am. Chem. Soc.* **2006,** *128*, 1664–1674.
187. Hošťálek, Z.; Mundil, R.; Císařová, I.; Trhlíková, O.; Grau, E.; Peruch, F.; Cramail, H.; Merna, J., *Polymer* **2015,** *63*, 52–61.
188. Myers, J. K.; Jacobsen, E. N., *J. Am. Chem. Soc.* **1999,** *121*, 8959–8960.
189. Tian, D.; Liu, B.; Gan, Q.; Li, H.; Darensbourg, D. J., *ACS Catal.* **2012,** *2*, 2029–2035.
190. Berkessel, A.; Brandenburg, M., *Org. Lett.* **2006,** *8*, 4401–4404.
191. Nielsen, L. P. C.; Stevenson, C. P.; Blackmond, D. G.; Jacobsen, E. N., *J. Am. Chem. Soc.* **2004,** *126*, 1360–1362.

14 X–Ray Analysis References

Bruker SAINT v8.38B Copyright © 2005-2019 Bruker AXS
Sheldrick, G. M. (1996). *SADABS*. University of Göttingen, Germany.
Dolomanov, O.V., Bourhis, L.J., Gildea, R.J, Howard, J.A.K. & Puschmann, H. , OLEX2, (2009), J. Appl. Cryst. 42, 339–341
C. B. Huebschle, G. M. Sheldrick and B. Dittrich, ShelXle: a Qt graphical user interface for SHELXL, J. Appl. Cryst., 44, (2011) 1281–1284
Sheldrick, G. M. (2015). *SHELXS v 2016/4* University of Göttingen, Germany.
Sheldrick, G. M. (2015). *SHELXL v 2016/4* University of Göttingen, Germany.
A. L. Spek, Acta Cryst. 2009, D65, 148–155.